Australian Government

Bureau of Meteorology

The Centre for Australian Weather and Climate Research

A partnership between CSIRO and the Bureau of Meteorology

CSIRO

‘Modelling and Understanding High Impact Weather’: extended abstracts of the third CAWCR Modelling Workshop, 30 November – 2 December 2009, Melbourne, Australia

CAWCR Technical Report No. 017

A.J. Hollis (editor)

www.cawcr.gov.au

‘Modelling and Understanding High Impact Weather’: extended abstracts of the third CAWCR Modelling Workshop, 30 November – 2 December 2009, Melbourne, Australia

CAWCR Technical Report No. 017

A.J. Hollis (editor)

November 2009

ISSN: 1836-019X

ISBN: 978-1-921605-47-5 (pdf)

Series: Technical report (Centre for Australian Weather and Climate Research.) ; no. 17.

The 3rd CAWCR Modelling Workshop is supported by Sun Microsystems.

Enquiries should be addressed to:

Andrew Hollis
Centre for Australian Weather and Climate Research:
A Partnership between the Bureau of Meteorology and CSIRO
GPO Box 1289
Melbourne VIC 3001
AUSTRALIA
a.hollis@bom.gov.au
Phone: 61 3 9669 4046
Fax: 61 3 9669 4660

Copyright and Disclaimer

CONTENTS

FOREWORD

The Centre for Australian Weather and Climate Research (CAWCR) is a partnership between Australia's leading atmosphere and ocean research agencies – the Bureau of Meteorology and CSIRO. The Centre was established in 2007 to provide the combined critical mass necessary to keep Australia at the forefront of climate, weather and oceans research. This year's CAWCR Workshop, '*Modelling and Understanding High Impact Weather'* is the third Modelling Workshop under the auspices of the joint Centre continuing the series originating within the Bureau of Meteorology Research Centre.

Australia faces significant and ongoing challenges from high impact weather realised on time scales from hours to those associated with climate change. There are many scientific questions to resolve. The key themes covered in this year's workshop are: (i) Tropical Cyclones; (ii) Heat, Drought and Fire Weather; and (iii) Mid-latitude and Convective Storms.

The workshop, by invitation only, includes participants from research groups around Australia. We also welcome a number of contributors from overseas research institutes and national meteorological services to the workshop, with invited keynote presentations from Jay Charney (US Forest Service), Peter Clark (UK Met Office), Erich Fischer (ETH Zurich, Switzerland), Yuki Honda (JMA, Japan) and Tom Knutson (GFDL, USA). We are grateful for these expert contributions and to all the participants' contributions to the debate and discussions.

We are particularly grateful to Sun Microsystems for their generous support of this workshop.

Finally, I would like to thank the Local Organising Committee for the workshop, comprising Debbie Abbs and John McBride (Co-Chairs), Kevin Hennessy, Andrew Hollis, Val Jemmeson, Graham Mills and Chris Tingwell.

Tom Keenan
Acting Director
Centre for Australian Weather and Climate Research:
A partnership between the Australian Bureau of Meteorology and CSIRO

November 2009

Extremes, climate change and disasters

Neville Nicholls
Monash University, Clayton, Australia

Australia has warmed about 0.75C since 1970, and on the back of this trend we have set many impressive new record extremes in the last year or so:

- Adelaide in 2008 saw 15 consecutive days above 35C – seven days more than the previous record heatwave duration.
- The Melbourne temperature on three successive days at the end of January 2009 exceeded 43C; we had never previously seen three days in a row reach 42C, let alone 43C. Then a week later Black Saturday set a new Melbourne record temperature of 46.4C, more than 3C hotter than the previous February record.
- The seven hottest August days ever recorded at Windorah in western Queensland all occurred this year. The new record August maximum temperature for Windorah is 38C; the record prior to this year was only 34.2C. Similar, unprecedented temperatures were observed in August across much of southern Queensland and northern New South Wales.
- Six of the hottest Sydney Septembers (average of MaxT and MinT) since 1851 (including the two hottest) have occurred in the last 10 years.
- This year (2009) will likely (unless we get a deluge or three in the next couple of months) be the 13th year in succession that Melbourne has experienced below average rainfall. Prior to this drought the longest such period was only six years long.
- Springtime (October) snow depths in the Australian snowfields have declined by 40% over the past 40 years, and this decline shows no evidence of halting.
- Finally, some good news: the average number of nights with frost has declined by about 30% over the past 50 years, across the country.

These recent trends and record extremes continue the pattern seen in previous decades. Alexander et al (2007) showed that maximum and minimum temperatures are increasing across most of Australia. In the east of the continent, maximum and minimum temperature have warmed about 2C since 1957. Consistent with this warming we have seen strong decreases in cold nights and cold days, decreases in frost days and cold spells, and increases in extremely warm nights. At any particular location, the increasing trend in the minimum temperature with fewer cool nights is generally larger than the trend for maximum temperature and cool days. This means that the diurnal range (the difference between the maximum and minimum temperatures) is decreasing. Trends in rainfall extremes vary throughout the seasons. The largest trend is the decrease in both the total rainfall and the maximum 1-day rainfall in southeastern Australia in March-May. In some places the trends in the average rainfall and the extremes are not in the same direction (that is, we are seeing more “droughts and flooding rains”). For example, the trend in the total amount of rainfall that falls on the day with the maximum rainfall is increasing almost everywhere, even in the southwest where total rainfall is decreasing, indicating that the intensity of the rainfall is increasing. In summer and spring, the trends in one day maximal rainfall increased almost everywhere over the period 1910-2005.

Is this pattern of records and trends evidence of a changing climate? And if so, is it caused by human actions? I would maintain that each of the above trends and records is so unlikely (in the context of a static climate) as to provide some evidence of a changing climate, and a climate that is fundamentally altering the risks from “high impact weather”. However, each record or trend, by itself may not be so unusual as to provide *convincing* evidence of a changing climate. For instance, historically (1856-1990) a drier than average year in Melbourne has been followed on 52% of occasions by a dry year the following year. Given this transition frequency, it is easy to calculate that you could expect a 13-year run of drier than average years to occur about once in 2500 years. So, the 13-year dry spell is unusual but perhaps not so unusual to convince us, by itself, that the climate is changing – there is still room for the hypothesis that the drought is just a fluke or natural variability. Collectively, however, the pattern of trends (a shift towards more frequent and extreme hot extremes, and drying along the southern coast of the continent) is what is anticipated from anthropogenic climate change. So the pattern of widespread records and trends might more likely convince us that the climate is changing. But how confident can we be of the reality or credibility of these changes, both observed and projected?

Our understanding of how climate extremes may or may not be changing, and the likely causes of these changes, and how they might change in the future, has grown rapidly over the past decade or two, since the establishment of the Intergovernmental Panel on Climate Change (Nicholls and Alexander, 2007). In 1990 and 1992 the Intergovernmental Panel on Climate Change (IPCC), in its first assessment of climate change and its supplement, did not consider whether extreme weather events had increased in frequency and/or intensity globally, because data were too sparse to make this a worthwhile exercise. In 1995 the IPCC, in its second assessment, did examine this question, but concluded that data and analyses of changes in extreme events were ‘not comprehensive’ and thus the question could not be answered with any confidence. Since then, concerted multinational efforts have been undertaken to collate, quality control, and analyse data on weather and climate extremes. A comprehensive examination of the question of whether extreme events have changed in frequency or intensity is now more feasible than it was 15 years ago, and statements about extremes in the latest IPCC assessment reflect this growing confidence.

In 2007, the Intergovernmental Panel on Climate Change’s Fourth Assessment summarised our understanding on changes in various types of extremes thus:

- Warmer and fewer cold days and nights (coldest 10%), and warmer and more frequent hot days and nights (hottest 10%) have *very likely* occurred over most land areas, while the frequency of warm spells and heat waves has *likely* increased. It is *likely* that human actions have contributed to this trend towards warmer extremes (and *more likely than not* that human actions have contributed to the increased frequency of heat waves). It is *virtually certain* that the trend towards warmer extremes will continue through the 21st century, and a trend towards more heat waves is *very likely*.
- The frequency of heavy precipitation events (or the proportion of total rainfall occurring in heavy falls) has *likely* increased over most areas, due *more likely than not* to human influences. It is *very likely* that this trend towards more extreme precipitation events will continue through the 21st century.
- It is *likely* that the area affected by droughts has increased in many regions since the 1970s, and it is *more likely than not* those human actions have contributed to this trend. It is *likely* that this trend will continue through the 21st century.
- There has been no clear trend in the annual numbers of tropical cyclones.

However, it is *likely* that intense tropical cyclone activity has increased in some regions since 1970, and *more likely than not* that human action has contributed to this trend. It is *likely* that this trend to more intense cyclone activity will increase through the 21st century.

- Stronger mid-latitude westerly wind maxima have occurred in both hemispheres in most seasons from at least 1979 to the late 1990s, and poleward displacements of corresponding Atlantic and southern polar front jet streams have been documented. Analyses of wind and significant wave height support reanalysis-based evidence for changes in Northern Hemisphere extratropical storms from the start of the reanalysis record in the late 1970s until the late 1990s. These changes have been accompanied by a tendency towards stronger winter polar vortices throughout the troposphere and lower stratosphere.
- It is *likely* that there has been increased incidence of extreme high sea level (highest 1% of hourly observed sea level), and *more likely than not* that this has been contributed to by human actions. It is *likely* that this trend will continue unless sea level influences from regional weather systems offsets the contribution from increased mean sea level.
- There is insufficient evidence to determine whether trends have occurred in “small spatial scale” events such as tornadoes, hail, lightning and dust storms.

In summary, the IPCC Assessment was that some extremes are changing, and will likely continue to change, due to human influences on the weather. But not all “high impact events” are changing; in some cases we cannot even monitor events sufficiently well to determine if they are changing, let alone whether any changes are the result of human actions. Yet, by definition, we are vulnerable to these high impact events, and changes in their frequency, intensity, location, or spatial scale are likely to have very serious consequences in many parts of the world. Most of the weather extremes examined by the IPCC (heat waves, drought, flood, tropical cyclones, extreme sea levels events) can have disastrous consequences. Changes in their frequency or intensity will likely have far graver consequences than might be imagined from a gradual warming of a degree or so over some decades.

So, what should we do? How should we react? Can we adapt to the projected changes? Should we even try? The IPCC, with the involvement of the UN International Strategy for Disaster Reduction (ISDR), has commenced the preparation of a Special Report on *Managing the Risks of Extreme Events and Disasters to Advance Climate Change Adaptation*. The report, to be completed in 2011, will focus on climate change and its role in altering the frequency, severity, and impact of extreme events or disasters, and on the costs of both impacts and the actions taken to prepare for, respond to, and recover from extreme events and disasters. The emphasis will be on understanding the factors that make people and infrastructure vulnerable to extreme events, on recent and future changes in the relationship between climate change and extremes, and on managing the risks of disasters, over a wide range of spatial and temporal scales. The assessment will consider a broad suite of adaptations, ranging from early warning to insurance to altered infrastructure and social safety nets. It will also explore the limits to adaptation, the conditions that can transition adaptation into maladaptation, and the human and financial consequences of those limits. Finally, the assessment will build links between communities focused on climate change and those focused on disaster risk reduction.

The Special Report, even in its preliminary stages, clearly recognizes the need for a variety of responses to the threat of changes in extreme events from climate change. The variety of responses can be exemplified by considering how disaster relief and disaster prevention organizations might respond to projected changes in two different extremes: heat-waves and drought. There seems little doubt that heat waves will continue to become more frequent and extreme, almost everywhere. So the development of early warning systems (eg., Nicholls et al., 2008) that allow emergency response organizations to take action to reduce the consequences of these events seems sensible. The availability of accurate short-term weather forecasts facilitates such actions. Drought, however, is more problematic. Predictions of changes in drought occurrence and behavior are far less certain, and short-term drought forecasts are also far less accurate than forecasts of next weekend's temperatures. Yet global warming of two or three degrees must surely change the behavior of droughts, even if we cannot, as yet, confidently predict exactly how and where these changes will appear. So, perhaps in this case we need to focus more on how to reduce vulnerability to droughts, especially in communities already vulnerable to drought impacts, rather than expecting to be able to use specific projections of drought changes.

Whatever the extreme in which we are interested, it is clear that improved predictions (from a day or so to a season or a year or more) can provide an important tool in adaptation and in minimizing the adverse impacts of extreme weather and climate events in a changing climate. Many predictions of climate and weather hazards have improved dramatically in recent decades (Nicholls, 2001). The quality of Bureau of Meteorology short-term forecasts in the lead up to the late January 2009 southeast Australia heat wave and the Black Saturday bushfires undoubtedly saved many lives. Further improving predictions of high-impact climate and weather events should be integral to any climate change adaptation strategy.

References

Alexander, L., Hope, P., Collins, D., Trewin, B., Lynch, A., and Nicholls, N. 2007. Trends in Australia's climate means and extremes: a global context. *Aust. Met Mag*., **56**, 1-18.

Nicholls, N. 2001. Atmospheric and climatic hazards: Improved monitoring and prediction for disaster mitigation. *Natural Hazards*, **23**, 137-155.

Nicholls, N., and Alexander, L. 2007. Has the climate become more variable or extreme? Progress 1992-2006. *Progress in Physical Geography*, **31**, 77-87.

Nicholls, N., Skinner, C., Loughnan, M., and Tapper, N. 2008. A simple heat alert system for Melbourne, Australia. *Int J. Biometeorology* DOI:10.1007/s00484-007-0132-5.

Bureau services perspective on the need for modelling and understanding high impact weather

Jon Gill

Weather Services Branch, Bureau of Meteorology

Introduction

There is no doubt that in recent decades we have witnessed substantial improvements in the performance of the Bureau of Meteorology's weather services, and that these improvements are fundamentally based on advances in numerical weather prediction and supporting decision-support systems. It is almost a truism that weather forecasts and warnings are reliant on numerical modelling. Of course, the greatest benefits arise when appropriate tools and training are available to allow forecasters to understand and exploit the guidance produced by numerical models. How the wealth of numerical weather prediction (NWP) guidance is effectively utilised in the forecast process is a substantial and important subject, but is not the focus of this paper. Nor will we concentrate on how the Bureau's services *routinely* depend on NWP, except to acknowledge fundamental and universal requirements, such as that NWP guidance be accurate and that it possess as much spatial and temporal detail as possible.

Instead, the focus is on the need for numerical modelling and understanding of high impact weather, with a particular focus on current gaps in the science that most directly impinge on the Bureau's highest priorities in weather services. The term 'high impact weather' by definition focuses on atmospheric phenomena that have significant impacts on socio-economic well-being. THORPEX focuses on high impact weather on the 1-day to 2-week timeframe. Others extend the definition to include climatic events such as drought. Although the current workshop takes the latter, broader meaning, this paper will concentrate on the former definition, confining its scope to weather (rather than climate). This is for two reasons: to keep the width of discussion manageable and because the Bureau itself distinguishes organisationally between climate and weather. Accordingly, the emphasis is on the traditional 'severe weather services' – tropical cyclones, fire weather and severe thunderstorms – along with subtropical and mid-latitude lows and their associated high impact weather (heavy rain, high winds), heat waves and dust storms. This list is prescriptive because the purpose of this paper is to explicitly identify where modelling can address specific high impact weather services needs.

Directions in weather services

In some ways, the demands of the user community for weather services is the same today as it has always been – that services be more accurate, more detailed, extend further in time and be available for more locations. These are fundamental requirements of forecast and warning services and each of them have been well-served by steady advances in NWP over recent decades. Increasingly, users are requiring information in ways that better match their decision-making. This includes risk-based activities that are planned on the basis of forecast uncertainty. Until such a time as a forecast is guaranteed to be perfect, users will demand information on the forecast likelihood, using probabilities and other metrics.

The number of different uses to which weather forecast and warning information is put is almost as large as the number of users. However, community surveys in Australia do reveal that some weather phenomena are of greater importance overall. Rain is routinely reported to be the most important weather element for most people. Not unexpectedly, severe weather also rates highly, especially for vulnerable communities. Users are interested in forecasts and warnings at all time scales, from nowcast to seasonal scales. Some users make decisions that are affected by events that fall within the 10-60 day 'predictability gap'. Modelling that successfully addresses this problem, even if only in a limited way, would produce a step-function improvement in weather forecast and warning services.

A major change to the Bureau's weather services program is occurring with the national roll-out of the Graphical Forecast Editor. Object guidance sourced from deterministic and ensemble-based NWP is a core input to the system and places modelling at the very heart of the forecast production chain. The GFE directly leverages improvements in modelling into improved services. The GFE will also provide an effective platform to translate ensemble-based guidance into probabilistic services, both grid-based and for specified locations.

Users also demand improvements in those areas that have stubbornly resisted our best efforts to date. Forecasting of short-term convective weather remains a high priority, as does tropical cyclone genesis and intensity prediction. From a community risk management perspective, these are the areas that demand the greatest attention.

The next section describes specific priority areas for modelling of high impact weather. If an area is not mentioned, it may not be because it is unimportant but rather because current modelling endeavours are – from a weather services perspective – successfully addressing the problem. Instead, the discussion focuses on those areas of modelling research that will make the biggest, additional contribution to the Bureau's high impact weather services.

Fire Weather

Much of the modelling requirements in support of the Bureau's fire weather services program are addressed through the research programs of the Bushfire Cooperative Research Centre (CRC), including the Fire Weather and Fire Danger project that seeks to *"improve operational utility of fire weather forecasts and outlooks, by providing better knowledge and understanding of wind, temperature and humidity structures and distributions, on the very short term (1-12 hours), short to medium term, and seasonal time scales."* The outcomes from this work have been instrumental in better understanding the dynamics of key fire weather features such as summertime wind-changes in southern Australia. Black Saturday has increased the focus of work of this kind. Priorities for fire weather modelling research are listed below and are based on recent Bushfires CRC priority-setting activities together with existing operational forecasting requirements:

Modelling requirement	**Description**
Improved modelling of key fire weather variables	There is an ongoing requirement to improve the modelling performance for key fire weather parameters. These include surface dewpoint and ground moisture. Better representation of fuel conditions is also required.
Discriminating extreme fire danger days from normal events	Although there have been major improvements in forecasting skill, with extreme fire danger now routinely forecast well in advance, there is a need to differentiate critical events such as Ash Wednesday, and Black Saturday from the "normal" extreme fire weather days.
Forecasting fire behaviour under extreme fire danger conditions, including very high resolution modelling of wind flow in complex terrain	The highest resolution operational NWP forecasts currently available in Australia have a grid spacing of approximately 5km. Variations of wind speed, direction, and gustiness on the scale in which firefighters are operating are not represented. The interaction of topography, variations in atmospheric instability and fires on forecast wind changes could be better forecast through the use of modelling with higher resolution.
Simulating and predicting fire behaviour of going fires	The impact of meteorological factors on the behaviour of going fires is made more complex when larger fires modify the meteorological environment. These are currently not modelled well by existing numerical weather and fire behaviour models. Improved fire modelling should be achieved through the use of two-way coupling in a 3D fire-atmosphere model.

Ensuring meteorological inputs to decision systems provide measures of probability for risk management; developing 'alternate scenario' methods	As decision makers are developing risk management strategies for a range of activities, meteorological forecasts that provide indications of uncertainty, alternate scenarios and relative probabilities of different outcomes are required. The behaviour of fires and the evolution of fire danger through a day can have a dramatically different character dependent on certain meteorological events, such as whether the inversion breaks in the lee of the ranges, and whether the wind change has a single or double structure. Such different scenarios are currently not forecast. The potential exists to use the spread of information available in ensembles and consensus forecast methods to predict the likely errors in each day's forecast and to build alternate forecast scenarios systematically into the forecast service.

Tropical Cyclones

Research requirements in support of the Bureau's operational tropical cyclone warning program were recently tabled at the Second International Workshop on Tropical Cyclone Landfall Processes held in Shanghai in October 2009. The following table lists the top 10 in ranked order. Provided for interest are the relative rankings assigned by other international warning centres. The requirements that are specifically related to modelling are shown in **bold**.

Research requirement	**Rank**			
(modelling requirements shown in italics)	**BoM**	**TPC/NHC**	**JTWC**	**JMA**
Statistically-based real-time guidance for track, intensity and precipitation (e.g. multi-model consensus approaches), provided to forecasters in probabilistic and other formats	1	3	5	1
Guidance for tropical cyclone intensity change, with highest priority on the onset, duration and magnitude of rapid intensification events	2	1	1	2
Guidance for tropical cyclone genesis that exhibits a high probability of detection and a low false alarm ration, and/or provides probability of genesis	3	7	3	11
Improved observational systems in the storm and its environment that provide data for forecaster analysis and model initialisation	4	2	2	3
Additional operational guidance on coastal inundation (e.g. storm surge and waves)	5	5	7	5
Guidance for tropical cyclone precipitation amount and distribution	6	11	11	4
Guidance for changes in tropical cyclone size/wind structure and related parameters	7	9	4	7
Enhancements to the operational environment to increase forecaster efficiency	8	4	6	10
Identification and then reduction of the occurrence of guidance and official track outliers, focussing on both large speed errors and large detection errors, and on specific forecast problems, including interactions between upper-level troughs and tropical cyclones, track forecasts near mountainous areas, and extra-tropical transition	9	6	8	9
Operational analysis of the surface wind field	10	8	9	6

The priorities for tropical cyclone modelling are consistent with some of the overall weather services directions, including the increased use of multi-model/consensus approaches to forecasting to better match operational and user decision-making.

Thunderstorms

Modelling in support of the Bureau's thunderstorm forecast and warning services can be categorised according to its role in forecasting the storm's evolution, from environmental assessment of the pre-storm conditions, through to initiation, and subsequent prediction of storm type, track, intensity and decay. In each of these areas, the requirements for modelling vary.

Modelling requirement	Description
Pre-storm environmental assessment - NTFGS	The National Thunderstorm Forecast Guidance System (NTFGS) is the Bureau's primary tool for assessing severe thunderstorm likelihood. The system provides good overall guidance, especially for surface-based storms. The migration from mesoLAPS to ACCESS may offer further opportunities to improve the system. Refinement of the NTFGS to accommodate additional upper-level processes is seen as desirable.
Pre-storm environmental assessment – multi-model ensembles	This requirement is consistent with the need to provide information that matches risk-based decision-making, including forecast uncertainty and confidence information and the use of probabilities
Thunderstorm initiation	Primary tools that currently support this are observational rather than modelling. However, research activities that address the use of real-time radar data in very high resolution modelling will offer some valuable tools to address this forecast requirement. The Strategic Radar Enhancement Project (SREP) will provide a valuable mechanism for advancing this work.
Thunderstorm track prediction – consensus nowcast products	Current research in the area of consensus thunderstorm nowcasts and strike probabilities (e.g. THESPA) is consistent with the needs of users and forecasters for information that is tuned to risk-based decision-making.
Pulse storms and flash flooding	One of the most challenging forecasting problems is the timely prediction of intense, short-term convection, including 'pulse' thunderstorms that lead to flash flooding. Very high resolution modelling that assimilates real-time data, including radar data, will offer opportunities to improve this important service gap.

Other synoptic scale phenomena: mid-latitude cyclones, east coast lows, dust storms, heat waves

The modelling requirements to support the forecasting of these synoptic scale phenomena and their associated high impact weather is generally consistent with the overall and long-standing drive towards more accurate short to medium range numerical prediction using dynamical models. Higher resolution models, with improved data assimilation methods, looking further ahead in time, are all desirable directions to be taking.

Ensemble-based predictions will also support the growing need for uncertainty and probability-based forecasts for these events. State health agencies have expressed a strong desire for heatwave warning services that are based on probabilistic estimates of temperature (both maximum and minimum) upon which they can activate scaled response plans.

Summary

The effectiveness of the Bureau's high impact weather services is fundamentally based on numerical modelling and supporting decision-support systems. Much of the improvements in the accuracy of services in recent years has been the result of ongoing advances in the science and technology of NWP, and this forward progress will continue as models become more accurate, more detailed and extend further in time. All high impact weather services benefit from this – 'a rising tide lifts all boats'. Equally, there is a growing demand across most high impact weather services for probabilistic and other uncertainty-based services which allow users (and forecasters) to better tune their risk-based decisions. For specific high impact weather phenomena, a number of priority areas for modelling work have also been identified in this paper.

Global climate change, natural disasters and property losses

John McAneney, Ryan Crompton, and Keping Chen
Risk Frontiers, Macquarie University, NSW 2109, AUSTRALIA

Globally, economic and insured losses from natural disasters are increasing dramatically. This presentation summarises results from a number of recent studies undertaken at Risk Frontiers to understand the causes underlying this increase, including the possible role of Anthropogenic Climate Change (ACC). This is an important issue for Risk Frontiers, which studies natural disasters with a view to helping the insurance sector better understand and price its exposure to natural catastrophes.

We begin with a re-analysis of the official Atlantic basin tropical cyclone database (HURDAT) (Chen et al., 2009); this study was undertaken at three different spatial scales – for all track segments over the entire basin; segments of tracks that made landfall on the continental US; and US landfalling segments alone. We find no systematic change in wind speed distributions at any of these spatial scales since the introduction of aircraft observations in the early 1940s. In contrast to the more recent data, the early record (1851 – 1943) has a marked and statistically significant over-representation of wind speeds largely corresponding to Saffir-Simpson Categories 1 and 2 and an under-representation of Categories 4 and 5 events; importantly, no single Category 5 event is recorded prior to 1924. Since property damage is a non-linear and increasing function of windspeed at landfall, we can be confident that increasing property losses due to hurricanes are not being driven by increases in frequency and intensity of the hazard.

In Crompton and McAneney (2008), we normalised the record of Australian historical insurance event losses (1967 – 2006) due to weather-related hazards in order to estimate likely losses should these historical events recur under 2006 societal factors. The normalisation adjusts for changes in building numbers and value and, in the case of tropical cyclones, regulated improvements in construction standards that following the destruction of Darwin by Cyclone Tracy in 1974. Once normalized in this way, weather-related losses exhibit no obvious trend over time that might be attributed to other factors, including ACC.

Lastly, Crompton et al. (2009) undertook a conceptually similar study to the above, this time looking at Australian bushfire property losses and fatalities over the period 1900 - 2009. After normalising the data to 2009 societal factors, the 2009 Black Saturday fires rank fourth in terms of property losses and second after the 1925 fire season in terms of the ratio of deaths to property losses. There is no obvious trend over time in the normalized data.

Collectively all of these studies suggest societal conditions are driving the increasing trend in disaster losses and, at least to this point in time, there is no evidence to ascribe increasing disaster losses to ACC. On the other hand, the success of improved building standards in reducing wind-induced losses from tropical cyclones is clear evidence that important gains can be made through disaster risk reduction. Moreover, land planning policies in hazard prone parts of this country that ignore the risk are inconsistent with their public safety obligations.

References

Chen, K., McAneney, K.J. and K. Cheung. (2009) Quantifying changes in wind speed distributions in the historical record of Atlantic tropical cyclones. *Natural Hazards–Earth Systems Science*, 9, 1749–1757, www.nat-hazards-earth-syst-sci.net/9/1749/2009/

Crompton, R.P. and K.J. McAneney, 2008. Normalised Australian insured losses from meteorological hazards: 1967-2006. *Environmental Science and Policy*. 11:371 - 378.

Crompton, P.A., McAneney, K.J., Chen, K., Pielke Jr., R. and K. Haynes, 2009. Normalised Australian bushfire property losses and fatalities: 1925–2008 (in preparation).

Advancing the understanding of Tropical Cyclones through numerical modelling

Noel E. Davidson, Chi Mai Nguyen, Yimin Ma, Marie-D. Leroux, Yi Xiao, Hongyan Zhu and Lili Liu

Centre for Australian Weather and Climate Research
n.davidson@bom.gov.au

Background

During the last 15 years, major improvements in the understanding and forecasting of TC motion have occurred. However, similar improvements for intensity and structure change have not eventuated. Currently there is little skill in TC structure and intensity forecasting. Possible reasons for this include: 1. insufficient horizontal and vertical resolution in numerical systems to represent the operative dynamical and thermodynamical processes, 2. paucity of observations necessary to define the intense inner-core structure, 3. lack of the required assimilation techniques to initialize the intense inner-core, 4. rapid dynamical error amplification due to barotropic and convective instabilities, and 5. sensitivity of prediction to parameterizations of convective and microphysical processes. These deficiencies are compounded by a lack of understanding of: 1. environmental influences on intensity, 2. internal structure change during intensification, and 3. the coupling between the atmosphere and the ocean. Forecasts of TC intensity and structure change, and particularly Rapid Intensification (RI) are critically important. The impact is felt via rapid changes in extreme winds, heavy rain and storm surge, but little is known about how these changes occur.

The presentation will focus on BMRC/CAWCR research to advance understanding of TC genesis, track, rapid intensification and extratropical transition, via application of numerical modelling to investigate the role of the large-scale environment (LSE), vortex structure (VS) and inner-core dynamics and thermodynamics, during TC life cycles.

CAWCR Research

(a) *Current TC Modelling Capabilities*

A major tool in BMRC/CAWCR TC research has been the availability of a near state-of-the-art TC modelling system for operations and research. The current operational TC forecast system, TC-LAPS (TC Limited Area Prediction System, Davidson and Weber, 2000) has been competitive with international forecast guidance since 1999. Its successor, built around the Australian Community Climate and Earth System Simulator, ACCESS, will provide unprecedented opportunities to make further improvements to initialization and prediction of both the large scale environment and the evolving structure of TCs via the application of 4D-VAR and non-hydrostatic dynamics. Initial research focus will be on initialization of the primary and secondary circulations of TCs, the moisture analysis and validation of track, structure and intensity.

Application of ACCESS to TC forecasting is illustrated in Fig. 1. It shows observed and forecast tracks and intensities for Typhoon Sinlaku, during the Tropical Cyclone Structure experiment, TCS08, over the Northwest Pacific. The forecasts were initialized when the storm was weak but undergoing rapid intensification (left panels), and when it was an intense circulation (right panels). The forecasts are based upon (i) a vortex specification designed to fit estimated vortex structure parameters, and (ii) application of 4DVAR in 5-cycles over a 24-hour period to initialize the primary and secondary circulations. The forecasts provide very useful guidance on intensity change, while not diminishing the quality of the track forecasts. Detailed analysis of the initial condition and forecast when the storm was intense (right panels) indicates that the 4DVAR at the model resolution used here (0.11^0 latitude-longitude) was not able to initialize the storm at the estimated intensity (935 hPa). However, the system still initializes a very intense storm (~ 950 hPa), maintains that intensity during the forecast (as observed), and still produces a very skilful track forecast. Components of TC-LAPS and ACCESS-TC have been and will continue to be major tools for studies on prediction and understanding of TC behaviour.

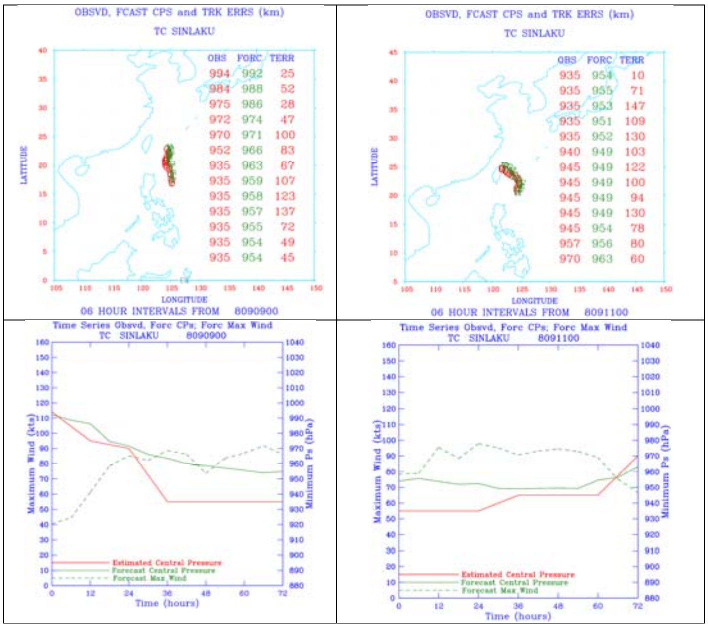

Figure 1. Observed (red) and forecast (green) tracks and intensities for Typhoon Sinlaku. 72 hour forecasts from base times 00UTC 9 and 11 September 2008. Central pressures are in hPa. Winds are in knots. The TERR column in the upper panels shows track errors in km.

(b) *Environmental Influences on Rapid Intensification, RI*

Figure 2, taken from Davidson et al. (2008) shows the evolving upper level environment for Hurricane Opal during RI. The diagram illustrates the rapid southeastward group propagation and slow phase propagation of Planetary Rossby Waves (PRWs) at upper levels. Opal underwent RI as the wave passed overhead. Simulations suggest (not illustrated here) that the dynamical influence of the wave on the Hurricane's low level circulation was to provide a favourable environment for RI (decreasing wind shear, a developing low to mid level cyclonic environment, modulation of the vertical motion field, enhanced boundary layer moisture, deep convective bursts). The case is one of many that highlight the important issue of analysis and prediction of the evolving large-scale flow and its impact on prediction of intensity and structure. A key issue is assimilation, prediction and verification of evolving PRWs and their impact on TC behaviour.

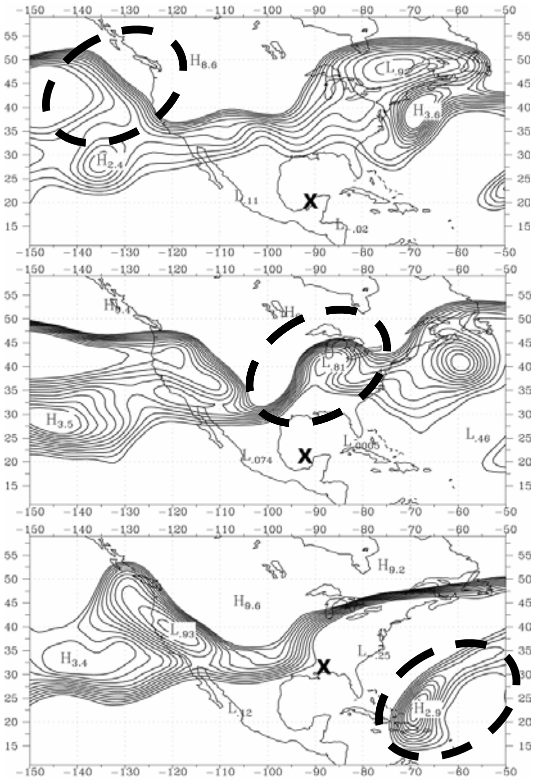

Figure 2. 200hPa potential vorticity for Opal at two day intervals commencing 0000 UTC 30 September 1995. PV Units are 10^{-6} K m^{2} s^{-1}. Contour interval is 0.5PVU. Only contours between 1 and 3 PVU are plotted. The ellipses mark the location of the leading synoptic-scale amplification at each time. 'X' marks Opal's location at analysis time.

(c) *Internal Structure Change during RI*

Figure 3, taken from high-resolution, 5-km simulations by Nguyen et al. (2008) show two distinct phases exhibited by a storm undergoing RI. In Fig. 3a a nearly circular, symmetric updraught defines the tropical cyclone eye-wall (symmetric phase). In contrast Fig. 3b shows a highly asymmetric eye-wall updraught dominated by three intense updraught cores (asymmetric phase). The intense updraught cores result from convective bursts, which are initiated and energized by (a) barotropic instability of the vortex ring during the symmetric phase, indicated by the PV ring structure in Fig. 3c, and (b) latent heat release from low-level moisture, and high energy (warm) air drawn in from the eye. The ascent and inflow associated with the convection concentrates the abundant eye-wall vorticity into an intense rotating core, known as a vortical hot tower (VHT). The development of the convective bursts disrupts the symmetry of the eye-wall and mixes the PV into a monopole structure. The VHT convection weakens a few hours later, influenced by large, local wind shear associated with the mean vortex, and after exhausting the Convective Available Potential Energy (CAPE). The system then relaxes back towards the more symmetric phase. The transition from symmetric to asymmetric phase sees a reduction in the intensification rate of the mean circulation. The transition back to the symmetric phase sees a significant increase in the mean intensification rate. The replenishing of the low-level moisture that fuels the next outbreak of VHTs occurs during the symmetric phase, when the evaporation from the ocean surface (enabled by the high wind speeds) exceeds the moisture consumption of the now reduced convection. The processes above describe a pathway to RI which occurs while the TC is still somewhat immature, as opposed to the situation for more intense systems, where RI tends to occur via eye-wall replacement cycles (Willoughby et al. 1982).

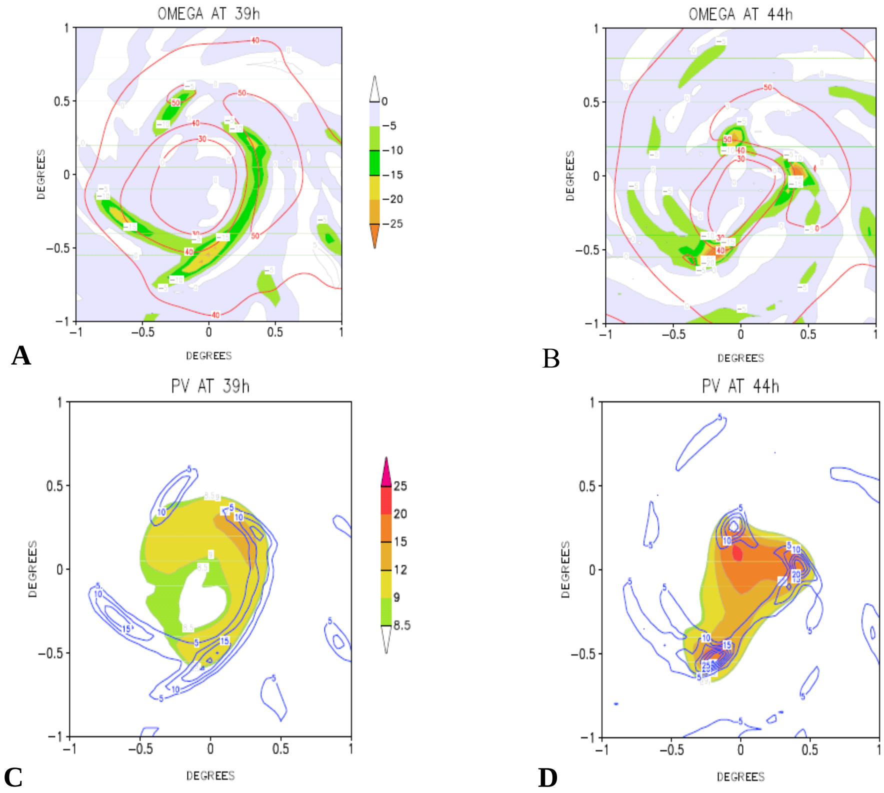

Figure 3. Vertical velocity (top panels, hPa/day) and Potential Vorticity (right panels, PVU) at 850 hPa during symmetric phase (left panels) and asymmetric phase (right panels).

We expect that advances in understanding internal structure changes will occur when experiments similar to those in this earlier study are repeated in the non-hydrostatic ACCESS-TC at increasingly higher resolution for Typhoons Sinlaku, Hagupit and Jangmi, observed during TCS08. The understanding of internal structure change and the development of inner-core asymmetries is critical for prediction of RI.

(d) *Vortex Structure*

Best track data sets are now designed to include the set of critical vortex structure parameters: Central Pressure (CP), Maximum Wind (VMAX), the Radius of Maximum Wind (RMW), the Radius to 34 knot winds (R34, gales) and the Radius of Outer Closed Isobar (ROCI). We can then ask the questions: What defines variability in vortex structure? How is vortex structure important for a storm's evolution? How well can we forecast vortex structure and the set of parameters that defines structure and intensity? Figure 4, taken from Ma and Davidson (2009) shows azimuthal-mean profiles from 7 different analytical forms of the near-surface wind for Hurricanes Bonnie (12UTC 23 August 1998) and Katrina (12 UTC, 27 August 2005). Symbols on the diagram show estimates of vortex parameters. The two storms have approximately the same intensity, but clearly possess important differences in their RMWs, R34s and outer structures. Accurate prediction of intensity (CP, VMAX) does not necessarily imply accurate prediction of storm structure (RMW, R34). Detailed analysis of simulations suggest that these differing wind structures may be associated with markedly different rainfall distributions, different storm surge potential, and possibly even different responses to the same large-scale forcing. We are investigating these important vortex structure issues, to study how vortex structure influences the subsequent behaviour of the vortex, and to determine whether it is possible to forecast changes in structure. Understanding vortex structure and how 4D-VAR builds the structures is critical to initialization and prediction of TC structure change and RI. This work will not only focus on prediction of the intensity of storms, but on prediction of a set of vortex structure parameters (CP, VMAX, RMW, R34 and ROCI) and storm asymmetries, which will provide new and important forecast guidance, as well as insights into TC processes.

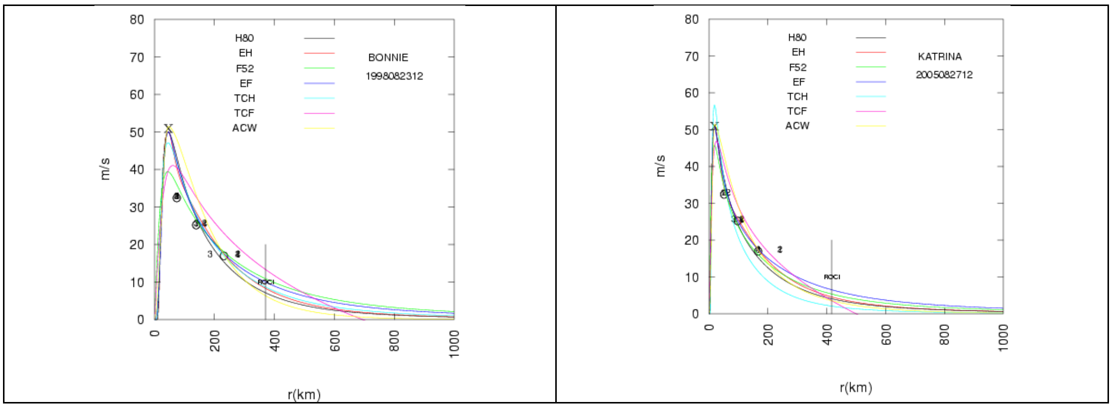

Figure 4. Radial distribution of mean tangential wind from 7 synthetic analytical forms for Hurricanes Bonnie (left panel) and Katrina (right panel). Symbols represent estimated values of (VMAX, RMW, R34, ROCI) on which the synthetic structures are calculated.

(e) *TC Motion*

With application of advanced observational technologies, sophisticated assimilation techniques, high-resolution modelling and ensemble/consensus forecasting methods, prediction of TC track has, in the mean, become highly skilful. However occasional poor forecasts do still occur. An example is shown in Fig. 5 which illustrates forecasts for Typhoon Sinlaku from base time 0000UTC, 9 September 2008.

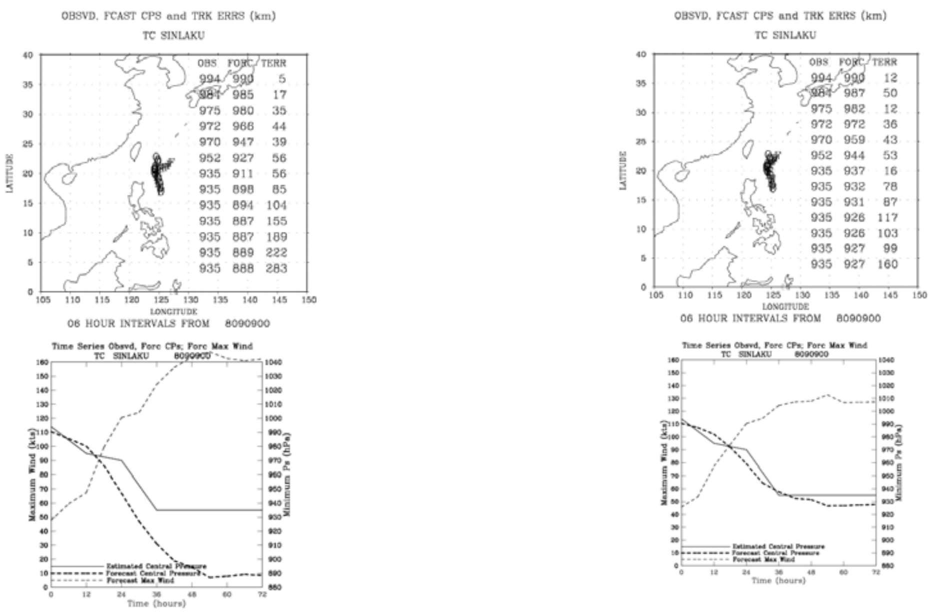

Figure 5. Observed and forecast tracks and intensities for Typhoon Sinlaku from base time 0000UTC 9 September 2008. Left panels show simulations initialized with an RMW = 55 km. Right panels with an RMW = 220 km.

The difference in the two forecasts is in the initial specification of the radius of maximum winds, 55 km (left panels) and 220 kms (right panels). Note that both the track and the intensity forecasts are improved with the larger RMW. During this time, Sinlaku exhibited multiple wind maxima at various radii and so its structure was difficult to define. Simulations suggest that as the environmental steering weakened, the storm's motion became somewhat more influenced by β–propagation. With stronger winds at large radii, this process was more active in the large RMW simulation and impacted on the storm's motion. For intensity, note that the forecast is sensitive to initial vortex structure. The small RMW vortex intensifies more rapidly and attains a maximum intensity far in excess of that observed. Even though both simulations are run with the same SSTs and the same environment, the large RMW simulation verifies better. Preliminary diagnostics suggest that with an initially large RMW, the simulation reproduces some aspects of the observed multiple wind maxima, which reduces the tendency for run-away intensification.

(f) *Extratropical Transition*

Observational diagnostics suggest that during Extratropical Transition (ET), Downstream Development (DD) frequently occurs at upper tropospheric levels (see also section (b) above). This is seen as a wave train of amplifying troughs and ridges developing eastward in time. The process is illustrated in Fig. 6 for Hurricane Wilma (2005). The top panels show the amplifying troughs and ridges at 200 hPa developing eastward and equatorward. The middle panels are cross-sections of potential vorticity along NW to SE sections and show large undulations in PV at upper levels as the wave propagates. The bottom panel is a time-longitude section of stream function anomaly at 200 hPa and illustrates the DD as successive ridges and troughs develop eastward in time. The black dot marks the storm's location.

The DD results in very rapid changes to the environment of the storm. A critical flow change appears to be the development of a large-scale, low- to mid- level trough, which wraps around the storm, seemingly holding it upright and allowing it to withstand the increasing wind shear associated with the approaching upper trough, until it can reach the favourable equatorward entrance region of the upper jet. A series of simulations have been run ranging in complexity from high-resolution, full physics integrations (to confirm that the simulations reproduce the ET) through to coarse-resolution, no-latent-heating runs with the TC vortex removed from the initial condition. The latter is used as a first approximation to the environment of the storm. The simulations suggest that the dry dynamics of the evolving environment can establish the wrap-around flow and the development of the low- to mid- level trough. The simulations also suggest that these features are associated with the maturing DD event and upper-level warming from subsidence within the environment during ET. This counter-intuitive process can (a) produce the low-level pressure trough that captures the storm, and (b) produce a partial inhibition to embedded convection, allowing the boundary layer to moisten via (i) sustained surface fluxes, and (ii) horizontal moisture advection of the wrap-around flow. This produces potential for more intense convective activity once the inhibition passes. These characteristics are consistent with proposed conceptual models of ET and with the enhanced vertical mass flux diagnosed by Davis et al. (2007).

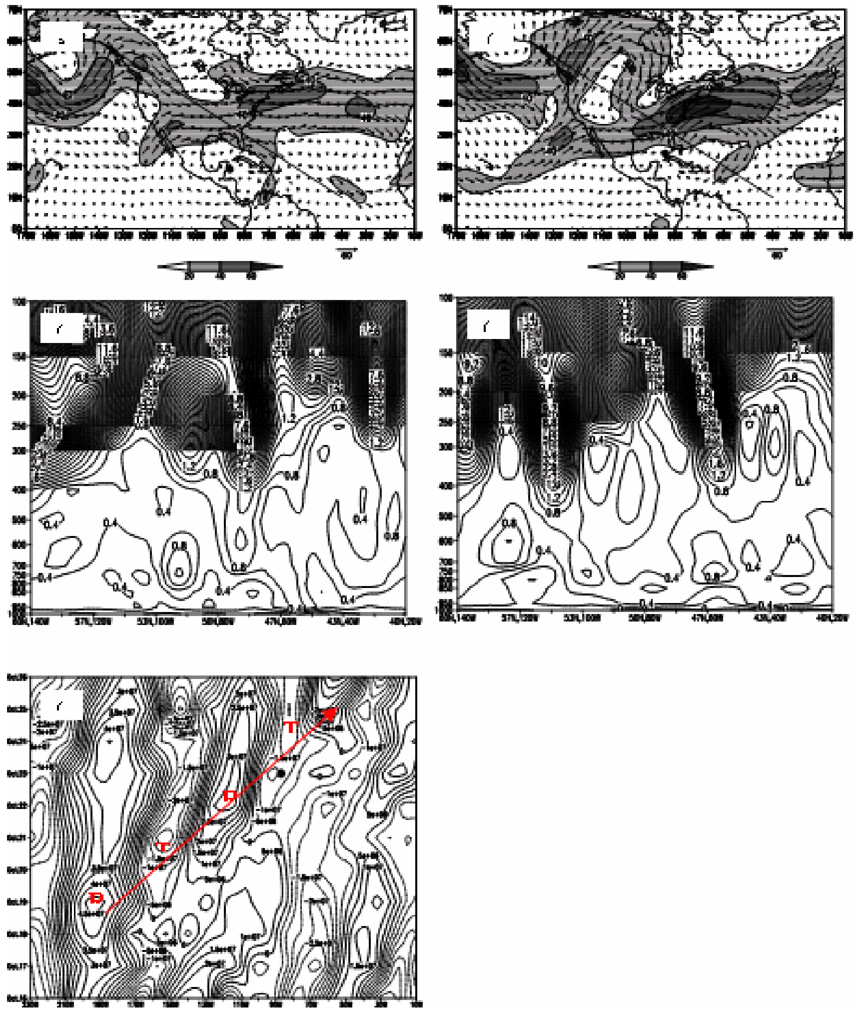

Figure 6. Top panels: For Hurricane Wilma, 200 hPa wind analysis for pre-ET (00UTC Oct. 21st 2005) and post-ET (00UTC Oct. 24th 2005). Isotachs are at 20 m/s intervals. Middle panels are cross-sections of potential vorticity along NW to SE sections shown in top panels. Bottom panel is a time-longitude section of stream function anomaly at 200 hPa for the period 16 to 26 October 2005**.** In the bottom panel, the line extending towards the top right corner of the diagram indicates successive developments, eastward in time, of ridges and troughs.

Summary

Major gaps exist in our understanding of Tropical Cyclone structure change and intensification, which in turn limit our ability to forecast critical and devastating TC events. The projects described here form a plan to systematically investigate initialization, prediction and diagnosis of TC behaviour, with a focus on structure change and rapid intensification.

ACCESS provides unprecedented and internationally-unique opportunities to investigate structure change and RI. Application of sophisticated data assimilation methods and a state-of-the-art numerical prediction system provide a framework for future research. The demonstrated high-quality performance of ACCESS, and ongoing collaboration between the CAWCR ACCESS Group and the UK Meteorological Office, suggest that ACCESS is eminently suitable for the research proposed here.

In this presentation we have illustrated (a) the power of a state-of-the-art numerical forecast system for prediction and diagnosis of TC behaviour, (b) some techniques for extracting basic dynamical information from complex numerical systems, and (c) some large- and meso- scale processes that seem important for understanding TC structure change.

Specific, future complementary research goals are:

- Enhancements for TC applications to 4D-VAR with respect to: (i) development of flow-dependent covariances, (ii) non-geostrophic dynamical constraints between the mass and wind fields, and (iii) techniques to account for important inner-core asymmetries for intense TCs during initialization.
- Prediction and predictability of RI.
- Initialization, prediction and verification of evolving Planetary Rossby Waves and their influence on the behaviour of TCs.
- Initialization, prediction and verification of vortex structure and structure change.
- Diagnosis and assimilation aspects of internal structure change and inner-core asymmetries during rapid and slow TC intensification.
- Boundary layer thermodynamics and the energy supply to the TC via heat and moisture fluxes that fuel the convective bursts required for RI (eg, Kepert and Wang, 2001).

References

Davidson, N.E. and H.C. Weber, 2000: The BMRC high resolution tropical cyclone prediction system: TC-LAPS. *Mon. Wea. Rev.*, **128,** 1245-1265.

Davidson, N.E., C.M. Nguyen and M.J. Reeder, 2008: Downstream Development during the Rapid Intensification of Hurricanes Opal and Katrina: the Distant Trough-Interaction Problem**.** Extended Abstracts. 28th AMS Conference on Hurricanes and Tropical Meteorology. 28 April – 2 May, 2008. Orlando, Fl., USA.

Davis, C.A., S.C. Jones, and M. Riemer, 2008: Hurricane Vortex Dynamics during Atlantic Extratropical Transition. *J. Atmos. Sci.*, **65**, 714–736.

Kepert, J.D. and Y. Wang, 2001: The dynamics of boundary layer jets within the tropical cyclone core. Part II: Nonlinear enhancement. *J. Atmos. Sci.*, **58**, 2485-2501.

Ma, Y. and Davidson, N.E., 2009: Surface Pressure Profiles and Initialization for Hurricane Prediction. Part I: Analysis of Observed and Synthetic Structures. For submission to *Mon. Wea. Rev.*

Nguyen, C.M., M.J. Reeder and N. Davidson, 2008: Intensity Forecasts for Hurricane Katrina (2005) from TCLAPS: Vortex and Structure Evolution and Forecast Sensitivity. Extended Abstracts. 28th AMS Conference on Hurricanes and Tropical Meteorology. 28 April – 2 May, 2008. Orlando, Fl., USA.

Willoughby, H., J. Clos, and M. Shoreibah, 1982: Concentric Eye Walls, Secondary Wind Maxima, and The Evolution of the Hurricane vortex. *J. Atmos. Sci.*, **39**, 395–411.

Comparing slab and height-resolving models of the tropical cyclone boundary layer

Jeffrey D. Kepert
Centre for Australian Weather and Climate Research,
Bureau of Meteorology, 700 Collins St, Melbourne Vic 3000.
Email: J.Kepert@bom.gov.au

Third Annual CAWCR Modelling Workshop, Melbourne, Australia, Nov 30 – Dec 2, 2009.

1. Introduction

Simple depth-averaged, or slab, models of the tropical cyclone boundary layer (TCBL) have had important practical uses, including for engineering design, climatological risk assessment studies and as components of tropical cyclone potential intensity models. Here, such models are compared to a fully height-resolving model, and it is shown that there are substantial differences in the simulations. The slab model produces excessively strong inflow and too great departure of the boundary-layer mean winds from gradient balance, due to excessive surface drag. The tendency of slab models to produce quasi-inertial oscillations is shown to be due to the inaccurate treatment of the vertically averaged nonlinear terms in the momentum equations, and not to the improper specification of the upper boundary condition as has recently been argued. Given the considerable deficiencies of slab models in representing the tropical cyclone boundary layer, it is impossible to recommend their further use.

2. Model Formulation

Two diagnostic models of the TCBL are used here, a slab model and a height-resolving model. Each diagnoses the boundary-layer flow as the response to a specified, optionally translating, pressure field representative of a tropical cyclone. Thus each model can be provided with identical forcing, thereby isolating the effects of the boundary-layer representation from the rest of the storm. The slab model is depth-averaged, while the height-resolving model solves the full three-dimensional equations of motion with a simple parameterisation of turbulent diffusion. Both use the same parameterisation of surface drag and, as far as is possible, boundary conditions. The thermodynamics of the boundary layer will not be studied, not because it is unimportant, but because the focus is on getting the flow correct, which is a necessary first step to calculating the flux and advection terms in the thermodynamic budgets. Details of the model formulation and derivation may be found in Kepert (2009).

3. Results

Figure 1 shows the boundary-layer flow in a stationary, axisymmetric cyclone with maximum gradient wind of 40 m s^{-1} at a radius of 40 km, according to the height-resolving model. The forcing vortex is the same as in Smith and Vogl (2008) for ease of comparison with their results. The depth of the inflow layer decreases rapidly with radius, from about 2 km at 300-km radius to below 400 m in the eye. This decrease is consistent with observations (e.g. Frank 1984; Kepert 2006a,b; Bell and Montgomery 2008), and linear models and scaling arguments that show that the boundary layer depth in the core of the storm scales as $I^{-1/2}$, where I is the inertial stability (e.g Rosenthal 1962; Eliassen and Lystad 1977; Kepert 2001). The maximum azimuthal wind is 43.2 m s^{-1} at a height of 400 m, and is about 8% supergradient.

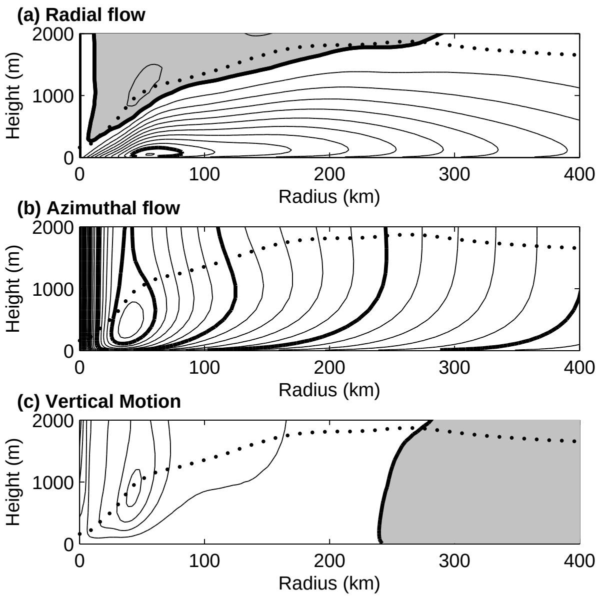

Figure 1: The boundary layer flow in a stationary storm simulated by the height-resolving model. (a) radius-height section of the radial wind, contour interval 1 m s^{-1}, multiples of 10 m s^{-1} shown bold, positive values shaded. (b) radius-height section of azimuthal wind, contour interval 2 m s^{-1}, multiples of 10 m s^{-1} shown bold. (c) radius-height section of the vertical velocity, contour interval 0.05 m s^{-1}, zero line shown bold, subsidence shaded. The dotted line in each panel indicates the level at which the stress magnitude reduces to 20% of its surface value.

The supergradient flow is mostly within the inflow layer, but does extend upwards into the outflow layer at the top of the boundary layer, and was extensively analysed by Kepert and Wang (2001).

The turbulent stress has maximum magnitude at the surface and decreases monotonically with height in this and similar simulations. The dotted lines in Fig. 1 show the height at which the momentum flux magnitude falls to 0.2 of its surface value; the value 0.2 was chosen as it roughly coincides with the top of the inflow layer. Clearly the turbulent transport of momentum is a significant part of the dynamics of the outflow layer, consistent with the discussion in Kepert and Wang (2001).

3.1 *Comparison of boundary-layer mean flow in slab and height-resolved models*

The flows from the slab and height-resolving models are compared in Fig. 2. This comparison uses the same forcing vortex and surface drag parameterisation in both models; the flow from the height-resolving model is averaged over the same height range as the prescribed boundary layer depth in the slab model. This height is less than the boundary-layer depth except in the inner core, but as can be inferred from Fig. 1, other reasonable choices will not dramatically change the results. The slab model has the stronger inflow except within the eye, most markedly so at and immediately outside of the radius of maximum winds (RMW). Thus the eyewall updraft is very much stronger in the slab model. The frictionally-forced updrafts outside of 250 km radius are more similar, because there the stronger $\partial u/\partial r$ term in the continuity equation compensates for the stronger inflow in the slab model. The height-resolving model has the height-mean azimuthal flow slightly subgradient except in the vicinity of the RMW, where it is slightly supergradient. This situation is in strong contrast to the slab model, which has much larger departures from gradient balance through most of the storm. Observations show that the azimuthal-mean surface inflow angle in tropical cyclones over the sea is usually in the range 20 – $25°$. For example, Hurricane Frederic (1979) had an azimuthal-mean surface inflow angle of 21 – $22°$, according to the over-water composite analysis of Powell (1980). The height-resolving model simulation shown in Fig. 2b has a surface inflow angle of 20 – $25°$ over most of the domain, reducing to smaller values inside of radius 70 km. Observations of the depth-averaged inflow angle are seldom reported, but can safely be assumed to be less than the surface value. The slab model inflow angle exceeds $20°$ between 70 and 360 km, and exceeds $30°$ from 90 to 220 km radius, which is unrealistically large.

One might suspect that the excess inflow in the slab model is because the surface drag there is calculated from the boundary-layer mean wind, whereas the height-resolving model uses the 10-m wind.

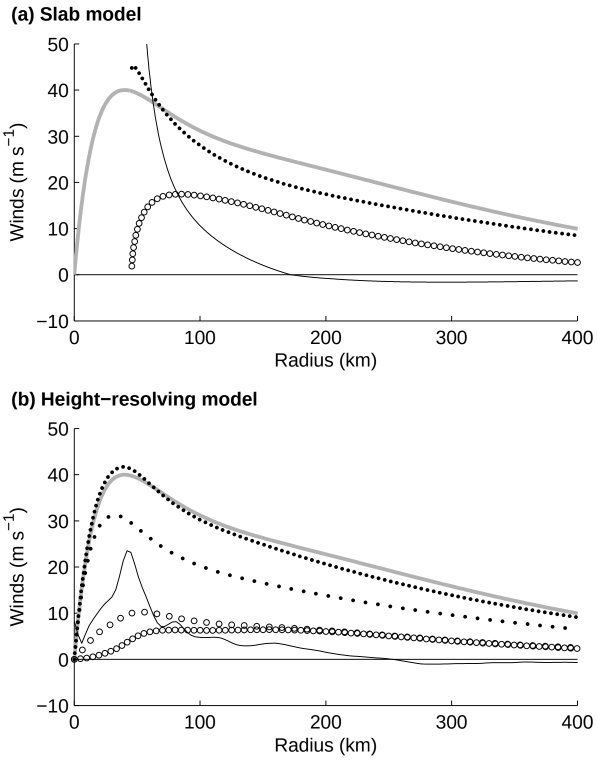

Figure 2: (a) Axisymmetric boundary layer flow according to the slab model. Gradient wind (thick grey), boundary-layer mean azimuthal (dots), inwards (open circles) and upwards (thin black, multiplied by 100) flow components. Parameter values are as in Smith and Montgomery (2008), including the boundary-layer height which is fixed at $h = 800$ m. (b) Simulation of the same vortex as in (a), except by the height-resolving model, as already shown in Fig. 1. Curves with closely-spaced symbols are averaged over the lower 800 m, while those with less dense symbols show the flow at 10-m height. The vertical velocity is at 800-m height.

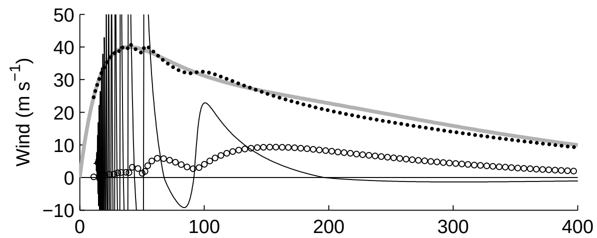

Figure 3: Boundary-layer flow simulated by the slab model as in Fig. 2a, except with C_D halved.

One can crudely correct for this by reducing the wind speeds in the surface stress calculation by a factor of, say, 0.7 – 0.9, to better represent the surface wind (see e.g. Powell and Black 1990; Kepert and Wang 2001; Franklin et al. 2003, and references therein regarding the choice of constant). Vickery and Twisdale (1995) reduce their surface drag coefficient by 50% for this reason. This adjustment reduces the departure of the boundary-layer flow from the gradient flow at large radii (Fig. 3). However, the solution now displays marked oscillations inwards of about 150 km radius, similar to those analysed by Smith and Vogl (2008, section 4.1) but beginning at much larger radius than they reported.

3.2 *Further results from axisymmetric slab models*

The slab model was tested on a variety of vortex radial profiles of differing sizes, intensities and structures, and found to produce unphysical results when applied to some vortex profiles. An example of especially pathological behaviour is shown in Fig. 4, where the model is forced with the gradient wind radial profile fitted to aircraft and dropsonde observations in Hurricane Georges by Kepert (2006a). The oscillations in $\overline{u}$ and $\overline{v}$ that are apparent inwards of $r = 150$ km are similar to those analysed near the RMW by Smith (2003) and Smith and Vogl (2008), and also shown here in Fig. 3, but have not previously been reported except near and within the RMW. They produce a strong oscillation in the vertical motion, to the extent that the frictionally-forced vertical motion near 50 km, or only twice the RMW, is actually downwards. In contrast, the modelled flow from the simulation in Kepert (2006a, Fig. 23a), which

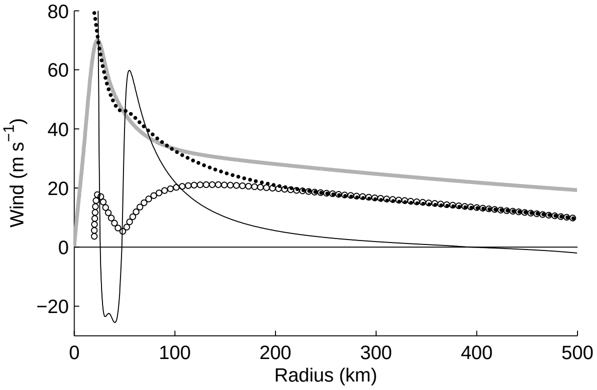

Figure 4: Simulated axisymetric flow in the boundary layer of Hurricane Georges on 19 Sept 1998, according to the slab model. Gradient wind (thick grey), boundary-layer mean azimuthal (dots), inwards (open circles) and upwards (thin line, multiplied by 100) flow components. Note the bimodal structure of the inflow and the consequent strong downdraft near radius 50 km. Model parameter settings were as in Fig. 2a.

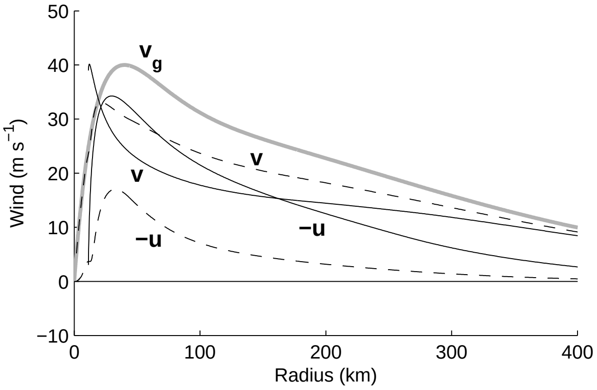

Figure 5: Simulations with the slab model with radially varying h. The depth h varies as $I^{-1/2}$, and is 800 m at $r = 500$ km. The dashed curves show the simulated flow with $w_s c = -0.057$ m s^{-1} as in Smith and Vogl (2008), while the thin solid lines have $w_{sc} = 0$, both with azimuthal and inflow components as marked. The thick grey curve is the gradient wind.

used the full 3-dimensional boundary layer model of Kepert and Wang (2001) and was shown to agree reasonably well with the observations, does not display this bizarre character. The case of Georges is particularly interesting, since analysis of dropsonde observations showed that the upper boundary layer flow was not supergradient, and simulation with the height-resolving model showed only very slightly supergradient flow (Kepert 2006a). In contrast, Smith and Vogl (2008) emphasise that supergradient flow is ubiquitous in their slab model.

Most published slab model applications use constant h, although the height-resolving model, linear models and observations show a marked reduction in boundary-layer depth towards the storm centre (section 3). Smith and Vogl (2008) present two calculations with such a variation, although they choose boundary-layer depths which are arguably too small, being around 100 m at the RMW. The simulation they presented used quite a large value of their shallow convection velocity scale, which controls the flux through the top of the boundary layer due to parameterised shallow convection, $w_{sc} = -0.057$ m s^{-1}. Fig. 5 presents a comparison of this simulation (dashed lines) to one with $w_{sc} = 0$ (thin solid lines), from which it is clear that omitting w_{sc} produces grossly excessive inflow. It not clear that it is physically reasonable to allow shallow convection to have such a large influence on the boundary-layer flow in the core of a tropical cyclone. This excessive inflow can also be controlled by reducing the ratio C_D/h, but this leads to an oscillating solution similar to that in Fig. 3. It was not possible to discover a satisfactory set of parameters for the slab model with radially varying h.

3.3 *Why is the slab model inaccurate?*

It has been shown that the slab model is inaccurate, when measured against the height-resolved model. A further model, intermediate between the slab and height-resolved models, has been developed (Kepert 2009). In this model, the vertical structure of the flow is parameterised by an Ekman-like spiral with two free parameters. Differential equations are derived for these parameters, and the model is solved

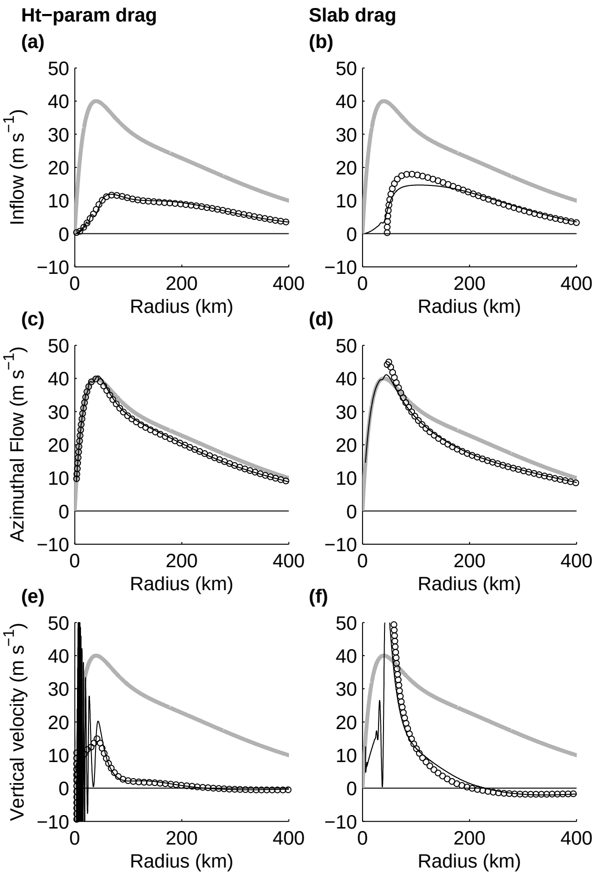

Figure 6: Boundary-layer flow simulated by four models. The left column is for the height-parameterised model and for the hybrid model with the same surface drag condition. The right column is for the slab model and for the hybrid model with the same surface drag condition. (a) Height-mean inflow for the height-parameterised (thin black curve) and hybrid model (ii) (circles), together with gradient wind (thick grey curve). (c) The height-mean azimuthal wind, models and line-styles as in (a). (e) The vertical motion in the limit $z \to \infty$, models and line-styles as in (a). (b) Height-mean inflow for the hybrid model (i) (thin black curve) and for the slab model (circles). (d) The height-mean azimuthal wind, models and line-styles as in (b). (e) The vertical motion in the limit $z \to \infty$, models and line-styles as in (b). The slab model simulation here omits vertical advection through the upper boundary, but is otherwise the same as shown in Fig. 2a.

by integrating them in from large radius. In contrast to the slab model, the more realistic vertical profile allows the application of the surface drag to the surface wind instead of the boundary-layer mean wind, and more accurate treatment of nonlinear terms. This model is considerably more accurate than the slab model, when measured against simulations from the height-resolving model. In addition, two further models that are hybrids of the slab and height-parameterised models were developed. Specifically, (i) a model with the slab model's treatment of the surface drag and height-parameterised model's treatment of the other nonlinear terms, and (ii) a model with the height-parameterised model's treatment of the surface drag and the slab model's treatment of the other nonlinear terms, are examined. Full details of these models are in Kepert (2009)

Solutions of these models with the usual forcing are shown in Fig. 6. The left column is for the models with the height-parameterised surface drag condition, while the right column is for those models which apply the surface drag to the boundary-layer mean wind. The open circles indicate that the nonlinear terms are calculated as in the height-parameterised model, while the thin black lines have slab-model style advection. Outside of about 200 km radius, the differences between the simulations are dominated by the method used for the surface drag, with the slab-model method leading to stronger inflow and weaker azimuthal flow. Inwards of about 200 km, the two simulations with slab-model surface drag diverge (right column), with the height-parameterised method of calculating the nonlinear terms leading to weaker inflow, the azimuthal flow being approximately in gradient balance, and the elimination of the singularity which terminated the slab model integration near the RMW. In the left column, the solution is nearly independent of how the nonlinear terms are calculated, except inside the RMW, where the slab-model method leads to high-frequency oscillations in w. The difference between the curves shows up at smaller radius than in the right column, because the flow is not so far from gradient balance and so the nonlinear terms are smaller and therefore less sensitive to their method of computation. These differences are representative of those found in other simulations. Slab-model drag leads to excessive inflow and departures from gradient balance, and slab-model style calculation of the nonlinear terms greatly increases the tendency of the solution to become singular or to oscillate (although it is the excess inflow, caused by the slab-model drag, that actually triggers the inflow).

4. Discussion and Conclusions

Marked differences in the boundary-layer flow occur between that predicted by a simple slab model and that predicted by a height-resolving model. In addition, the slab model was shown to be capable of quite pathological behaviour for some reasonable parameter settings, and has an unphysical sensitivity to f (not shown here). Analysis of the reasons for these properties shows that two factors are responsible:

1. the calculation of the surface drag using the boundary-layer mean wind rather than the surface wind, and

2. the inaccurate treatment of the nonlinear terms in the depth-averaging.

The first of these is problematic at all radii, while the second becomes significant in the inner core. There is some uncertainty in what values of physical parameters should be applied, and arguably a smaller value of C_D can be justified in the slab model since the drag is being applied to the boundary-layer mean wind. This adjustment reduces the excess inflow and subgradient flow in the slab model, but can trigger the quasi-inertial oscillation, so cannot be regarded as an improvement. These results confirm and help explain the recent TCBL model intercomparison by Khare et al. (2009), who found that the slab model was significantly less accurate than the linear model of Kepert (2001) when compared to observational analyses.

The slab model is known to be subject to quasi-inertial oscillations (Smith 2003; Smith and Vogl 2008). It was shown that these oscillations are triggered by the excess inflow in the slab model, and persist because of the inaccurate treatment of the nonlinear terms. This point is important, since Smith and Vogl (2008) have argued that these oscillations are an artifact of prescribing the pressure gradient at the top of the boundary layer in regions of outflow. Their argument, if correct, would preclude the use of diagnostic models of the boundary layer, including nearly all of those discussed in the introduction, in the most important part of the storm. Fortunately, their argument is incorrect. It is not the prescribed pressure gradient that is responsible for the oscillations, but rather the excess inflow that triggers them, and the inaccurate treatment of the nonlinear advection terms that allows them to persist. A more reasonable treatment, as in the height-parameterised model, greatly reduces the propensity to oscillate, while extensive experience with the height-resolved model suggests that extra degrees of freedom in the vertical completely eliminates this problem.

Simplified models of the TCBL are useful for a number of purposes, with major applications including climatological risk assessment and engineering design. The considerable inaccuracies demonstrated here implies that slab models can no longer be recommended for such purposes. Such applications have demonstrated satisfactory agreement between model and observations (Vickery and Twisdale 1995; Thompson and Cardone 1996; Vickery et al. 2000, 2009), but the slab model output has in such cases been rather empirically adjusted before comparison with observations. While these authors are to be commended for their validation efforts, it appears that the tuning of these adjustments has concealed fundamental deficiencies in the model.

Another important application of simplified models has been as a component of tropical cyclone potential intensity (PI) models. Recently, Smith and Montgomery (2008) have shown that further approximations within a slab model, including those made in Emanuel's PI model, can produce large changes in the flow. Those differences are of similar magnitude to the differences between slab and height-resolved models demonstrated here. The results in this paper support the conclusion of Smith and Montgomery (2008) as to the need to improve the boundary-layer component within existing PI models. However, it is very clear that simply relaxing some approximations but remaining with the slab model approach would be replacing one inaccurate model with another. A better solution could be an extension of the height-parameterised model presented here, to include prediction of the thermodynamic parameters. Research is continuing to develop such a model.

Recently, Smith et al. (2009) have argued that boundary layer dynamics play a crucial role in tropical cyclone intensification. Their arguments are strongly influenced by the slab model results of Smith and Vogl (2008), so the fact that slab models overestimate the depth-mean inflow and the strength of the supergradient flow may be cause to doubt their reasoning. Indeed, while Smith and Vogl (2008) emphasise the ubiquity of supergradient flow in the slab model, analysis of observations shows that not all storms contain boundary layer supergradient flow, consistent with simulation of these storms by the height-resolving model (Kepert 2006a; Schwendike and Kepert 2008). Further, Smith et al. (2009) do not give the mechanism by which the boundary layer dynamics and supergradient flow leads to an adjustment in the cyclone's mass field, necessary for intensification. Schubert et al. (1980) studied geostrophic adjustment of the first internal mode in initially balanced vortices and showed that wind forcing can lead to a significant adjustment of the mass field provided that the scale of the forcing is less than the Rossby radius of deformation, $L_R = NH/I$, where N is the Brunt-Väisälä frequency, H is the vertical scale, and I is the inertial stability. In the cyclone core, L_R for the first internal mode is similar to or less than the RMW, so the mass field will adjust to the wind field for deep imbalances. However, for shallow regions of imbalance, as in the supergradient flow at the top of the boundary layer, L_R is much less, and most of the kinetic energy in the imbalance will be lost as inertia-gravity waves. In this context, the outflow immediately above the supergradient wind maximum (Fig. 1) can be regarded as a continuously-forced inertia wave that adjusts the wind back to the mass field, with little if any impact on the mass. (This is not an exact analogy, since diffusion is non-negligible in this layer.) In general, idealised models are valuable because their use may lead to understanding. Whether the systematic biases in slab models have led Smith et al. (2009) to an untenable hypothesis of tropical cyclone intensification remains to be seen.

References

Bell, M. M. and M. T. Montgomery, 2008: Observed structure, evolution and potential intensity of category five Hurricane Isabel (2003) from 12 – 14 September. *Mon. Weather Rev.*, **136**, 2023–2046.

Eliassen, A. and M. Lystad, 1977: The Ekman layer of a circular vortex. A numerical and theoretical study. *Geophysica Norvegica*, **7**, 1–16.

Frank, W. M., 1984: A composite analysis of the core of a mature hurricane. *Mon. Weather Rev.*, **112**, 2401–2420.

Franklin, J. L., M. L. Black, and K. Valde, 2003: GPS dropwindsonde wind profiles in hurricanes and their operational implications. *Weather and Forecasting*, **18**, 32–44.

Kepert, J. D., 2001: The dynamics of boundary layer jets within the tropical cyclone core. Part I: Linear theory. *J. Atmos. Sci.*, **58**, 2469–2484.

———, 2006a: Observed boundary–layer wind structure and balance in the hurricane core. Part I: Hurricane Georges. *J. Atmos. Sci.*, **63**, 2169–2193.

———, 2006b: Observed boundary–layer wind structure and balance in the hurricane core. Part II: Hurricane Mitch. *J. Atmos. Sci.*, **63**, 2194–2211.

———, 2009: Comparing slab and height-resolving models of the tropical cyclone boundary layer. *Q. J. R. Meteorol. Soc.*, revised and resubmitted.

Kepert, J. D. and Y. Wang, 2001: The dynamics of boundary layer jets within the tropical cyclone core. Part II: Nonlinear enhancement. *J. Atmos. Sci.*, **58**, 2485–2501.

Khare, S. P., A. Bonazzi, N. West, E. Bellone, and S. Jewson, 2009: On the prediction of over-ocean hurricane surface winds and their uncertainty. *Q. J. R. Meteorol. Soc.*, **135**, 1350–1365.

Powell, M. D., 1980: Evaluation of diagnostic marine boundary-layer models applied to hurricanes. *Mon. Weather*

Rev., **108**, 757–765.

Powell, M. D. and P. G. Black, 1990: The relationship of hurricane reconnaissance flight-level wind measurements to winds measured by NOAA's oceanic platforms. *J. Wind Eng. Ind. Aero.*, **36**, 381–392.

Rosenthal, S. L., 1962: A theoretical analysis of the field of motion in the hurricane boundary layer. National hurricane research project report no. 56, U. S. Department of Commerce.

Schubert, W. H., J. J. Hack, P. L. Silva, and S. R. Fulton, 1980: Geostrophic adjustment in an axisymmetric vortex. *J. Atmos. Sci.*, **37**, 1464–1484.

Schwendike, J. and J. D. Kepert, 2008: The boundary–layer winds in Hurricanes Danielle (1998) and Isabel (2003). *Mon. Weather Rev.*, **136**, 3168–3192.

Smith, R. K., 2003: A simple model of the hurricane boundary layer. *Q. J. R. Meteorol. Soc.*, **129**, 1007–1027.

Smith, R. K. and M. T. Montgomery, 2008: Balanced boundary layers used in hurricane models. *Q. J. R. Meteorol. Soc.*, **134**, 1385–1395.

Smith, R. K., M. T. Montgomery, and V. S. Nguyen, 2009: Tropical cyclone spin-up revisited. *Q. J. R. Meteorol. Soc.*, **135**, 1321–1335.

Smith, R. K. and S. Vogl, 2008: A simple model of the hurricane boundary layer revisited. *Q. J. R. Meteorol. Soc.*, **134**, 337–351.

Thompson, E. F. and V. J. Cardone, 1996: Practical modeling of hurricane surface winds. *J. Waterway, Port, Coastal and Ocean Eng.*, **122**, 195–204.

Vickery, P. J., P. F. Skerjl, A. C. Steckley, and L. A. Twisdale, 2000: Hurricane wind field model for use in hurricane simulations. *J. Engineering Structures*, **126**, 1203–1221.

Vickery, P. J. and L. A. Twisdale, 1995: Wind field and filling models for hurricane wind-speed predictions. *J. Structural Eng.*, **121**, 1700–1709.

Vickery, P. J., D. Wadhera, M. D. Powell, and Y. Chen, 2009: A hurricane boundary layer and wind field model for use in engineering applications. *J. Appl. Meteorol. Clim.*, **137**, In press, doi:10.1175/2008JAMC1841.1.

Numerical modelling of tropical cyclone formation: Insights into dynamic and thermodynamic processes.

Kevin Tory

Centre for Australian Weather and Climate Research, Melbourne, Victoria, Australia.

Introduction

Tropical Cyclone (TC) formation has long been considered the least well understood component of the TC life-cycle. TC formation is a multi-scale process from cloud- through to synoptic scales. Until recently observations of sufficient temporal and spatial resolution have not been available to comprehensively understand the cloud and mesoscale processes. However, in the last five years or so high resolution cloud-resolving numerical weather prediction (NWP) systems have been used to simulate TC formation and hindcast real TC formation events. Detailed analyses of these modelled events led to a significant shift in TC formation theories, that provided great insight into understanding real events, and provided a framework for understanding recent high-resolution observation data from sources such as airborne Doppler radar (e.g., Reasor et al. 2005). These theories also helped target observational resources during field campaigns. In this paper a brief overview is provided of the main advances in TC formation understanding enabled by NWP studies. The content draws heavily on a soon to be published chapter on TC formation (Tory and Frank, 2010).

Competing theories

Prior to high-resolution cloud-resolving NWP TC formation studies and modern observation techniques, TC formation research initially focused on the synoptic climatology and meteorology that brought about favourable environments for TC development. In the 1990's studies appeared focussing on mesoscale formation processes, in particular the role of Mesoscale Convective Systems (MCSs) in intensifying cyclonic circulations sufficiently to give the TC a "crank start". Vorticity convergence near the freezing level in the expansive MCS stratiform precipitation region spins up a mid-level circulation termed the mesoscale convective vortex (MCV). MCVs were central to the dominant theories of the 1990's, including the MCV merger theory of Simpson et al. (1997) and Ritchie and Holland (1997), the showerhead theory of Bister and Emanuel (1997) and the bottom-up theory of Montgomery and Enagonio (1998). The merger theory proposed that vortex interactions between two or more MCVs led to the formation of a single larger vortex with a sufficiently enhanced surface cyclonic circulation for the TC to become self-sustaining. The showerhead theory proposed that the enhancement of the surface cyclonic circulation can be achieved in a single MCS, when the MCV mid-level circulation is advected downwards by subsidence in the stratiform precipitation region. Importantly the showerhead theory recognised the importance of enhanced humidity for TC formation. These two theories have been labelled "top-down" because they propose mid-level cyclonic circulation is projected or transported down to the surface. The bottom-up theory focussed on low-level cloud-scale cyclonic vorticity anomalies that develop in the deep convective clouds. The surface circulation is enhanced when these smaller vortices interact with the mid-level MCV to form a single vertically aligned vortex on the scale of the MCV.

Much debate followed the publication of these somewhat opposing theories, a debate that has been mostly quelled by recent NWP studies. Cloud resolving simulations have shown that modelled TC formation is considerably more complex than the above theories suggest, and that elements of all theories are possible in the real world but only aspects of the bottom-up theory appear to be universal. While the showerhead mechanism for humidification is probably too simplistic, the importance of humidification has since been confirmed.

Vortex interactions

Early simulations capable of representing and resolving cloud-scale features (hereafter termed "realistic" simulations), were performed at 3 km grid spacing. TC formation occurred in the convective complex where synoptic ambient vorticity is enhanced and deep convection favoured. Consistent with the bottom-up theory, multiple relatively short-lived convective bursts led to the generation of vorticity anomalies termed vortical hot towers (VHTs, Hendricks et al. 2004, Montgomery et al. 2006). Multiple merger of VHTs led to the gradual construction of a central monolithic vortex that formed the core of the TC. An example of VHT merger is given in Fig. 1. Such behaviour has also been identified in coarser resolution studies with paramterized convection, although those VHTs were necessarily larger in size and fewer in number (e.g., Tory et al. 2006, 2007).

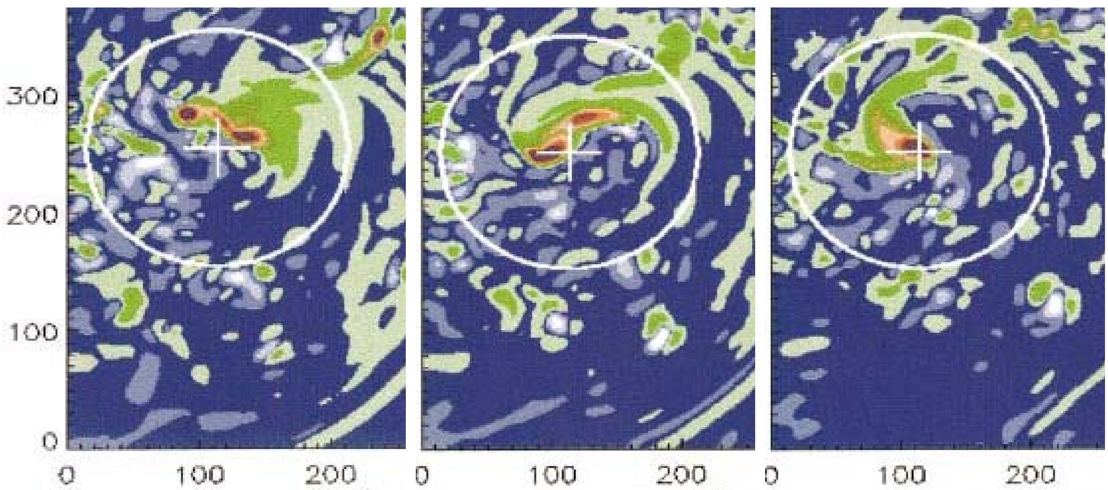

Fig. 1: Merger of absolute vorticity anomalies during the simulation of Hurricane Diana (1984) from Hendricks et al. (2004).

System-Scale Intensification (SSI)

The multiple short-lived convective outbreaks provide sporadic bursts of diabatic heating that contribute to a net pseudo-steady heat source. Solutions to the Eliassen balanced vortex model (Eliassen 1951) show that a steady heat source in a rotating fluid introduces an in-up-out secondary circulation that enhances the system-scale primary circulation. The realistic simulations of Hendricks et al. (2004) and Montgomery et al. (2006) were compared with the Eliassen model. Sufficient similarity between the secondary circulations led them to conclude that the ensemble of heat sources in the VHTs drove a secondary circulation (100's of km in scale) in a manner akin to the Eliassen model, which in turn intensified the developing cyclonic circulation (hereafter termed System-Scale intensification, SSI). Similar conclusions were drawn in the coarser resolution studies of Tory et al. (2006, 2007).

The Eliassen balanced vortex model solutions show that the magnitude of the SSI increases with the intensity of the primary circulation, i.e., the intensification rate increases non-linearly for a given steady heat source. In reality heating is not steady, but when integrated spatially and temporally across the formation region, it resembles a slowly varying heat source with a spatially and temporally variable perturbation. It is likely that the energy from the perturbation is lost to gravity waves, whereas the slowly varying heat source feeds the SSI (Willoughby 2009). Willoughby showed that as the primary circulation intensified increasingly shorter periods of heating could contribute to the SSI. Thus the greater the primary circulation the more efficient the SSI is for a given steady heating, and the smaller-scale and more sporadic the heating can be to still induce an SSI response.

Thermodynamic transition

The previous section highlighted the importance of large-scale and persistent diabatic heating to maximise the efficiency of the SSI. TC development requires essentially a troposphere-deep diabatic heat source, which means lower troposphere evaporation and associated cooling must be minimized. Evaporative cooling induced subsidence results in lower tropospheric divergence, which acts to weaken vorticity and thus oppose the low-level TC spin-up.

Idealized modelling studies of Nolan (2007) showed strong low-level vorticity enhancement did not develop until the lower to middle troposphere humidity was significantly enhanced (> 80%). Thermodynamic theory shows the potential for downdrafts is reduced with increasing humidity, and thermal stability ($\partial\theta/\partial z$) increasing towards moist neutrality. The Nolan study confirmed the hypothesis of Bister and Emanuel (1997) that humidification was essential for TC formation. Interestingly, convective mixing humidifies and stabilizes the immediate environment, and thus sustained convection will reduce the potential for downdrafts with time, and favour deep, broad convection that more efficiently fuels the SSI.

Marsupial pouch theory

It has long been known that strong vertical wind shear and the influx of dry air can be destructive to developing and mature TCs alike. The realistic modelling studies of recent times have helped identify the vulnerability of the developing TC. Convective activity must be persistent and widespread to drive the SSI and contribute towards the thermodynamic adjustment that favours deep, broad convection. This brewing of TC ingredients must be confined to avoid dilution with the outside environment. Dunkerton et al. (2008) found that TCs that form in African easterly waves develop within a region of closed circulation (relative to the mean wave propagation), and that the TC core forms where the circulation is in near-solid body rotation (i.e., weak horizontal shear). An example is illustrated in Fig. 2.

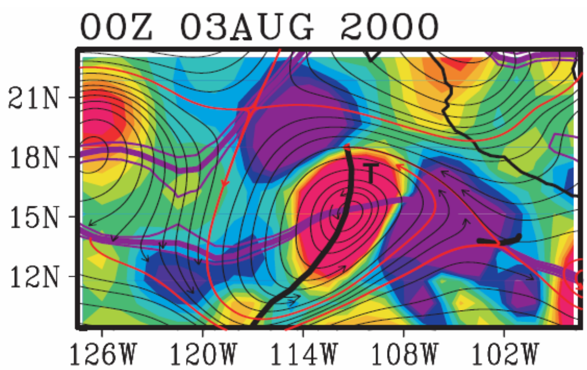

Fig. 2: Mean flow relative streamlines at 600 hPa during the formation of Tropical Storm Fabio, from Fig. 22 of Dunkerton et al. (2008). The red stream lines in the centre of the figure illustrate the approximately closed region. The Okubo-Weiss parameter is shaded, warm colours indicate flow in near solid body rotation, cold colours represent strongly sheared flow.

Dunkerton et al. (2008) likened the closed circulation to a marsupial pouch that nurtures the TC embryo until it is ready to emerge from the parent wave. In that protected environment persistent convection can slowly adjust the thermodynamic state to favour deep, broad convection, and the circulation intensifies non-linearly with time. It is this author's belief that most TCs form in similar protected environments characterized by a core region of near-solid body rotation.

Summary

Realistic modelling studies in recent years have provided tremendous insight into the dynamics and thermodynamics of TC formation that has enabled great advancement in the understanding of TC formation in the real world. The modelling has (i) helped sort out the debate over TC formation as a top-down or bottom-up process; (ii) highlighted the dual role of VHTs in forming the TC vortex core and providing the diabatic heat sources that drive the SSI; (iii) helped demonstrate the importance of humidification to promote deep broad-scale convection that more efficiently drives the SSI; and (iv) helped identify and illustrate the protected environments in which TC embryos form.

References

Bister, M., and K. A. Emanuel, 1997: The genesis of Hurricane Guillermo: TEXMEX analyses and a modeling study. *Mon. Wea. Rev.*, **125**, 2662—2682.

Dunkerton, T. J., M. T. Montgomery, and Z. Wang, 2008: Tropical cyclogenesis in a tropical wave critical layer: Easterly waves. *Atmos. Chem. Phys. Disc.* http://www.atmos-chem-phys-discuss.net/8/11149/2008/acpd-8-11149-2008.html

Eliassen, A., 1951: Slow thermally or frictionally controlled meridional circulation in a circular vortex. *Astrophys. Norv.*, **5,** 19–60.

Hendricks, E. A., M. T. Montgomery and C. A. Davis, 2004: On the role of "vortical" hot towers in hurricane formation. *J. Atmos. Sci.*, **61**, 1209—1232.

Montgomery, M. T. and J. Enagonio, 1998: Tropical cyclogenesis via convectively forced vortex Rossby waves in a three-dimensional quasigeostrophic model. *J. Atmos. Sci.*, **55**, 3176—3207.

Montgomery, M. T., M. E. Nicholls, T. A. Cram and A. Saunders, 2006: A vortical hot tower route to tropical cyclogenesis. *J. Atmos. Sci.*, **63**, 355—386.

Nolan, D. S., 2007: What is the trigger for tropical cyclogenesis? *Aus. Met. Mag.*, **56**, 241-266.

Reasor, P. D., M. T. Montgomery and L. F. Bosart. 2005: Mesoscale observations of the genesis of Hurricane Dolly (1996). *J. Atmos. Sci.*, **62**, 3151–3171.

Ritchie, E. A. and G. J. Holland, 1997: Scale interactions during the formation of Typhoon Irving. *Mon. Wea. Rev.*, **125**, 1377—1396.

Simpson, J., E. A. Ritchie, G. J. Holland, J. Halverson and S. Stewart, 1997: Mesoscale interactions in Tropical Cyclone Genesis. *Mon. Wea. Rev.*, **125**, 2643—2661.

Tory, K. J. and W. M. Frank, 2010: Global Perspectives on Tropical Cyclones. 2nd Edition. Chapter 3: Tropical Cyclone formation. World Meteorological publication. Eds. Jeff Kepert and Johnny Chan.

Tory, K. J., M. T. Montgomery, N. E. Davidson and J. D. Kepert, 2006: Prediction and diagnosis of Tropical Cyclone formation in an NWP system. Part II: A diagnosis of tropical cyclone Chris formation. *J. Atmos. Sci.*, **63**, 3091–3113.

Tory, K. J., M. T. Montgomery and N. E. Davidson, 2007: Prediction and diagnosis of Tropical Cyclone formation in an NWP system. Part III: Developing and non-developing storms. *J. Atmos. Sci* ., **64**, 3195—3213.

Willoughby, H. E., 2009: Diabatically induced secondary flows in Tropical Cyclones. Part II: Periodic forcing. *Mon. Wea. Rev.*, **137**, 822—835.

Tropical Cyclones and Climate Change: Modeling Approaches at GFDL

Thomas Knutson, Morris Bender, Steve Garner, Isaac Held, Shian-Jiann Lin, Joe Sirutis, Robert Tuleya[1], Gabriel Vecchi, and Ming Zhao

Geophysical Fluid Dynamics Laboratory/NOAA
Princeton, New Jersey U.S.A.

Introduction

Recent statistical analyses comparing Atlantic hurricane activity to the secular rise in tropical Atlantic sea surface temperatures (SSTs) since 1950 (Emanuel, 2007) have raised concern that global warming could produce a dramatic future increase in Atlantic basin hurricane activity. However, such a projection is based on extrapolation of a statistical relation, and alternative statistical models can be constructed that project relatively small changes in Atlantic tropical cyclone activity with projected 21st century climate warming (Vecchi et al. 2008). To address this problem using a dynamical modeling approach, we have undertaken several tropical cyclone/climate modeling studies at GFDL, with a regional atmospheric model for the North Atlantic basin, a hurricane prediction model for case studies, and a new global atmospheric model aimed at tropical cyclone simulation.

Regional model (18 km grid) simulations

We first developed a regional atmospheric downscaling model for the Atlantic basin. Our strategy was to demonstrate that our regional downscaling model would be a useful tool for the study of Atlantic hurricane climate and its variability. To do this, we performed a "proof of concept" experiment (Knutson et al. 2007), in which we supplied (via interior spectral nudging) only the large-scale time-evolving atmospheric fields (domain wavenumbers 0-2) to a regional model of the Atlantic basin, and then allowed the model to develop tropical storms and hurricanes based on those conditions (Fig. 1). A 27-season sample using this approach demonstrates that the regional model can indeed recover substantial information about hurricane counts (Fig. 2), with a year-to-year variability correlation (model vs observed) of 0.84.

[1] Affiliation of Robert Tuleya is Old Dominion Univ., Norfolk, Virginia, U.S.A.

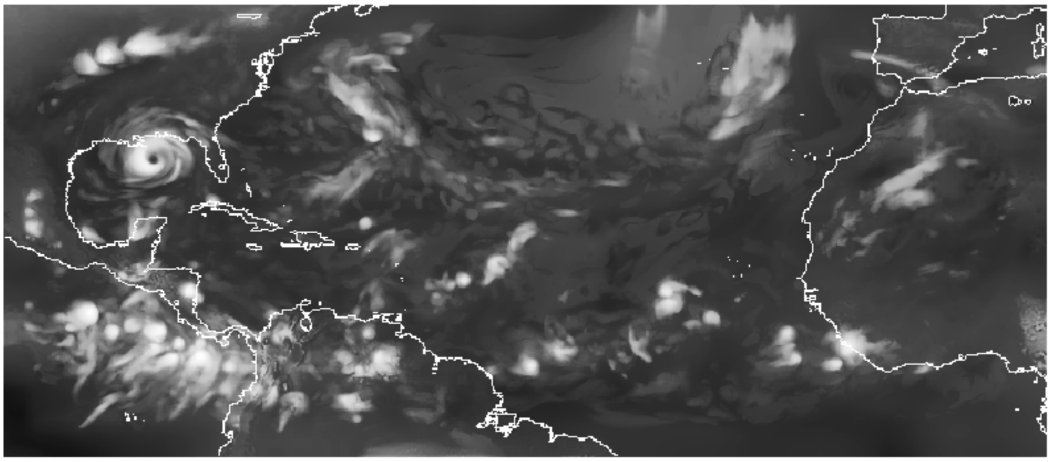

Fig. 1. Snapshot of model outgoing longwave radiation (W m-2) illustrating scales of disturbances in the regional model. A model-generated hurricane is seen approaching the U.S. Gulf Coast for the 2005 season simulation.

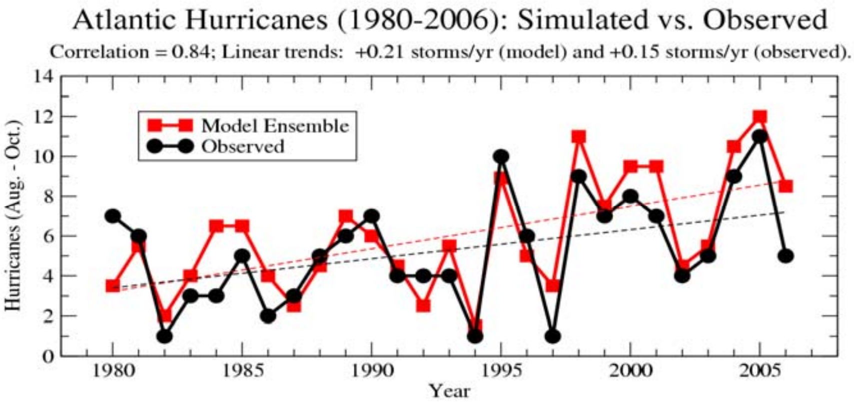

Fig. 2. Annual number (Aug.-Oct. of simulated and observed Atlantic basin hurricanes for the years 1980-2006, based on downscaling of NCEP Reanalyses into a regional climate model.

Having established that the regional model simulates a credible base level and interannual variability of hurricanes when supplied with "perfect" large-scale information, we then re-ran those 27 seasons, but modifying the atmospheric conditions according the mean climate change simulated for the late 21st century (IPCC A1B scenario) by an ensemble of 18 CMIP3 climate models (Knutson et al. 2008). In this experiment, the number of tropical storms and hurricanes was reduced compared to the control runs (Fig. 3). While the reduced number of storms is a common result across most of the intensity classes simulated by the model regional model, at the highest model simulated intensities, the opposite occurs, as there is some increase in the number of the most intense hurricanes. Specialized follow-on experiments (Garner et al. 2009) suggest that the main driver of the reduced number of tropical storms in the warmer climate is the change in circulation (such as wind shear) rather than the stabilization due to enhanced upper tropospheric warming relative to the surface warming.

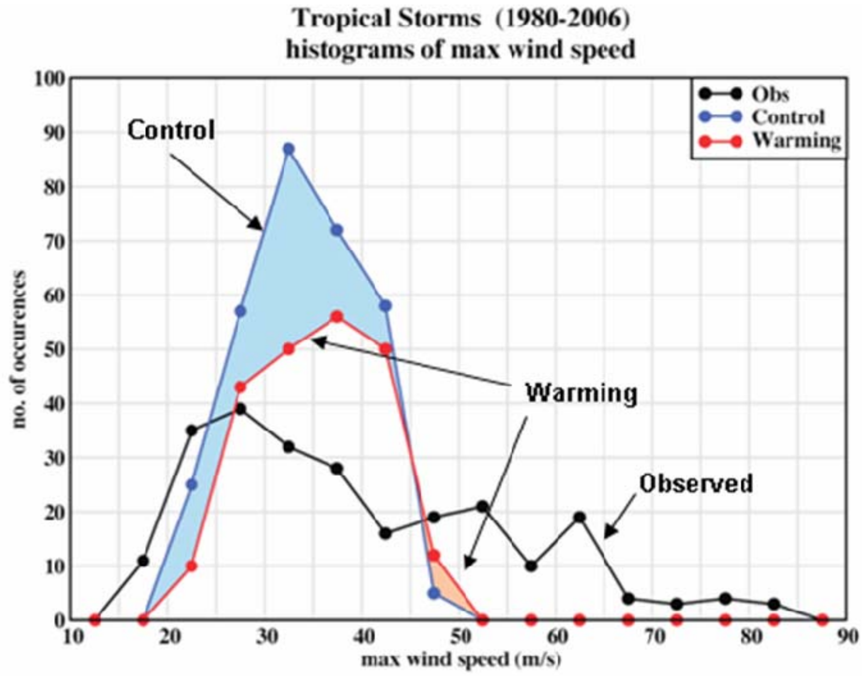

Fig. 3. Distribution of maximum surface wind speeds of tropical cyclones simulated for the years 1980-2006 (control) using NCEP Reanalysis forcing, or simulated for a warmed climate version of these conditions. See Knutson et al. 2008 for details.

The initial sets of climate change experiments with the regional downscaling climate model (Fig. 3) used an 18-model ensemble mean climate change as the projection of late 21-century conditions. Further tests are being conducted using climate change conditions from several individual climate models that make up the 18-model ensemble (Fig. 4), in order to explore the robustness of the simulated response of Atlantic hurricane activity to a range of climate model projections from several individual CMIP3 models.

The regional modeling experiments just described used a model with horizontal grid spacing of 18km, a choice which was dictated by available computing resources, as these experiments required approximately 1.5 Million CPU hours to perform. However, even with this large computational expense, the model failed to simulate the most intense (and most damaging) hurricanes: the maximum simulated wind speeds were only about 47 m/s (Fig. 3). To address this shortcoming, we performed an additional downscaling step, in which each individual storm case from the 27 seasons using the regional model was further downscaled into a 5-day run of the GFDL hurricane prediction system. That operational system, with a triply nested moveable mesh and horizontal grid spacing as fine as 9km--and including ocean coupling--does simulate the more intense hurricanes reaching categories 3 and 4. Results from the model under warm climate conditions, which are currently under review, will be reported on at the meeting.

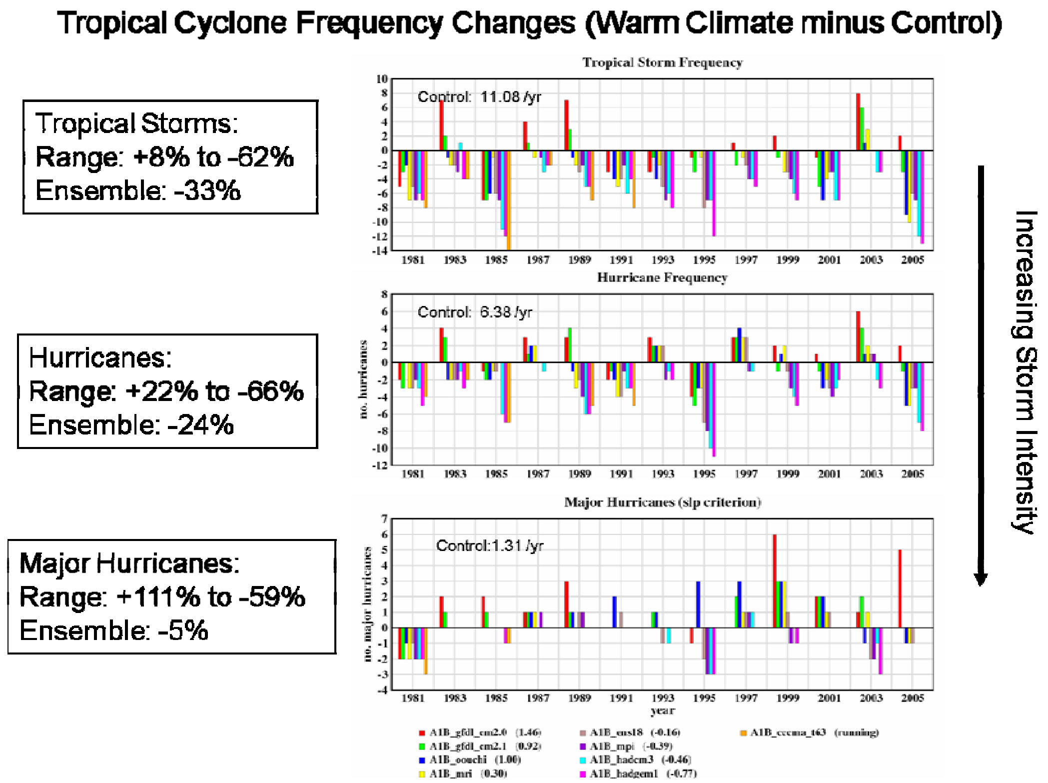

Fig. 4. Tropical storm, hurricane, and major hurricane count changes between control and warm climate experiments with the GFDL Zetac regional model. The sets of shaded bars for each labeled year represent results obtained from different global climate model projections in the downscaling experiments. Results are shown for each individual Aug.-Oct. season simulated, which include the odd years from 1981 through 2005.

Global model (50 km grid) simulations

A global modeling framework has been developed at GFDL which, as a global model, has certain inherent advantages over a regional model approach. For example the model does not require atmospheric boundary conditions and interior spectral nudging toward the NCEP Reanalysis, as was used for the regional model. The only required boundary conditions are sea surface temperatures and sea ice. Also, the global model provides information on all basins from a single set of runs.

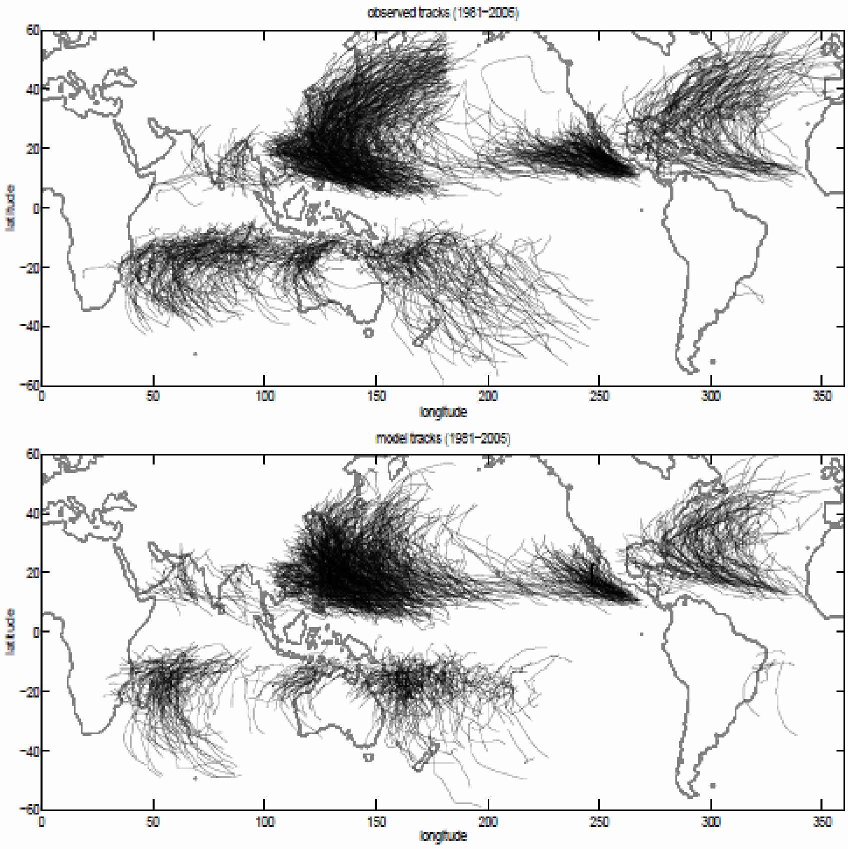

Fig. 5. (Top) Observed hurricane tracks for 1981-2005. (Bottom) Simulated hurricane tracks from the GFDL HIRAM 50-km grid atmospheric model, run over observed SSTs for 1981-2005. Adapted from Zhao et al. (2009).

The simulated tracks from this model (Fig. 5) have considerable resemblance to the observed tracks, although shortcomings are apparent, such as the lack of storms over the central Southern Indian Ocean. As shown in Fig. 6, the model ensemble (n=4) hurricane counts are surprisingly well-correlated with the observed counts in the Atlantic (r=0.83), and also well-correlated in the Northeast Pacific (r=0.62) and Northwest Pacific (r=0.52) basins. In contrast, correlations are much lower for the other basins (~0.3 for the Southwest Pacific and insignificant for the Indian Ocean basins.

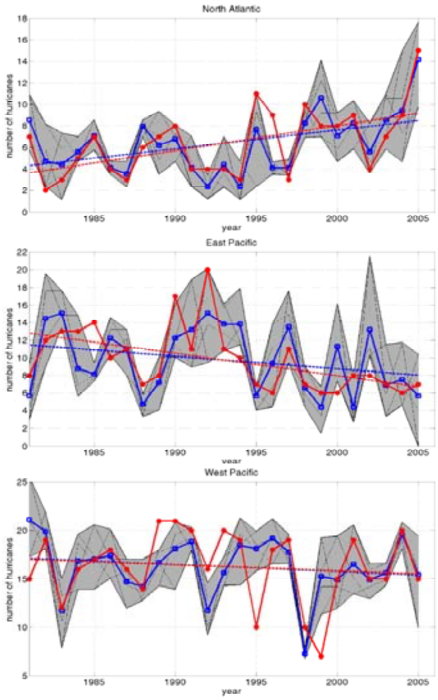

Fig. 6. Simulated vs. observed hurricane interannual variability for (top) Atlantic, (middle) East Pacific, and (bottom) Northwest Pacific basins. These experiments use a 50-km grid global atmospheric model forced by observed SSTs and sea ice for 1980-2006. The curve of connected circles is the observed number of hurricane-strength tropical cyclones while the curve of connected open boxes and shading are the ensemble mean and range, respectively, of counts across a 4-member simulated ensemble. Model timeseries are normalized by a constant multiplicative factor to have the same mean number of storms as observed. Straight dashed lines on each panel are linear trends of the time series. Adapted from Zhao et al. (2009).

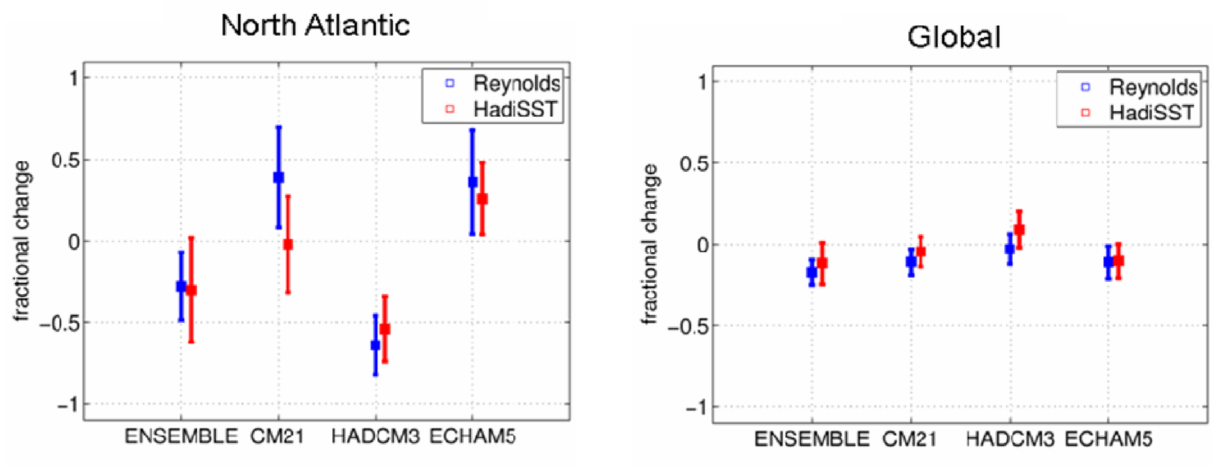

Fig. 7. Model projections of fractional changes in hurricanes for (left diagram) North Atlantic or (right diagram) all basins combined, for the late 21st century using a 50 km grid global atmospheric model to downscale climate model SST projections from three individual climate models or from an 18-model ensemble. The two different projections shown for each model are obtained using two different control run cases based on

different observed SST data sets. The vertical bars denote 90% confidence intervals. Adapted from Zhao et al. (2009).

The global model, when forced with SST changes from either an ensemble of climate models or three different individual climate models shows a fairly consistent decrease in hurricane counts globally (Fig. 7), with three of four experiments indicating a decrease. For the Atlantic basin, the results based on downscaling different climate models are more mixed, with results from the 18-model ensemble result and one individual model showing a decrease, while the results from the other two individual models show either little change or an increase.

Summary and concluding remarks

While some recent statistical analyses of Atlantic hurricane activity have raised concern that global warming could produce a dramatic future increase in Atlantic basin hurricane activity, this result is not supported by our dynamical modeling studies, which show relatively modest changes in Atlantic and global hurricane activity as a response to substantial 21st century projected climate warming. Our findings receive some additional support from our analyses of the observational record, which attempt to correct for possible missing storms early in the record (Vecchi and Knutson, 2008; Landsea et al. 2009). Dynamical models provide an important additional perspective to the tropical cyclone/climate change problem that is complementary to-- if not superior to-- that of statistical approaches.

References:

Emanuel, K., 2007a: Environmental factors affecting tropical cyclone power dissipation. *J. Climate*, **20,** 5497–5509.

Landsea, C., G. A. Vecchi, L. Bengtsson, & T. R. Knutson, 2009: Impact of duration thresholds on Atlantic tropical cyclone counts. *J. Clim*., in press.

Knutson, T. R., J. J. Sirutis, S. T. Garner, I. M. Held, and R. E. Tuleya, 2007: Simulation of the recent multidecadal increase of Atlantic Hurricane activity using an 18-km-Grid Regional Model. *Bull. Amer. Meteor. Soc.*, **88**(10), 1549-1565.

Knutson, T. R., J. J. Sirutis, S. T. Garner, G. A. Vecchi, and I. M. Held, 2008: Simulated reduction in Atlantic hurricane frequency under 21st century warming conditions. *Nature Geoscience*, **1,** 359-364.

Vecchi, G. A., K. L. Swanson, and B. J. Soden, 2008: Whither hurricane activity. *Science*, **322** (5902), doi:10.1126/science.1164396.

Vecchi, G. A., and T. R. Knutson, 2008: On estimates of historical North Atlantic tropical cyclone activity. *J. Clim.*, **21**, 3580-3600.

Zhao, M., I. Held, S.-J. Lin, and G. A. Vecchi, 2009: Simulations of global hurricane climatology, interannual variability, and response to global warming using a 50km resolution GCM. *J. Clim*. In press.

Tropical cyclones and climate change: the Tropical Cyclone Climate Model Intercomparison Project

Kevin Walsh and Sally Lavender
School of Earth Sciences, University of Melbourne, Victoria, Australia
Hiroyuki Murakami
Meteorological Research Institute, Tsukuba, Japan
Enrico Scoccimarro
INGV, Bologna, Italy
TCMIP project members[1]

Introduction

The possible effect of climate change on tropical cyclones remains one of the most controversial topics in modern meteorology. Opinions on this issue range from flat denial that there could be any effect to predictions of large increases in tropical cyclone incidence and intensity that are already detectable in the observed record. A range of techniques have been used to make inferences about this topic, ranging from purely statistical analyses to sophisticated fine-resolution models to fundamental theories of atmospheric behaviour.

The debate about the effects of climate change on tropical cyclones is going through the same stage as the controversy regarding the possible effects of man-made increases in carbon dioxide on global climate passed through some years ago. In both topics, initial theoretical work established that such an effect was consistent with our understanding of atmospheric physics – for tropical cyclones and climate change, this was the work of Emanuel (1987). For global climate change, this was followed by a period of model development and experimentation, accompanied by argument over both the existence and the magnitude of the possible climate change signal. This debate is now essentially over: there are few serious climate scientists who still believe that there is no significant global effect. Numerous detection and attribution studies have shown that the observed 20th and early 21st century warming is consistent with climate model predictions based on the observed increases in greenhouse gas concentration in the atmosphere. These same climate models project even larger changes later this century.

In contrast, for tropical cyclones and climate change, the debate continues. There are two fundamental reasons why this is so. Unlike the global climate record of (for example) land-based screen temperature, there is considerable controversy about the consistency of the tropical cyclone record, due to significant changes in observing systems over several decades. Unlike the land-based temperature record, the main tropical cyclone records, the best track data, were never intended to be used as climate data sets. As a result, little attention was paid to ensuring that the measuring techniques used to construct them were consistent from year to year. The other issue limiting scientific conclusions from this debate is that until very recently, climate model simulations of the observed distribution of tropical cyclone extreme wind speeds were poor. This is also in contrast to the quality of the simulation of global average temperature and regional distribution of temperature: since this is considerably easier to simulate, its quality has always been better. One of the crucial steps in the debate on the causes of the observed increase in global average temperature over the past century or so was the development of an ability to simulate that

[1] See http://www.earthsci.unimelb.edu.au/~kwalsh/tcmip_index.html for a complete list

increase and the relative contributions of the various climate forcings (aerosols, solar radiance, greenhouse gas concentrations) to observed climate change. Thus the causes of global climate change were able to be identified, through the process of detection and attribution.

Recent improvements in climate model simulations of tropical cyclones have the same potential to resolve arguments about the causes of observed trends in tropical cyclone characteristics, provided of course that there is agreement on the magnitude and direction of observed trends. Leaving aside the question of observed trends for the moment, this article focuses on recent developments in tropical cyclone climate models, including the Tropical Cyclone climate Model Intercomparison Project.

Tropical cyclones as simulated by climate models

A recent review of the quality of tropical cyclone simulation in climate models is contained in Walsh (2008). In a nutshell, this paper concluded that the simulation of tropical cyclone formation and tracks by climate models is reasonable for the best models. In contrast, the simulation of tropical cyclone intensity distributions is inadequate, largely a result of coarse resolution. While the simulation of tropical cyclone formation and tracks does not depend so much on model resolution as intensity does, there is still considerable room for improvement in climate model simulations of these variables. This is important as there have been observed trends in track and formation regions that are less controversial than trends in observed wind speeds. Thus climate models used for attribution studies need the best possible simulation of these trends that can be obtained for relatively coarse model resolutions, which in this context means horizontal resolutions from 30-200 km.

One issue that was identified by Walsh (2008) was that many climate model studies of tropical cyclones had been performed to date but that almost all of them used different criteria to define a model-generated tropical cyclone. One way to circumvent this issue would be to define a simulated tropical cyclone in the same way that observed tropical cyclones are defined: by simply counting all of the storms that had 10 metre wind speeds in excess of 17.5 ms^{-1} and had the warm core structure of tropical cyclones. Nevertheless, this is a very severe test for a climate model of coarser resolution, indeed an unfair test as it compares a model of limited resolution with reality which has effectively unlimited resolution. Climate models are usually validated by comparing their performance against observations that have been degraded to a similar resolution to the model. Walsh et al. (2007) proposed the same process for tropical cyclone simulation: to degrade data from weak, observed tropical cyclones to the resolution of the climate model and determine what are their maximum wind speeds at that resolution. Additionally, this serves as a way of comparing the results of climate models running at slightly different resolutions. In this way, the native ability of the model to generate tropical cyclones is assessed in a resolution-appropriate fashion.

This was the philosophy behind the proposed Tropical Cyclone climate Model Intercomparison Project (TC-MIP)[2]. Like all intercomparison projects, this project proposes and defines common metrics for the assessment of climate models of tropical cyclones (e.g. Camargo et al. (2007); Yokoi et al (2009)) Here, we reanalyse the CMIP3 model output and recent high-resolution climate models, using common metrics, including two separate detection routines. Due to space limitations, we only supply samples of the analysed data.

[2] http://www.earthsci.unimelb.edu.au/~kwalsh/tcmip_index.html

CMIP3 model output

The CSIRO detection scheme of Walsh et al. (2007), a resolution-dependent scheme, and the Camargo and Zebiak (2002) basin-dependent schemes are applied here. Fig. 1 shows genesis rates from the CSIRO Mk 3.5 model (T63 resolution) for the two schemes compared with the genesis rates from the best track data. It is clear that based on the CSIRO detection scheme the Mk 3.5 model slightly undersimulates tropical cyclone formation. The Camargo scheme, because of its basin-dependent threshold criteria, gives more information about the pattern of formation than it does about the absolute numbers of storms formed. From this scheme, the CSIRO Mk 3.5 model appears to be simulating rather more formation in the Indian Ocean than in the Southwest Pacific, and also is generating anomalous formation in the North Central Pacific.

Fine-resolution model output

While analysis of the CMIP3 data is instructive, none of the models included in that archive were designed to simulate a good climatology of tropical cyclone formation. More recent, finer-resolution results have the potential to give much better simulations of numbers and patterns of formation. Fig. 2 shows sample results from the MRI AGCM (20 km resolution) and the CMCC-INGV coupled GCM at T159 resolution (about 80 km resolution). Both give good simulations of the observed pattern of formation, although both appear to be simulating slightly too few storms in the Australian region. More results are presented at the workshop.

References

Camargo, S.J., Barnston, A.G., Emanuel, K.A., 2007. Tropical cyclone genesis potential in climate models. *Tellus, 59A*, 428-443.

Camargo, S.J., Zebiak, S.E., 2002. Improving the detection and tracking of tropical storms in atmospheric general circulation models. *Wea. Forecast*., *17*, 1152-1162.

Emanuel, K.A., 1987. The dependence of hurricane intensity on climate. *Nature, 326*, 483-485.

Walsh, K., 2008. The ability of climate models to generate tropical cyclones: implications for prediction. In *Climate Change Research Progress*, L. Peretz (ed.), Nova Publishers, pp. 313-329

Walsh, K., Fiorino. M., Landsea, C. and McInnes, K., 2007.Objectively-determined resolution-dependent threshold criteria for the detection of tropical cyclones in climate models and reanalyses. *J. Climate, 20*, 2307-2314.

Yokoi, S., Takayabu, Y. and Chan, J., 2009. Tropical cyclone genesis frequency over the western North Pacific simulated in medium-resolution coupled general circulation models. *Clim. Dyn.*, DOI 10.1007/s00382-009-0593-9.

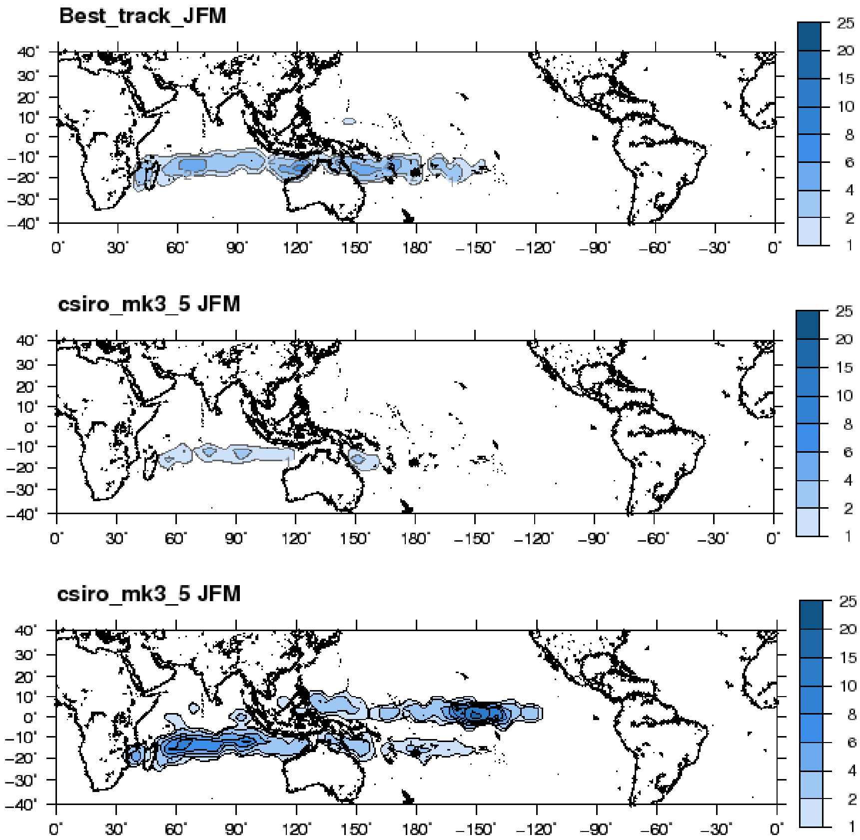

Fig. 1. Global tropical cyclone genesis for JFM from (top) IBTracs best track data; and as generated by the CMIP3 CSIRO Mk 3.5 data from (middle) the CSIRO detection scheme; and (bottom) the Camargo detection scheme.

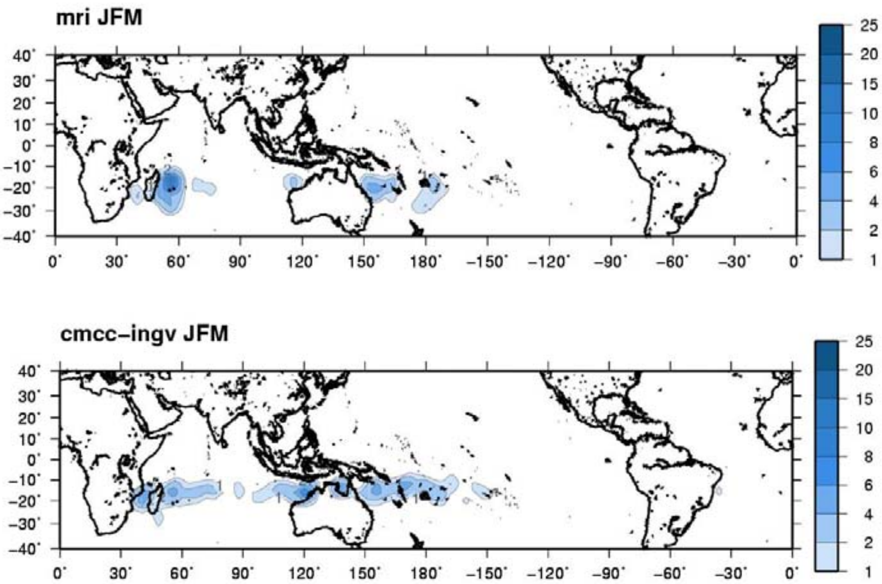

Fig. 2. The same as Fig. 1 for (top) the MRI model and (bottom) the CMCC-INGV model as described in the text.

Downscaling tropical cyclones for climate change studies

Debbie Abbs
Centre for Australian Weather and Climate Research,
CSIRO Marine and Atmospheric Research,
Private Bag 1,
Aspendale, Victoria, 3195.
Australia

Introduction

Tropical cyclones (TCs) are amongst the World's most destructive and costly natural hazards; thus accurate estimates of future changes in their frequency, intensity and location would be of great value. Formation of tropical cyclones generally occurs within a band between 5° and 25° from the Equator. The climatology of TCs in the Australian region (Figure 1a) is based on the southern hemisphere tropical cyclone (TC) archive constructed in the National Climate Centre of the Bureau of Meteorology. The climatology can be characterised by a preferred region of occurrence between 10 and 20°S with maxima occurring off the Queensland and Western Australian coastlines and in the Gulf of Carpentaria.

Throughout the world, tropical cyclone (TC) activity and intensity are variable on the intra-seasonal, inter-annual, inter-decadal and multi-decadal timescales. Australian region tropical cyclone numbers are correlated with indices of the El Niño Southern Oscillation (ENSO) from the central and eastern equatorial Pacific, indicating a remote effect on tropical cyclone numbers. Tropical cyclone activity is lower in the Australian region during El Niño events, while La-Niña events typically produce the opposite conditions (e.g. Kuleshov *et al.* 2008, Ramsey *et al.* 2008). Other large scale patterns affecting TC occurrence in the region are the 40-60-day Madden-Julian Oscillation (MJO) (Hall *et al.* 2001) and the Inter-decadal Pacific Oscillation (IPO) (Grant and Walsh 2001).

There is substantial evidence that the large-scale environment in which TCs form and evolve is changing as a result of global warming. Projected changes in tropical cyclones are subject to the sources of uncertainty inherent in climate change projections. These include the future climate-forcing scenario (e.g. greenhouse gas and aerosol emissions), model dynamics and physics, errors in the modelled tropical cyclone climatology, regional changes in environmental conditions and climate drivers such as ENSO. Consequently there is large uncertainty in projected TC changes. In recent years, there have been a growing number of studies using results from medium and high resolution GCMs. The results from these studies are summarised by Knutson *et al.* (2006) and indicate a consistent tendency for fewer tropical cyclones globally in a warmer climate. The fourth assessment report of the United Nations Intergovernmental Panel on Climate Change (IPCC 2007) considered that it is likely that storm intensity will continue to increase through the 21st century, and declared it more likely than not that there has been some human contribution to the increases in tropical cyclone intensity, although this contribution may be very small compared to natural variability. However, there are significant regional variations in the direction of the changes and these vary between models.

Model and methodology

The model used in this study is the CSIRO Conformal-Cubic Atmospheric Model (CCAM) of McGregor and Dix (2001). In the simulations considered herein, the region of interest lies over the Australia region and has a grid spacing of approximately 65 km. Two sets of simulations are considered: (1) an ensemble of 15 climate simulations nested in NCEP reanalyses and (2) an ensemble of 12 simulations nested in GCMs sourced from the IPCC CMIP3 archive. The reanalysis-based results are used to determine whether or not the model can reproduce the spatial occurrence and inter-annual variability of TCs in the region. A good representation of these characteristics provides some confidence in the suitability of the modelling system for providing projections of changes in TC activity. Archived 12 hourly outputs from CCAM are used to detect and track tropical cyclone-like vortices (TCLVs) which are subsequently analysed to identify possible changes in their frequency and intensity.

The TCLV detection and tracking scheme was modified from that of Nguyen and Walsh (2001). The detection criteria are:

1. A vorticity more negative than -10^{-5} s^{-1} (in the Southern Hemisphere);
2. There must be a closed pressure minimum, taken to be the centre of the storm, within 250 km of a point satisfying criterion 1;
3. There must be rotation, defined by wind direction, around the storm centre;
4. The maximum 10m wind speed must be greater than 11.5 ms^{-1};
5. The mean wind speed in the area 500 km × 500 km around the centre of the storm at 850 hPa must be higher than that at 300 hPa;
6. The system must be warm cored. The total of the tropospheric temperature anomalies at 750, 500 and 300 hPa in the centre of the storm must be greater than zero. These anomalies are calculated relative to the mean environmental temperature at each level in the region 750 km east and west and 500 km north and south of the storm centre.

In this study, we focus on the tropical waters in the Australian region, with the region of interest being from 90° to 180°E and from the equator to 50°S. Within this domain, tropical cyclogenesis is not allowed poleward of 30°S, however if a TCLV forms within the 0° to 30°S band and tracks poleward, it will continue to register as a cyclone providing that it continues to satisfy the relevant criteria. Once the TCLV has existed for a period of at least 12 hours, criterion 6 is relaxed and the TCLV tracked until it no longer satisfies any of the remaining five criteria. Tracks of less than 24 hours duration are discarded from the final results. The wind speed threshold used in this study is lower than the grid-spacing based “standard” value (16 ms^{-1}) suggested by Walsh *et al*. (2007). A manual examination of the raw model outputs indicated that the lower value was more appropriate.

Results

Reanalysis-based simulations

The climatology based on an ensemble of 15 climate simulations nested in NCEP reanalyses is presented in Figure 1(b) and can be compared with the climatology presented in Figure 1(a). The results show a good qualitative agreement in the preferred regions of occurrence, with maxima in the Coral Sea, the Gulf of Carpentaria and off the coast of north Western Australia. In all regions, the modeled frequencies are less than observed with, on average, approximately 60% of the observed number of TCs simulated by CCAM. The underestimate in TC occurrence is most likely due to the relatively coarse grid spacing used in this study. The ability of the model to simulate the inter-annual variability of TCs occurring in the region has been examined and the ensemble-average correlation between observed and modelled annual TC numbers is 0.3. While this value is relatively low, it compares favourably with results obtained by Zhao *et al.* (2009) for the South Pacific from their 50 km global climate model simulation. The ratio of the number of TCs occurring during El Niño years to that occurring during La Niña years is 0.74 while that obtained from the model ensemble average is 0.64. These results indicate that, on average, CCAM is able to simulate the spatial characteristics of TC occurrence in the Australian region and that the configuration used for the reanalysis-based simulation is able to differentiate between El Niño and La Niña events.

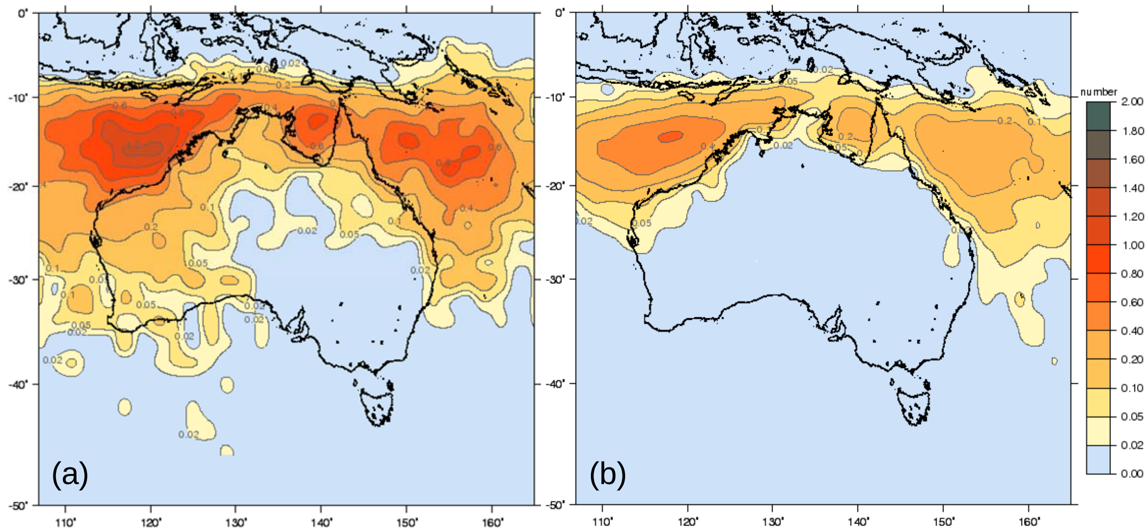

Figure 1: (a) Average annual distribution of TCs in the Australian region. Occurrence is expressed as the number of cyclones per year within a 2x2 degree grid cell. Figure based on data from the Bureau of Meteorology Best Track dataset. (b) Climatology of TCs based on the ensemble average of 15 simulations nested in NCEP reanalyses. Occurrence is the number of cyclones per year within a 2x2 degree grid.

Climate change simulations

The climate change projections are from an ensemble of 12 simulations nested in GCMs sourced from the IPCC CMIP3 archive. The simulations considered include climate change forcing using variations of 2 different methods. Six simulations nudge the CCAM atmosphere towards the large scale fields from the host GCM while the remaining 6 simulations only force CCAM with bias-corrected SSTs from the host model.

The modelled average annual occurrence of tropical cyclones for the 30-year period corresponding to 1971-2000 is not shown but is similar to that in Figure 1(b). The ensemble average projected changes are shown in Figure 2.

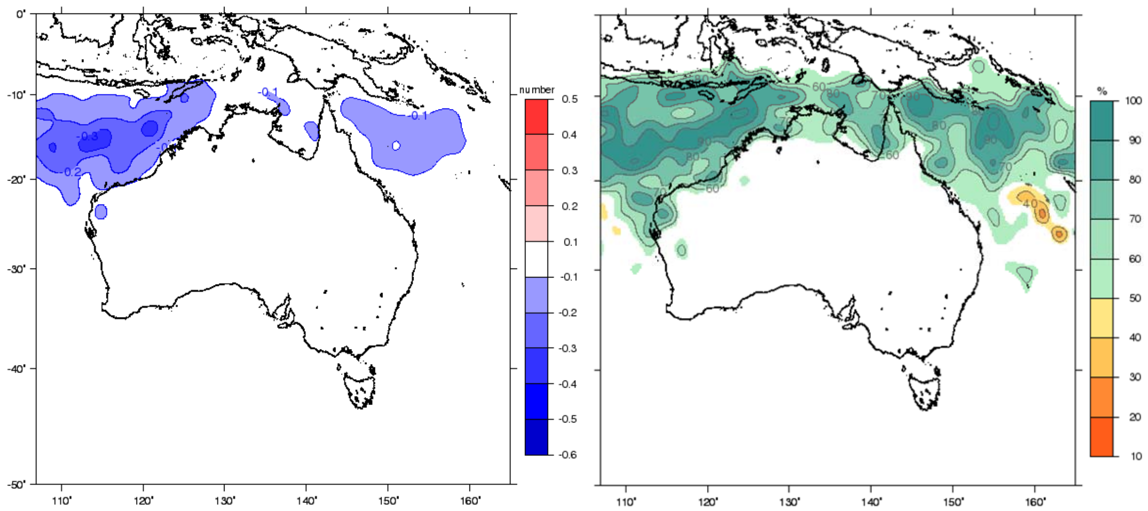

Figure 2: Projected changes in the annual occurrence of TC-like vortices for 2046-2065, relative to 1971-2000, based on the results from 12 climate simulations (left), with shading indicating regions of decreased occurrence of events. Inter-model ‘consensus’ for direction of change (right), with shading indicating regions where more than 50% of simulations project a decrease in TC occurrence.

These results show a strong tendency for a decrease in TC numbers in the Australian region, especially in the region of current preferred occurrence. Further analysis of these simulations has investigated potential changes in the duration, genesis latitude and decay latitude of TCs. On average, the simulations show an approximately 50% decrease in occurrence for the Australian region, a small decrease (0.3 days) in duration and a southward movement of approximately 1 degree in both genesis latitude and decay latitude. On average, the southward movement in decay latitude is greater off the Queensland coast than off the coast of Western Australia.

Changes in intensity

The simulations described above are too coarse for an assessment of changes in TC intensity. Thus a subset of detected TC-like vortices from one CCAM simulation has been further downscaled to a grid-spacing of 15 km for 40-year time slices centred on 1980, 2030 and 2070. For each time slice 100 events were modelled. While this grid spacing is still inadequate to resolve the fine-scale structure of TCs, the results do show a distinct shift towards deeper pressures and a flattening of the maximum wind speed distribution with a larger percentage of TCs producing high larger wind speeds in the 2070 climate than either the 1980 or 2030 climates. A larger population of storms needs to be downscaled at higher resolution (e.g. 5 km grid spacing) before quantitative projections of changes in intensity and rainfall can be produced. This is a focus of current downscaling activity.

Comparison with other studies

A number of global climate modelling studies have appeared in the international literature since 2000 which investigate the impact of climate change on the global occurrence of tropical cyclones. A consistent result from each of these studies (Sugi *et al.* 2002; McDonald *et al.* 2005; Oouchi *et al.* 2006*;* Zhao *et al*. 2009*)* is for a decrease in Southern Hemisphere tropical cyclone occurrence late in the 21st Century. Most studies project an increase in tropical cyclone intensity.

References

Grant, A.P., and K.J.E. Walsh, 2001: Interdecadal variability in north-east Australian tropical cyclone formation. *Atmospheric Science Letters*, doi:10.1006/asle.2001.0029.

Hall J.D., A.J. Matthews, and D.J. Karoly, 2001: The modulation of tropical cyclone activity in the Australian region by the Madden-Julian oscillation. *Mon. Wea. Rev*.,**129,** 2970-2982.

IPCC, 2007: Climate Change 2007: The Physical Science Basis. Contribution of Working Group I to the Fourth Assessment Report of the Intergovernmental Panel on Climate Change. S. Solomon, D. Qin, M. Manning, Z. Chen, M. Marquis, K. B. Averyt, M. Tignor, and H. L. Miller (eds.). Cambridge University Press, Cambridge, United Kingdom and New York, NY, USA, 996 pp. (2007).

Knutson, T.R., and co-authors, 2006: Possible relationships between climate change and tropical cyclone activity. Topic 4.2, 6th WMO International Workshop on Tropical Cyclones (IWTC-VI), Costa Rica, Nov. 2006.
http://severe.worldweather.org/iwtc/document/Topic_4_2_Tom_Knutson.pdf]

Kuleshov, Y., L. Qi, R. Fawcett, and D. Jones, 2008: On tropical cyclone activity in the Southern Hemisphere: Trends and the ENSO connection, *Geophysical Research Letters*, **35**, L14S08, doi:10.1029/2007GL032983.

McDonald, R.E., D.G. Bleaken, D.R. Cresswell, V.D. Pope, and C.A. Senior, 2005: Tropical storms: representation and diagnosis in climate models and the impacts of climate change. *Clim. Dyn.,* **25:** 19-36, DOI: 10.1007/s00382-004-0491-0.

McGregor, J. L., and M.R. Dix, 2001: The CSIRO conformal-cubic atmospheric GCM. *Proc. IUTAM Symposium on Advances in Mathematical Modelling of Atmosphere and Ocean Dynamics*, Limerick, Ireland, P. F. Hodnett, Ed., *Fluid Mechanics and Its Applications*, **61**, 307-315.

Oouchi, K., J. Yoshimura, H. Yoshimura, R. Mizuta, S. Kusunoki, and A. Noda, 2006: Tropical cyclone climatology in a global-warming climate as simulated in a 20 km-mesh global atmospherc model: Frequency and wind intensity changes. *J. Meteorol. Soc. Japan*, **84**, 259-276.

Ramsay, H.A., L.M. Leslie, P.J. Lamb, M.B. Richman, and M. Leplastrier, 2008: Interannual Variability of Tropical Cyclones in the Australian Region: Role of Large-Scale Environment. *J. Climate*, **21**, 1083–1103.

Sugi, M., A. Noda, and N. Sato, 2002: Influence of global warming on tropical cyclone climatology: an experiment with the JMA global model. *J. Meteorol. Soc. Japan*, **80**, 249-272.

Walsh, K.J.E., M. Fiorino, C.W. Landsea, and K.L. McInnes, 2007: Objectively Determined Resolution-Dependent Threshold Criteria for the Detection of Tropical Cyclones in Climate Models and Reanalyses. *J. Climate*, **20**, 2307–2314

Zhao, M., I. Held, S.-J. Lin, and G. Vecchi, 2009: Simulations of global hurricane climatology, interannual variability, and response to global warming using a 50km resolution GCM. *J. Clim*. In press (2009).

Challenges and opportunities in operational Tropical Cyclone forecasting

Andrew Burton
Bureau of Meteorology, Perth, Australia

Introduction

This paper highlights challenges and research opportunities relating to operational tropical cyclone (TC) forecasting. It draws significantly on input from a recent survey of the three Australian Tropical Cyclone Warning Centres (TCWCs) as well as the outcomes from the Sixth International Workshop on Tropical Cyclones (IWTC-VI; 2006) and the Second International Workshop on Tropical Cyclone Landfall Processes (IWTCLP-II;2009).

The paper provides some operational perspective on TC forecasting and then discusses contemporary forecasting challenges and identifies opportunities for research focused on establishing good decisions amongst client groups. A key theme of this paper is summarised by a quote taken from the proceedings of IWTC-V (WMO 2002): "*Establish good decisions as the goal of research rather than good predictions, good theories or good models.*" This statement was echoed at IWTC-VI (WMO, 2006) where the gap between research findings and the ability to transfer the information into operational techniques was recognised.

Achievements

Before considering the forecast challenges facing Australian TCWCs it is worth reflecting on recent advances in Australian tropical cyclone warning services. Over the last decade Australian TCWCs have developed an efficient operational forecast process well supported by systems (particularly TC Module). This has enabled TCWCs to increase the quantity and range of products, enhance briefing services and increase forecast lead times while assimilating a greater breadth and complexity of observational data and forecast guidance.

Numerical Weather Prediction (NWP) guidance has improved track prediction and consensus forecast methods have yielded additional improvements in the accuracy and stability of predictions. Multi-model consensus TC track forecasting became a focus for a group of researchers associated with the Naval Postgraduate School in Monterey through their ties to the Joint Typhoon Warning Centre. Australian TCWCs were early adopters of these methods and have contributed to further developments (Burton 2006; Elsberry et al 2008).

The three TCWCs have also recently adopted a consistent pressure-wind relationship that will improve both operational consistency and the transparency and internal consistency of the Australian "best track" dataset (Courtney and Knaff, 2009). Further work is required to improve the consistency, transparency and reliability of the database. A consistent Dvorak reanalysis of the satellite era requires considerable time from an experienced Dvorak analyst but there are intermediate steps that can be taken to improve the database's utility for research and risk assessment.

Forecast process

Operational forecast process is focused on the efficient and effective combination of science with risk management elements to deliver guidance to decision makers in government, industry and the community. One of the key characteristics of operational tropical cyclone forecasting is the requirement for efficient processes. In the twenty four hours before TC impact the demand for up-to-date information creates a work schedule in which every minute counts. Research findings need to be transferred into operations with this context in mind. Forecast guidance information will fail to influence decision making if it can not be accessed quickly and incorporated into the forecast process efficiently.

Operational tropical cyclone forecasting utilises objective and subjective guidance and incorporates a layer of risk analysis to determine its outputs. Ideally TCWCs would assess the meteorology and leave the risk assessment to others; however the risk assessment element cannot be avoided when producing deterministic products. Risk is a product of probability and consequence. Deterministic forecasts that represent the most probable outcome will often not represent the highest risk. To provide the best possible service to communities TCWCs occasionally need to present a forecast scenario that is the highest risk but not the most likely outcome.

Challenges and opportunities

Forecasting storm surge

Warnings for storm tides provide a good example of the need for warnings to focus on risk rather than probability. The storm tide risk at a particular community is sensitively dependent on the track of the tropical cyclone. The probability of a very large storm tide at any given location is small even when an intense cyclone is within 18-24 hours of landfall (a lead-time at which evacuation must generally be considered); however because the consequence of a large storm tide can be catastrophic, the risk remains high. By agreement with emergency management agencies the current approach is focused on providing communities with a worst-case scenario. The track that would result in the worst storm surge is the one used to assess the storm tide risk, even if that track is considered unlikely. Hence the desire to improve the specification of the meteorological forcing in storm surge models (from the parametric models typically used) can conflict with the need to be able to choose the worst-case track scenario. Further developments in storm surge modelling are required, but the outputs need to be able to be incorporated into the operational setting outlined above.

Perceptions of accuracy

The degree to which industry and community decision makers incorporate forecasts into their decision making depends on their perceptions of forecast accuracy. Government, industry and community perceptions of accuracy in tropical cyclone forecasting are not a simple function of the mean absolute error of the predictions. Whilst track prediction has steadily improved when viewed in terms of mean errors, the occasional "big bust" can have a disproportionate effect on client confidence. IWTC-VI (WMO, 2006) resolved that: "*There's greater value in focussing resources on researching extreme events (not forgetting though that weak TCs can produce major floods).*" Research aimed at identifying the causes of large forecast errors has potential to provide greater improvements to decision making "on the ground" than an overall reduction in mean absolute error.

Incorporating EPS guidance

Recent advancements in ensemble prediction systems (EPS) and a concomitant growth in the quantity of probabilistic guidance information have not been transferred into operational forecasting process in a systematic fashion. The incorporation of EPS guidance into operational forecast process requires research into the methods for combining multi-model EPS outputs, development of a forecast process based on the outcomes of that research and the development of tools (or enhancement of existing tools) to support that process. One of the challenges to overcome is the lack of verification for EPS guidance. Probabilities assigned in EPS displays are based on the percentage of ensemble members that incorporate a specific outcome. Forecasters are left to guess the degree to which the spread of the ensemble members captures the true spread of possible outcomes. The current lack of verification of probabilistic guidance provides an opportunity to develop a common methodology for application across NWP suites to facilitate the optimal use of multi-model EPS.

Intensity analysis

Track forecasts have steadily improved over the last two decades, but intensity forecasts have shown only marginal improvement (WMO 2006). Indeed it is difficult to measure improvement (or degradation) in intensity forecasting because there is a lack of precision in intensity analysis[1]. Tropical cyclone analysis has a strong reliance on remote sensing via satellite and the principal

[1] Even defining what is meant by "intensity" can be problematic, as there are issues with using either central pressure or wind speed as the metric of intensity.

method for determining intensity remains the Dvorak method; for which the root mean square error is generally recognised as being of the order of +/-0.5T (Brown and Franklin 2004, Knaff et al 2009). The accuracy of the technique is greatest for systems with well defined eye patterns and is less for systems below hurricane-force (Knaff et al 2009). The greatest forecasting challenges occur during the formative and weaker phases and there is a need for improved observations during this period to facilitate better analysis, as a poor analysis will generally lead to a poor forecast.

Installation of a number of new oil and gas platforms off the North West shelf offers opportunities to increase in situ observations and radar coverage in the area. There may also be opportunities to gather funds for observational field experiments in the region that could serve as verification for remote sensing techniques and NWP. An offshore-radar, in combination with the outcomes of the Strategic Radar Enhancement Project, may offer significant improvements to NWP forecasts through assimilation of detailed structure information.

Forecasting genesis and intensity

The history of TC track forecasting suggests that the optimum approach to improved genesis/intensity forecasts will be to incorporate consensus methods as soon as possible while continuing to work on the skill of individual elements of guidance. Whilst consensus methods for track forecasting have been the subject of considerable research consensus methods for intensity forecasting are still in their infancy (Burton 2006). Unlike track forecasting in which access to a simple text file (the output of a vortex tracker) is sufficient to create another consensus member, creating a consensus approach to intensity forecasting may require greater access to model fields. This may limit the ability of Australian TCWCs to capitalise on the work of US researchers as they did in order to implement consensus track forecasting. Hence there is a need for Australian researchers to work in this area if Australian communities are to obtain benefit from the improvements likely to follow from consensus intensity forecasting methods. For longer lead times, attention should be paid to achieving the optimal mix of dynamical and statistical aids.

Optimising the skill of individual guidance elements requires research into how to gain optimal skill from individual NWP models. The appropriate use of intensity diagnostics (such as the Okubo-Weiss parameter, or differential warm air advection displays), the choice of other fields to overlay and the design of a process that incorporates these into an effective and efficient forecast process is work that remains to be done and for which there is a clear need.

Rainfall forecasting

There is a need for improved prediction of TC-related precipitation, both temporal and spatial, at landfall. Flooding remains the largest overall impact in most landfall events and despite some improvement there remains a large degree of uncertainty in rainfall forecasts. The dependence of rainfall totals on translation speed and system structure indicates that to some extent improvements in flood forecasting will be dependent on improved track and structure forecasting.

Opportunities for partnership with industry

Burgeoning industry in TC prone areas, particularly in the North West of Australia, provides an opportunity for funding of research that can improve decision making for government, industry and communities. The window of opportunity is open now while a number of large projects are still in the planning phase. Offshore industry clients typically have a requirement for forecasts with longer lead times. Service expectations of the three key user groups are not static and are continually being updated; inevitably towards longer lead times, greater detail and improved accuracy in forecasts. There are opportunities to have new services developed under finance from industry before eventually being made accessible to the wider community.

Wave forecasting

Offshore industry has a greater interest in marine hazards than the general community. There is a need for improved wave guidance through coupling of ocean wave models with TC NWP. Once again an EPS approach is required to enable services to be delivered within a risk management framework that accounts for uncertainties in forecasting track, structure and intensity.

Summary of research priorities from a services perspective

1. Greater focus on the transfer of research into operations. *"Establish good decisions as the goal of research rather than good predictions, good theories or good models."* (WMO, 2002)
2. Further improvements in track landfall forecasts, particularly:
   a. Investigation of instances of large forecast errors, and
   b. Extension of current consensus methods to allow for systematic incorporation of multi-model EPS guidance and the production of improved probabilistic forecasts.
3. Improvements in guidance for genesis/intensity forecasting. There is a need to improve NWP guidance on intensity (where we take intensity forecasting to incorporate the issue of cyclogenesis). General improvements in model skill need to be complemented with development of displays of parameters such as Okubo-Weiss, or using EPS displays of key parameters (eg. intersection of high vorticity with low vertical shear).
4. Consensus methods for intensity forecasting. There is a need to develop an efficient consensus methodology for combining EPS outputs from multiple models, with statistical guidance where appropriate, as the basis for probabilistic forecasts of intensification/decay.
5. Improved predictions of TC-related precipitation (both temporal and spatial) following landfall. Flooding remains the largest overall impact in most tropical cyclone landfalls and despite some improvement there remains a large degree of uncertainty in rainfall forecasts.
6. Improved wave guidance through coupling of ocean wave models with TC NWP. Once again, an EPS approach is required to account for deficiencies in forecasting intensity, structure and track. A single coupling of the best ocean wave model to the best tropical cyclone model would not establish the basis for the best decisions to be made.
7. Advances in understanding and prediction of TC structure and intensity.
8. Further observation systems/platforms within the TC and its environment.
9. Improved TC database to enhance its utility for research and risk assessment.

References

Brown, D.B., and J.L. Franklin, 2004: Dvorak TC wind speed biases determined from reconnaissance-based best track data (1997-2003). *26th Conf. Hurr. And Trop. Meteor.*, Miami, FL, Amer. Meteor. Soc., 86-87.

Burton, A., 2006: Sharing experiences in operational consensus forecasting. Topic 3a, *Proceedings of the Sixth WMO International Workshop on Tropical Cyclones*, San Jose, Costa Rica, 21-30 November 2006.

Courtney, J., and J.A. Knaff, 2009: Adapting the Knaff and Zehr pressure-wind relationship for operational use in TCWCs. *Australian Meteorological & Oceanographic Journal*, 58, 167-179.

Elsberry, R.L., J.R. Hughes, and M.A. Boothe, 2008: Weighted Position and Motion Vector Consensus of Tropical Cyclone Track Prediction in the Western North Pacific. *Mon. Wea. Rev.*, 136, 2478–2487.

Knaff, J.A., D.P. Brown, J. Courtney, G.M. Gallina and J.L.Beven II, 2009: An Evaluation of Dvorak Technique-Based Tropical Cyclone Intensity Estimates. *Wea. Forecasting, (submitted).*

WMO. 2002. *Topic Chairman and Rapporteur Reports of the Fifth WMO International Workshop on Tropical Cyclones*. WMO TD-No. 1136. WMO, Geneva. (Cited November 2009 on line at http://www.aoml.noaa.gov/hrd/iwtc/)

WMO. 2006. Workshop Topic Reports, Sixth WMO International Workshop on Tropical Cyclones. *Tropical Meteorology Research Programme Report Series. TMRP No. 72*. WMO, Geneva.

Coupled Tropical Cyclone modelling and adaptive dynamical initialisation

P. A. Sandery and G. B. Brassington
Centre for Australian Weather and Climate Research,
Bureau of Meteorology, Melbourne, Australia

Background

The impact of air-sea coupling on tropical cyclone (TC) intensity change and the ocean response in the Australian region has recently been investigated using a coupled limited-area model (CLAM) (Sandery et al, 2009:1). The coupled model was based on the Australian Bureau of Meteorology's Tropical Cyclone Limited Area Prediction System (TC-LAPS) and a regional version of the BLUElink ocean forecasting system. The study centred on a series of case study forecasts that included original and uncoupled runs and an inertial coupled ensemble, all using the same atmospheric model physical parameters and initial and boundary conditions. The results showed that in each of the cases, the use of reanalysed sea surface temperatures significantly improved the prediction of TC intensity change in the intensification phase.

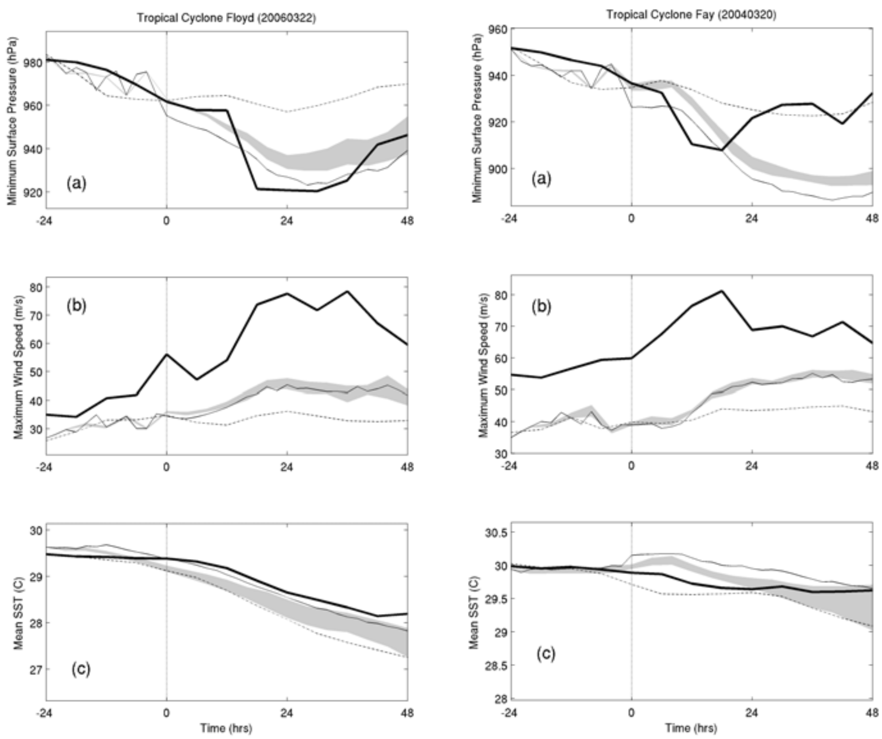

Figure 1. Comparison of TC-LAPS operational forecast (dashed line), CLAM ensemble experiments (denoted by gray area), the Bureau of Meteorology's posterior analysis (solid heavy line) and the uncoupled simulation (solid line) for (a) minimum surface pressure, (b) maximum wind speed and (c) mean SST following the estimated contact area of the storm for the TC Floyd and TC Fay cases.

Figure 1 illustrates the impact of different SSTs, air-sea coupling and the importance of track prediction in two cases. The TC Floyd case is an example where the predicted track was good and storm induced cooling was not significant. Rather there was a transition of the storm to higher latitudes to a cooler SST environment. The small difference (~0.5^{o}C) in mean contact area SSTs illustrates the importance of obtaining accurate SSTs for forecast initial conditions. The TC Fay case is an example where error in the track prediction led to large divergence, 24 hours after forecast base-time, between the forecasted and the analysed TC (Figure 2).

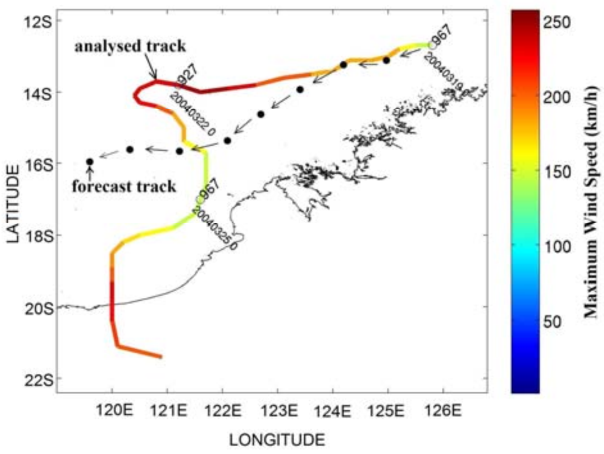

Figure 2. Analysed track from the Joint Typhoon Warning Centre and average of the forecast tracks from all model runs for TC Fay. Colour scale corresponds to maximum wind speed. Timestamps and lowest central pressures for the analysed track correspond to the locations denoted by circles. Solid black dots that denote average forecast track are 12 hours apart.

The TC Fay case highlights the complexity of TC and ocean prediction in the Australian region. In this case, the predicted track was oriented with the shelf break and the degree of cooling on the left side of the track was not realised in the simulation. This is because there was not the same available source of cooler water on the shelf as there was further offshore. The real TC ventured to an area over deeper ocean, where at maximum intensity, the storm induced cooling appears to have been highly significant (as seen in the observations) and to have caused de-intensification and recurvature (Figure 3). The forecasted TC did not experience de-intensification largely because of a combination of track error and proximity to different oceanic environments.

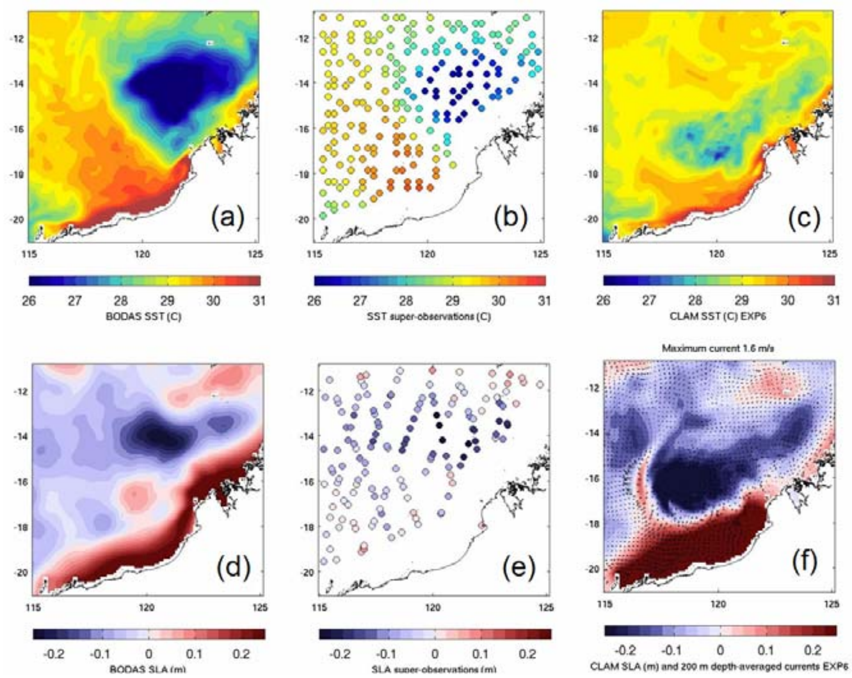

Figure 3. Ocean response to tropical cyclone Fay around 24th March 2004. (a) BLUElink Ocean Data Assimilation system (BODAS) analysed SST. (b) SST super-observations from the AMSR-E microwave sensor and (c) simulated SST from CLAM. Figures d-f as per a-c and illustrate corresponding sea-level anomalies and depth-averaged currents up to maximum 200 m depth.

The results from the coupled tropical cyclone modelling studies also show that dynamic air-sea coupling has an impact on intensity in cases where storm induced SST cooling is significant and is likely to be important for predicting the rate of TC intensity change and peak intensity in these cases. No negative impact was found in the forecasts of TC intensity change and track in the cases where SST cooling was not a significant factor. A definite coupled signal exists, which suggests biases in the atmospheric model that could potentially be removed.

The results highlight the relative increased complexity of tropical cyclone prediction in the Australian region compared to other regions. This is because the region where tropical cyclones form and are supported is characterised by a mixture of areas of warm shelf waters and deep ocean with heat content and mixed layer depths that vary at the mesoscale (O 10-100 km). In the vicinity of the shelf break, other processes, such as internal waves and density fronts, may also influence the ocean response. Furthermore, climatological sea surface temperatures are approximately 2^{o}C warmer and salinities are several psu lower in the equatorial Western Pacific Ocean than in the equatorial Atlantic Ocean. This suggests the work required to vertically mix cooler waters to the surface, which depends on the potential energy of the stratification and the density structure, may be greater in the Australian region.

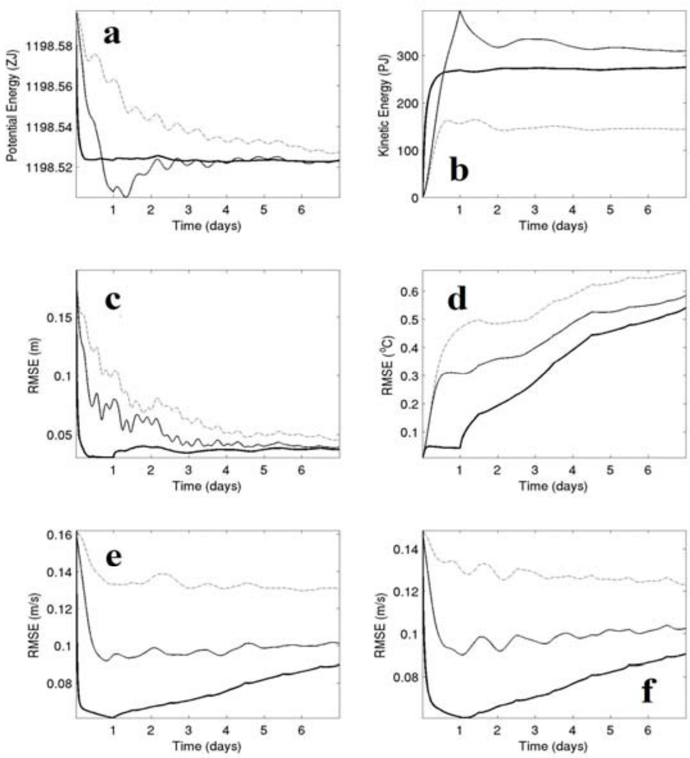

Figure 4. Comparisons of adaptive initialization (heavy solid line), incremental analysis update (solid line) and 'nothing' (dashed line) in a regional CLAM model with respect to (a) total potential energy (ZettaJoules), (b) total kinetic energy (PetaJoules), (c) RMSE sea-level (m), (d) RMSE temperature (°C), (e) RMSE zonal current component (ms^{-1}), (f) RMSE meridional current component (ms^{-1}). The initialisation period is the first day and the reference fields for the RMSEs are the OceanMAPS behind real-time analysis. In this example the regional model domain is 90^{o}E-135^{o}E, 30^{o}S-15^{o}N, and incorporates the Australian northwest shelf, South Equatorial Current and flow through the complex straits and passages of the Indonesian Throughflow.

Adaptive Dynamical Initialisation

To address the issue of providing reliable ocean initial conditions for CLAM an adaptive nonlinear dynamical initialization (ANDI) scheme has been developed (Sandery et al, 2009:2). The ocean initialisation system provides significant improvements over current methods for both introducing information from analyses and minimizing discontinuities (shock) (Figure 4). The method provides the capability of generating ensemble forecasts using different initial conditions (Figure 5). ANDI is close to being an optimal initialisation scheme and places the emphasis for accurate forecasting on the observation network, the physical models and the analysis system.

Conclusions

A coupled model is likely to add value to TC forecasting if initial conditions are adequately constrained to observations and there is skill in the component models and forecast track. This is because it has the potential to account for the many ocean-related factors that govern TC intensity change. In cases where the ocean does not play a significant role there will be no negative impacts. Furthermore, a coupled model closes the surface flux budget and can provide improved prediction of the ocean response to the TC, such as storm induced cooling and coastal sea-level change.

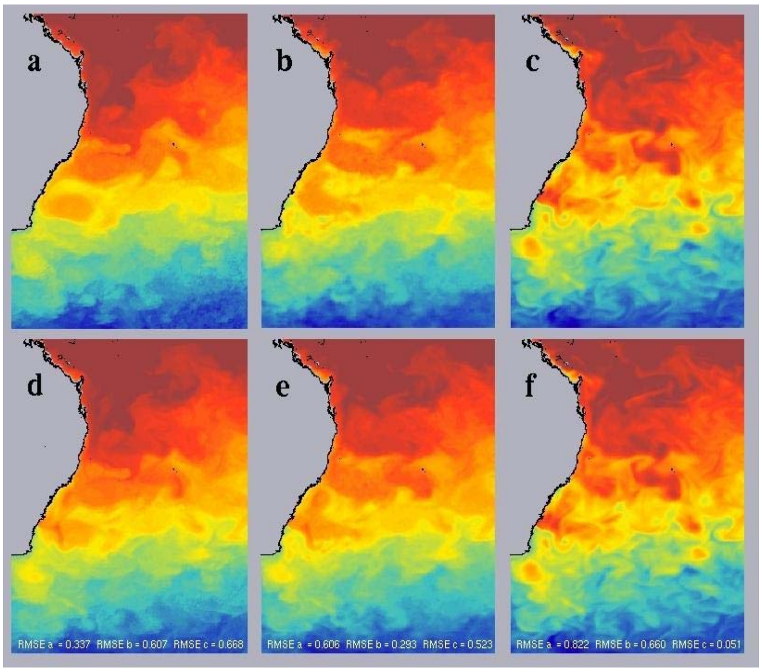

Figure 5. Example of adaptive initialisation to different SST analyses around 1st August 2009. (a) CSIRO AVHRR 10 day composite. (b) RAMSSA. (c) BODAS. Panels d-e are the result of initialising the CLAM model to the corresponding fields above.

References

Sandery, P. A., G. B. Brassington, A. Craig and T. Pugh, 2009. Impacts of ocean-atmosphere coupling on tropical cyclone intensity change and ocean prediction in the Australian region. *Submitted to Monthly Weather Review*.

Sandery, P. A., G. B. Brassington and J. Freeman, 2009. Adaptive Nonlinear Dynamical Initialisation. *Submitted to Journal of Geophysical Research Oceans*.

Use of NWP models to diagnose, understand and predict unusual fire weather events – can we get more from what we already have?

Joseph J. Charney
United States Forest Service, Northern Research Station
East Lansing, Michigan, USA

Numerical Weather Prediction (NWP) models are routinely employed in all forms of operational weather forecasting, at virtually all spatial and temporal scales for which forecasts are prepared. General circulation models are employed for global-scale climate predictions, with mesoscale models commonly used to downscale those predictions for regional application. Routine, daily weather forecasts rely heavily upon synoptic simulations on continental scales for the 12 to 70 hour time windows. Modeling systems such as the Rapid Update Cycle (RUC) employ state-of-the-science NWP and data assimilation techniques to provide the best possible mesoscale analysis for the 0 to 12 hour time windows, for use in nowcasting, short-term severe weather warnings, and rapid response disaster planning.

All of the NWP applications mentioned above, as well as many others, rely heavily upon mesocale models. After the earliest mesoscale models became available to the research and operational community in the early 1970s, most of the model development efforts during the following two decades concerned improving the ability of the models to reproduce and predict the mesoscale processes and structures associated with severe weather, such as mid-latitude convective storms, heavy precipitation, and tropical cyclones. As a result of this focus, many of the physical paramaterizations and model physics options in mesoscale models were developed to improve the depiction of precipitation systems and the environments in which these systems develop. At the same time, tools that would help forecasters interpret model output and highlight the locations where severe weather is most likely to occur were formulated and implemented, relying heavily upon an ingredients-based methodology (e.g. upward motion, high humidity, vertical wind shear, and statically unstable air are ingredients for severe convective storms). Finally, numerous field programs were undertaken to better understand the mesoscale processes associated with severe weather, and the data collected from these field programs were used to improve the depiction of these processes in mesoscale models.

In the last twenty years, mesoscale models have come to be relied upon for much more than forecasts of severe weather. Mesocale models are now routinely employed to predict drought, to assess hydrological impacts, to determine the potential for wind energy, and for numerous other applications. This presentation will focus on the application of mesoscale models to fire weather prediction, both for research and operational forecasting purposes. Specifically, it will address how the development of mesoscale models and the tools used to analyze and interpret mesoscale model output have optimized the implementation of mesoscale model products for severe weather forecasting, and will highlight current research and development efforts that are working to provide similar impacts for fire weather forecasting and research applications.

While it is well-known that the primary ingredients for fire weather forecasts are high winds, low humidity, and high temperatures near the ground, meteorological indices designed to be sensitive to spatial and temporal variations in those ingredients are not commonly used in all weather forecast offices. Additionally, indices and diagnostics that highlight when meteorological processes could lead to sudden changes in those primary ingredients are even less common. Haines (1988) introduced a lower atmospheric stability index (later termed the Haines Index), an empirical formulation designed to account for the role of static stability and dry air in the lower troposphere on the growth of large fires. Potter (2002) analyzed the vertical energy exchanges suggested by the physical quantities used in the Haines Index, Jenkins (2004) examined the mixed-layer structures represented by different HI values, and Potter (2005) looked at the role of vertical exchange of humidity above a fire The physical relationships investigated in these studies provide a starting point for understanding the impact of vertical energy exchanges above a fire on the primary fire weather ingredients. At the same time, Mills (2005a) reported on the mesoscale conditions involved in the Ash Wednesday fires of 1983, Mills (2005b) looked at the mesoscale conditions associated with two severe fire weather days in 2003, and Zhong (2005) verified the performance of a mesoscale model developed fire weather applications. These studies highlight the ability of mesoscale models to resolve important fire weather structures, while also suggesting that fire weather forecasts are strongly sensitive to the performance of certain mesoscale model elements, such as planetary boundary layer and land surface exchange parameterizations.

In the last two years, numerous new studies have employed mesoscale models investigated other aspects of fire-atmosphere interactions. Sun et al. (2009) analyze the vertical coupling between a combustion parameterization and mixed layer structures in a large-eddy simulation model. Mölders (2008) and Colle (2009) have investigated the application of ensemble modeling techniques to high fire danger episodes. Zimet and Martin (2007), Mills (2008a,b), Charney and Keyser (2009), and Miretzky (2009) presented case studies and analyses of sudden surface drying around a fire. Additionally, field studies documented in Clements et al. (2008), Hiers et al. (2009), and Heilman et al. (2009) addressed the mesoscale conditions around and above a fire that contribute to high spatial and temporal resolution changes in the relevant fire weather ingredients.

These recent and ongoing research efforts will be discussed in the context of how new tools can be developed that use mesoscale model output that is currently available to operational forecasters to enhance fire weather forecasts.

References

Charney JJ and Keyser D (2009) Mesoscale model simulation of the meteorological conditions during the 2 June 2002 Double Trouble State Park wildfire. *Int. J. Wildland Fire*, in press.

Colle BA, Erickson M, and Charney JJ (2009) Verification of short-range ensembles for fire threat days over the Northeast U.S. 8th Symposium on Fire and Forest Meteorology, 12-15 October, 2009, American Meteorological Society, Kalispell, MT.

Haines DA (1988) A lower atmosphere severity index for wildland fires. *National Weather Digest* **13**, 23–27.

Hiers KJ, Ottmar R, Butler B, Clements C, Vihnanek B, Dickenson M, and O'Brien J (2009) An overview of the Prescribed Fire Combustion and Atmospheric Dynamics Research Experiment (Rx-CADRE). 4th International Fire Ecology & Management Congress: Fire as a Global Process, 30 November – 4 December 2009, Savannah, GA.

Heilman WE, Zhong S, Charney JJ, Hom J, Clark K, Bohrer G, Skowronski N, Bian X, and Kiefer MT (2009) Development of modeling tools for predicting smoke dispersion from low intensity fires. 4th International Fire Ecology & Management Congress: Fire as a Global Process, 30 November – 4 December 2009, Savannah, GA.

Jenkins MA (2004) Investigating the Haines Index using parcel model theory. *Int. J. Wildland Fire* **13**, 297–309.

Mills GA (2005a) A re-examination of the synoptic and mesoscale meteorology of Ash Wednesday 1983. *Australian Meteorological Magazine* **54**, 35–55.

Mills GA (2005b) On the subsynoptic-scale meteorology of two extreme fire weather days during the eastern Australian fires of January 2003. *Australian Meteorological Magazine* **54**, 265–290.

Mills GA (2008a) Abrupt surface drying and fire weather. Part 1: overview and case study of the South Australian fires of 11 January 2005. *Australian Meteorological Magazine* **57**, 299–309.

Mills GA (2008b) Abrupt surface drying and fire weather Part 2: a preliminary synoptic climatology in the forested areas of southern Australia. *Australian Meteorological Magazine* **57**, 311-328.

Miretzky B (2009) A model based analysis of the synoptic and mesoscale processes associated with subsidence into western Great Lakes wildfire environments. Ph.D. Thesis, U Wisconsin-Madison, Department of Atmospheric and Oceanic Sciences.

Mölders N (2008) Suitability of the Weather Research and Forecasting (WRF) model to predict the June 2005 fire weather for Interior Alaska. *Wea. Forecasting* **23**, 953-973.

Potter BE (2002): A dynamics based view of atmosphere-fire interactions. *Int. J. Wildland Fire* **11**, 247-255.

Potter BE (2005) The role of released moisture in the atmospheric dynamics associated with wildland fires, *Int. J. Wildland Fire* **14**, 77–84.

Sun R, Krueger S, Jenkins M, and Charney J (2009) The importance of fire/atmosphere coupling and boundary layer turbulence to wildfire spread. *Int. J. Wildland Fire* **18**, 50-60.

Zhong S, In HJ, Bian X, Charney J, Heilman W, and Potter B (2005) Evaluation of real-time high-resolution MM5 predictions over the Great Lakes region. *Wea. Forecasting* **20**, 63–81.

Zimet T, Martin JE, Potter BE (2007) The influence of an upper-level frontal zone on the Mack Lake wildfire environment. *Meteorological Applications* **14**, 131–147.

Rossby waves, fronts and fires

Michael J. Reeder
School of Mathematical Sciences, Monash University, Victoria
michael.reeder@sci.monash.edu.au

Severe fire weather conditions in southern Australia are invariably associated with strong anticyclones, which direct very dry northerlies or northwesterlies on their western flanks from the interior of the continent across the region. These hot, dry airstreams precede the passage of strong cold fronts, which are subsequently followed by strong southerlies or southwesterlies.

This pattern of severe fire weather is associated with propagating Rossby waves, which grow to large amplitude and eventually irreversibly overturn. As an illustration of this, the potential vorticity (PV) on the 350 K isentopic surface on Black Saturday at 0600 UTC 7 February 2009 is shown in Fig. 1. Stratospheric air on this isentropic surface is characterized by cyclonic PV greater than about 1.5 PVU (meaning, in the southern hemisphere, PV less than about -1.5). For the most part, stratospheric air on this surface lies to the south of the continent with tropospheric air to the north. A prominent stratospheric filament lies roughly northwest-southeast from northwestern Australia to New Zealand. Likewise, a tropospheric filament lies across Victoria and the Tasman Sea. This pattern is characteristic of anticyclonic Rossby wave overturning. The process of overturning produces the low-level anticyclone and dry conditions over southern Australia, while simultaneously producing an upper-level trough and often precipitation in northeastern Australia. In this connection, floods occurred across much of Queensland around the time of Black Saturday. Hence, the heatwave in the southeastern part of the continent and heavy rain in the northeastern part can be viewed as two sides of the same coin.

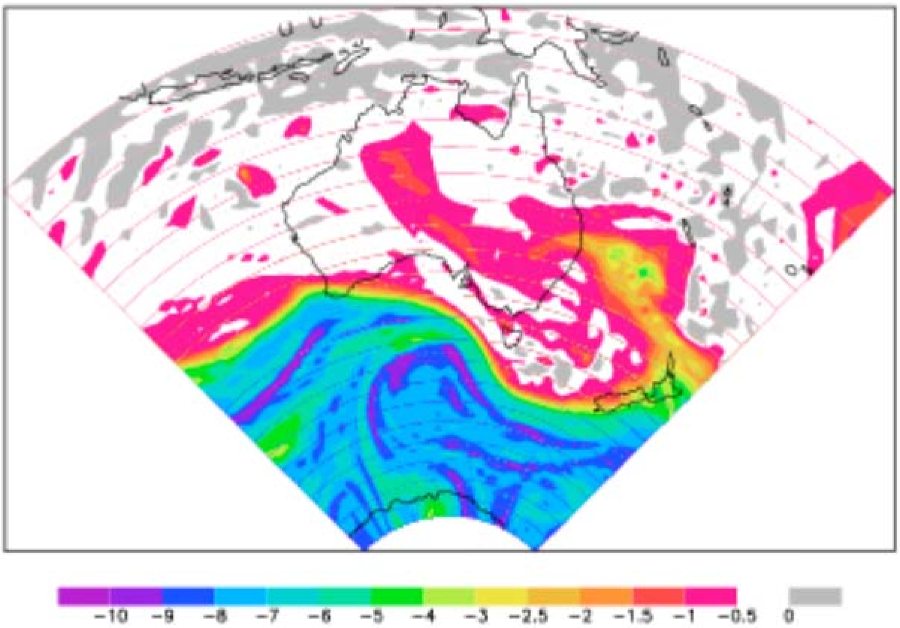

Figure 1. Potential vorticity on the 350 K isentopic surface at 0600 UTC 7 February 2009. Cyclonic potential vorticity exceeding 0.5 PVU is coloured.

Figure 2 shows the perturbation meridional wind on the 350 K isentropic surface *averaged* for all days in the period 1989 – 2006 on which a cold front passed Melbourne and produced a change of at least 20^{o}C. The perturbation is defined relative to the mean for all days in December – February in the period. Six days prior to the passage of the front, a packet of Rossby waves lies in the Atlantic. Subsequently, the packet propagates westward and amplifies. The passage of the front is associated with a large-amplitude packet centred on Melbourne.

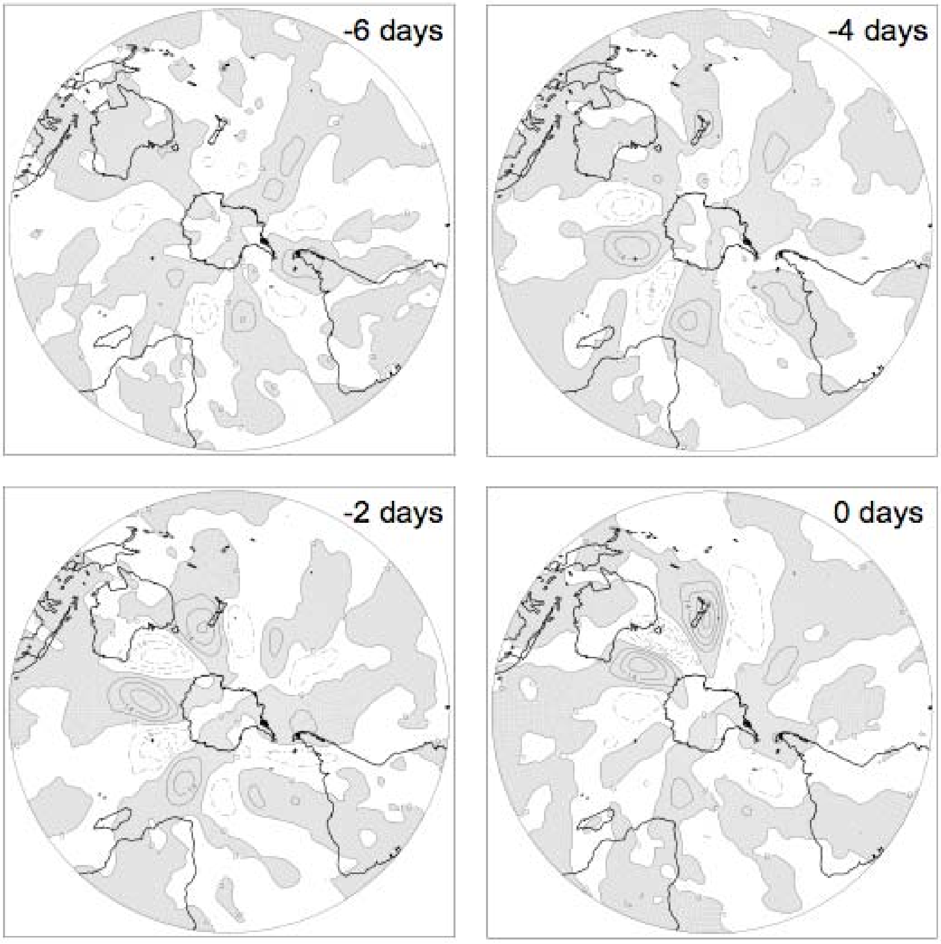

Figure 2. Isotachs of perturbation meridional wind on the 350 K isentopic surface, 6, 4 and 2 days prior to the passage of a strong front and on the day of the passage. Solid lines are positive (southerlies) and dashed lines negative (northerlies). Southerlies are shaded also.

Although not shown here, all major fires in Victoria (as defined by the Department of Sustainability web site) have been associated with a pattern of overturning Rossby waves.

Acknowledgement

Aspects of this work have been done in collaboration with my colleagues Olivia Martius (ETH, Zurich), Ruth Musgrave (Scripps Institution of Oceanography, San Diego) and Thomas Spengler (GFDL, Princeton).

Predicting environments of dry lightning ignitions

Andrew J. Dowdy[A, B] and Graham A. Mills[A, B]

[A]*Centre for Australian Weather and Climate Research, 700 Collins St, Docklands, Victoria, Australia.*
[B]*Bushfire Cooperative Research Centre, 340 Albert St, East Melbourne, Victoria, Australia.*

Introduction

Fires caused by lightning (hereafter referred to as lightning-fires) are responsible for a large proportion of the area burnt by wildfires throughout Australia and the world. A greater understanding of lightning-fires could be expected to produce benefits such as reducing the response time to these fires and the damage that they cause.

The chance of fuel ignition by lightning is relatively independent of fuel moisture, with some fuels igniting even though they may be very wet (Latham *et al*. 1997). In contrast, the chance that an ignition is sustained is highly dependent on fuel moisture (Wotton and Martell 2005). The high dependency of ignition survival on fuel moisture is the reason why the concept of ‘dry lightning’ (i.e. lightning which occurs without significant rainfall) is of importance.

A method for forecasting dry lightning has been developed by Rorig and Ferguson (1999) (hereafter RF99) in the Pacific Northwest of the U.S.A., based on high atmospheric instability (as represented by a large temperature difference between 850 hPa and 500 hPa) and low atmospheric moisture levels (as represented by high dewpoint depression at 850 hPa). This method is tested in this study for southeast Australian conditions, using NWP forecasts from MESOLAPS (Puri *et al*. 1998) combined with lightning, fire and rainfall observations.

Dataset preparation

Lightning stroke data were obtained from the commercial provider GPATS Australia. To classify whether a particular lightning stroke is ‘wet’ or ‘dry’, rainfall data have been obtained from a gridded analysis of rainfall observations (for details see http://www.bom.gov.au/climate/austmaps/metadata-daily-rainfall.shtml). Lightning-fire data were obtained from the Department of Sustainability and the Environment, Victoria, for fires ignited on public land.

The lightning-fire dataset contains the time that a fire was first observed, not the time that a fire was ignited. The lightning stroke closest in time prior to the first observation of a lightning-fire is used here as the most likely fire ignition time, provided that the lightning stroke occurred within an area of 0.05 degrees (~5 km) in both latitude and longitude of the fire ignition location. A maximum time of 3 days between the lightning and the fire first being observed has been used to provide a high degree of confidence in the lightning-fire ignition times. It is estimated, based on modelling lightning occurrence as a Poisson distribution, that more than 99% of ignition days will be correct as calculated using this method for the available lightning and lightning-fire datasets.

The relationship between dry lightning and fire occurrence

The number of lightning strokes that occurred during the period of this study (1 January 2000 until 31 January 2009) is shown in Fig. 1, distributed by the rainfall which accompanied them (using 1 mm bins to categorise the rainfall data). This is shown for strokes that were matched to fires as well as for strokes that were not matched to fires. The chance of fire per stroke is also shown for each rainfall amount.

RF99 use a rainfall threshold for defining dry lightning as less than one tenth of an inch (i.e. 2.54 mm). This value is similar to that for southeast Australian conditions, since the chance of fire per stroke increases very rapidly for rainfall amounts less than about 2-3 mm, with the average value occurring for rainfall amounts of about 5-7 mm.

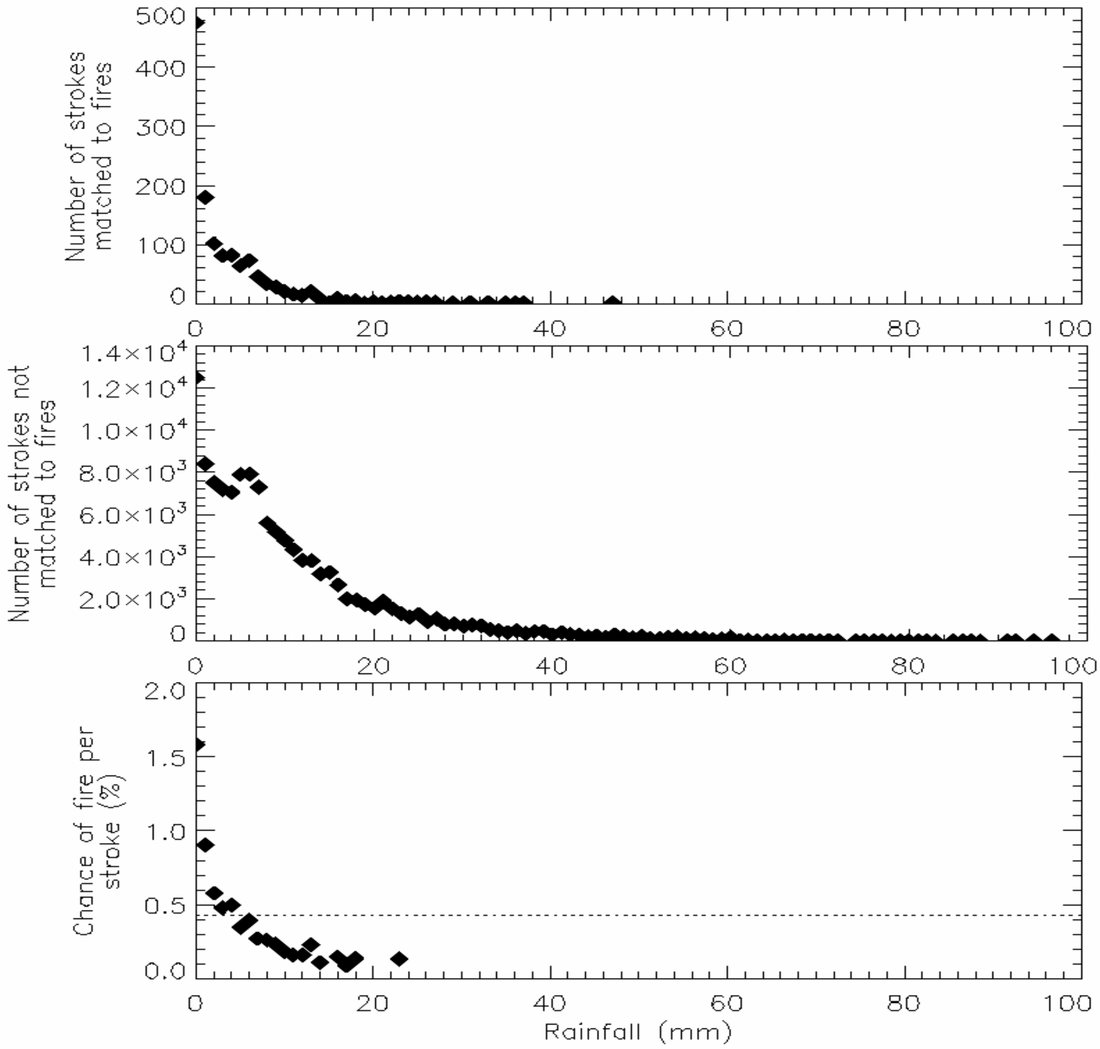

Fig. 1. The number of lightning strokes distributed by rainfall, shown for strokes that were matched to fires (upper panel) and for strokes that were not matched to fires (middle panel). The chance of fire per stroke is also shown (lower panel), with the dotted line representing the average chance of fire per stroke. The chance of fire per stroke has only been shown for values where the chance of fire per stroke multiplied by the total number of strokes is greater than 5 to avoid showing data that is based on very small sample proportions.

Modelling dry lightning

To examine the RF99 method for southeast Australian conditions, Fig. 2 shows lightning strokes categorised by the 850 hPa dewpoint depression and the 850 hPa – 500 hPa temperature lapse for 1700 AEDT (obtained from MESOLAPS). Plots are shown separately for dry strokes and wet strokes, (using the 2.54 mm rainfall threshold to define 'dry' or 'wet' lightning), as well as the ratio of dry strokes to all strokes (i.e. the sum of the number of dry strokes and the number of wet strokes) to provide an indication of the chance of dry lightning. Lightning data are used only for the period 1500-1900 AEDT from the start of November until the end of March. This time restriction produces a more targeted analysis, similar to that used by RF99, since this is when the vast majority of the lightning-fire ignitions occur.

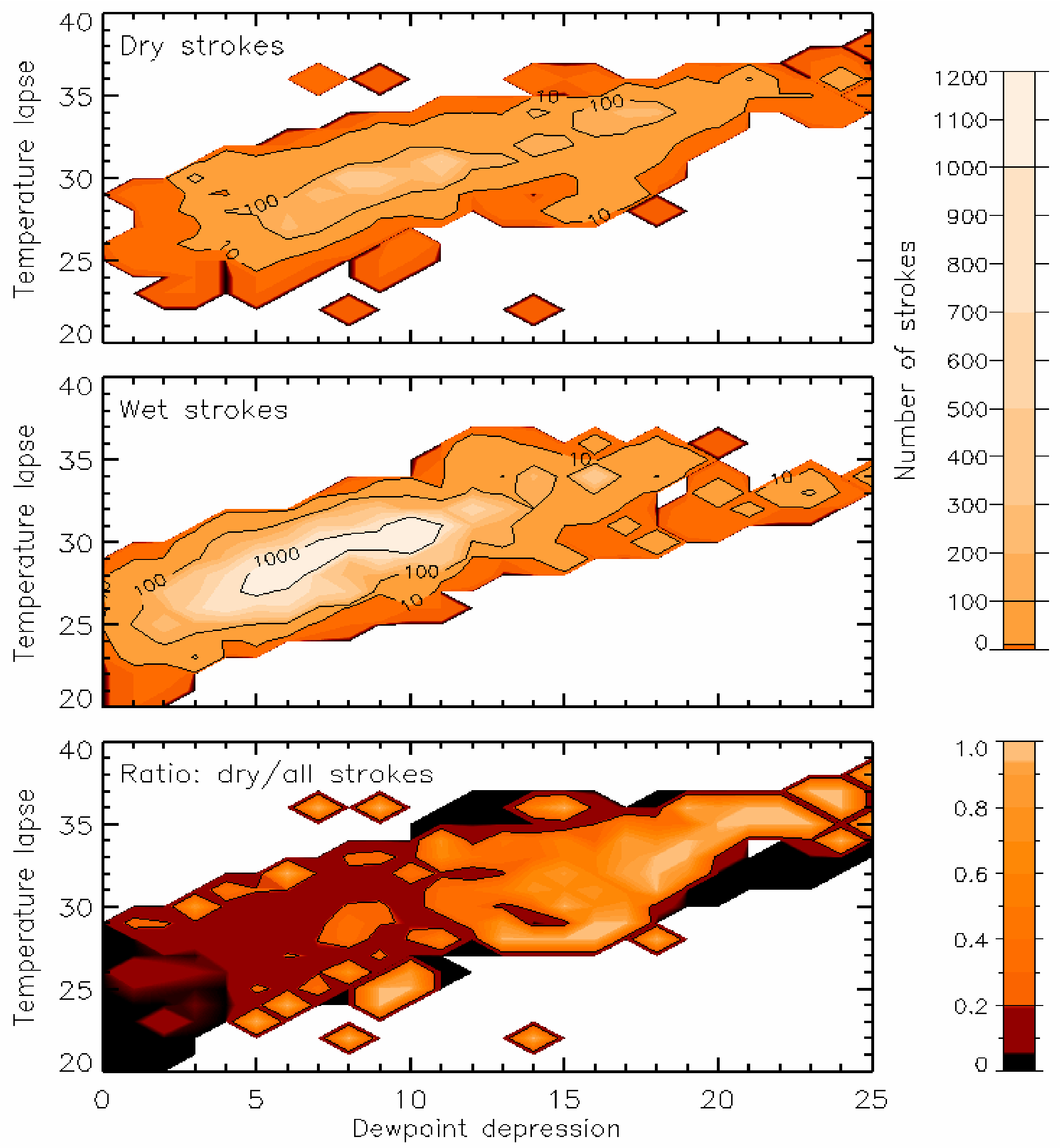

Fig. 2. The number of dry lightning strokes (upper panel) and wet lightning strokes (middle panel), distributed using the 850 hPa dewpoint depression and the 850-500 hPa temperature difference. The ratio of dry strokes to all strokes is also shown (lower panel) to provide an indication of the chance of dry lightning.

The results shown in Fig. 2 are consistent with the results of RF99 for the Pacific Northwest U.S.A. in that a similar rainfall dependence and phase space is apparent. There is typically a high (low) chance of dry lightning for high (low) values of the 850 hPa dewpoint depression (hereafter DPD) and the 850 hPa – 500 hPa temperature lapse (hereafter TL).

The dependence of the chance of fire per stroke on the DPD and TL (not shown) is very similar to the dependence of the chance of dry lightning on the DPD and TL (Fig. 2). High (low) values of DPD and TL typically indicate a high (low) chance of fire per stroke. Based on these dependencies, it was determined that ~75% of the increased number of fires that occur for high values of DPD (> 10˚C) and TD (> 30˚C) can be accounted for by the increased frequency of dry lightning as indicated by high values of DPD and TD.

Discussion

The climate of the Pacific Northwest U.S.A where the RF99 method was developed is considerably wetter and more humid than the southeast Australian climate, although it is similar in that lightning predominantly occurs in the mid-afternoon during the summer months. The fact that the results are reasonably similar in both regions indicates that the physics behind dry lightning may be somewhat universal: i.e. high-based thunderstorms with low atmospheric moisture at lower levels produce favourable conditions for the occurrence of dry lightning.

In addition to dry lightning, there are many other factors which can influence the chance of fire from the occurrence of lightning, such as traditional fire weather parameters (e.g. screen-level wind speed, relative humidity and temperature, as well as fuel moisture content). A number of these factors could be combined into an index which, when combined with lightning forecasts, could potentially produce forecasts of lightning-fire probabilities. Such an index could also be produced for statistical downscaling of lightning-fire occurrence from climate datasets (e.g. NWP climate simulations or reanalysis data), allowing the influence of climate change on lightning-fire occurrence to be investigated.

References

Latham D., Burgan, R., Chase, C. and Bradshaw, L. 1997. Using Lightning Location in the Wildland Fire Assessment System. *United States Department of Agriculture, Intermountain Research Station*, General Technical Report INT-GTR-349.

Puri, K., Dietachmayer, G.D., Mills, G.A., Davidson, N.E., Bowen, R.A. and Logan, L.W. 1998. The new BMRC Limited Area Prediction System (LAPS). *Australian Meteorological Magazine,* **47**, 203-223pp.

Rorig, M.L. and Ferguson, S.A. 1999. Characteristics of Lightning and Wildland Fire Ignition in the Pacific Northwest. *Journal of Applied Meteorology*, **38**, 1565-1575pp.

Wotton, B.M. and Martell, D.L. 2005. A lightning fire occurrence model for Ontario. *Canadian Journal of Forest Research*, **35**, 1389-1401pp.

Meteorological drivers of extreme bushfire events in southern Australia

Graham Mills

Centre for Australian Weather and Climate Research, Melbourne, Victoria, Australia

Introduction

Bushfires occur regularly during summer in southern Australia, but only a few of these fires have such an impact that they form part of the national psyche. These events become iconic due to their effects, either in terms of loss of life or economic and social cost. Such events include Black Friday (1939), the Hobart fires (1967), Ash Wednesday (1983), the Canberra bushfires (2003), and most recently Black Saturday in February 2009. In most of these events the weather of the day was statistically extreme in terms of heat, (low) humidity, and wind speed, and in terms of antecedent drought. There are a number of reasons for conducting post-event analyses of the meteorology of these events. One is to identify any meteorological circulation systems or dynamic processes occurring on those days that might not be widely or hitherto recognised, to document these, and to develop new forecast or guidance products. The understanding and prediction of such features can be used in the short term to assist in effective management of fires and the safety of firefighters and in the medium range to assist preparedness for the onset of extreme conditions. The results of such studies can also be applied to simulations of future climates to assess the likely changes in frequency of the most extreme fire weather events, and their documentary records provide a resource that can be used for advanced training purposes. In addition, particularly for events further in the past, revisiting these events using reanalysis data sets and contemporary NWP models can also provide insights unavailable at the time of the events.

Over the past few years the Bushfire CRC’s Fire Weather and Fire Danger project in CAWCR has studied the mesoscale meteorology of a number of major fire events, including the days of Ash Wednesday 1983, the Dandenong Ranges fire in January 1997, the Canberra fires and the Alpine breakout fires in January 2003, the Lower Eyre Peninsula fires in January 2005 and the Boorabbin fire in December 2007-January 2008. Various aspects of these studies are described below, including the structures of dry cold frontal wind changes, the particular character of the cold fronts associated with the most damaging fires in southeastern Australia, and some aspects of how the vertical temperature and humidity structure of the atmosphere may affect the fire weather at the surface. As this is a modelling workshop, the results will not only show how far NWP has come in the past 40 years, but also throw out a few challenges to model performance.

Dry cool changes

The dry cool changes of southern Australia are of particular concern to fire agencies because of their potential to change the flank of a fire burning under (typically) northwesterly winds to a long headfire burning under southwesterly winds. Accordingly, the forecast time of the “wind change” is critical for fire management decisions and firefighter safety.

During the 1980’s, with the coincidence of a surge in interest engendered by the Cold Fronts Research Program, together with the two highly visible cold frontal passages associated with the Melbourne dust-storm and a week later the Ash Wednesday fires in February 1983, concepts of pre-frontal troughs (PFT: Reeder 1986, Physick 1988) and of coastal surging of fronts (Garratt 1986) were developed to explain the apparent disparity between what had been analysed as a cold front on the synoptic analyses and the “early” arrival of the cool change through central Victoria. As NWP models developed through the mid-1990’s, and operational NWP model resolution increased to the scale where many of these processes were better resolved, guidance products that demonstrate the evolving structure of the cool changes were developed. The case study of the cool change on the day of the Dandenong Ranges fire (21 January 1997, Mills 2002) provides an example. Figure 1 shows the forecast wind and surface potential temperature forecasts for that day, with the times selected to demonstrate the evolving structure of the change as it moved through Victoria.

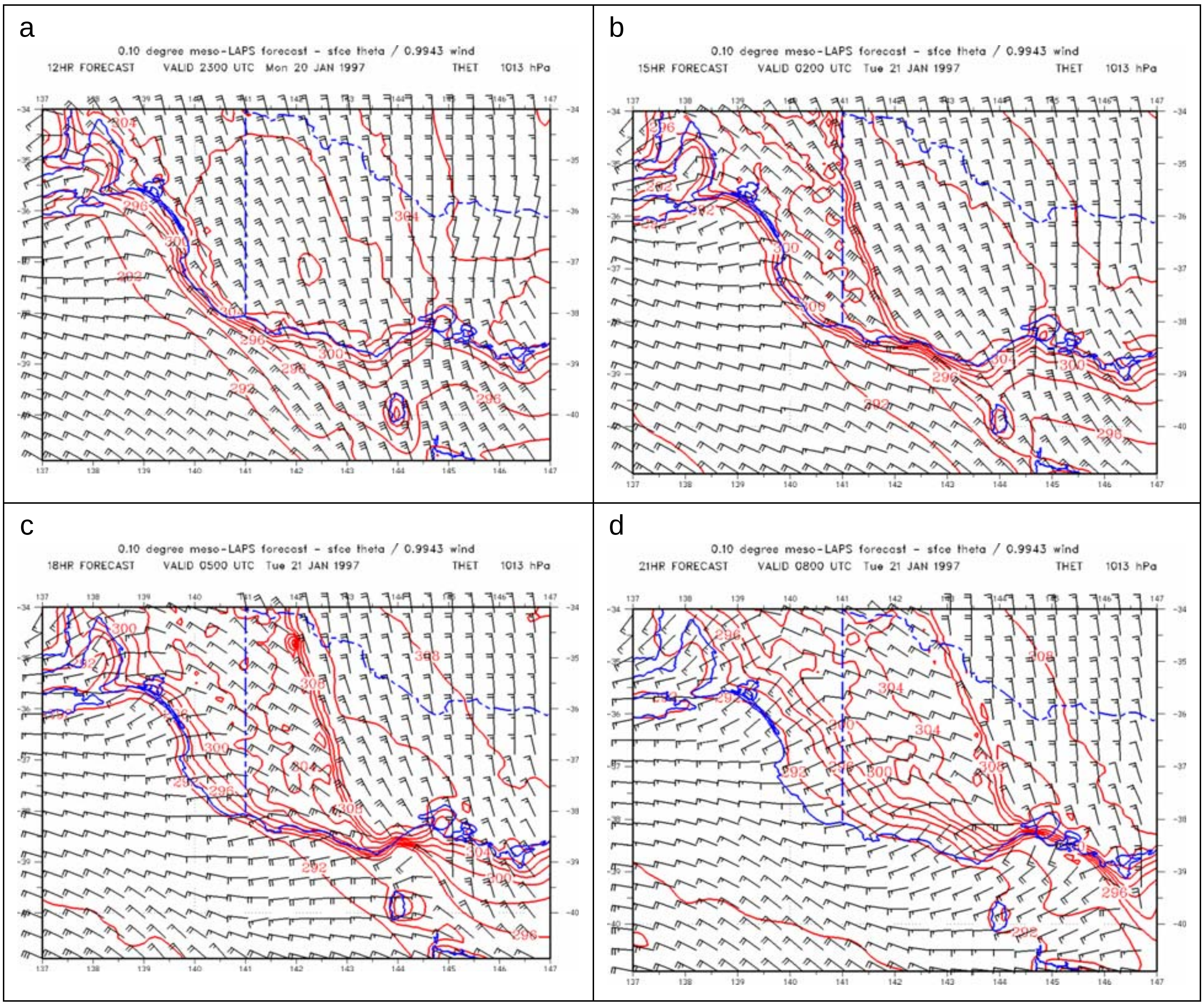

Fig. 1. Lowest sigma level potential temperature (K) and ~70 m wind barbs from a 0.1^{o} grid hindcast for the Dandenong Ranges fire event. Forecasts are valid at 2300 UTC 20 January 1997 (a), and 0200 (b), 0500 (c) and 0800 (d) UTC 21 January 1997.

Bearing in mind the association of the start of the wind change with the warm-air edge of a frontal temperature gradient, Fig. 1 reveals a number of interesting features. At 2300 UTC (Fig. 1a) the synoptic “front” can be inferred, from the cyclonic curvature of the wind field near the westernmost of the plotted isentropes, to be off the southeast SA coastline. An incipient PFT is forming on or just inland of SA’s southeast coast, and over western Bass Strait the offshore flow and offshore temperature gradient indicates that an internal boundary layer (IBL) is forming as the hot, continental air is cooled from below as it flows over the ocean. Two hours later (Fig. 1b) a well-developed PFT has moved into western Victoria, and a very strong temperature gradient has developed along the Victorian coast west of Cape Otway as the offshore winds back under the joint influence of the positive pressure anomaly generated by the denser air in the IBL and the negative pressure anomaly due to the hot (less dense) air overland, with the net effect being a strengthening of the coastal temperature gradient. However at this time the only cool change overland is in the far southwest of Victoria, and associated with the PFT.

By 0500 UTC (Fig. 1c) the change has surged northeastwards from the change of coastal orientation at Cape Otway, ahead of the extrapolated position of the PFT, and has just started to move inland along the coastline west of Cape Otway to the border. Three hours later (Fig. 1d) the surging coastal change is approaching Port Phillip, with an extremely abrupt directional shift, and tightly packed isentropes. Inland, the PFT has continued to move eastwards, but has weakened somewhat under the influence of post-frontal diabatic heating

Another example of the crucial role of coastal diabatic heating gradients in modifying cool change structure occurred on the evening of 30 December 2007, when a strong wind change caused disastrous changes in fire behaviour during the Boorabbin fire in WA. A west coast trough change was moving through southwest WA during the daytime of 30 December (Fig. 2a), but crucially a very strong temperature gradient was forming along the coastline near and west of Esperance (YEST). The resulting intensified pressure gradient led a strong southerly wind surge to move inland (Fig. 2b). Between Southern Cross (YSCR) and Kalgoorlie (YPKG), where the fire was running actively to the southeast ahead of the change, the west coast trough change reaches the area first as a southwesterly change, and the southerly surge follows a little later, with an increase in wind speed. Observations at Southern Cross are consistent with this forecast, with winds shifting through west-southwest to southwest between 1800 and 2000 WDT (0900-1100 UTC), and then shifting southerly and increasing in speed at about 2100 WDT (1200 UTC). These variations had major ramifications for the spread of the fire, with its northeast flank breaking out with the arrival of the first change, and the second shift to stronger southerlies exacerbating the spread of the fire, estimated at some 6 km/hr (Paul de Mar, personal communication), during that period.

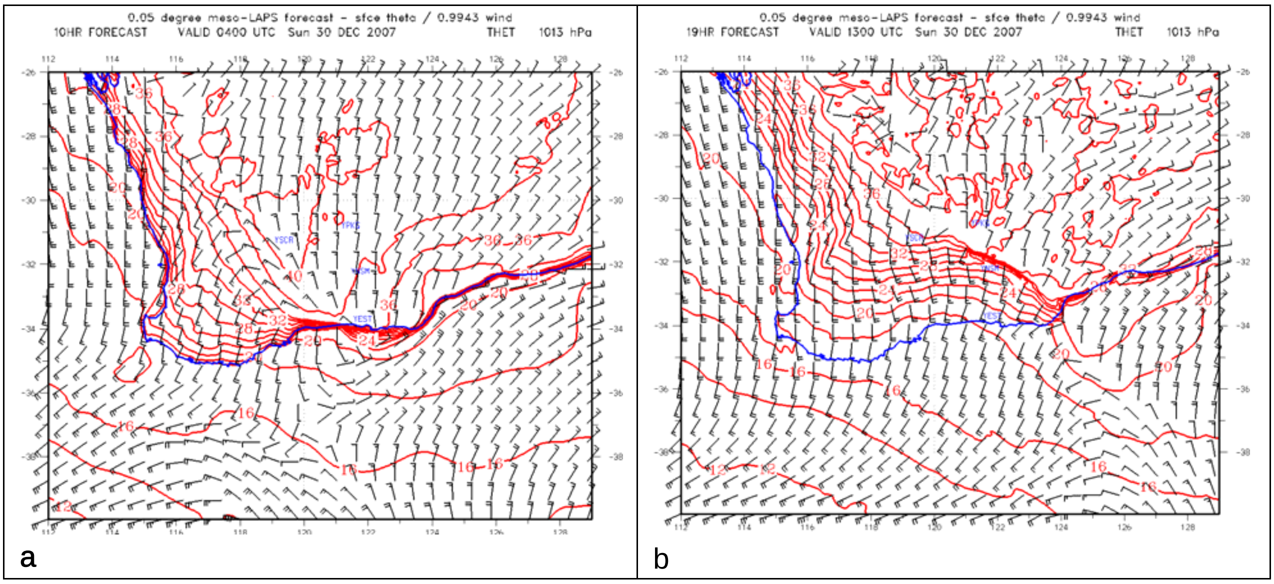

Fig. 2. Lowest sigma level potential temperature (K) and wind barbs at ~70m from a 0.1^{o} grid hindcast from a 0.05^{o} degree grid version of meso-LAPS (Puri et al 1998). The simulations are valid at 0400 UTC (a) and 1300 UTC (b) 30 December 2007.

These and other case studies suggest that diabatic processes, in conjunction with a necessary synoptic-scale frontogenetic environment, play a crucial role in determining the various morphologies of cool changes in Australia. If one also includes topographic blocking as an additional control, then many of the types of cool change known by local names, such as the Southerly Burster of coastal NSW, the Storm Bay low of southeast Tasmania (Mills and Pendlebury 2003), the Canberra afternoon “sea breeze” change (Mills 2007), and even some smaller scale features (eg Mills and Morgan 2006) can be explained in a common framework, and more details are found in those papers.

These and many other studies provide fascinating insight into the physical processes that generate these particular cold frontal morphologies, and mesoscale NWP models subjectively appear to forecast both their arrival times and associated weather sequences with extremely good levels of accuracy. Quantifying this impression is rather more difficult, given the complexity of defining a unique wind change time, and one of our projects has attempted to do just this.

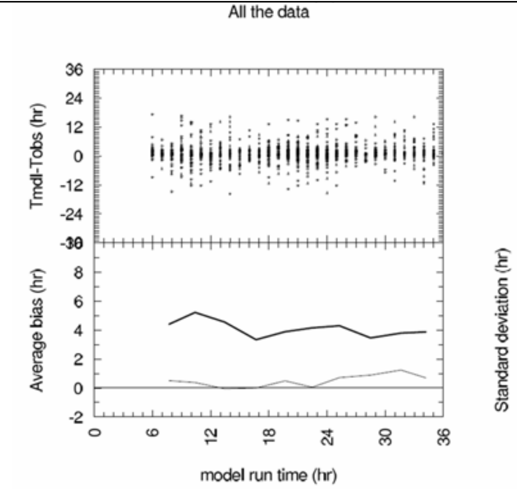

Fig. 3. Scatterplot of wind change timing error versus forecast lead time for Victorian Regional Forecast Centre wind change forecast days, with the lower graphs of showing the smoothed mean (thin line) and standard deviation (thick line) of error.

Huang et al (2008) have developed algorithms to determine wind change times from both observation and NWP model hourly (or more frequent) time series, and have shown that the highest resolution operational NWP model has an excellent performance in forecasting the timing of these wind changes (Fig. 3), and in particular shows little bias in timing error for lead-times out to 36 hours. While there is considerable scatter, much of this is due to the difficulty in many circumstances of determining a unique wind change time.

These results are extremely encouraging, but there is still room for improvement. Figure 3 indicates the degree of uncertainty that is inherent in contemporary mesoscale NWP predictions, and perhaps indicates that an ensemble-type approach is likely best practice for some time. In addition, nowcasting methods using AWS and Doppler radar observations, perhaps combined with extrapolation techniques, might be used for short-term updating when the wind change is very close.

The deep, strong fronts

The rapid fire spread following the post-change increase in wind speeds shown in Fig. 2 is a graphic example of the need to understand the structure of these changes, and be able to differentiate them from those after which the wind speed decreases. Ash Wednesday is a classic example of the former type, demonstrated in the anemograph record (Fig. 4) from Melbourne Airport for that day.

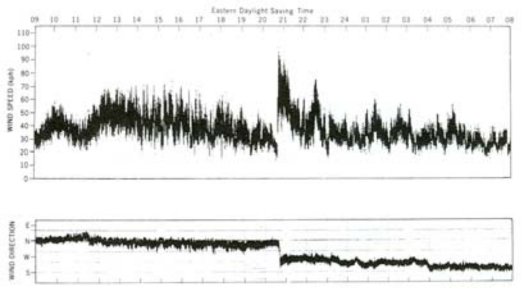

Fig. 4. Dines anemograph record from Melbourne airport on 16 February 1983. Upper panel is wind speed (km/hr), lower panel wind direction(degrees)

The wind was strong for many hours before the cool change, but increased dramatically with its passage, and then only very slowly declined. The dramatic effects of this on the fire spread are shown in Oliver (1984), and Bureau of Meteorology (1984) attributed the “blow-up” behaviour of the fires on that day to be partly due to the rapid eastward movement of the front. The availability of global NCEP and ERA40 reanalysis data allows retrospective modelling studies of events such as this, and based on these reanalyses, mesoscale NWP hindcasts provide data sets that can be used to diagnose the particular mesoscale meteorological characteristics of the event. To justify conclusions based on these diagnostic studies it is essential that the hindcasts reproduce the important weather of the day, and Fig. 5 shows such a forecast for Ash Wednesday, with the wind change just approaching Melbourne, and 20-30 kt winds covering a wide area west of the front. The quality of this forecast allows some confidence in using the NWP fields as a basis for a synoptic-diagnostic study.

Inspecting sequences of surface and synoptic analyses showed a number of apparently climatologically extreme features, including a very high amplitude upper trough and strong jet streak over southwest WA 24 hours earlier, and what subjectively appeared to be an unusually intense temperature gradient at 850 hPa (Fig. 6). A vertical cross-section, orientated southwest-northeast through the front over western Victoria (Fig. 7) shows a deep baroclinic zone with strong temperature gradient extending well west of the initial cool change and also through the depth of the troposphere, and with the jet stream extending down the sloping isentropes in the post-frontal air. The depth of this cold air, and the sustained temperature gradient in the cold air, generates the pressure gradient that drives the strong post-frontal winds.

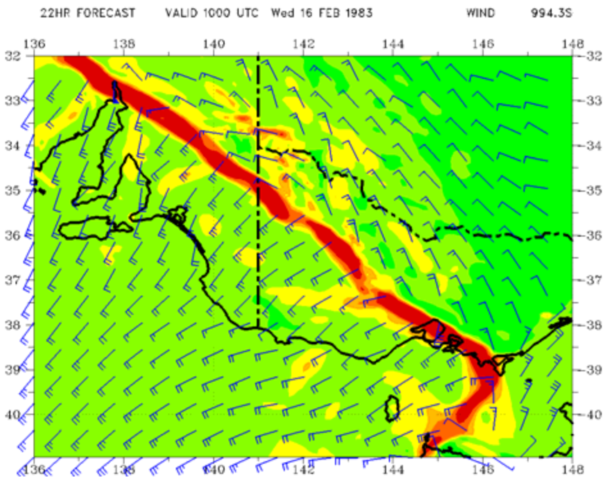

Fig. 5. Ten-hour 0.05^{o} grid forecast of ~70m wind barbs, and shaded, the Wind Change Range Index, with darker shading indicating more rapid rate of change of wind direction.

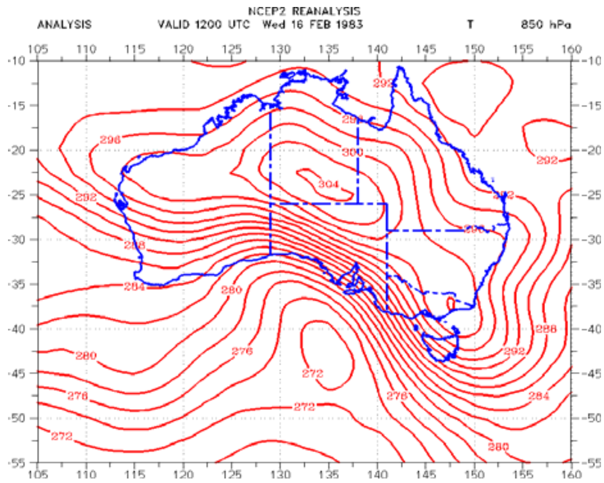

Fig. 6. NCEP-NCAR reanalyis field of 850 hPa temperature at 1200 UTC 16 February 1983.

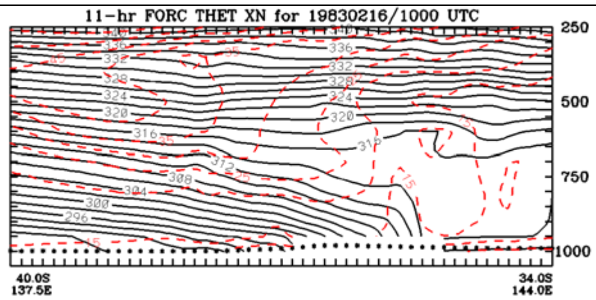

Fig.7. Cross-section of potential temperature (K, black contours), and wind speed (m sec^{-1}, dashed contours) through a southwest-northeast line crossing the coast near Mt. Gambier

In order to assess whether this 850 hPa temperature pattern (Fig. 6) is unusual for typical summertime cold fronts, the magnitude of the temperature gradient at 850 hPa was calculated at each reanalysis gridpoint (2.5^{o} intervals) over a 10^{o} x 5^{o} rectangle covering southeast Australia, and the highest value in the rectangle was calculated for analyses at 12-hour intervals for the 40 summers from December 1963 to February 2003 – some 7000 analyses. Ordering these by the magnitude of the temperature gradient ranked Ash Wednesday 1983 as the 10th highest in the data set, and if ordered by the magnitude of the east-west component of the temperature gradient it was the 5th highest in the 40 years. Clearly the day was meteorologically very extreme. It was also noted that several of the other dates in the top 30 temperature gradients (listed in Mills 2005a) were also associated with severe fire events. On 15 of these 30 days the fires that occurred were of sufficient impact that reports were readily found describing the incidents.

There are few rigorous data sets describing fire behaviour available to test any statistical relationship between the magnitude of the temperature gradient and the fire activity or effect. However, one statistic that is perhaps recorded more reliably than many others are deaths from bushfires. Emergency Management Australia maintains a disasters database[1] that lists bushfire deaths, and in the 40 years of this meteorological study, some 80% of deaths in southeastern Australia occurred on those 30 days of the most extreme temperature gradients.

The fact that the strength of the east-west component of the temperature gradient appears to have a role in discriminating these events suggests that the isotherms are oriented more north-south in these cases, which further suggests that high temperatures are likely on the eastern side of the gradient. This distribution can be visually presented in terms of a scatterplot of maximum value of the

[1] http://www.ema.gov.au/ema/emadisasters.nsf/webEventsByCategory?OpenView

temperature gradient plotted against the highest temperature in the subgrid (Mills 2005a, his Fig. 16). The extension of this analysis to cover the 46 summers to the end of February 2009 is shown in Fig. 8, with notable (documented) events highlighted. The clustering of events in the top right hand section of the phase-space is clear, and it is striking that in the 6 years since the Mills (2005) study the Hobart fire day has moved from 30th to 40th on the list of strongest temperature gradients, while the days of the Stawell fires on New-Years Eve 2005, the Brisbane Ranges fires in January 2006, and Black Saturday in February 2009 are notable additions.

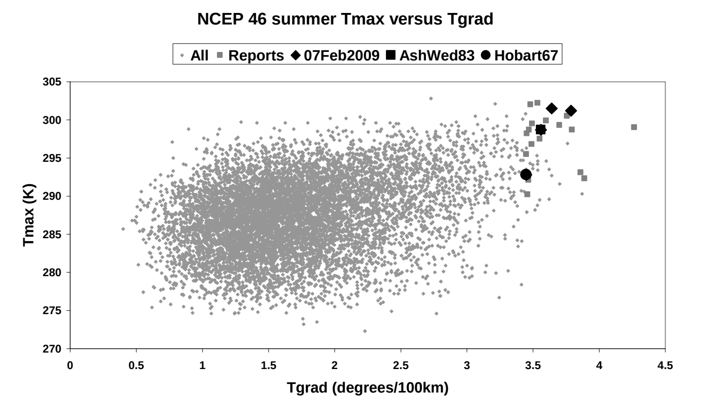

Fig. 8. Scatterplot of maximum value of temperature gradient at 850 hPa in the sub-grid over southeastern Australia versus the highest temperature at 850 hPa in the subgrid, based on NCEP reanalysis data for the summer months from December 1963 to February 2009. Significant events are highlighted.

The simplicity of this measure, being based only on 850 hPa temperature, together with the ever increasing quality of medium-range global forecasts, makes a medium range alert system attractive. While this would not provide a forecast of the weather-element sequence associated with any particular front, in the medium range that is not the vital need – it is the warning that extreme fire weather is likely that would allow increased time to implement preparedness measures.

Similarly the measures shown in Fig. 8 can also be calculated from GCM model simulations of current and future climate to assess changes in frequency of such events under differing climate scenarios. Hasson et al. (2009) have reported such a study, based on IPCC model scenarios, and have shown an increasing trend in the number of extreme frontal passages with time, depending on the degree of anthropogenic forcing specified in the GCM simulation, albeit with considerable model-to-model scatter. This study should be revisited with future GCM simulations.

Vertical humidity structures – the "dry slots"

Assessing the time-series of AWS data from Canberra Airport after the fires on 18 January 2003, the sharp decline in humidity (Fig. 9) was striking, and its cause was investigated. As similar behaviour was seen in AWS observations from several stations in the elevated regions of southeast NSW that day, it is more likely to be a mesoscale meteorological feature rather than (as was suggested in the immediate aftermath of the event) due to fire-induced vertical circulations. As fine fuel moisture content responds rapidly to changes in atmospheric humidity, it can be hypothesised that the lowering atmospheric humidity might lead to an increase in fire activity. Analysis showed that a mid-tropospheric dry band, clearly identifiable in geostationary satellite water vapour channel imagery, moved over Canberra at around the same time as the dewpoint decreased rapidly (Mills 2005b). It was proposed that dry convective mixing through a very deep mixed layer (extending to 600 hPa at Wagga that morning) would potentially allow the mid-tropospheric dry air to mix to the surface. A second mechanism, enhanced mixing caused by perturbations to the entrainment layer by the frontal updraft associated with the easterly cool change that arrived a little after 0700 UTC, was also proposed.

Modelling the event provides support for these hypotheses, but also poses a significant challenge for modellers. A mesoscale NWP forecast of screen level dewpoint (Fig. 10) shows two axes of minima in the dewpoint field – one oriented northwest-southeast that aligns with the satellite-observed dry feature, and one roughly parallel to the coast and advancing westwards ahead of the advancing easterly change that supports the enhanced frontal mixing hypothesis. However the challenge lies in the absolute value of the dewpoint minima – the lowest values forecast are around 0C, while dewpoints lower than -10C were observed at many stations. Even allowing for non-linearity in dewpoint calculations, this is a significant difference.

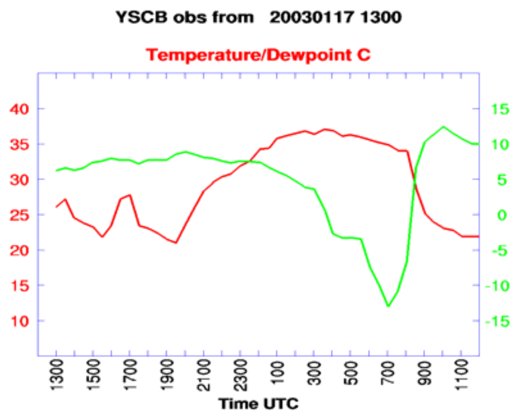

Fig. 9. Time series of temperature (left) and dewpoint (right) observations at Canberra Airport from 1200 UTC 17 January 2003.

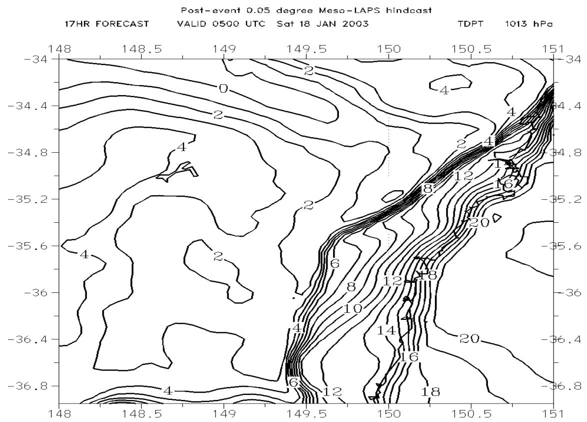

Fig. 10. 0.05^{o} meso-LAPS forecast of screen level dewpoint (C) valid 0500 UTC 18 January 2003.

This study may only have been of phenomenological interest, but two years later similar behaviour was seen in association with the Lower Eyre Peninsula fires on 11 January 2005 (Mills 2008a), and two overseas case studies of abrupt lowering of surface humidity associated with upper-tropospheric subsidence and enhanced fire behaviour were published – the Mack Lake fire (Zimet et al 2007) and the Double Trouble State Park fire (Kaplan et al 2008). These studies, and some anecdotal reports of unusual fire activity during prescribed burns, suggest that effort directed towards understanding and accurately forecasting these events might aid fire managers, and the synoptic climatology and case studies of easterly changes in Mills (2008b) and Mills (2007) are a step towards this.

Discussion

The examples discussed above are only a very small part of the possible range of subsynoptic meteorological phenomena that might affect fire behaviour, and are very much focussed on the author's own work. There are many other studies, and many avenues for further studies, that provide increased understanding of the synoptic drivers of major fire events.

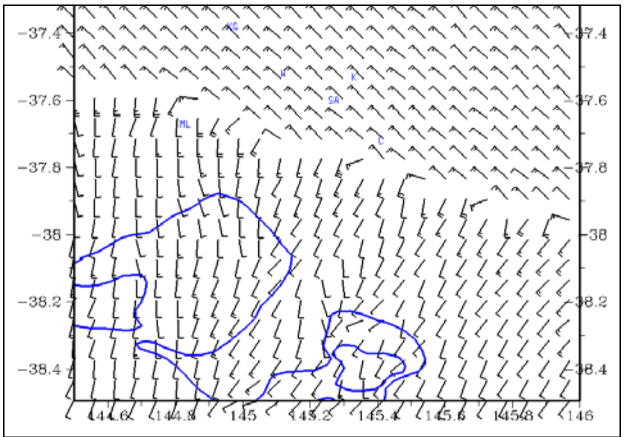

Fig. 11. Twenty-five hour forecast of the Black Saturday cool change screen level wind speed and direction using a version of the ACCESS NWP system, with nesting down to 3km grid-spacing.

Continuing NWP system development suggests that forecasts of these features will continue to improve. An example (and thanks to Les Logan and Kamal Puri for providing these forecasts) is the 3 km ACCESS NWP simulation (Fig. 11) of the Black Saturday cool change, with the change structure, the strong winds just behind the change, and then the lull in the winds over the Melbourne basin, all well simulated. However, there is a long way to go before forecasts of actual fire behaviour are routine, and there are many steps along that path that need to be taken. One obvious evolutionary step is to continue down the path of higher and higher resolution meteorological modelling, so that the spatial and temporal variations of the wind flow on the scale of the topography in which a fire is burning are resolved. How to communicate this detail in a way that it can be effectively used in making fire management decisions is of course a major additional step.

Understanding and then predicting the way that a fire may interact with the atmosphere is a field that is hardly tapped as yet. The coupled modelling approaches of Linn et al (2002) and Coen (2005) show the excitement that lies in following that path. While these studies are moving towards routine prediction of fire behaviour with coupled models, idealised studies that increase our understanding of how the atmosphere and a fire interact, using very high resolution modelling and a specified heat source to represent the fire (eg Kiefer et al 2009, Cunningham and Reeder 2009), can provide giant steps forward in our understanding of how the vertical structure of the atmosphere affects how the atmosphere-fire feedback processes develop.

References

Bureau of Meteorology, 1984. Report on the meteorological aspects of the Ash Wednesday fires – 16 February 1983. Bureau of Meteorology, Australia 143pp.

Coen, J.L., 2005. Simulations of the Big Elk Fire using coupled atmosphere-fire modelling. *Int. J. Wildland Fire 14*, 49-59.

Cunningham, P., and M. Reeder 2009. *Geophysical Research Letters* 36, L12812, doi:10.1029/2009GL039262.

Garratt, J.R. 1986. Boundary layer effects on cold fronts at a coastline. *Bound. Layer. Met.* ***36***. 101-105.

Hasson, A.E.A., G.A.Mills, B.Timbal, and K.Walsh, 2009. Assessing the impact of climate change on extreme fire weather events over southeastern Australia. *Climate Research* ***39***, 159-172.

Huang Xin-Mei, Ma Yimin, and G.A. Mills 2008. Objective verification of operational mesoscale NWP model wind change forecasts. CAWCR Technical Report CTR008, 72pp.

Kaplan, M.L., C. Huang, Y-L. Lin, and J.J. Charney 2008. The development of extremely dry surface air due to vertical exchanges under the exit region of a jet streak. *Meteorol. Atmos. Phys. 102,* 63-85.

Kiefer, M.T., M.D. Parker, and J.J. Charney 2009. Regimes of dry convection above wildfires: idealised numerical simulations and dimensional analysis. *J. Atmos. Sci. 66*, 806-836.

Linn, R., J. Reisner, J.J. Colman and J. Wintercamp 2002. Studying wildfire behaviour using FIRETEC. *Int. J. Wildland Fire 11*, 233-246.

Mills, G.A., 2002: A case of coastal interaction with a cold front. *Aust. Meteor. Mag.* ***51***, 203-221.

Mills, G.A., 2005a. A re-examination of the synoptic and mesoscale meteorology of Ash Wednesday 1983. *Aust. Meteor. Mag.* ***54***, 35-55.

Mills, G.A., 2005b. On the sub-synoptic scale meteorology of two extreme fire weather days during the Eastern Australian fires of January 2003. *Aust. Meteor. Mag.* ***54***, 265-290.

Mills, G.A., 2007. On easterly changes over elevated terrain in Australia’s southeast. *Aust. Meteor. Mag.* ***56***, 177-190.

Mills, G.A., 2008a. Abrupt surface drying and fire weather Part 1: Overview and case study of the South Australian fires of 11 January 2005. *Aust. Meteor. Mag.* ***57***, 299-310.

Mills, G.A., 2008b. Extreme surface drying and fire weather Part 2: A preliminary synoptic/dynamic climatology in the forested areas of southern Australia. *Aust. Meteor. Mag.* ***57***, 311-328.

Mills, G.A. and S. Pendlebury, 2003. Processes leading to a severe wind-shear incident at Hobart Airport. *Aust. Meteor.Mag.* ***52***, 171-188.

Mills, G.A., and E. Morgan, 2006. The Winchelsea Convergence – using radar and mesoscale NWP to diagnose cool change structure. *Aust. Meteor. Mag.* ***55***, 47-58.

Puri, K., G. S. Dietachmayer, G. A. Mills, N. E. Davidson, R. A. Bowen, and L. W. Logan, 1998: The new BMRC Limited Area Prediction System, LAPS. *Aust. Meteor. Mag.,* ***47,*** 203–223

Physick, W.L. 1988. Mesoscale modelling of a cold front and its interaction with a diurnally heated land mass. *J.Atmos. Sci.* ***45***, 3169-3187.

Oliver, J., Britton, N.R., and James, M.K., 1984. The Ash Wednesday Bushfires in Victoria. *Disaster Report No 7,* Centre for Disaster Studies, James Cook University of North Queensland, Townsville, Australia. 147pp

Reeder, M.J. 1986. The interaction of a surface cold front with a prefrontal thermodynamically well-mixed boundary layer. *Aust. Meteor. Mag.* ***34***, 137-148.

Zimet, T., Martin, J.E., and Potter, B.E., 2007. The influence of an upper-level frontal zone on the Mack Lake wildfire environment. *Meteorol. Appl. 14*, 131-147.

Climate change impacts on fire weather

Christopher Lucas

Centre for Australian Weather and Climate Research

Melbourne, VIC Australia

Introduction

Over the last decade, Australia has seen a very high level of bushfire activity. The focus and impact of this activity has been on the populous southeast, but relatively high levels of fire activity have been experienced nationally. The source of this increase in fire activity has been the subject of public debate. Is it related to climate change, or is it the result of insufficient fire and land management practices? Given the high impact on bushfires on society, answering these questions has important implications for the management and control of this phenomenon.

This paper will contribute to this debate by investigating how the observed fire weather has changed in recent decades. How large are the changes in fire weather? Where are they occurring? How well do they agree with previous projections of the impact of climate change? Answering these questions is the main thrust of this paper.

Data

The data used in this study are the high quality fire weather data described by Lucas (2009). Briefly, these data compute a daily value of the McArthur Forest Fire Danger Index (FFDI) from 1500 local time observations of relative humidity and wind speed along with maximum temperature. The drought factor calculation is based on the Keetch-Byram Drought Index (KBDI) and uses the daily rainfall observations from 0900 LT. There are 77 stations available, although not all are used. The dataset extends from 1973 to the present.

These data are processed and analysed to produce seasonal time series of the median and 90th percentile FFDI. The seasons are the standard meteorological seasons (i.e. DJF, MAM, JJA and SON). The median provides information on the general nature of the season. A higher median means a generally greater fire weather danger during that season. The 90th percentile provides insight into the upper extremes of a given season; what the worst fire weather days in a given season are like. An annual measure, cumulative FFDI (ΣFFDI) -- the sum of all FFDI values over 1 year (defined here from July through the following June) -- is also used.

An important finding of Lucas (2009) is the quantification of the errors in the seasonal distribution of FFDI associated with inhomogeneities in the wind speed data, present to some degree at all stations in the dataset. With this knowledge and a quantification of the wind inhomogeneities, adjustments can be made to the median and 90th percentile FFDI to accurately place current and past observations of FFDI into a historical context free from the effects of instrumentation changes and other technical issues. Note that *individual* observations are not corrected with this methodology, only the seasonal statistics. A similar correction can also be applied to ΣFFDI.

Projected impacts of climate change on fire weather

Henessey et al. (2005) and Lucas et al. (2007) used the results of climate simulations from the CSIRO CCAM Mark 2 and Mark 3 models to estimate the likely effects of global warming on fire weather in south-eastern Australia. Projections were made for 2020 and 2050 using a both high and low emissions scenarios. From these climate simulations, projected changes in maximum temperature, humidity rainfall and wind speed were applied to the observed meteorological observations (centred on 1990) for each year/model/forcing scenario (8 in total). Fire dangers were re-computed and compared to the current climatology to ascertain the projected changes to fire weather.

Table 1. Expected trends in DJF median FFDI from the climate change simulations. Units are points of FFDI per decade.

site	2020 Mk 2	2020 Mk 3	2050 Mk2	2050 Mk3
Melbourne AP	0.2	0.1	0.4	0.1
Sydney AP	0.2	0.1	0.2	0.1
Canberra	0.3	0.1	0.6	0.1
Hobart	0.0	-0.0	0.0	0.0
Adelaide	0.2	0.1	0.1	0.1

The largest changes to the fire danger variables occurred in the maximum temperature and the rainfall. Changes to wind speed and relative humidity were comparatively small. Typically, maximum temperatures increased by around 0.9^{o}C and 2.8^{o}C in 2020 and 2050, respectively, Annual rainfall changes were more variable and showed model-dependent effects. Simulations using CCAM Mk 2 showed decreasing annual rainfall at in both 2020 and 2050. However, using the Mark 3 model, rainfall actually increased in some locales, particularly by 2050. At Sydney Airport (AP), annual average rainfall is projected in increase by over 25% by 2050 in the Mark 3 High scenario.

Overall, these changes result in an overall increase in the fire weather danger in most locations. By 2020, the high forcing scenarios show changes in ΣFFDI of around 10% in most locales.. By 2050, the increase is even stronger, with changes in ΣFFDI of 25-35%. The projected changes are not linear, but rather accelerate between 2020 and 2050. There is also a spatial dimension to the change, with projected 2050 changes being lower in South Australia and Tasmania. The projections show negligible change to fire weather danger in Hobart, even by 2050.

By examining the median statistics of the simulated data, an estimate the expected trend can be made. These are summarized in Table 1 for 2020 and 2050 from the strong global warming scenarios in those studies for the capital cities in the southeast. At the locations selected, the trends are generally on the order of 0.1-0.2 points per decade. At a few other sites, more inland than those listed here, the trends were 2-3 times larger

Lucas et al. (2007) also noted changes in the seasonality of the fire danger. Of all the changes in the active fire season, the changes in DJF were usually the smallest. Instead, the largest changes were typically observed in spring (SON), with a sharp increase in median FFDI predicted. There was also some tendency towards higher trends in the autumn (MAM), although this was not as consistent across the stations studied. In general, this implies an earlier start to the fire season and an increased number of dangerous fire weather days in spring.

Observed trends in FFDI

Figure 1 shows a time series plot of the observed median and 90th percentile FFDI in DJF at Melbourne Airport. The solid lines are the wind-corrected values, dotted lines are the raw values. The strength of the 4 breakpoints in the monthly mean wind time series are on the order of 2-3 km/h at this station (relatively small) and hence the corrections applied to the time series are also relatively minor. See Lucas (2009) for full details of the breakpoint analysis and correction.

The two time series show a distinct change in behaviour in 1997. Before that date, the median FFDI was typically around 7; afterward, a value of 9 or above is not unexpected. Both the 2006-07 and 2008-09 summers has median FFDI above 12, the 'high' fire danger rating. A similar pattern is seen in the 90th percentile, with values around 25 before 1997 and values of 35 and above after that date. In both series, the interannual variability is considerably larger after 1997. The number of extreme fire weather days, both in the summer and otherwise, has also seen an increase since the late-1990s. These general pattern of a sharp change in the character of fire weather are seen at many stations in the southeast.

Figure 1 also shows a trend line, computed using ordinary least squares-regression for each series from the period 1973 through 2009. The trends are quite obvious, with values of 0.6 and 2.5 points of

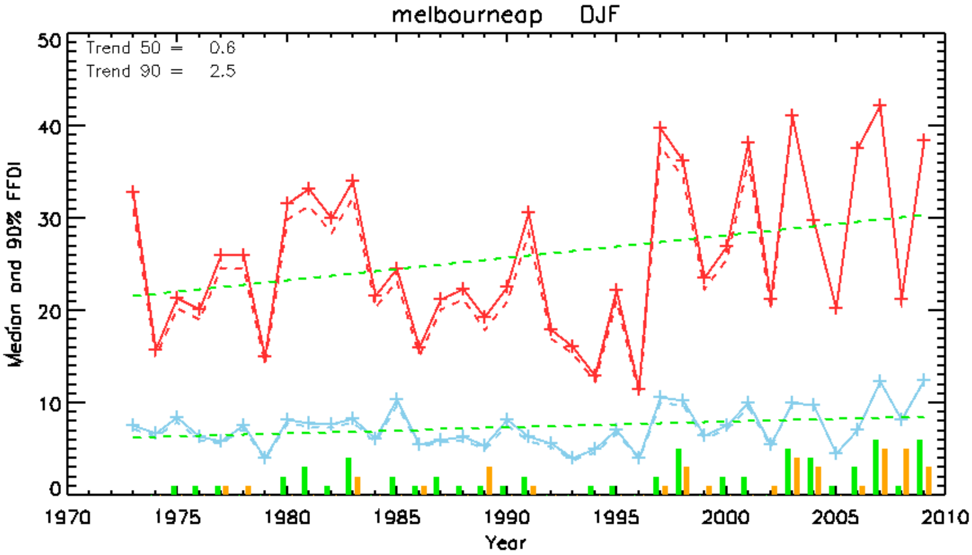

Figure 1. Time series of the median (blue) and 90th percentile (red) FFDI during DJF at Melbourne AP. The uncorrected values of each series are also shown (dashed lines), as well as the computed trend lines. Along the bottom, the number of extreme fire weather days (FFDI > 50) in DJF (green, on left) and in other seasons (orange, right). The same scale is used for this plot but for the number of days.

FFDI per decade. However, in both series the trends are only significant at the 90%-level. The values of the trends are large, but the variance in the series reduces the significance.

This same procedure is applied nationally to 42 of the stations in the fire weather dataset described earlier. Figure 2 shows the observed trends in median FFDI during the summer months (DJF); Figure 3 shows the trends for spring months (SON).

In DJF, the highest trends are seen in the general Murray-Darling Basin (MBD) region, with strong trends extended roughly from Adelaide to northern NSW (Cobar and Dubbo) and southward to Wagga. The peak trend value of 2.5 points per decade is observed in Mildura. Strong positive trends are also noted in western QLD and southern NT. Over the remainder of the country, trends are smaller and generally insignificant. A few negative trends are seen, notably in Giles and Forrest in eastern WA. In general, this same pattern is seen in the 90th percentile trends for DJF (not shown).

By way of contrast, a greater portion of Australia has observed significant positive trends in FFDI during spring (Fig 3). As before, strong trends are observed in the MDB and in central Australia. Further, significant trends are seen throughout VIC, southward into TAS and along the central NSW coast. In the west, a region of significant positive trends is seen in a large portion of central and western WA. A significant positive trend is also noted in Darwin.

Although not shown, the other two seasons also display large regions of significant positive trends. In autumn (MAM), most of eastern Australia, from central QLD to southern NSW, shows strong trends in median FFDI in excess of 1 point per decade. In winter (JJA), the trends are weaker but widespread across the majority of the country at least the 90% significance level.

Discussion

Fire weather is clearly changing across Australia, with a tendency towards more dangerous conditions being observed across the country. Significant trends in median and 90th percentile FFDI are observed in all seasons, but overall, it is the summer months – the peak of the southern fire season-- that shows the least amount of change. The largest changes are occurring in the spring and autumn, broadly consistent with the model projections. The fire season is lengthening, with an earlier start and a later end. The number of 'extreme' fire weather days is increasing in spring, summer and autumn. In a

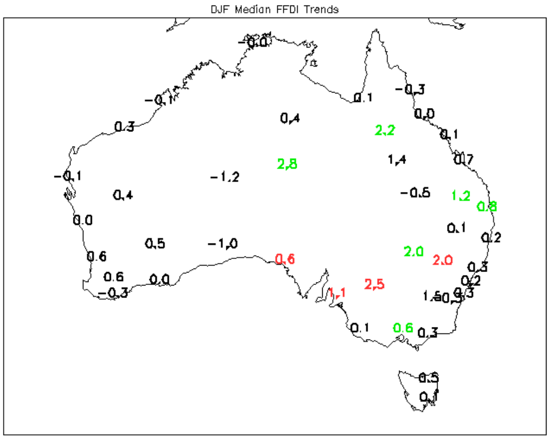

Figure 2. Computed trends in median FFDI during DJF. Values are in points per decade. Colour of number indicates level of significance, where black is non-significant, green is 90%, orange is 95% and red is 99%.

regional sense, the Murray-Darling Basin region is seeing the biggest change in fire weather danger, with significant positive trends observed in all four seasons. In general, the eastern portion of Australia is seeing larger trends in more seasons, but almost every region shows some degree of change

In southeastern Australia, the observed changes in fire weather are happening more quickly than suggested by the simulations (Table 1). The trends in median FFDI are stronger than projected in most seasons, particularly in the MDB. Something similar was suggested in Lucas et al (2007) with apparent jumps in ΣFFDI since the early 2000s. The analysis here, correcting for the wind inhomogeneities in the data, supports those claims, although lessens the magnitude of the jumps. In any case, there is ample evidence of changes in the last decade or so are approaching the magnitude of changes expected for 2050.

In the end, the cause of the rapid changes in fire weather still remains subject to some uncertainty. The possibility of interdecadal variability cannot be ruled out; the longer-term records shown in Lucas et al. (2007) clearly indicate that possibility. If there is a significant effect of longer-term variability, the recent weather may not reflect the true longer-term trends. In the southeast, there is also likely a link with the ongoing drought, where the influence of climate change is suggested but not confirmed. There is also the possibility that the estimations of the trend are incorrect. Trend calculations are sensitive to the choice of the start or end date. The 1973-75 period, the start time of the calculation here, was the wettest period in the 20th Century throughout Australia, resulting in a extended period of low fire dangers. This could be inflating the values of the trends in the present.

More broadly, fire weather is clearly changing for the worse in recent decades. However, a direct attribution to anthropogenic climate change cannot be made at this time. The role of fuel and fire management practices on the occurrence and outcome of bushfires remains uncertain. Excess fuel loads could certainly be driving some of the severity of the fires. Answering this question is not clear cut as the response of the vegetation to enhanced CO2 and a changing climate remains uncertain. A considerable amount of work remains in order to untangle cause and effect in this trickly question.

References

Hennessy, K., C. Lucas, N. Nicholls, J. Bathols, R. Suppiah and J. Ricketts, 2005: *Climate change impacts on fire-weather in south-east Australia*. Consultancy report. CSIRO Marine and Atmospheric Research and Australian Government Bureau of Meteorology, 88 pp,.

Lucas, C., K. Hennessy, G. Mills and J. Bathols, 2007: *Bushfire weather in southeast Australia: Recent trends and projected climate change impacts*. Consultancy report for The Climate Institute of Australia. Bushfire CRC and CSIRO Marine and Atmospheric Research, 79 pp.

Lucas, C.,2009: On developing a historical fire weather dataset for Australia. In press, *Austr. Meteor. Oceangraphic Journal*.

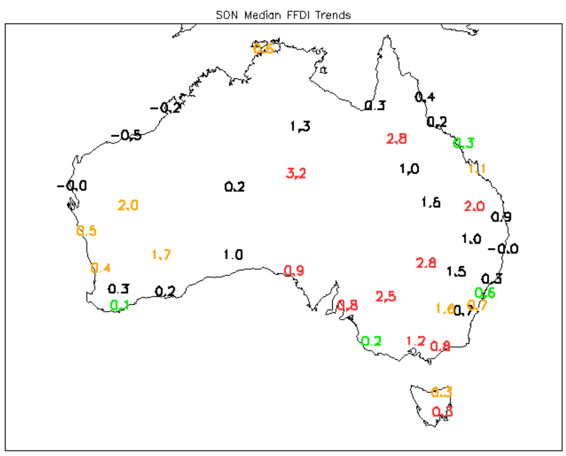

Figure 3. As in Figure 2, expect for SON median FFDI.

European heatwaves in a changing climate

Erich M. Fischer[1,2], and Christoph Schär[1]

1 Institute for Atmospheric and Climate Science, ETH Zurich, Switzerland
2 National Center for Atmospheric Research (NCAR), Boulder, United States

Introduction

Changes in the frequency, intensity and duration of climate extremes have socio-economic impacts that reach far beyond the effects of rising global mean temperatures. Recent European summer heatwaves have demonstrated how dramatically single extreme events can affect even today's society. The record-breaking 2003 heatwave increased mortality by around 35,000 heat-related deaths across Europe (e.g., Vandentorren et al. 2004; Hémon and Jougla, 2004; Schär and Jendritzky, 2004). Similar albeit weaker impacts have been observed during the 1976 heatwave, which caused an average mortality increase of 20–30% in Birmingham (Ellis et al., 1980), and during the 1994 heatwave, which led to a statistical excess over mean mortality rates of about 10% in Belgium (Sartor et al., 1995).

In addition to the severe health effects, the 2003 heatwave further caused crop failure, forest fires, a mass loss of up to 10% in Alpine glaciers (Haeberli et al. 2005), anomalous permafrost melt in high Alpine areas and consequently exceptional rockfall events (e.g. Gruber et al. 2004). The heatwave-associated lack of precipitation and enhanced evaporation severely reduced river discharges and lake levels. Even the energy sector (higher demand for cooling, reduced production of nuclear and fossil-fuelled power plants cooled with river water), the drinking water supply (water quality), fisheries in lakes and rivers (low flow and high water temperatures) and the transport sector (inland navigation) where affected by the excessive heat.

Observed trends in the frequency of heatwaves

Changes in climatic extremes such as heatwaves may relate to changes in the temperature mean and variability. Several studies have demonstrated that the intensity of extremes is more sensitive to changes in variability than mean (e.g. Katz and Brown, 1992).

Over recent decades the annual number of warm extremes has increased significantly as a result of an asymmetric pronounced warming of the upper tails of the temperature distribution (Klein Tank et al. 2005, Moberg and Jones 2005). Based on homogenized long-term temperature series at 54 European stations, Della-Marta et al. (2007) concluded that the daily maximum temperature variance has significantly increased by 6% since 1880 associated with a warming of 1.6K. Fig. 1 reveals that the length of heatwaves has doubled and the frequency of hot days has almost tripled in the same period.

This is consistent with a global trend to significantly more warm nights and slightly more hot days, which has been identified in a numerous temperature series across the globe (Alexander et al. 2006, Frich et al., 2002). However, in contrast to observed trends in Europe, over most regions the cold tail of the temperature distribution has warmed more than the warm tail.

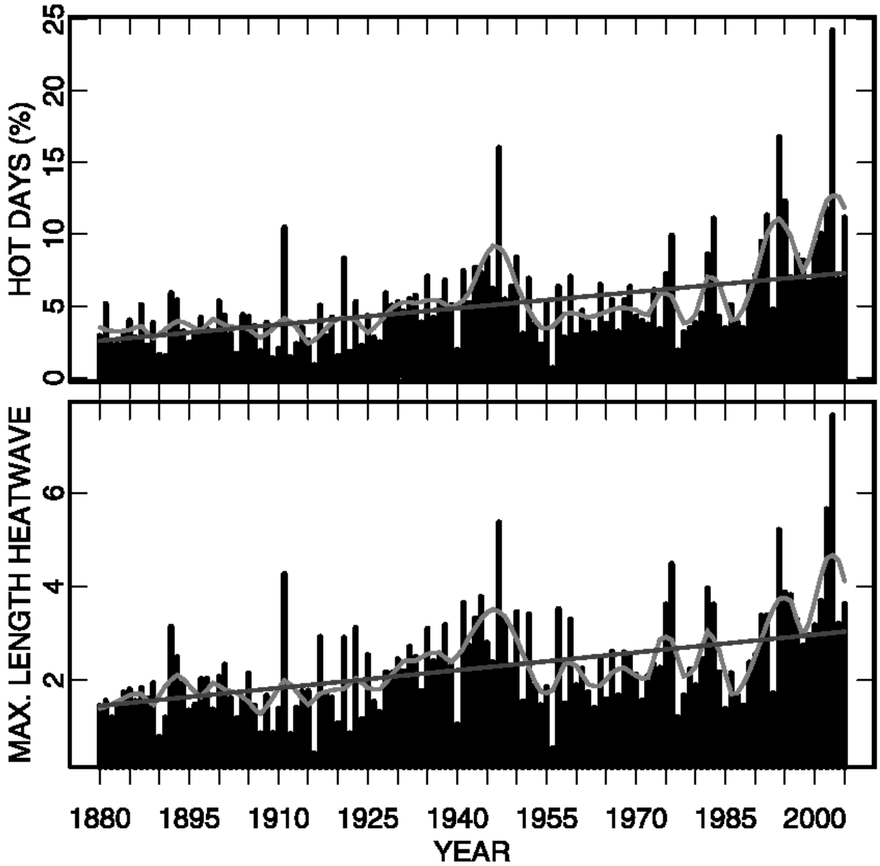

Figure 1: (top) Number of hot days (percentage of summer days when maximum temperature exceeds long-term daily 95th percentile) and (bottom) maximum heatwave duration [in days] from 1880 to 2005 over western Europe (Della-Marta et al. 2007).

The above findings raise the question whether the increasing frequency of heatwaves can be attributed to anthropogenic greenhouse warming. While an individual extreme event, such as the 2003 heatwave, cannot be attributed to one external influence in a simple deterministic sense, a change in the probability of such events might be attributable (Palmer and Räisänen, 2002). Stott et al. (2004) used a methodology to estimate the contribution of anthropogenic greenhouse gases to the risk of the occurrence of heatwaves. They concluded that human-induced greenhouse warming has at least doubled the likelihood of a heatwave similar to 2003 to occur.

Physical mechanisms underlying European summer heatwaves

The following three large-scale mechanisms have been identified as fundamental factors in producing summer heatwaves in Europe: (a) persistent anticyclonic circulation anomalies, (b) sea surface temperatures (SSTs) in the North Atlantic, Mediterranean and/or Indian Ocean and (c) anomalous land surface conditions.

Characteristically heatwaves are associated with quasi-stationary anticyclonic circulation anomalies. These anomalies produce subsidence, clear skies, warm-air advection, and prolonged hot conditions at the surface (Black et al., 2004; Meehl and Tebaldi, 2004; Xoplaki et al. 2003). The positive geopotential height anomalies are generally most distinct in the mid and upper troposphere. Near the surface, however, the anomalies are often less pronounced. Fischer et al. (2007a) suggested that the absence of pronounced anomalies in surface pressure fields arises from a heat low mechanism, which reduces SLP over the extensively heated continental surface.

The European summer climate is highly sensitive to water temperatures in the surrounding oceans. Sutton and Hodson (2005) have highlighted the role of the Atlantic Multidecadal Oscillation (AMO) in modulating boreal summer climate on multidecadal time scales. There is also evidence that SSTs may affect not only mean temperatures but also extreme events on seasonal and subseasonal timescales. Cassou et al. (2005) have suggested that the anomalous diabatic heating in the tropical Atlantic Ocean, which is related to SST anomalies, significantly favours anticyclonic circulation regimes over Europe.

Regarding the 2003 heatwave, there is an ongoing scientific debate whether the SST anomalies over the North Atlantic and the Mediterranean contributed decisively to the heatwave or, on the contrary, they were induced by the intense positive tropospheric temperature anomalies. Black and Sutton (2006) suggested that the SST anomalies in both the Indian Ocean and in the Mediterranean Sea significantly contributed to the anomalous temperature and precipitation throughout the 2003 heatwave. Feudale and Shukla (2007) confirmed that the Mediterranean Sea was warmed by the strong anticyclonic circulation, but also contributed towards strengthening the circulation, thereby providing additional memory to the system and playing the role of a positive feedback. However, all available atmospheric GCM simulations with prescribed SST significantly underestimate the 2003 heatwave, even on a seasonal time scale.

Fischer et al. (2007b) and Vautard et al. (2007) revealed that most of the recent European summer heatwaves have been preceded by a pronounced spring precipitation deficit (see Fig. 2a). In 2003, average precipitation was reduced by more than 50% in the four months between February and May 2003 (Fischer et al. 2007b). These anomalous spring conditions were associated with high shortwave net radiation due to low cloudiness and an exceptionally early vegetation onset (Zaitchik et al. 2006). These 3 factors contributed to rapid soil drying and reduced latent cooling, which amplify the summer temperature extremes.

Based on a regional climate model experiment, Fischer et al. (2007b) estimated that the number of extremely hot summer days would have been substantially reduced (50–80%) in the absence of anomalous soil drying (see Fig. 2).

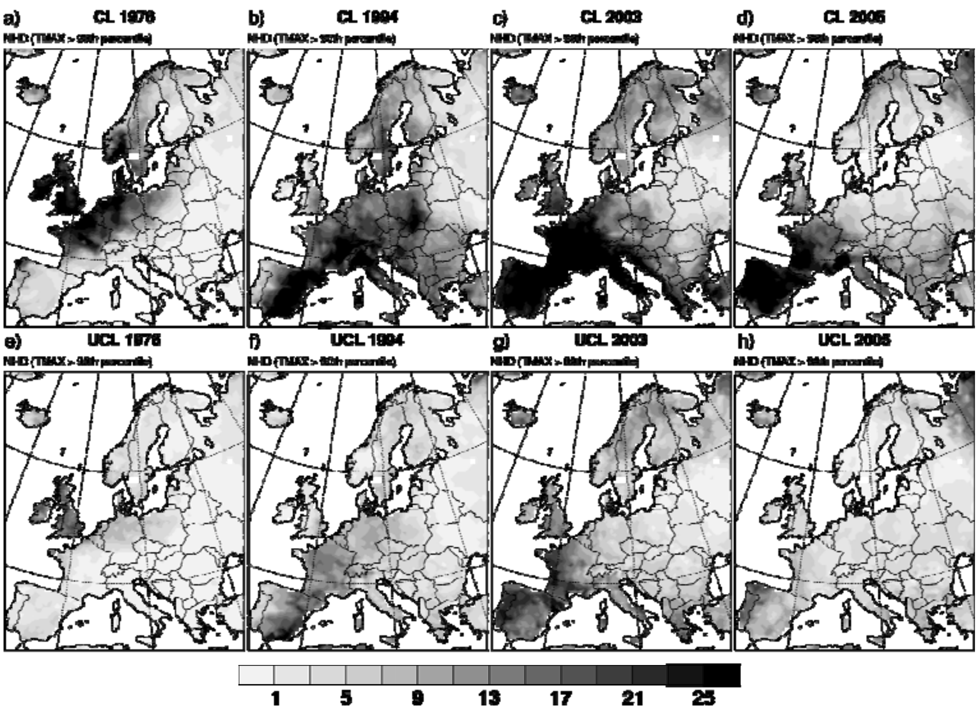

Figure 2: Number of hot days (days with daily maximum temperatures warmer than the local climatological 90th percentile) during the summers (JJA) 1976, 1994, 2003, and 2005 as simulated (a–d) with a regional climate model with a fully interactive land surface model and (e–h) with a regional climate model without land-atmosphere coupling (prescribed climatological mean soil moisture cycle) (Fischer et al. 2007b).

Projections of the European summer climate

In the 21st century, the warming of summer temperatures over Europe is projected to continue at a rate somewhat greater than on the global mean. Furthermore, recent model studies (based on global and regional climate models) have suggested that the recent trend towards more frequent, pronounced and longer lasting heatwaves is very likely to be continued and even intensified in the future (IPCC 2007 and references therein). Schär et al. (2004) suggested that at the end of the 21st century every second summer could be as warm or warmer than 2003 due to a projected increase in mean and variability. These findings are in line with numerous regional studies, which project a tendency to higher interannual summer temperature variability particularly over central, western and eastern Europe (Schär et al., 2004; Rowell, 2005; Clark et al., 2006; Giorgi et al., 2004; Seneviratne et al., 2006b; Vidale et al., 2007; Lenderink et al., 2007). Also on daily time scale the projected increase is larger for the warm tail of the distribution than for the median (Kjellström et al., 2007; Fischer and Schär 2009a).

We analysed future changes in impact-relevant summer heatwave indices based on 6 high-resolution regional climate models of the multi-model scenario experiment of the ENSEMBLES project. To assess changes in extended hot episodes, we define a heatwave to be a spell of at least six consecutive days with maximum temperatures exceeding the local 90th percentile of the control period (1961-1990). Fig. 3 depicts changes in the frequency of heatwave days (HWF90), and these show large increases in the Mediterranean region. Averaged over the Iberian Peninsula and the Mediterranean, HWF90 is projected to increase from about 2 days per average summer (1961-1990) to around 6-24 days in 2021-2050 (not shown) and 27-67 days in 2071-2100 (see Fig. 3). The average number of heatwaves (HWN90) increases from one every 3-5 summers (1961-1990) to about 2-3 heatwaves per season (2071-2100) (Fischer and Schär 2009b).

The projected changes in frequency and intensity of heatwaves may relate to changes in large-scale atmospheric circulation (e.g. Meehl and Tebaldi, 2004) and/or small-scale physical processes related to soil processes determining the partitioning of latent and sensible heat fluxes or to the surface radiation budget (shortwave and longwave radiation) (Seneviratne et al., 2006; Vidale et al. 2007; Lenderink et al, 2007).

These projections for southern Europe are concerning since they imply a strong increase in the frequency of dangerous health conditions within the 21st century.

Despite substantial agreement across a wide range of climate models, studies reveal considerable uncertainties in the projection of the European summer climate. Buser et al. (2009a, 2009b) used a Bayesian methodology to derive probabilistic climate change scenarios. They find that estimates of continental European summer temperature changes strongly depend upon the underlying bias assumptions, thereby leading to significantly larger uncertainties than in other seasons.

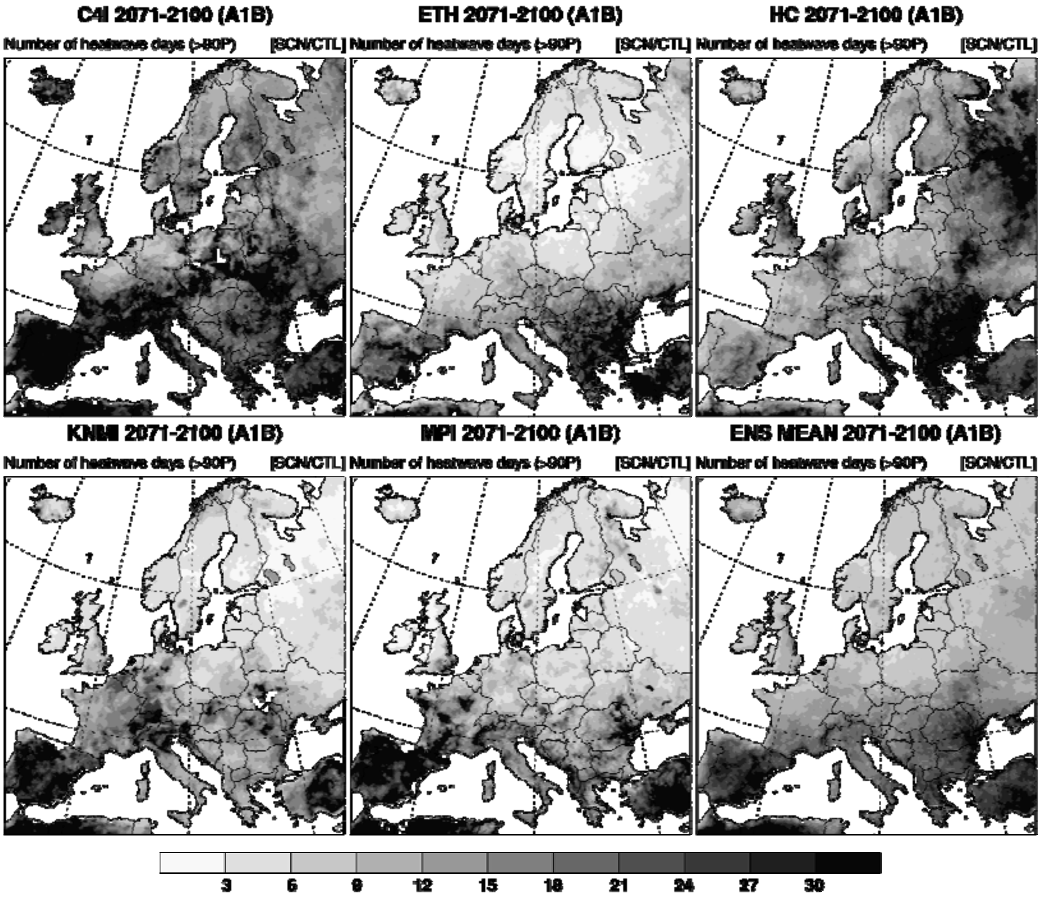

Figure 3: Projected changes in frequency of summer heatwave days, expressed as ratio SCN (2071-2100)/CTL (1961-1990). Results are based on 5 regional climate models of the ENSEMBLES multi-model project with an A1B greenhouse gas scenario. The bottom right panel shows the ensemble mean (Fischer and Schär 2009b).

References

Alexander, L., X. Zhang, T. Peterson, J. Caesar, B. Gleason, A. K. Tank, M. Haylock, D. Collins, B. Trewin, F. Rahimzadeh, A. Tagipour, K. Kumar, J. Revadekar, G. Griffiths, L. Vincent, D. Stephenson, J. Burn, E. Aguilar, M. Brunet, M. Taylor, M. New, P. Zhai, M. Rusticucci, and J. Vazquez-Aguirre, 2006: Global observed changes in daily climate extremes of temperature and precipitation. *J. Geophys. Res.*, **111**, doi:10.1029/2005JD006290.

Black, E., M. Blackburn, G. Harrison, and J. Methven, 2004: Factors contributing to the summer 2003 European heatwave. *Weather*, **59**, 217–223.

Brockhaus, P., P. Bechtold, O. Fuhrer, C. Hohenegger, D. Lüthi, C. Schär, 2009: The ECMWF IFS convection scheme applied to the COSMO-CLM limited-area model. *Quart. J. Roy. Meteor. Soc.*, submitted.

Buser, C.M., H.R. Künsch, D. Lüthi, M. Wild and C. Schär, 2009a: Bayesian multi-model projection of climate: Bias assumptions and interannual variability. *Climate Dynamics*, **33** (6) 849-868, doi: 10.1007/s00382-009-0588-6

Buser, C.M., H.R. Künsch and C. Schär, 2009b: Bayesian multi-model projections of climate: Generalization and application to ENSEMBLES results. *Climate Research*, submitted.

Cassou, C., L. Terray, and A. S. Phillips, 2005: Tropical Atlantic influence on European heatwaves. *J. Climate*, **18**, 2805–2811.

Clark, R. T., S. J. Brown, and J. M. Murphy, 2006: Modeling Northern Hemisphere summer heat extreme changes and their uncertainties using a physics ensemble of climate sensitivity experiments. *J. Climate*, **19**, 4418–4435.

Della-Marta, P. M., J. Luterbacher, H. v. Weissenfluh, E. Xoplaki, M. Brunet, and H. Wanner, 2007b: Doubled length of Western European summer heatwaves since 1880. *J. Geophys. Res.*, **112**, doi:10.1029/2007JD008510.

Ellis, F., H. Prince, G. Lovatt, and R. Whittington, 1980: Mortality and morbidity in Birmingham during the 1976 heatwave. *Q. J. Med.*, **49**, 1–8.

Feudale, L. and J. Shukla, 2006: Role of Mediterranean SST in enhancing the European heatwave of summer 2003. *Geophys. Res. Lett.*, **34** (3), Art. No. L03811

Fischer, E. M., S. I. Seneviratne, D. Lüthi, and C. Schär, 2007a: Contribution of land–atmosphere coupling to recent European summer heatwaves. *Geophys. Res. Lett.*, **34**, doi:10.1029/2006GL029068.

Fischer, E. M., S. I. Seneviratne, P. L. Vidale, D. Lüthi, and C. Schär, 2007b: Soil moisture–atmosphere interactions during the 2003 European summer heatwave. *J. Climate*, **20**, 5081–5099.

Fischer, E. M. and C, Schär, 2009a: Future changes in daily summer temperature variability: Driving processes and role for temperature extremes. *Clim. Dyn*, 10.1007/s00382-008-0473-8.

Fischer, E. M. and C, Schär, 2009b: High-impact European heatwaves in a changing climate, submitted.

Frich, P., L. Alexander, P. Della-Marta, B. Gleason, M. Haylock, A. Klein Tank, and T. Peterson, 2002: Observed coherent changes in climatic extremes during the second half of the twentieth century. *Climate Res.*, **19**, 193–212.

Giorgi, F., X. Bi, and J. Pal, 2004: Mean, interannual variability and trends in a regional climate change experiment over Europe. II: Climate change scenarios (2071-2100). *Clim. Dynam.*, **23**, 839–858.

Gruber, S., M. Hoelzle, and W. Haeberli, 2004: Permafrost thaw and destabilization of Alpine rock walls in the hot summer of 2003. *Geophys. Res. Lett.*, **31**, doi:10.1029/2004GL020051.

Häberli,W., F. Paul, S. Gruber, R. Frauenfelder, M. Hoelzle, A. Kääb, H. Machguth, J. Noetzle, C. Rothenbühler, D. Von derMühl, and M. Zemp, 2004: Effects of the extreme summer 2003 on glaciers and permafrost in the Alps. *Geophysical Research Abstracts*, **6**.

Hémon, D., E. Jougla, C. J, F. Laurent, S. Bellec, and G. Pavillon, 2003: Surmortalité liée à la canicule d'août 2003 en France. *Bulletin Epidémiologique Hebdomadaire*, **45–46**, 1–5.

Hohenegger, C., P. Brockhaus, C.S. Bretherton and C. Schär, 2009: The soil moisture-precipitation feedback in simulations with explicit and parameterized convection. *J. Clim.*, **22** (19), 5003–5020.

Katz, R. W. and B. G. Brown, 1992: Extreme events in a changing climate: Variability is more important than averages. *Climatic Change*, **21**, 289–302.

Kjellström, E., L. Bärring, D. Jacob, R. Jones, G. Lenderink, and C. Schär, 2007: Modelling daily temperature extremes: recent climate and future changes over Europe. *Climatic Change*, **81**, 249–265.

Klein Tank, A., G. Können, and F. Selten, 2005: Signals of anthropogenic influence on European warming as seen in the trend patterns of daily temperature variance. *Int. J. Climatol.*, **25**, 1–16.

Meehl, G. A. and C. Tebaldi, 2004: More intense, more frequent, and longer lasting heatwaves in the 21st century. Science, 305, 994–997.

Moberg, A. and P. Jones, 2005: Trends in indices for extremes in daily temperature and precipitation in central and western Europe, 1901–99. *Int. J. Climatol*., **25**, 1149–1171.

Palmer, T. N. and J. Räisänen, 2002: Quantifying the risk of extreme seasonal precipitation events in a changing climate. *Nature*, **415**, 512–514.

Räisänen, J., U. Hansson, A. Ullerstig, R. Döscher, L. Graham, C. Jones, H. Meier, P. Samuelsson, and U. Willen, 2004: European climate in the late twenty-first century: Regional simulations with two driving global models and two forcing scenarios. *Clim. Dynam*., **22**, 13–31.

Rowell, D. P., 2005: A scenario of European climate change for the late twenty-first century: seasonal means and interannual variability. *Clim. Dynam.*, **25**, 837–849.

Sartor, F., R. Snacken, C. Demuth, and D.Walckiers, 1995: Temperature, ambient ozone levels, and mortality during summer, 1994, in Belgium. *Environ. Res.*, **70**, 105–113.

Schär, C., P. L. Vidale, D. Lüthi, C. Frei, C. Häberli, M. A. Liniger, and C. Appenzeller, 2004: The role of increasing temperature variability in European summer heatwaves. *Nature*, **427**, 332–336, doi:10.1038/nature02300.

Schär, C. and G. Jendritzky, 2004: Hot news from summer 2003. *Nature*, **432**, 559–560.

Seneviratne, S. I., D. Lüthi, M. Litschi, and C. Schär, 2006: Land-atmosphere coupling and climate change in Europe. *Nature*, **443**, 205–209.

Stott, P. A., D. A. Stone, and M. R. Allen, 2004: Human contribution to the European heatwave of 2003. *Nature*, **432**, 610–614.

Sutton, R. T. and D. L. R. Hodson, 2005: Atlantic ocean forcing of North American and European summer climate. *Science*, **309**, 115–118.

Vandentorren, S., F. Suzan, S. Medina, M. Pascal, A. Maulpoix, J. C. Cohen, and M. Ledrans, 2004: Mortality in 13 French cities during the August 2003 heatwave. *Amer. J. Public Health*, **94**, 1518–1520.

Vautard, R., P. Yiou, F. D'Andrea, N. d. Noblet, N. Viovy, C. Cassou, J. Polcher, P. Ciais, M. Kageyama, and Y. Fan, 2007: Summertime European heat and drought waves induced by wintertime Mediterranean rainfall deficit. *Geophys. Res. Lett.*, **34**, doi:10.1029/2006GL028001.

Vidale, P. L., D. Lüthi, R.Wegmann, and C. Schär, 2007: European summer climate variability in a heterogeneous multi-model ensemble. *Climatic Change*, **81**, 209–232.

Xoplaki, E., J. F. Gonzalez-Rouco, J. Luterbacher, and H. Wanner, 2003: Mediterranean summer air temperature variability and its connection to the large-scale atmospheric circulation and SSTs. *Clim. Dynam.*, **20**, 723–739.

Zaitchik, B., A. K. Macalady, L. R. Bonneau, and R. B. Smith, 2006: Europe's 2003 heatwave: a satellite view of impacts and land-atmosphere feedbacks. *Int. J. Climatol.*, **26**, 743–769.

Defining and predicting Excessive Heat events, a National system

John Nairn[1], Robert Fawcett[2] and Darren Ray[1]

[1]South Australian Regional Office, Adelaide
[2]National Climate Centre, Melbourne,
Australian Bureau of Meteorology

Introduction

Heatwaves are one form of severe weather expected to become worse in Australia under global warming (Solomon et al. 2007). In Australia, heatwaves are defined by the achievement of a minimum sequence of consecutive days with daily maximum temperatures (T_{max}) reaching a designated threshold. Definitions that only apply to individual locations impede our ability to understand and respond appropriately to heatwaves. Daily maximum temperatures are only part of the story when we consider impacts on human health, agriculture, infrastructure, demand on utilities and other environmental hazards such as fire. Incorporating minimum temperature through the average daily temperature is also important (Nicholls et al. 2008, Pattenden et al. 2003), which is not surprising. The extent to which heat load is dissipated overnight ahead of the following high heat day dictates the accumulating thermal load impacting vulnerable people and systems.

In this presentation, we describe a set of three new excess heat indices (EHIs) which we propose for use in real-time and historical climate monitoring of heat-waves across Australia. A scheme for their operational implementation will be outlined, together with possibilities for extension into real-time weather forecasting.

These indices provide a means by which the community can gauge their historical sensitivity to accumulated excess heat load, peak load and duration. Mitigation and response capabilities will also benefit from access to time series and spatial tools applicable to past and forecast events.

Method

The EHIs we propose here are based on average daily temperature (ADT), defined as the average of the maximum and minimum temperature (T_{min}) within a 24-hour 9 am to 9 am (local time) day, which corresponds to the daily temperature observation cycle in Australia. In practice, this means that the early morning T_{min} typically follows the afternoon T_{max} in time.

The first EHI we propose is an acclimatisation index, defined as EHI(accl.) = $(T_i + T_{i-1} + T_{i-2})/3 - (T_{i-3} + \ldots + T_{i-32})/30$, where T_i is the ADT for day *i*. In other words, EHI(accl.) is the difference between the mean ADT over a three-day period and the mean ADT over the preceding thirty days. Positive values are associated with relatively hot weather, or excess heat, negative values with relatively cool weather. This index is very much a relative one – excess heat according to this index is possible in summer and winter alike. Also, its values are not expected to become more extreme under a general warming trend.

The second EHI is more an absolute index, and is defined as EHI(sig.) = $(T_i + T_{i-1} + T_{i-2})/3 - T_{95}$, where T_{95} is the 95th percentile of ADT. We use the 30-year period 1971-2000 for the calculation of T_{95}, and the calculation is across all days in the year. With this second index, excess heat is typically only possible in the summer half-year, because hot winter weather isn't hot by annual standards. The comparison against T_{95} gives a measure of the statistical significance of the event. Unlike EHI(accl.), this index is expected to become more extreme under a general warming trend, provided a fixed climatological period for T95 is adopted. Lastly, the excess heat factor (EHF) is defined as EHF = | EHI(accl.) | × EHI(sig.), which obviously implies that sign(EHF) = sign(EHI(sig.)) – EHI(accl.) acts as an amplification term on EHI(sig.).

These three indices obviously require continuous time series of daily maximum and minimum temperature. While these can of course be obtained from station-based data, for climate monitoring purposes we use the new Australian Water Availability Project (AWAP) daily temperature analyses (Jones et al. 2009). Initially we use the low resolution (0.25°) analyses, although the high resolution (0.05°) might be used in time. Gridded forecast values of three indices could be obtained for the next four of five days using the new experimental OCF/AWAP daily temperature forecast system, OCF from ACCESS NWP or from forecaster generated data (optimally within Graphical Forecast Editor).

Results

Figures 1, 2 and 3 show station-based and grid-interpolated results for Adelaide in January and February 2009. The station-based results are obtained using the Adelaide (Kent Town) site (023090), supplemented by Adelaide (West Terrace) site (023000) data in the early part of the base period 1971-2000 to calculate T_{95}. Figure 1 shows daily maximum and minimum temperature – actual station data (solid lines) from Adelaide (Kent Town), and grid-interpolated data (34.921°S, 138.622°E) from the 0.25° AWAP daily temperature analyses. While there is a clear bias in the daily temperature data, the manner in which the two EHIs are calculated largely removes this bias, although as seen in Figure 2, the peak values of the grid-interpolated results are slightly lower than the station-based results. This slight discrepancy is amplified in the EHF calculation (Figure 3), but these results would not lead to a qualitative difference in the interpretation of their results. The three-day EHIs and EHFs in Figures 2 and 3 are plotted against the *last* day of the three-day calculation period. [A forecast strategy would differ, EHIs and EHFs would be plotted against the *first* day of the three-day calculation period, whilst minimum precedes maximum temperatures in forecast systems.]

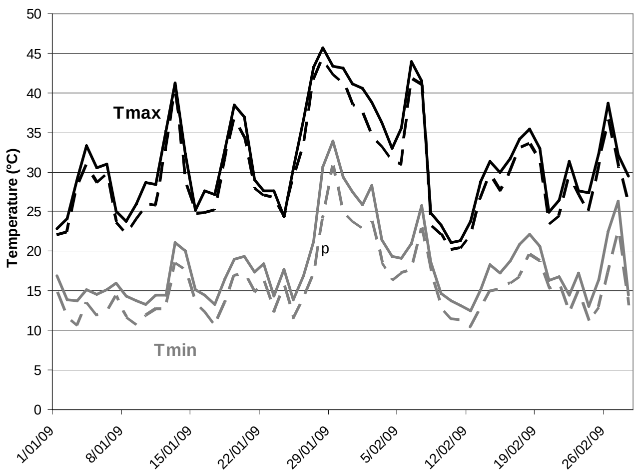

Fig. 1: Station (solid) and grid-interpolated (dashed) daily Tmax (black) and Tmin (grey) at Adelaide for January and February 2009. Following normal Bureau of Meteorology convention, daily maximum (*minimum*) temperatures are recorded for the 24 hours from (*to*) 9 am on the designated day.

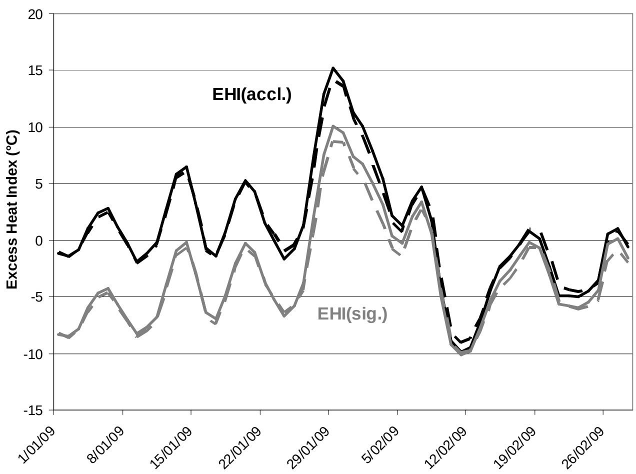

Fig. 2: Station (solid) and grid-interpolated (dashed) daily EHI(accl.) (black) and EHI(sig.) (grey) at Adelaide for January and February 2009. The three-day EHIs are graphed against the last day of the three-day period.

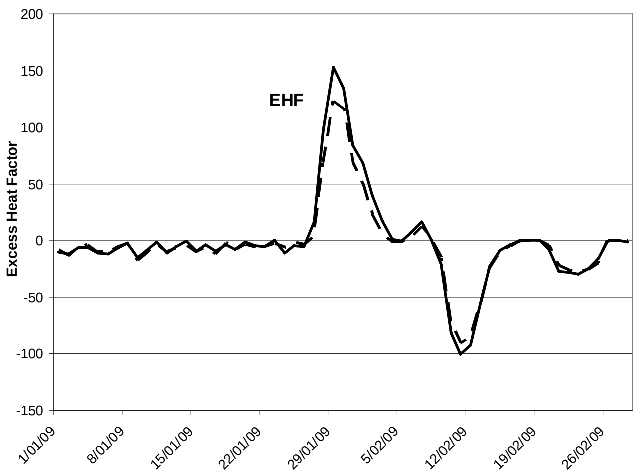

Fig. 3: Station (solid) and grid-interpolated (dashed) EHF at Adelaide for January and February 2009. The three-day EHFs are graphed against the last day of

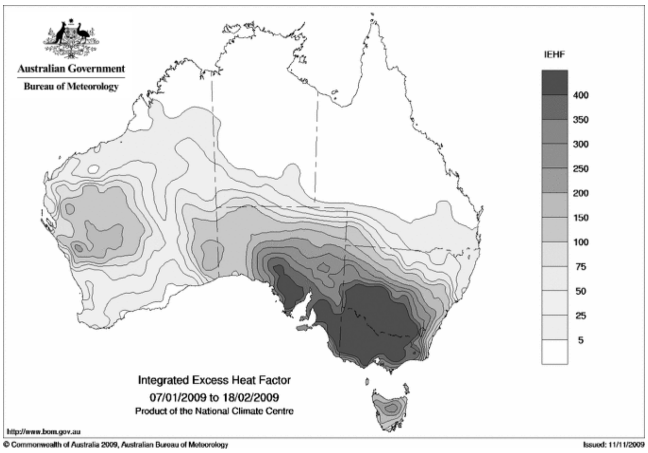

Fig. 4: Integrated EHF across Australia for 7 January to 18 February 2009.

three-day period.
Daily values of the EHIs can of course be mapped, but it is also useful to integrate or sum the daily values across an entire heat wave. Figure 4 shows the integrated EHF from 7 January to 18 February 2009, where only positive daily values of the EHF contribute to the integration – negative values are treated as if they were zero. As with Figures 2 and 3, the range of days represented in Figure 4 refer to the last days of the three-day triplets used in the EHF calculations.

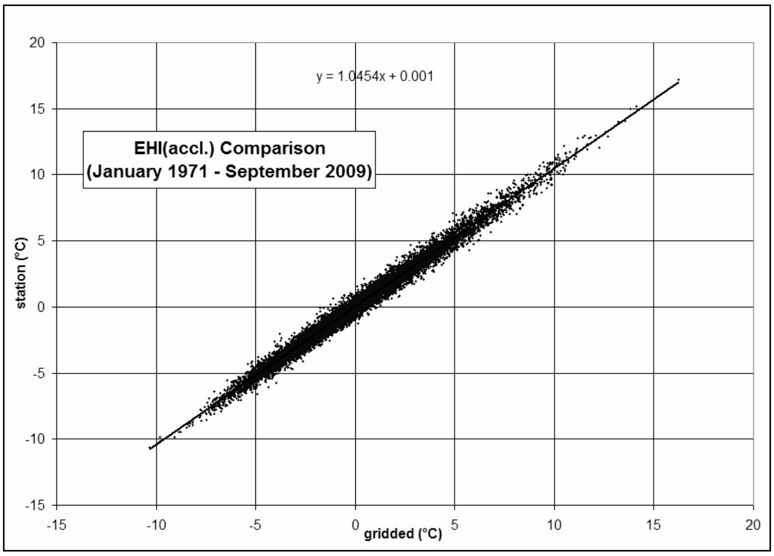

Fig. 5: A comparison between grid-interpolated (horizontal axis) and station-based (vertical axis) EHI(accl.) for Adelaide (Kent Town) over the period January 1971 to September 2009. The linear regression is shown as a solid line, together with the regression equation**.**

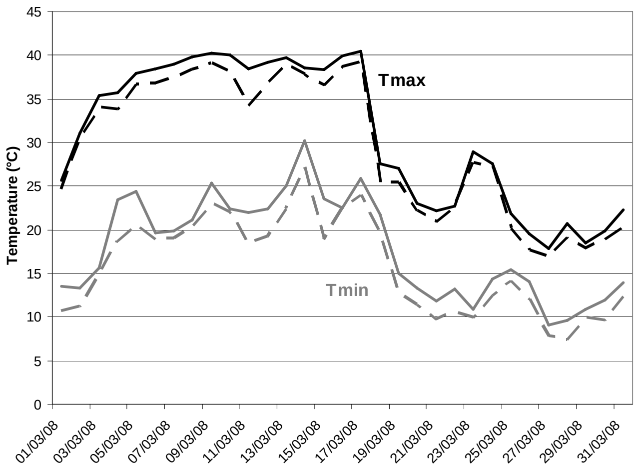

Fig. 6: As per Fig. 1, but for March 2008.

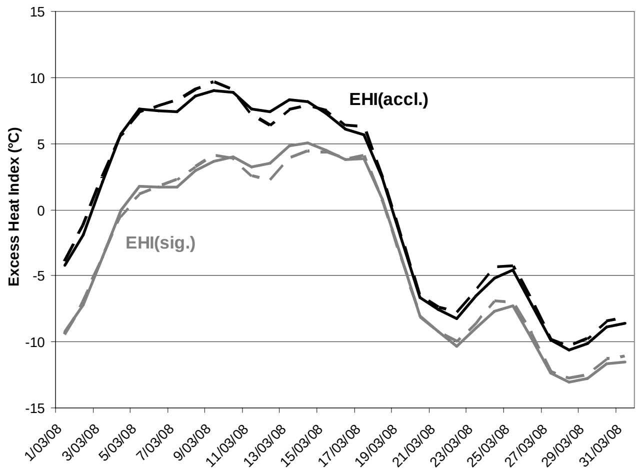

Fig. 7: As per Fig. 2, but for March 2008.

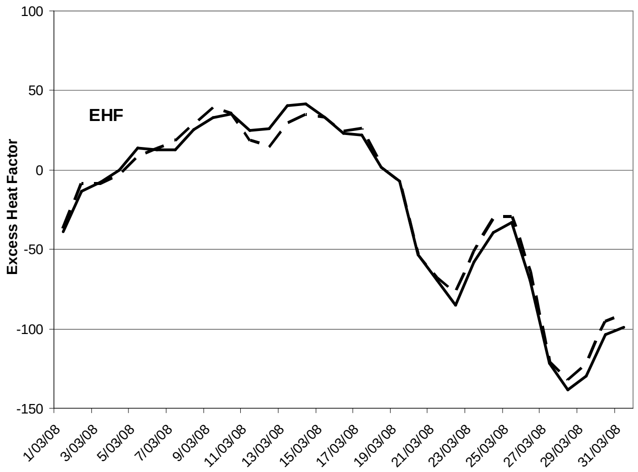

Fig. 8: As per Fig. 3, but for March 2008.

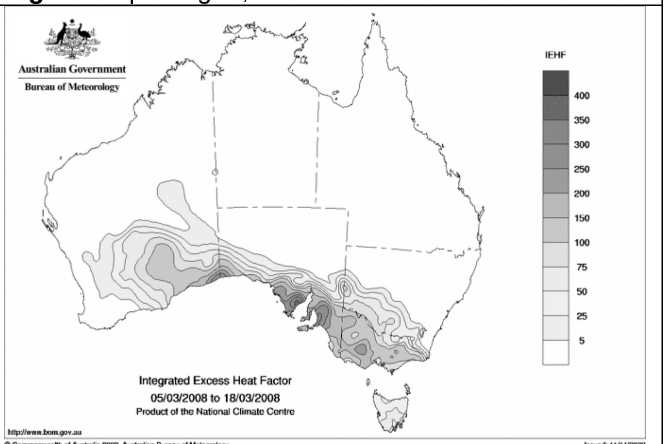

Fig. 9: Integrated EHF across Australia for 5 to 18 March 2008.

Figure 5 shows an extended comparison between the gridded and station-based EHI(accl.) values at Adelaide. Relative to the grid-interpolated values, the station-based values show very little bias but a slight increase (4.5%) in amplitude. This is not altogether surprising, in that the daily temperature analyses represent (to some extent) local areal averages.

Figures 6 to 9 show results (analogous to Figures 1 to 4) for the March 2008 Adelaide heatwave. This Adelaide heatwave was of lesser intensity but longer duration than the subsequent event in 2009 – peak EHI(accl.) values reached +10°C in 2008 compared with +15°C in 2009, while peak EHI(sig.) values reached +5°C in 2008 compared with +10°C in 2009. On the other hand, the EHI(accl.) index remained positive for 16 consecutive daily values in the 2008 event, compared with 14 consecutive daily values in 2009, while 2008 showed greater consistency in the elevation of its temperatures.

Discussion

As seen above the ability to objectively contrast the peaks, ingredients and length of excess heat factor across heat waves provides a new opportunity to test which aspect(s) of an event is impacting heat vulnerable systems. Excess Heat Factor load can also be assessed as demonstrated in Figures 4 and 9, where integrated or summed EHF is presented as an event assessment, once again relevant to any agency, community group or business sector wishing to evaluate their resilience thresholds. This application could also prove highly useful for state and federal government relief arrangements (NDRRA) whereby threshold temperature criteria are currently being developed in order to include heatwaves as a natural disaster.
An interesting challenge is presented to current NWP standards by the longevity of the record breaking Adelaide heatwaves presented. Direct model output and OCF guidance is limited to about 8 days. Experiments are required to establish the utility of 15 and 30 day NWP forecast period objective guidance.

Time series analysis of Adelaide's 120 year temperature record using this technique also produces insights into heatwave climatology. Ranking of events based upon EHF peak and load are not presented.

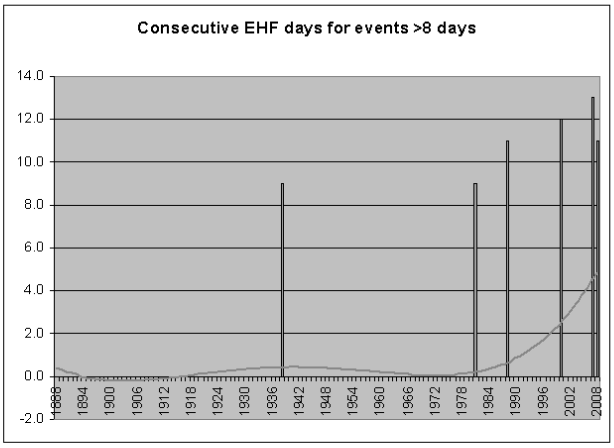

Fig. 10. Length of Adelaide EHF events when greater than 8 days by year.

References

D A Jones, W Wang and R Fawcett, 2009. *High-quality spatial climate data sets for Australia*. Australian Meteorological and Oceanographic Journal (in press).

Natural Disaster Relief and Recovery Arrangements http://www.ema.gov.au/www/emaweb/emaweb.nsf/Page/Emergency_ManagementRecovering_from_Emergencies

N Nicholls, C Skinner, M E Loughnan, N Tapper. *A simple heat alert system for Melbourne, Australia.* Int J Environ Biometeorology (in press, 2008).

M Nitschke, G Tucker, P Bi. *Morbidity and mortality during heatwaves in metropolitan Adelaide.* Med J Aust 2007; 187{11/12}:662-665.

S Pattenden, B Nikiforov and B G Armstrong, *Mortality and temperature in Sofia and London.* J Epidemiol Community Health 2003;57;628-633.

S Solomon, D Qin, M Manning, Z Chem, M Marquis, K B Averyt, M Tignor, H L Miller (Eds.). *IPPC Fourth Assessment Report (AR4). Climate Change 2007: The Physical Science Basis. Contribution of Working Group 1 to the Fourth Assessment Report of the Intergovernmental Panel on Climate Change.* Cambridge University Press, Cambridge, United Kingdom and New York, NY USA, 966 pp.

Influence of model performance on estimated changes in Australian drought under enhanced greenhouse condition

Dewi G.C. Kirono and David M. Kent

CSIRO Marine and Atmospheric Research, Centre for Australian Weather and Climate Research (CAWCR), Aspendale, Vic, Australia 3170

Introduction

In Australia, the range of projected changes in rainfall (one of the most important climate factors for water management including drought management), allowing for model-to-model differences, is relatively large (CSIRO and BoM 2007). To address this issue, previous studies (e.g. Suppiah et al. 2007; Watterson 2008; Kirono and Kent 2009) attempt to select or to treat Global Circulation Models (GCMs) according to criteria related to the model's performance, with the reason being that the better a model is in reproducing the present regional climate the more likely it is that it will provide reliable guidance for changes in regional climate. The first two mentioned studies (Suppiah et al. 2007 and Watterson 2008) assessed GCMs performance based only on a model's ability to simulate the observed mean pattern of rainfall over the whole Australian region. The latter (Kirono and Kent 2009) examined GCM performance based not only on the mean climatology but also the interannual variability and long-term trends for each of the twelve regions being considered. The two last measures are important for drought projections related studies, because if the models cannot reproduce the interannual variability the models will presumably not be able to simulate the droughts correctly. This paper examines the relationship between a GCM's ability to reproduce the observed historical climate and the estimated changes in drought affected area it simulates under enhanced greenhouse conditions. The drought analyses are conducted for the twelve regions as shown in Figure 1.

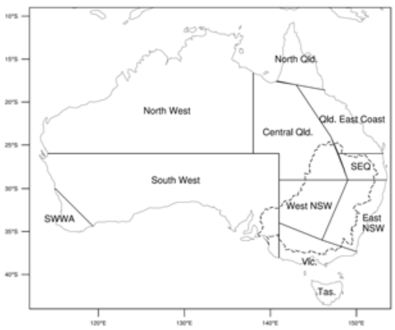

Figure 1. Distribution of 12 regions considered in this study.

Data and methods

The 20^{th} century (1900-2000) and future simulated annual rainfall from the 14 GCMs considered in this study are obtained from the Coupled Model Intercomparison Project 3 (CMIP3) database (www-pcmdi.llnl.gov). Simulations were forced using observed atmospheric emissions of greenhouse gases and sulphate aerosols for 1900-2000, and the SRES-A1B and –A2 emissions scenario for 2001 onward.

The model performance scores are obtained from Kirono and Kent (2009). In their study, the Euclidean distance score to a perfect score of 1 (Δ_{SS}) were calculated for each region shown in

Figure 1. The lower the values, the higher model's reliability in reproducing the observed present day climatology (see Kirono and Kent 2009 for more details).

We analyse the drought events based on the annual rainfall time series. A critical threshold of the 5th percentile of rainfall at each location is used to diagnose drought events. This is chosen by referring to the Australian National Drought Policy (NDP) and Hennessy et al. (2008). For each grid cell and for each GCM the threshold for drought is calculated for the period 1900-2007. The projected changes at each grid cell for each GCM for the next 100 years is then calculated relative to these thresholds. After a time series of drought/non-drought years for each grid cell of each GCM are prepared, the projections for the areal extent is calculated each year as the percentage area of a region affected by a drought event. The changes in affected area in the future (~2030) relative to the present (1900-2007) can be then calculated for each region. By definition, each region has an average of about 5.6% of the area experiencing drought simulated over the period 1900-2007.

Results

Figure 2 shows the range of the Euclidean distance from perfect skill score, Δ_{SS}, for each region for the 14 GCMs considered here. The lower the values, the higher model's reliability in reproducing the present day climatology. According to this measure, most models perform reasonably well over most regions. In particular, all models perform relatively well over Central Qld, MDB, East NSW, North West, and South West. In some regions there is a clearer range that can be used to distinguish between the better and poorer GCMs (e.g. North Qld and Qld East Coast). In particular, a large range is observed for small regions such as SWWA, TAS and Vic. A possible reason for this is that, in smaller regions, fewer grid cells are included in the skill score calculation and the result is dominated by either good or poor cells.

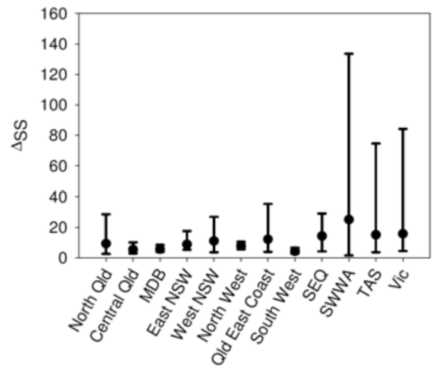

Figure 2. Range (mean, and max-min) of the Euclidean distance from perfect skill score (Δ_{SS}).

The relationship between a GCM's ability to represent the present day climate and the sign and magnitude of the projected changes in drought occurrence by ~2030 is presented in Figure 3. The relationship is relatively strong for some regions (Qld East Coast and Tas) and is relatively weak elsewhere. Over the North Qld, Qld East Coast and Tas regions, the correlation is positive suggesting that models with a lower Δ_{SS} (i.e. higher reliability) tend to indicate smaller positive and/or negative changes. Over the SWWA, the correlation is negative, although not significant, implying that a model with higher reliability tends to suggest a large positive change in drought affected area.

The influence of treating/selecting a model based on its past climate performance in the development of projections can also be explored by comparing the best estimate (multi-model mean) of projected changes obtained from all 14 model (with and without model performance weighting) and from selected models as shown in Figure 4. The subset models (7 GCMs) are representative of the top half of the sample models. Since model evaluation is performed for each region, the subset of the models included for a given region may not necessarily the same for all regions. Figure 4 also plots the changes based on 7 randomly chosen models. Apparently, drought projections based on all models without the weights are largely similar to those with the weights. A very small discrepancy between the two is only observed for the areas where the range of skill score is relatively large such as SWWA, TAS, and Vic. Overall, the projections from the subset of the top 7 models are not the same with those from all models. Compared to all 14 models, the top 7 models indicate: a larger decrease in drought affected area in North Qld; a smaller increase in MDB, East NSW, Qld East Coast, SEQ, and TAS; and a larger increase in West NSW, SWWA, and Vic. The projections based on 7-randomly chosen models are largely similar to those based on all 14 models. This suggests that the difference in projected changes based on the 7 top model and on all models can not be simply by chance.

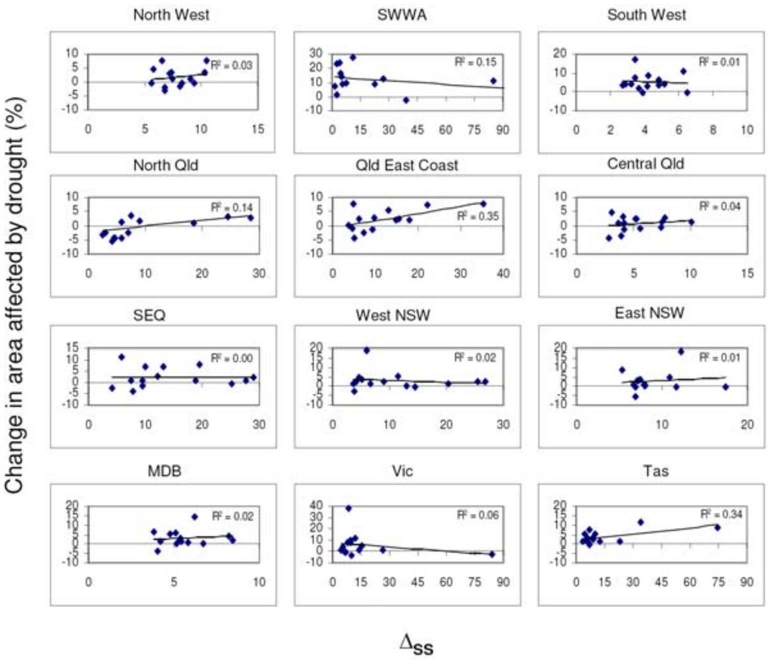

Figure 3. The relationship between model reliability in reproducing present day climate (Δ_{SS}) and projected change in area affected by drought in ~2030 relative to that in present (1900-2007)..

For some regions, the sample of better models can also potentially reduce the range of model-to-model uncertainty (not shown here). For example, the range of projected area affected by drought for ~2030 over the Qld East Coast region is 2.2% to 11.7% based on all 14 models and is 1.0% to 8.7% based on the top 7 models.

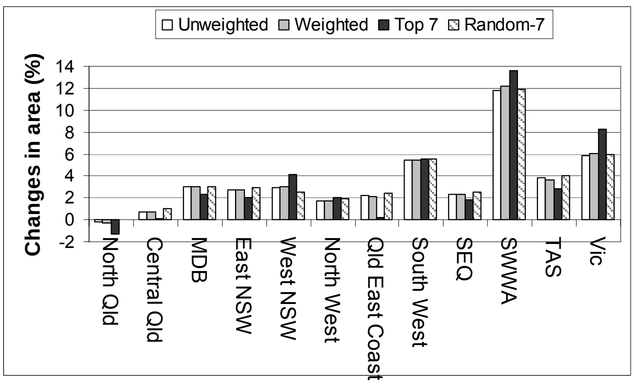

Figure 4. Projected changes in the area affected by drought in ~2030 based on all 14-unweigthed models, all 14-weighted models, top 7 models, and 7-randomly chosen models.

Concluding remarks

This paper demonstrates that the correlation between a GCM's skill score and the projected changes in drought affected area is not consistent across regions. The relationship is relatively strong for some regions (SWWA, North Qld, Qld East Coast and TAS) and is relatively weak elsewhere. However, even for regions showing a good relationship when the skill score is applied to weight a given model, it shows hardly any impact on the overall projections as the use of all 14 GCMs without weighting. This is perhaps due to the fact that each weighting was normalised such that the summation of the weightings was 1 resulting in the weightings range that is so small (e.g. from 0.075 to 0.047 for Vic region). This raises a question as to how to weight the different model results based on their performance, which is beyond the scope of this paper. When the raw skill scores are used to a select model, which in our case is the top 7 models, a clear difference in the future drought projections between the better and poorer performing GCMs emerges eventhough it is not the same for all regions. The model-to-model uncertainty is also found to be smaller when the projections are based on the better models in some regions. This is encouraging in a sense that for some regions it seems possible to reduce the uncertainty in future climate projection by selecting GCMs based on a certain criteria. As global and regional climate modelling improves, it is likely that more reliable and consistency in the future projections will be available in the future. Until then, drought projections for regions showing no correlations between model performance and model projections are probably best determined using future climate projections from most of the available GCM simulations.

Acknowledgements

This paper is based on the research partially funded by the Australian Climate Change Science Project (ACCSP). We thank Ramasamy Suppiah for constructive comments in the internal peer reviewing process of this paper.

References

CSIRO and BoM. 2007. Climate change in Australia, *Technical report*, 148pp. http://www.climatechangeinaustralia.com.au/resources.php

Hennessy, K., Fawcett, R., Kirono, D., Mpelasoka, F., Jones, D., Bathols, J., Whetton, P., Stafford Smith, M., Howden, M., Mitchell, C., Plummer, N. 2008. An assessment of the impact of climate change on the nature and frequency of exceptional climatic events. CSIRO and Bureau of Meteorology, 33 p. http://www.bom.gov.au/droughtec.

Kirono, D.G.C., Kent, D.M., 2009. Assessment of rainfall and potential evaporation from global climate modles and its implications for Australian regional drought projection. *Int. J. Climatol. Submitted.*

Suppiah, R., Hennessy, K.J., Whetton, P.H., McInnes, K.L., Macadam, I., Bathols, J.M., Ricketts, J.H., Page, C.M. 2007. Australian climate change projections derived from simulations performed for the IPCC 4th Assessment Report. *Aust. Met. Mag. 56*,131-152.

Watterson, I.G. 2008. Calculation of probability density functions for temperature and precipitation change under global warming, *J. Geophys. Res., 113*, D12106, doi:10.1029/2007JD009254.

The meteorology of Australian heatwaves

John L McBride, Graham A Mills and Alan G. Wain
Centre for Australian Weather and Climate Research
700 Collins St., Docklands, Melbourne, 3000.
j.mcbride@bom.gov.au, g.mills@bom.gov.au, a.wain@bom.gov.au,

Introduction

Three major heatwaves occurred in Australia during the period 2008-2009. All were characterised by their longevity and by the fact that temperature-duration records occurred over large areas of the continent. The major finding of this study is that the three heatwaves were associated with a continental-scale lower tropospheric warm anticyclone. In each case the anticyclone was of maximum amplitude at either the 700 or 500 hPa level, with a large amplitude anticylonic curvature of the polar jetstream on its high latitude side. This study documents the existence of the "warm-anticyclone weather system" and makes hypotheses as to how the system leads to such temperature records.

The heatwaves

Each of the heatwaves was documented in Special Climate Statements issued by the National Climate Centre of the Bureau of Meteorology (National Climate Centre, 2008, 2009a, 2009b).

- The first occurred between approximately from the 2 to 18 March 2008 and affected much of Southern Australia. Many stations across three states, Western Australia, South Australia and Victoria, set new records for number of days exceeding particular thresholds. Examples include Adelaide which had 15 consecutive days exceeding days exceeding 35°C and 13 exceeding 37.8°C (100°F), the previous records being 8 days and 7 days respectively (National Climate Centre, 2008)
- The second heatwave is the period leading up to and including the tragic "Black Saturday" bushfire event of 7 February 2009 on which 173 lives were lost in the state of Victoria due to bushfires. The preceding heatwave had two major episodes of exceptional high temperatures from 28 to 31 January and from 6 to 8 February. Over the five days 27-31 January 2009, maximum temperatures were 12-15°C above normal over much of Victoria and southern South Australia. Both Adelaide and Melbourne set records for the most consecutive days above 43°C over the period 27-30 January. Nearly half of Tasmania had its hottest day on record on 30 January. Launceston Airport (39.9°C) broke its previous record (37.3°C) by 2.6 degrees. On 7 February (the day of the fires) many all-time site records were set in Victoria, including Melbourne (154 years of record), where the temperature reached 46.4°C, far exceeding it's previous all-time record of 45.6°C and 3.2°C above the previous February record. (National Climate Centre, 2009a)
- The third was a winter heatwave across the northern half of the continent during August 2009. All-time record daily August maximum temperatures were set over 25% of the continent, including 55% of Queensland, 39% of the Northern Territory and 23% of New South Wales. Numerous stations set records for the most consecutive August days above 30°C. Between 10 and 24 August, Alice Springs in the Northern Territory experienced 14 days out of 15 above 30°C, as compared with the previous record of 8 days in a month above that threshold. (National Climate Centre, 2009b)

The meteorology of the events

Weather charts, operational forecast output and vertical soundings have been examined for the three events. All three cases were characterised by the development of a continental-scale region of warm, dry air in the lower troposphere between the surface and 500hPa. We have named it a “warm-anticyclone” as it appears as an anticylonic gyre at either the 700 or 500 hPa level, and is of scale approximately 30 degrees longitude by 20 degrees latitude. Its surface manifestation is as a low-pressure trough. Technically the system could be described as a “blocking pattern” as it is consistent with geostrophic easterly flow at 500 hPa. However, none of the three events were collocated with a split jet configuration; they did not have surface anticyclones; and they were at too low a latitude to be recorded as “blocking” by operational Blocking Index monitoring. Another characteristic of the flow is a mid-tropospheric anticyclonically curved jetstream on the poleward side of the anticyclone.

The mechanisms for build-up of the heat could be
- advection from lower latitudes,
- large-scale subsidence transporting higher potential temperature air from upper levels, or
- surface heating, development of the diurnal mixed layer , and replacement from below by the new mixed layer for the successive day.

Inspection of trajectories and vertical profiles leads us to the conclusion that surface heating is the dominant mechanism.

Inspection of hemispheric 500 hPa charts reveals that mid-tropospheric warm anticyclones are not uncommon phenomena in the subtropics. The key to a heat-wave seems to be that they occur over the continent after an extended period of drought. The role of drought is proposed to be that it leads to enhanced surface sensible heat-flux. This in turn leads to the development of a deep mixed layer which can be recirculated in the anticyclonic gyre. The presence of the gyre in observations is illustrated in Figs, 1, 2, 3, each of which show backward trajectory calculations for low and middle level air in the respective three heat-wave events.

Conclusions

The warm lower tropospheric anticyclone has been identified as the key weather-system associated with each of the three heat-waves. The mechanism for development of the anticylone is not known; but inspection of hemispheric charts reveals they are common in the subtropical mid-level flow. It is proposed that heat waves occur when these anticyclones occur over the continent under dry conditions. The trajectory calculations reveal that the gyre-type circulation allows the day-time heated mixed layers to remain over the continent. This provides a mechanism for tropospheric heat storage. This is added to by subsequent day-time heating. Modelling and observational studies are required to investigate the hypothesis that the presence of drought and low soil moisture leads to a feedback process allowing build-up of excessive warm air.

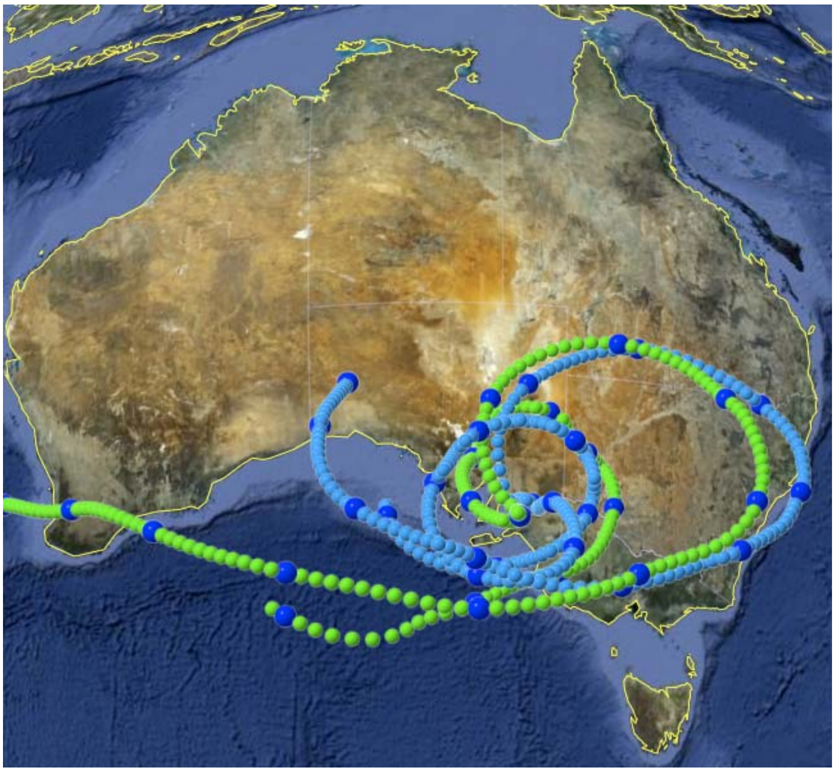

Fig.1 Heat-wave one: March 2008. Five-day backward trajectories calculated using the HYSPLIT trajectory model based on operational NWP (ACCESS) fields. The back-trajectories are from the city of Adelaide. Starting times are for 00UTC 24 10 March 2008 and 00 UTC 14 March 2008. Trajectories are shown for air ending over Adelaide at those times at the 850 hPa level (blue) and for the 700 hPa level (green).

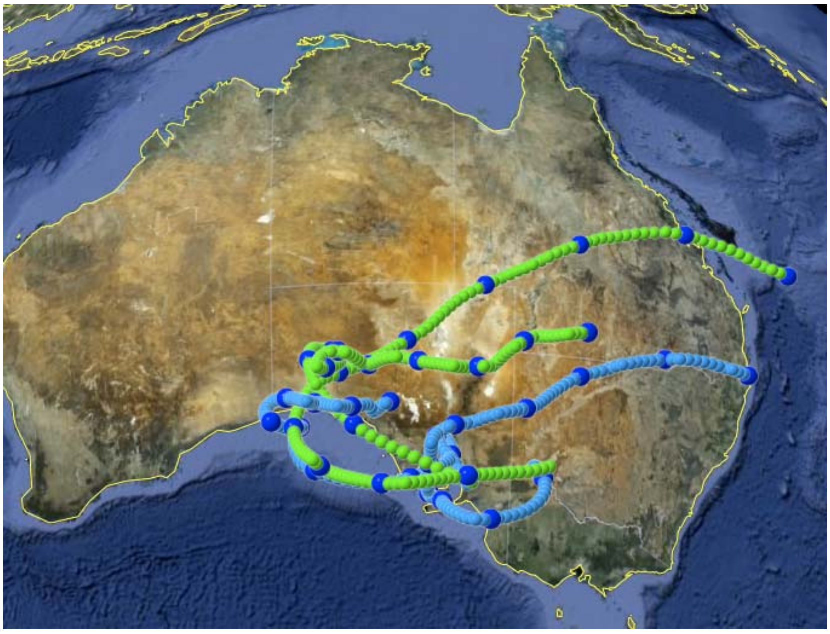

Fig. 2 Heat-wave two: January-February 2009 – Black Saturday. Five-day backward trajectories calculated using the HYSPLIT model trajectory model based on operational NWP (ACCESS) fields. The back-trajectories are from the cities of Adelaide and Mildura, ending at 850 hPa (blue) and 700 hPa (Green) on 6 February 2009.

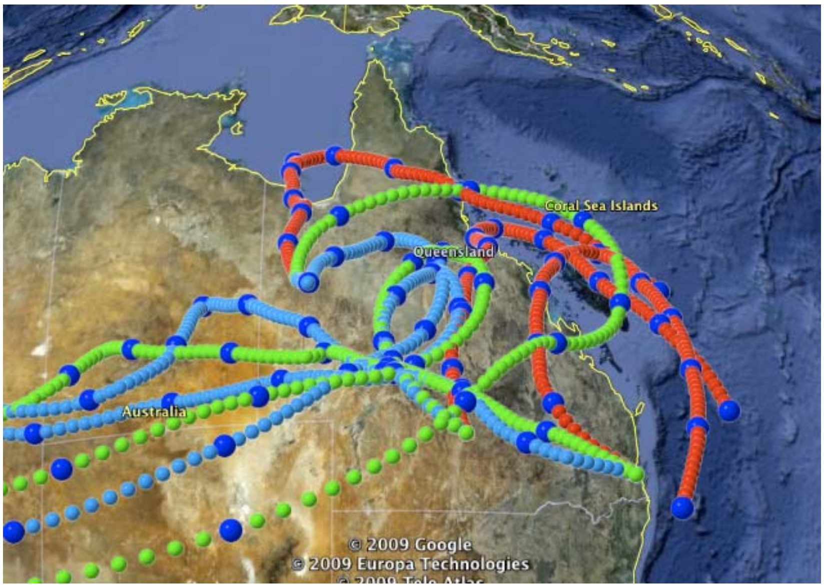

Fig. 3 Heat-wave three: August 2009. Five-day backward trajectories calculated using the HYSPLIT trajectory model based on operational NWP (ACCESS) fields. The back-trajectories are from the cities of Brisbane, Charleville and Mt Isa, ending at the surface (red) 850 hPa (blue) and 700 hPa (Green) on 24 August 2009.

References

National Climate Centre, 2008. An Exceptional and Prolonged Heatwave in Southern Australia, *Bureau of Meteorology, Special Climate Statement 15.*

National Climate Centre, 2009a. The exceptional January-February 2009 heatwave in southeastern Australia, *Bureau of Meteorology, Special Climate Statement 17.*

National Climate Centre, 2009b. Exceptional winter heat over large parts of Australia, *Bureau of Meteorology, Special Climate Statement 18.*

HYSPLIT and ACCESS simulations of the September 2009 East Australian continental scale dust storm

Alan G Wain, John L McBride, and Graham A Mills
Centre for Australian Weather and Climate Research
700 Collins St., Docklands, Melbourne, 3000.
a.wain@bom.gov.au, j.mcbride@bom.gov.au, g.mills@bom.gov.au

Introduction

In the week of 21 to 27 September 2009 Australia experienced two continental-scale dust-storms, three days apart. The dust storms were high impact events causing a spectacular bright red haze and low visibility at dawn in Sydney and airport closures in both Sydney and Canberra. The event has been labelled "red dawn" by Sydney journalists. These events are not unprecedented, two notable prior ones being the Melbourne dust-storm of February1983 and the continental-scale dust-storm of October 2002. This paper uses the HYSPLIT trajectory and dispersion model (Draxler and Hess, 1998) to simulate the sequence of events of September 2009. The paper has two major emphases, the first being to investigate the ability of the model to simulate the event. The second and major emphasis is to use the model to understand the dynamics and physical processes occurring.

Control simulation.

The simulations are carried out with the HYSPLIT dispersion model, dust being generated and dispersed through the dust being modelled as PM-10 (aerosol particles exceeding 10 micro-metre diameter). Dust is generated by "sand-blasting" when the surface wind exceeds a defined threshold (here 10m/sec), over regions defined to have soil characteristics, soil dryness and vegetation cover conducive to dust generation such that they can be considered dust source region. In the simulations described here, the source regions are defined climatologically, based on the regions of the country with a high occurrence of wind-blown dust according to the observations of Mctainsh and Pitblado (1987). These source regions are designated by the black hatching in the panels of Fig.1. Once generated the dust is dispersed and advected in a lagrangian framework by the HYSPLIT model, which takes its meteorological fields from a background numerical weather prediction model, in this case the Bureau of Meteorology operational ACCESS global model. For the control simulation used here, the meteorological model (ACCESS) is restarted very six hours observations with the dust concentrations from the end of the previous six-hour simulation set as initial fields for HYSPLIT. This configuration has been developed through a series of simulations of earlier dust events as described by Wain et al. (2006).

The sequence of events is shown in Figure 1, which is a panel of presentations of PM10 concentrations for the control simulation. As can be seen, the dust is first generated behind a cold front in South Australia on 21 September. Subsequently on 22 September it spreads behind the front and into the Tasman Sea in a branch-prefrontal trough. When the dust-storm passes through Sydney along the east coast on 23 September it follows the line of the surface cold front, the leading edge of the dust-storm being effectively a visualisation of the dome of cold frontal air. In the lower panel, the original dust-storm moves northward across Queensland and the Northern Territory, leaving clear skies across South Eastern Australia. A second low pressure system with an associated surface front develops on 25 September and a second dust-storm, again in the cold dome behind the front, passes through Sydney on the morning of 26 September.

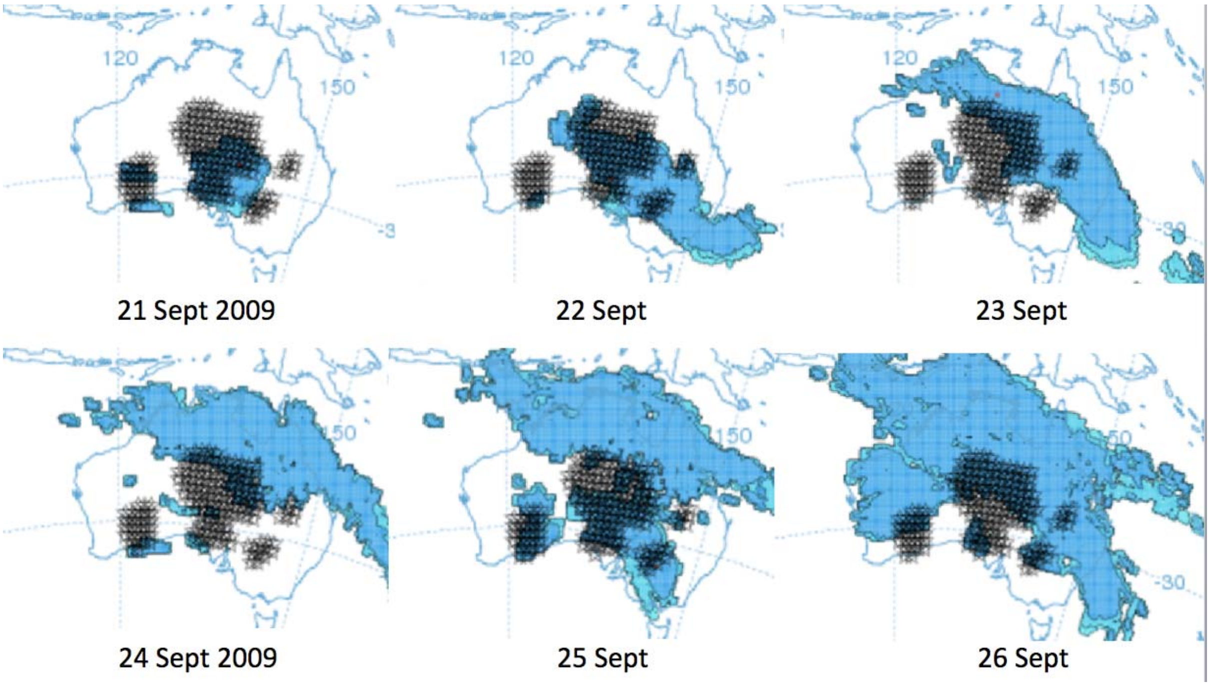

Fig.1 Concentrations of PM-10, representing ground-generated dust, in the HYSPLIT-ACCESS control simulation. The black hatching represents the locations where the model allows dust to be generated (source regions). The blue shades represent various concentrations of PM-10 averaged between the surface and 2000 metres height. Each panel is for 0600 local time on the respective calendar date along the Australian East coast.

Subjectively the control simulation reproduces the major features and the timing of both dust-events very well. The timing of the dust storm passages through the major population centres was correct as was the coincidence of the dust front with the surface-wind frontal passage. A potential weakness is the residual dust off the northwest coast at the end of the simulation, which we have no evidence occurred in nature. We are currently investigating the source of this weakness.

A visual illustration of the skill of the control simulation is shown in Fig.2 which shows the MODIS terra satellite visual channel image on 23 September (upper panel) with a clear depiction of a brown cloud of dust inland and parallel to the coast. The lower panel shows the HYSPLIT simulation for the same time period plotted on the same projection, revealing a remarkable level of skill. The skilfulness of the model was such that after the first event the simulations were forwarded to the Queensland Forecast office of the Bureau of Meteorology. Successful real-time forecasts were made for the second event, including the fact that dust concentrations would be significantly smaller than occurred in the first event.

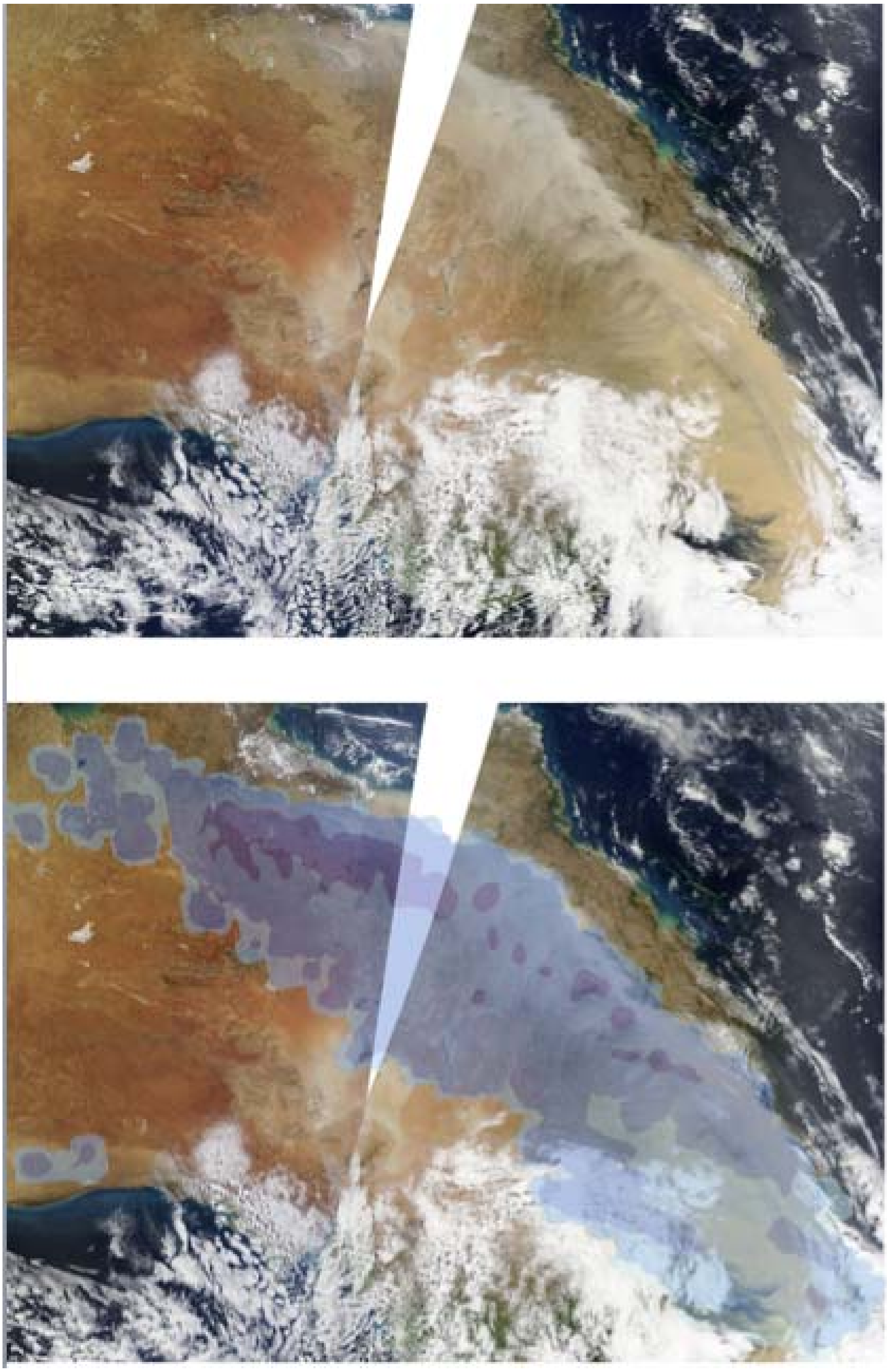

Fig. 2 MODIS terra satellite image for 26 September 2009 showing a brown cloud of dust inland and parallel to the eastern coastline of Australia (upper panel). The lower panel is the same image with the simultaneous concentration overlaid of dust (PM-10) for the control HYSPLIT-ACCESS simulation described here.

Scientific questions and ongoing model experimentation

The format of a short abstract precludes detailed discussion of physical hypotheses. Model runs with multiple sources combined with HYSPLIT forward and backward trajectories are being carried out to understand the underlying dynamical processes. Questions being addressed are:

a) the role of the drought. All major continental scale dust-storm events have occurred after periods of prolonged drought. The drought can provide dry soil as a source of dust. However, the authors believe the major role is that the altered Bowen ration (or greater sensible heat flux) leads to more intense fronts with stronger winds
b) The mechanisms through which the dust is restricted to the “cold-air-dome” of the front, and by which it spreads laterally to take up the several thousand kilometre horizontal scale of the front.
c) The relative roles of dust generation in the northerly flow ahead of the front versus generation in the cold air behind the front.
d) The source regions for the dust: Northern Lake Eyre, versus Channel country, versus the Mallee and the relative contributions of each.

These investigations are ongoing. Progress on answering them will be given in the aural presentation.

References

Draxler, R.R. and Hess, G.D. 1998. An overview of the HYSPLIT_4 modelling system for trajectories, dispersion and deposition. *Aust. Met. Mag.*, **47**, 295-308.

McTainsh, G.H. and Pitblado, J.R. 1987. Dust Storms and related phenomena measured from meteorological records in Australia. *Earth Surface Processes and Landforms*, **12**, 415-24.

Wain, A.G., Lee S., Mills G.A., Hess G.D., Cope M.E. and Tindale, N. 2006. Meteorological overview and verification of HYSPLIT and AAQFS dust forecasts for the duststorm of 22-24 October 2002. *Aust. Met. Mag.*, **55**, 35-46.

Modelling of convective and other high-impact weather events

Peter Clark, Met Office, UK [1]

Introduction

Despite the relatively benign climate of NW Europe and especially the UK, highly damaging events do, nevertheless, occur. Their relative rarity itself presents a challenge, since authorities may not be adequately prepared and, more commonly, when they are the general public affected by the event may not take warnings and instructions sufficiently seriously.

The UK spends autumn and winter (and some summers!) beneath the N Atlantic storm track. The vast majority of extra-tropical cyclones have little damaging impact, but occasional storms cause substantial damage and loss of life. Short-term effects can affect hundreds of thousands of people and take weeks to recover from, while costs of repair to property can cost billions of pounds. Examples include the 'Great Storm' of 16th October 1987 and the 'Burns Night Storm' of January 1990, which both caused widespread damage to SE England. December 1999 was notable for storm 'Anatol' which hit Denmark, SW Sweden and N Germany on the 3rd, storm 'Lothar', which caused major damage across France, southern Germany and Switzerland on the 26th, followed the next day by storm 'Martin' which hit Southern France and Northern Spain. .

Much fluvial flooding results from periods of high storm activity, leading to a slow build-up of groundwater. Damage and loss-of-life from rain due to individual intense autumn and winter storms is less common, but can occur, often when substantial orographic enhancement of rain occurs in slow-moving systems or when storms involve strong embedded convection. For example, both effects in one storm produced rainfall totals exceeding 160 mm over the Lake District, which lead to severe flooding of the city of Carlisle on 7th and 8th January 2005 (Roberts *et al.*, 2009), while mid-level convection, probably enhanced by orography, in a quasi-steady occluded front produced rainfall totals exceeding 125 mm which led to the flooding of the town of Morpeth on 6th September 2008.

A number of damaging flood events occur during the summer months and are caused by deep convection, often, but not always, organised into mesoscale convective systems. While less than common over mainland Europe, flash-flooding due to high rainfall accumulations (e.g. of order 200 mm in a few hours) can lead to severe damage and loss of life over the UK. The Lynmouth flood on the night of 15th August 1952 caused 34 deaths and much property damage, while the Boscastle flood of 16th August 2004 caused in excess of half a billion pounds of damage and necessitated the rescue of many people . The Ottery St Mary hail storm of October 2008 was notable in producing extreme convective precipitation (in excess of 180 mm over a few hours) so late in the year, local

---

[1] Address for correspondence: **Met Office** Joint Centre for Mesoscale Meteorology Meteorology Building, University of Reading, PO Box 243, Earley Gate, Reading, Berkshire, RG6 6BB, United Kingdom.
Email: peter.clark@metoffice.gov.uk

flooding being exacerbated by the blocking of drains caused by the high accumulation of soft hail (Grahame, *et al.*, 2009).

Research experience using the UM

The Met Office Unified Model (MetUM) has been developed to make it suitable for use at resolutions around 1 km (Lean *et al.*, 2007, Roberts and Lean, 2008), including progress on data assimilation (Dixon *et al.*, 2009). As discussed below, convection triggering turns out often to be of secondary importance, because mesoscale forcing (e.g. convergence lines) dominates, but in weakly forced circumstances (e.g. 'airmass convection') the development of convection depends very much on the model formulation. Horizontal and vertical mixing are both important for different reasons. Vertical mixing controls the depth of the boundary layer but also entrainment from above. It therefore tends to control initiation. Horizontal mixing controls the horizontal scales which develop through instability.

We have adopted a philosophy of retaining, where possible, the existing MetUM BL scheme (Lock et al., 2000), as this should still be appropriate at 1.5 km grid length. The intention has been to use the local part of this scheme outside the BL, but this has only been fully possible from version 7.3 of the MetUM. A '2D-Smagorinsky-Lilly' scheme has been implemented for horizontal mixing. (The Smagorinsky-Lilly scheme is also available in 3D for use at higher resolution). This seems to perform better than the fixed ∇^4 mixing used previously, primarily because much of the time it does much less mixing. It is recognised, however, this is very much an area of pragmatic tuning.

The MetUM microphysics has been extended to (optionally) include prognostic rain, ice, snow and graupel, but is currently being run with prognostic rain, a single combined ice and snow prognostic and no graupel. The main justification for this is that no forecast benefit has been found over the UK for running with a more complex scheme. (Benefit of prognostic rain **has** been found, primarily in orographically enhanced rain but also in increasing the lifetime of convective cells). Furthermore, it is possible that with more prognostics, interactions between mixing and microphysics may become more important. Development continues, including addressing some conservation issues arising from the semi-Lagrangian advection scheme and coupling warm autoconversion to an aerosol variable.

The Convective Storms Initiation Project (CSIP) took place over central southern England over summer 2005 (after a pilot study over July 2004). It was very successful, achieving 18 'Intensive Observation Periods' (IOPs). Modelling studies have been (and still are being) undertaken for most of the CSIP IOPs, with, on the whole, a remarkable degree of success. Most have used the MetUM at resolutions around 1 km; the model was in use operationally at 4 km resolution, and this usually provided initial and boundary conditions. IOPs varied widely, but a common feature of those with surface-forced convection was de-stabilisation by advancing upper level PV-anomalies, the cold air beneath upper-level PV anomalies being as important in producing instability as surface heating. Convection was often inhibited by the presence of one or more warm, dry layers above the boundary layer which were shown to be extensive and often contiguous on horizontal scales of (at least) 100 km. These allowed the build-up of CAPE and often restricted the triggering of convection to specific regions favoured by mesoscale processes. The origin of the inhibiting layers is not always clear, but some, at least, probably arise from the downward transport of the remains of tropopause folds. .

This experience has lead to a ‘three component’ view of the forecast problem. The first component is the synoptic and meso-alpha scales. These are generally well forecast on 24-48 h timescales (though not always) and regional ensemble systems such as MOGREPS-R show significant uncertainty at these scales. The second component is mesoscale interaction with the surface. The coast of the UK forms an enormous roughness and (often) thermal contrast which leads to numerous convergence (and divergence) lines, often penetrating at least 100 km inland. Orography also plays an important (and sometime surprising) role. These lines (or zones) can have a huge influence on the location of triggering of convective cells, which form the third component. The last has very little predictability, and is poorly represented in ~1 km models anyway.

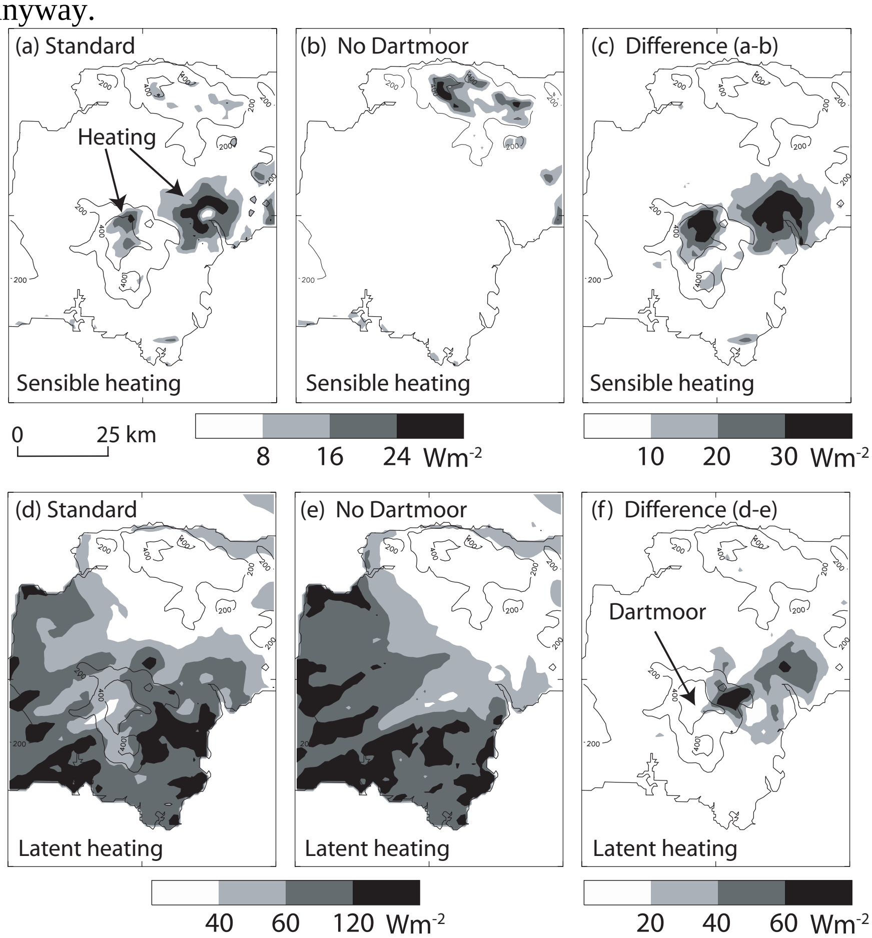

Figure 1 Difference in surface heat fluxes between runs with and without Dartmoor for CSIP IOP 1 simulations.

Most success has been achieved where the first two components are well forecast, in the case of the second component because of a reliable model response to the meso-alpha forcing. For example, Lean *et al.*, 2009, showed a remarkably high level of predictability of single deep (and quite intense) storm cluster which triggered over the SW Peninsula during CSIP IOP 1. Model experiments showed that this arose from a combination of:

1. A low-level tongue of high θ_w air beneath a ‘lid’ behind an upper front, leading to a narrow region of conditional instability near the leading edge of the lid.
2. Weakening of the lid along a convergence line along the SW Peninsula (normal to the front) caused by the land/sea contrast (mainly roughness).

3. Low-level warming along one segment of this convergence line caused by the clearance of cloud downwind of Dartmoor due to stability effects on the flow over Dartmoor.

Figure 1 shows the impact of removing Dartmoor on surface heat fluxes. The additional heating with Dartmoor downstream is sufficient to enable the boundary-layer air to penetrate the low-level ‘lid’. Figure 2 shows the development of convection in a standard run, which develops a deep cell in the right place, with one without Dartmoor. The grey shades show θ_s above lifting condensation level, θ_w below[2]. Both indicating lifting along a convergence line at 08 UTC, but only the full run show θ_w below cloud becoming high enough to exceed that at the ‘lid’ at around 2.5 km.

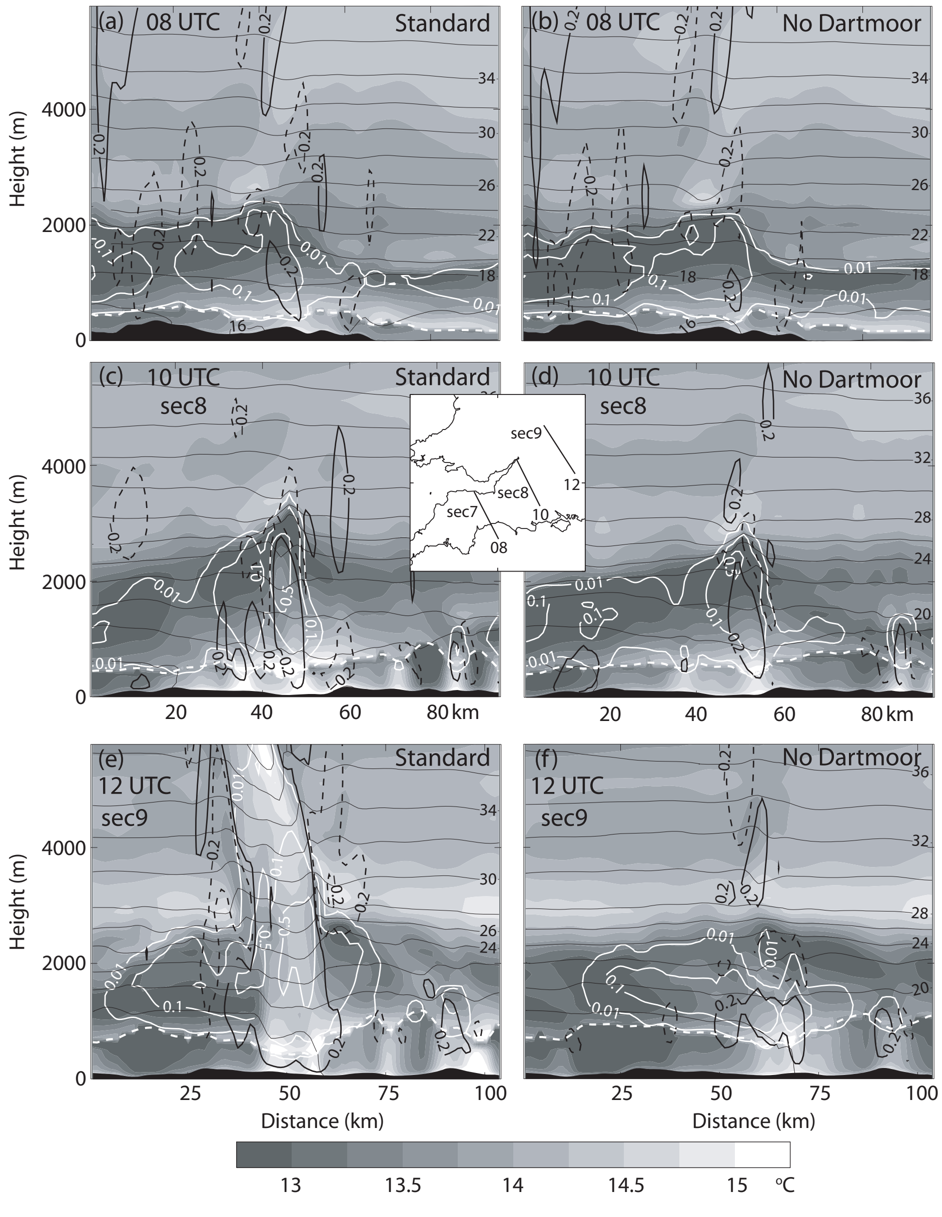

Figure 2 Cross sections approximately following the mean low-level flow from model simulations of CSIP IOP 1. Grey shades show θ_s above lifting condensation level (white dotted), θ_w below. Block contours are vertical velocity, white cloud liquid water content. Top to bottom, 08, 10 and 12 UTC. Standard run left, run without Dartmoor right.

[2] θ_s is the value of θ_w air would have if saturated. A parcel lifted wet-adiabatically to a reference level is buoyant if θ_s at that level is less than θ_w of the parcel.

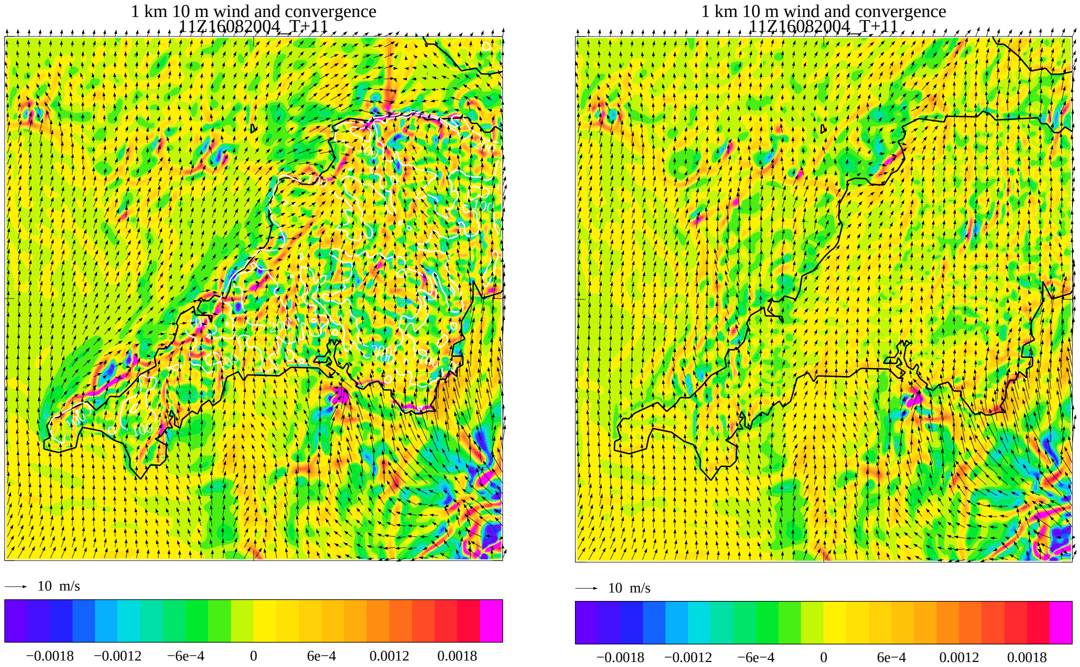

Figure 3 Simulations of the Boscastle flood event with a 1 km resolution model. Arrows show 10 m wind, colours show 10 m divergence. Left shows reference run, right a run with no orography and the land fluxes set to those over the sea.

Similarly, the Boscastle flood has been shown to have been caused by the repeated triggering of convective cells at the intersection of two (again, roughness contrast-driven) convergence lines along the northern coast of the SW Peninsula (Figure 3). Retrospectively, experiments using a repeated, random perturbation strategy have shown that the rain was remarkably predictable, though models have failed to produce the observed peak accumulations, probably because of inadequate resolution.

Not all storms are equally predictable. CSIP IOP 18 and one of the CSIP pilot cases were quite similar; both showed two mechanisms at work; primary initiation caused by coastal convergence and orography, secondary by convergence along a cold-pool caused by outflow from the primary storm. In both cases, the initial triggering and subsequent cold-pool initiation and propagation were well predicted by the MetUM (e.g. Figure 4) though the cold pool is sensitive to model physics (especially micro-physics). The pilot case, however, also showed secondary (or tertiary) initiation caused by modulation of the convective inhibition by gravity waves initiated by the primary or secondary storm (Morcrette *et al.*, 2006). Model studies to date have failed to reproduce the gravity-wave mechanism with sufficient accuracy. Likewise, storms with little surface forcing may have little predictability, though storms with similar structure may occur with different timing and/or location. For example, and succession of MCSs which developed during CSIP IOP 3 and led to severe flooding of the Glastonbury festival was poorly forecast, but 1 km resolution forecasts did develop MCSs with similar structure.

Orographic enhancement of precipitation over the UK is often by the ‘seeder/feeder process’, which enhances frontal precipitation and is generally well represented in models of order 1 km resolution. We have a number of examples of significant flooding events involving orographic enhancement being forecast much better by a high-resolution model. For example, Roberts *et al.*, 2009, in a case study of the Carlisle Flood, show that a 1 km version of the MetUM coupled to a catchment model forecast river flows 12 h or more ahead at least as accurately as driving the same model with observed rainfall. The

‘Morpeth’ flood involved embedded convection, but was also well forecast overall in a hindcast using a1.5 km model, largely because the stationary occluded front was well forecast but also because of interaction with orography.

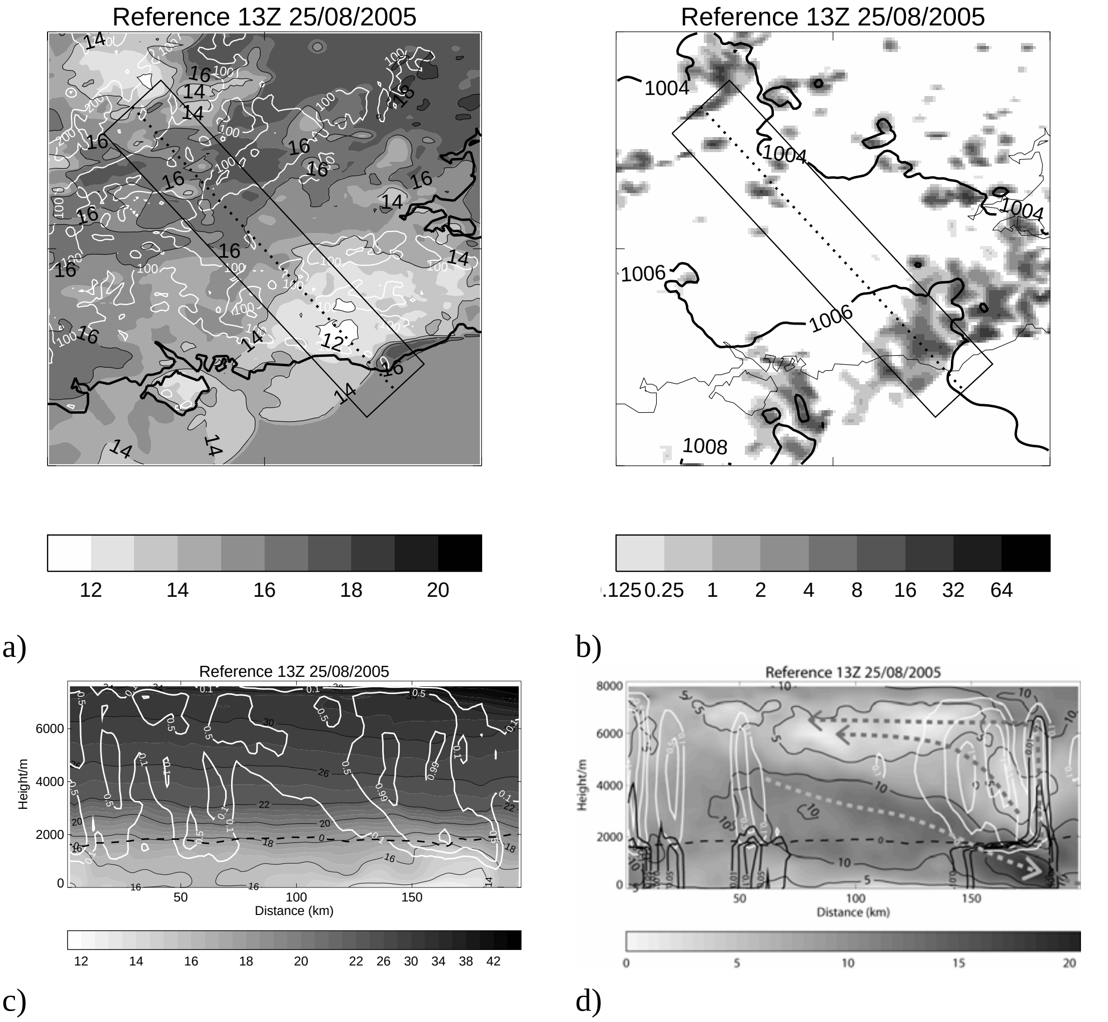

Figure 4 1.5 km horizontal grid model forecasts at 1300 UTC, 25/08/2005. a) shows bottom level (5 m) potential temperature (left, °C), b) shows mean sea level pressure (contours, hPa) and rainfall rate (shaded, mm h-1) . The dashed lines and solid boxes show, respectively, the centre and extent (200 km x 40 km) of average cross sections shown in c) and d). White contours on left panels show orography at 100 m intervals. c) shows potential temperature (shaded, thin black contours in °C; note non-linear scale) and cloud fraction (white contours, 0.1,0.5 and 0.99 shown). d) shows horizontal windspeed along the direction of the cross section (shaded, thin black contours at 5 m s^{-1} intervals), rain mixing ratio (g kg^{-1}, thick black contours) and total ice+snow mixing ratio (g kg^{-1}, white contours). Note, rain contours are 10 times smaller than ice to allow for different order of magnitude of fall speeds. Thick dashed gray arrows in d) show schematic system-relative flow. The propagation speed based on leading edge of precipitation along each line is 13.6 m s-1 at 1200 UTC and 15.8 m s-1 at 1300 UTC. Dashed black lines in all c) and d) are freezing level.

High-impact wind events can arise from convection; indeed, the precursor storm which led to a remarkably intense tornado (for the UK) over Birmingham was studied during CSIP. However, most wind-damage is associated with extra-tropical cyclones, and one feature of these which has been studied using mesoscale models in recent years is the so-called ‘Sting Jet’. This was first hypothesised by Browning *et al.* (2004) in a study of the 1987 Great Storm, and was first identified in simulations using the MetUM by Clark *et al.* 2005. More recent work (e.g. Parton *et al.*, 2008) has confirmed the presence of the Sting Jet in a number of storms and has confirmed that certain minimum resolution requirements are required to enable the sting jet to form in models. Horizontal resolution of at least 12 km seems to be necessary (well within the capabilities of current regional models); of more interest is that a vertical resolution in the mid-troposphere of order 250 m is needed.

Summary

Convective-scale NWP is showing considerable promise in very short range prediction of convection over the UK, and the Met Office has recently implemented a 1.5 km resolution forecast model in support of prediction of severe weather, especially extreme rainfall. Nevertheless, we must regard ourselves as just starting out in a new field and many challenges lie ahead. In particular, we need to understand when model predictions are reliable (often because of the role of predictable surface forcing) and when they are not. We need to understand more what scales are reliable in different circumstances and why, if possible predicting these parameters with the forecast. Application of km-scale modelling is a major issue and we need to manage expectations and, in particular, ensure that the finest detail is not taken too seriously.

Acknowledgements

Implementation of convective-scale NWP has required effort from very many people and space does not permit acknowledgement by name. The author would like to acknowledge the effort of the many who have contributed (and continue to do so).

References

Done, J.M., Craig, G.C., Gray, S.L., Clark, P.A. and Gray, M.E.B., 2006, Mesoscale simulations of organised convection: Importance of convective-equilibrium, *Quart. J. Roy. Meteorol. Soc*., **132**, 737 – 756.

Dixon M, Li Z, Lean H, Roberts N, and Ballard S.P. , 2009 Impact of Data Assimilation on Forecasting Convection over the United Kingdom Using a High-Resolution Version of the Met Office Unified Model, *Mon Wea Rev.*, **137**, 1562–1584.

Brian Golding, Peter Clark and Bryony May, 2005, The Boscastle Flood: Meteorological Analysis of the Conditions Leading to Flooding on 16 August 2004, *Weather*, **60**, 230-235.

Grahame, N., Riddaway, R., Eadie, A., Hall, B. and McCallum, E., 2009, Exceptional hailstorm hits Ottery St Mary on 30 October 2008, *Weather*, 255-263.

Hohenegger, C., D. Lüthi, and C. Schär, 2006: Predictability Mysteries in Cloud-Resolving Models. *Mon. Wea. Rev.*, **134**, 2095–2107.

Humphrey W Lean, Peter A Clark, Mark Dixon, Anna Fitch, Richard Forbes, Carol Halliwell and Nigel M Roberts, 2007, Characteristics of High Resolution NWP Models for Forecasting Convection over the UK, *Mon. Wea. Rev*., **136**, 3408-3424.

Humphrey W. Lean, Nigel M. Roberts, Peter A. Clark, Cyril Morcrette, 2009, The Surprising Role of Orography in the Initiation of an Isolated Thunderstorm in Southern England, *Mon. Wea. Rev*., **137**, 3026-3046.

Lock, A.P., Brown, A.R., Bush, M.R., Martin, G.M. and Smith, R.N.B., 2000, A New Boundary Layer Mixing Scheme. Part 1: Scheme Description and Single-Column Model Tests. *Mon. Wea. Rev.*, **128** 3187-3199.

Morcrette, C. J., Browning, K. A., Blyth, A. M., Bozier, K. E., Clark, P. A., Ladd, D., Norton, E. G. and Pavelin, E., 2006, Secondary initiation of multiple bands of cumulonimbus over southern Britain. Part I: An observational case study, *Quart. J. Roy. Meteorol. Soc*., **132**, 1021 – 1051.

G. A. Parton, G. Vaughan, E. G. Norton, K. A. Browning, P. A. Clark, 2008, Wind profiler observations of a sting jet, *Quart. J. Roy. Meteorol. Soc*., **135**, 663-680.

Roberts, N. and Lean, H., 2008, Scale-selective verification of rainfall accumulations from high-resolution forecasts of convective events. *Mon. Weather. Rev.*, **136**, 78-97.

Roberts, N. M., S. Cole, R. M. Forbes, R. Moore and D Boswell, 2009. Use of high-resolution NWP rainfall and river flow forecasts for advanced warning of the Carlisle flood, *Meteorol. Apps.* 16, 23 – 34.

Small-scale forecasting challenges associated with East Coast Lows

Rob Webb

Bureau of Meteorology, New South Wales Regional Office

Introduction

East Coast Lows (ECL) are regular visitors to the NSW coast, with a number of significant coastal impacts occurring annually (Speer et al 2009). Heavy rain and flooding, gales and coastal erosion have all become synonymous with these systems and NSW communities have suffered significant damage as a result. In the June 2007 ECL alone, the damage bill in the Newcastle area was estimated to be more than 1.5 billion dollars. There are many challenges that remain regarding how to provide the most effective warning service to coastal communities under threat from these destructive systems

Most commonly east coast lows conjure mental pictures of flooded towns, ships in distress, damaged houses and stark beach escarpments, a result of high seas. The cause of this more intense damage is quite often related to swathes of particularly severe weather that occur in narrow bands and for relatively short periods of time. From a communications point of view, it is difficult to hold the attention of the community for several days and the real challenge comes from designing a warning system and guidance products capable of providing rapid escalation of the threat message.

This paper outlines some of the small scale forecasting challenges associated with ECLs, the services by which community threats are communicated, the role of computer models in providing services and opportunities for development.

Discussion

Often the perception surrounding ECLs is that they are a single ‘event’ that bring about ongoing damage over the space of several days. Recent advances in observational networks have provided insight into the nature of the threat they pose and at the same time highlighted areas for improvements in the way numerical weather prediction models can be used to enhance the services the Bureau provides.

Flooding

Flooding from ECLs can come from two main sources. Firstly, the accumulation of rainfall over the course of a day or two can cause serious riverine flooding.

For relatively short periods within such events, intense rainfall can increase threat levels significantly. In 1984, areas south of Wollongong received over 500mm in 6 hours and over 700mm in 12 hours (Shepherd and Colquhoun, 1985). In August of 1998, areas around Wollongong received over 200mm in 3 hours and over 700mm over 2 days (Evans and Bewick, 2001). In the June 2007 ECL, Newcastle was inundated after serious flash flooding affected the town. In January 2008 more than 280mm fell in 6 hours at Bald Mountain in the far northeast of NSW and more recently in November 2009, Coffs Harbour was flooded after more than 189 mm fell in only 3 hours.

In many of these events, flood and severe weather warnings were current but one of the remaining challenges is to forecast the most likely onset time of the heaviest rain. In the case of the June 2007 event, the intense rainfall occurred along the convergence line between gale force southeast winds and much lighter west to northwest winds. Figure 1 shows a radar image at the time of significant flash flooding over the Newcastle area.

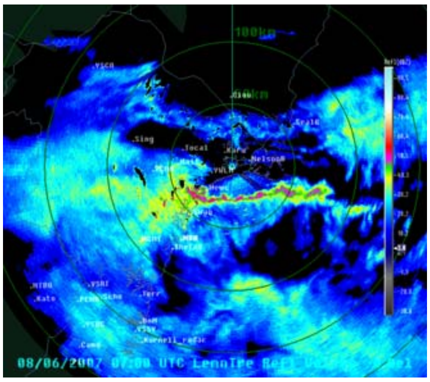

Fig 1: Radar image from the June 2007 East Coast Low showing an intense east west oriented line of convection. This line's continual movement over Newcastle led to serious flash flooding.

The actual distribution of intense short term rainfall relies on the optimal combination of a variety of factors. The complex interaction between the persistent low level convergence and mid and upper level flow can modulate the location, intensity and duration of the rainfall. Such interaction is difficult to nowcast, particularly given the sparse upper air network. A good conceptual model, awareness of the potential range of outcomes and a close eye on radar, satellite imagery and model data can assist forecasters to fine tune warning products in order to raise the awareness of emergency services and the community to the level of threat.

The importance of forecasting periods of more intense rain is not just applicable to flash flooding. The ability to predict the rainfall rate for hydrologists can lead to more accurate predictions of flood peak both in time and height. In NSW recent attempts at quantitative precipitation forecasting are designed to best link with the operations of the operational hydrologists. This not only promotes better services but a stronger appreciation for the dependencies of rainfall variability on the threat in the community.

Damaging Winds

Damaging winds regularly occur in the strong pressure gradients associated with east coast lows. Episodes of damaging winds will often occur over a series of days but a significant proportion of the damage may involve narrow swathes of very intense wind for periods of a few hours.

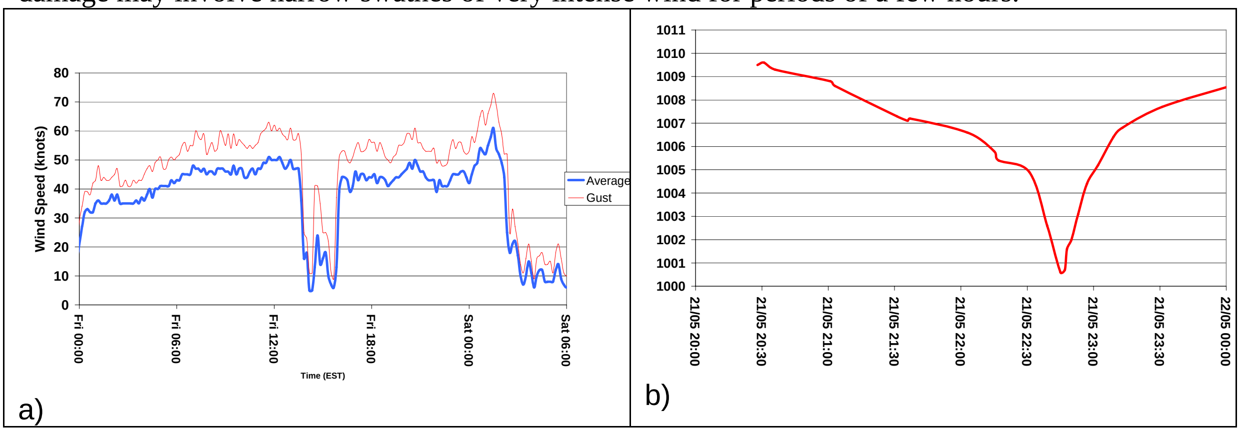

Fig 2: a) Anemograph from Norah Head just south of Newcastle on Friday 8 June 2007 and Saturday 9 June 2007 and Fig 2b) Barograph from Ballina AWS in the 4 hours between 2000 EST and midnight EST on 21 May 2009. This coincides with the passing of the vortex shown in Figure 3b

During the ECL event in May of 2009, an analysis of radar imagery showed 8 rotational centres crossing the southeast Queensland and northeast NSW coast over the course of 3-4 days. Some of these were coincident with a significant increase in wind and others an increase in rainfall. The maximum wind gusts recorded at Byron Bay during on of the vortices was 72 knots; comparable to

Cat 3 tropical cyclones. Figure 3b shows one of the intense vortices that crossed the coast near Ballina during the evening of 21 May 2009. Prior to impact, some NWP guidance indicated the potential for such vortices and led forecasters to a more detailed analysis of satellite imagery. The vortex was identified on satellite imagery approximately 6-8 hours prior to this image and the potential threat was indicated via live radio interviews in the area. The barograph from Ballina AWS which was in the vicinity of this vortex can be found in Figure 2b. This shows a drop in pressure 5 Hpa in 30 minutes

Another very severe source of wind damage associated with East Coast Lows has been documented in studies of cool season tornadoes (Mills and Hanstrum 1998). Convective uplift within regions of very strong low level shear has been shown to be a favourable location for tornado formation and there have been records of strong winter season tornadic activity in coastal NSW. Such events are difficult to forecast in specific locations but environments of enhanced risk of tornado development can be indentified.

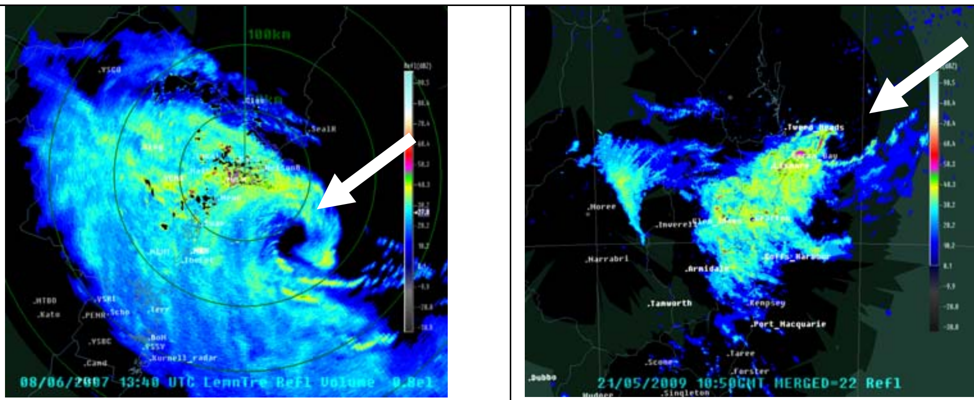

a b

Fig 3: a) 11:40pm radar image 8 June 2007 showing a vortex associated with increased wind speeds in the Newcastle area. b) 8:50pm 21 May 2009 radar image showing an intense vortex indicated by the arrow. As this low crossed the coast the pressure dropped 6 hPa in 45 minutes.

In the June 2007 ECL, a broad area of strong gales was evident for many hours and these were responsible for the difficulties experienced by a large container ship that ran aground near Newcastle. During the evening of the 8^{th}, a tight circulation appeared to move along a strong convergence line and briefly increased average wind speeds to 61 knots with gusts to 73 knots at Norah Head AWS, just south of Newcastle. Figure 2a shows the anemograph from Norah Head during this period. The lull in wind speed on Friday 8th between 1200 EST and 1800 EST occurred as a strong convergent line moved north to south across the area.

Along with the wind comes the potential for significant wave generation and coastal erosion. More transient in nature and often more complex to predict is the impact of sea-water inundation of coastal areas at high tide. A combination of astronomical tide, storm tide and riverine flooding can cause significant transient damage along the coastal interface.

All of the above small scale changes make the provision of services for East Coast Low challenging.

Services

The major impact from east coast lows can stretch over many days and their broad development and evolution is typically well captured in numerical guidance. The services provided for such events can sometimes begin 5-7 days prior as operational meteorologists start to discuss future events with emergency services and in some cases over media broadcasts. At this point in time impacts are described in terms of broad threats. Even in broad terms, such discussions can reduce the impact of a low by allowing pre-deployment of resources to the area by emergency services agencies. Closer to the event the Bureau is able to better delineate the threat and hopefully provide more advice on longevity and impact. Currently most regional forecasts only extend four days in advance and qualitative information can be included in these to emphasise the key impacts. Emergency Services

are generally briefed on the range of computer model scenarios, overlaid with the experience of the forecast office as to how such events develop.
Severe Weather Warnings are the primary focus of the Bureau's warning system and can be used to simply describe the evolving threat in the 1-2 days leading up to the initial impact. At such range, they still discuss the threat in terms of its broad evolution. It is at this time, strategies such as media releases can be used to better focus the media and community on the threat at hand. It is important that people be placed in the best possible position to respond to the developing threat.

As an event progresses, the service must be able to escalate appropriately to meet the needs of not only the broad ongoing threat but also the shorter, but very significant intense damage occurring on smaller scales.

Using computer models

Meteorologists can use an ingredients-based approach to forecasting the weather, assembling a picture of the expected range of outcomes and linking these to service decisions. Clearly computer modelling plays a major role throughout the life of an ECL. As the event unfolds the forecaster can use the information provided in a number of ways. Sometimes as important as the service is the risk approach to mobilising resources both internally and externally. Model output and experience can be used to change the operational posture of the forecasting centre; being prepared to change service direction makes the transition faster.

Vital pieces of the puzzle are the development of the low level mid level and upper level characteristics of the event. The goal of the forecasters, quite aside from warning the community, is to assess the model against current observational data and look for any variations in development or 'tracers' in the observational data that may allow the nowcasting process to begin in earnest. The use of a well designed data viewer in such circumstances allows forecasters to sift through the multitude of possible outcomes and develop a strong conceptual model of the evolving atmosphere.

Recent advances in techniques linking observational data with model data may prove a vital tool in operational readiness and warning strategy. One such technique (Seed 2005) links radar, rain gauge and short range NWP to produce probabilistic rainfall data.

Conclusion

This discussion provides a broad summary of some of the small scale forecasting challenges associated with ECLs in the context of the services provided by the Bureau of Meteorology and importantly the way computer models are used in the forecast process. With future advancements in the data viewing capability, model accuracy and service structure, the future looks bright for mitigating the impact of these extreme weather events.

References

Ebert, E.E., 2001: Ability of a poor man's ensemble to predict the probability and distribution of precipitation. *Mon. Wea. Rev.*, 129, 2461-2480.

Evans, J and Bewick, B. 2001: The Wollongong Flash Flood Event 15-19 August 1998, *Bureau of Meteorology Technical Report* 73.

Mills, G.A., Hanstrum, B.N. 1998: Australian cool season tornadoes, Part III: Use of an NWP model to identify potential for cool season tornado occurrence. Sixth Australian Severe Storms Conference, 23-27 August 1998, Bardon, Queensland pp103-107.

Seed, A.W. 2005: STEPS: an empirical treatment of forecast uncertainty. *BMRC Research Report* no. 111, Bureau of Meteorology Research Centre pp.131-137.

Shepherd, D. J. and Colquhoun, J. R. 1985: Meteorological aspects of an extraordinary flash flood near Dapto NSW. *Aust. Met. Mag*. 33 pp 87-102.

Speer, M, Wiles, P. and Pepler, A.: 2009: Low pressure systems off the New South Wales coast and associated hazardous weather: establishment of a database. *Aust. Met. Oceanogr. J.*, 58, 29-39

Woodcock, F. and Engel, C. 2005: Operational Consensus Forecasts. *Wea. Forecasting*, 20, 101-11.

Impact of assimilation resolution in areas that are densely observed and populated

Chermelle Engel, Peter Steinle and Chris Tingwell
Centre for Australian Climate and Weather Research, a partnership between CSIRO and the Bureau of Meteorology

Introduction

High impact weather often involves localized intense weather phenomena affected by things such as coastlines and topography. In order to accurately predict the performance of these phenomena it is important for forecasters to have access to accurate high-resolution NWP forecasts.

The accuracy of high-resolution model forecasts depends upon two factors being: the accuracy (and representativeness) of NWP modeling, and the accuracy of the initial conditions. NWP models respond to initial conditions in a non-linear manner (Davies et al., 2005). Therefore with current progress towards higher resolution NWP modeling, it is important to address the corresponding importance of high-resolution initial conditions.

High-resolution initial conditions are dependent upon a number of different factors including: background and observed error characterizations, background forecasts, observation networks and approximations to the full non-linear models for use in variational assimilation. A full discussion of the impact of each of these affects is out of the scope of this abstract but will be discussed in brief during the presentation (for more information see Rawlins et al. (2005) or Lorenc (2003)). In order to assess to the overall impact of the resolution of the initial conditions on NWP forecasts, we designed the following experiment.

Three different configurations of the 12.0km ACCESS-A model were run using: 80.0-, 37.5- and 12.0 km initial conditions (determined from ACCESS-G, ACCESS-R and ACCESS-A assimilation runs respectively) interpolated on to the ACCESS-A 12.0km grid (see Table 1).

Table 1: Configuration of various ACCESS systems

ACCESS System	Horizontal Grid		Vertical Levels (Lid ~62 km)	Physics Settings	Time Step	LBC from system
	UM	VAR				
G	N144 ~ 80 km	~160 km	L50	Met Office Global (N320)	600	n/a
R	37.5 km	75 km	L50	Met Office Global (N320)	600	G
A	12.5 km	36 km	L50	Met Office NAE	180	R

The impact of these different resolution initial conditions was assess by making 24 hour ACCESS-A forecasts and assessing the impact on verification statistics. We used a sample of ten runs, spaced at least 5 days apart over the December 2008 and August 2009 period.

Results

Verification statistics were produced against both assimilated grids (using ACCESS-A assimilations as a truth-proxy), and also against observations. The resolution of the initial conditions were found to have a discernable affect on the verifications throughout the 24 hour period, with the “gap” between verifications closing throughout the 24 hour period.

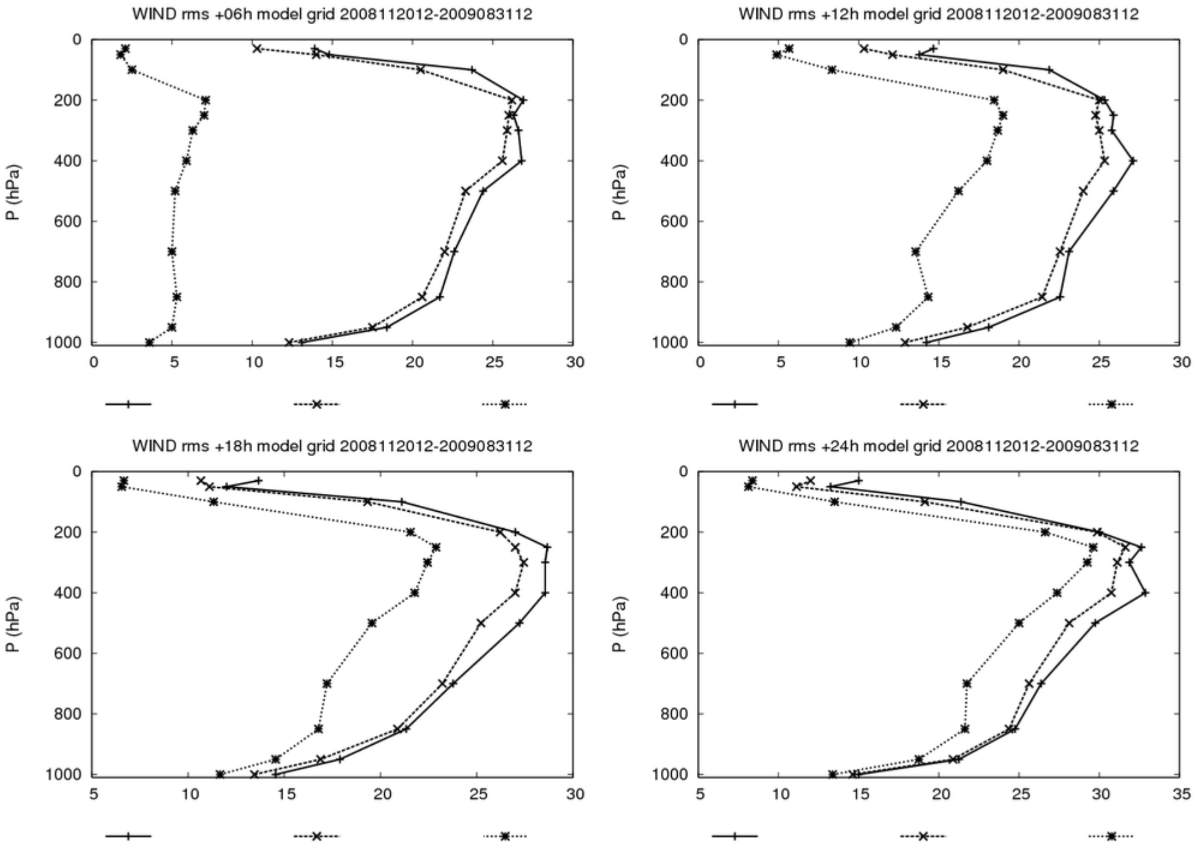

Fig. 1: Wind RMS verification statistics for 80.km/12.0km (solid), 37.5km/12.0km (dashed) and 12.0km/12.0km (dotted) for forecasting periods (left to right, top to bottom): +6, +12, +18 and +24 hours, for all pressure levels (as verified against ACCESS-A assimilation grids).

When verified against observations large degradations in comparative performance were found along densely observed and coastal areas for weather elements such and u- and v- 10 m wind, raising implication for high-impact weather forecasts. These results will be discussed as part of the presentation.

References

Davies, T., Cullen, M. P., Malcolm, A. J., Mawson, M. H., Staniforth, A., White, A. A. and Wood. N. 2005: A new dynamical core for the Met Office's global and regional modelling of the atmosphere. *Q. J. R. Meteorol. Soc.*, **131**, 1759-1782.

Lorenc, A. C. 2003: Modelling of error covariances by 4D-Var data assimilation. *Q. J. R. Meteorol. Soc.*, **129**, 3167-3182.

Rawlins, F., Ballard, S. P., Bovis, K. J., Clayton, A. M., Li, D., Inverarity, G. W., Lorenc, A. C. and Payne, T. J. 2007: The Met Office global four-dimensional variational data assimilation scheme. *Q. J. R. Meteorol. Soc.*, **133**, 347-362.

Heavy rain forecasts using the ACCESS model

Elizabeth Ebert

Centre for Australian Weather and Climate Research (CAWCR):
A partnership between the Bureau of Meteorology and CSIRO
Melbourne, Australia

Some early precipitation results shown at the 2008 CAWCR Modelling Workshop suggested that the quantitative precipitation forecasts (QPFs) from the ACCESS model were more accurate than rainfall predictions from the older GASP and LAPS models. This year an evaluation of more than 12 months of precipitation forecasts from the ACCESS and legacy systems is now possible, and confirms that there are indeed significant improvements in the new system. Both the location and amount of rainfall are more accurately predicted in the ACCESS system, with the improvement being most pronounced for the global model.

Results will be shown for forecasts of Australian rainfall over the past year, as well as for one or two recent heavy rain events. Two of the newer spatial verification approaches, namely the Contiguous Rain Area (CRA) object-based verification and the neighbourhood (fuzzy) verification approach, provide forecast users with additional information on QPF performance for rain events and as a function of scale.

NWP aspects of the Strategic Radar Enhancement Program – A Preview

Peter Steinle and Alan Seed

CAWCR – A partnership between CSIRO and the Bureau of Meteorology

Introduction

The Australian Bureau of Meteorology operates a network of approximately 60 radars to support its weather forecasting and warning services. The radar data has traditionally been used in a qualitative fashion via various visualization systems. The latest round of enhancements started in 2003 with the Radar Network and Doppler Services Upgrade (RNDSUP, Bally et al., 2007 and Seed at al., 2007).

During the life of RNDSUP, the Bureau's NWP systems were not suitable for the direct use of radar data, and so the program was focussed on developing nowcasting applications. With the introduction of the Australian Community Climate and Earth Simulator System (ACCESS), radar assimilation within mesoscale NWP systems has now become a possibility. The atmospheric prediction component of ACCESS is based on the Met Office Unified Model (UM) and associated four dimensional variational assimilation system (VAR, Rawlins et al., 2006 and Lorenc et al. 2000). This software has been used to assimilate radar data by the Joint Centre for Mesoscale Meteorology, University of Reading/Met Office, and the performance of the atmospheric modelling system is discussed in Lean et al. (2008).

In this year's federal budget, the Australian Government announced the Strategic Radar Enhancement Program (SREP). This is a $48M project over 7 years that is to provide for 4 new radars and improve the underlying science to assimilate radar data into the Bureau's NWP models. The expectation is for the NWP component of SREP to deliver operational systems to the Bureau capable of assimilating radar reflectivity and Doppler data.

This preview will outline some of the issues to be considered and a nominal "gold plated" target will be sketched out. The number of uncertainties and constraints associated with the project mean that the ideal system will probably not be feasible on current computing resources, but is a potential configuration after the 2015 upgrade. In the interim, this system will still provide a number of very high resolution NWP systems for the major urban areas and their environs that are suitably well served by the Bureau's observing network.

Potential NWP systems

The Bureau's current high resolution systems consist of 5km systems located over each of the state capitals and surrounding areas. Forecasts for these systems are initiated using initial conditions interpolated from the broader scale regional model (37.5km). The systems being developed as part of SREP are intended to gradually supersede the current high resolution systems.

Many major NWP centres are in the process of developing or implementing systems capable of assimilating radar data in an operational context, e.g. JMA (Honda et al. 2004), UK Met Office (Lean et al. 2008), NCAR (Huang et al. 2008), Meteo-France (Brousseau et al.2008) with other systems being developed in Korea, Germany and Canada. Features of these systems include resolutions of around 2km, shorter data cut-offs than synoptic scale systems, non-hydrostatic forecast models, variational analysis, and possibly a rapid update cycle. These features are generally considered as a minimum set to adequately forecast convective systems, and provide forecasts in a timely fashion.

These systems have been shown to improve the accuracy and detail of NWP, particularly during the 6-18 hour lead time which is a critical period for tactical decision making for many users. A key component of these systems is the use of suitably high time and space resolution information – which translates to the assimilation of radar data. The Doppler wind information drives the high resolution near-surface winds analyses, potentially having significant impact on air pollution modelling, fire weather, airport management and the like. The radar reflectivity on the other hand has been demonstrated in these systems to make a significant improvement to the first 12 hours of the rainfall forecasts. Finally, given the short life time of many mesoscale systems, it is essential to have the numerical guidance available as soon as possible. A common method for achieving this is the use of a rapid (e.g. hourly) update.

The development of such systems relies on several assumptions: that higher resolution assimilation over Australia will provide some benefit relative to downscaling, that a suitable quality controlled and close to homogenised radar data set is available and finally that the NWP system is capable of assimilating radar data.

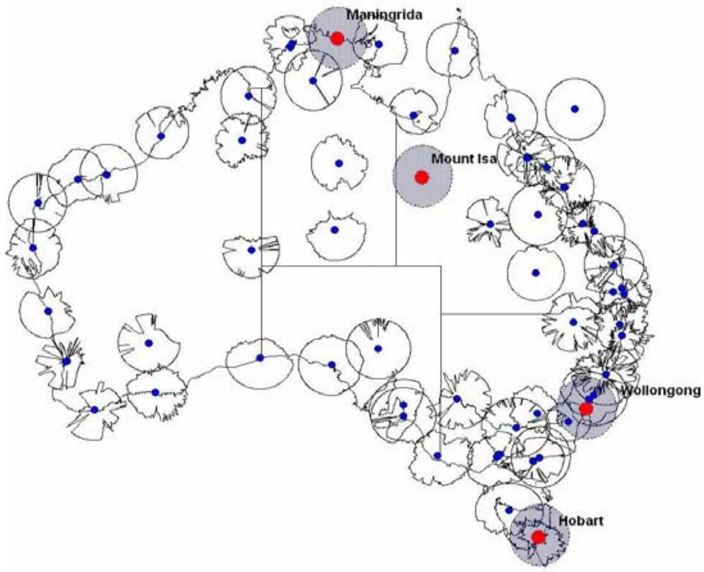

Fig. 1. The Australian Bureau of Meteorology's national radar network with indicative coverage for each station. The new SREP radars are shaded.

The advantages of assimilating at higher resolution over the Australian region have been shown in several studies, such as Chattopadhay et al. (2008), Vincent et al. (2008), Vincent and Kepert (2008) and Engel (this workshop). Based on these results, and overseas experience it is reasonable to expect that the combination of assimilation and a higher resolution model should yield significant improvement over the current 5km downscaled systems.

The Bureau's radar network is shown in Fig. 1 and consists of a variety of instruments of varying ages. The network is therefore not only inhomogeneous in coverage but also in accuracy and calibration. One of the first tasks of the SREP project is to generate a national, calibrated, quality controlled, composite radar reflectivity data set suitable for use within NWP. This data set will also be used for quantitative rainfall estimation and prediction.

The possibility of the UM and VAR system to use radar reflectivity and Doppler winds has been demonstrated in the UK Met Office. It is expected that ACCESS mesoscale systems should therefore be possible over Sydney, Melbourne and Brisbane at least. These three centres have the advantage of being mostly surrounded by relatively dense observations, including a rain gauge network suitable for calibrating precipitation estimates.

There are however considerable uncertainties associated with this project, not the least of which is acquiring appropriately skilled staff. The other unknown is how the ACCESS systems will perform at these resolutions on the Sun Constellation, although this can be partially ameliorated by adjustments to resolution, domain size, and the length and frequency of forecasts.

Despite these uncertainties there are some advances to the 5km city-based systems that are clearly feasible in the short term. The most obvious is adding an assimilation component, using the same observations as the regional system, and a possible resolution increase. These short term upgrades will then form the basis for advanced mesoscale NWP systems. Overseas experience has also shown that assimilating reflectivity data can add value to systems with resolutions around 10km – i.e. the resolution of the national NWP system ACCESS-A. With the development of a national, calibrated radar product this also becomes feasible. These two starting points lead to the possible outlines for the SREP systems outlined in Table 1. This outline relies heavily on the projected performance of the new computer and the performance of the NWP systems in the tropics. The outline is therefore an aspirational or "gold standard" target.

References

Bally, J,. A. Bannister, K. Cheong, G. Dance, T. Keenan, T., and P. Purdam, 2007: *"The Australian Nowcasting System"*. Proceedings of the 33rd AMS Radar Conference, 2007, Cairns.

Brousseau, P., F. Bouttier, G. Hello, Y. Seity, C. Fischer, L. Berre, T. Montmerle, L. Auger, and S. Malardel, 2008: "*A prototype convective-scale data assimilation system for operation : the Arome-RUC*". HIRLAM Technical Report **68**, 23–30.

Chattopadhyay, M., C. L. Vincent, and J. D. Kepert, 2008: *"MALAPS and MesoLAPS: A case study of East Coast Low event of 27th June 2007"*. CAWCR Research Letters, **1,** pp. 24–30.

Honda, Y., M., Nishijima, K. Koizumi, Y. Ohta, K. Tamiya, T. Kawabata and T. Tsuyuki, 2005: *"A pre-operational variational data assimilation system for a non-hydrostatic model at the Japan Meteorological Agency: Formulation and preliminary results"*. QJRMS., **131**, pp. 3465-3475.

Huang, X.-Y., T. Auligne, D. Barker, Y. Chen, M., Demirtas, Y.-R. Guo, M. Krysta, R. Li, H.-C. Lin, Z. Liu, S., Rizvi, H. Shao, C. Snyder, T. Vukicevic, Q. Xiao, D. Wang, W. Wang and X. Zhang, 2009: *"AFWA DA FY08 Weather Research and Forecasting Data Assimilation Improvement and Support"*. http://www.mmm.ucar.edu/wrf/users/wrfda/pub-doc.html

Lean, H.W., P.A. Clark, M. Dixon, N.M. Roberts, A. Fitch, R. Forbes and C. Halliwell, 2008: *"Characteristics of High-Resolution Versions of the Met Office Unified Model for Forecasting Convection over the United Kingdom"* Mon.Wea.Rev. **136** pp.3408-3424.

Lorenc, A.C., S.P. Ballard, R.S., Bell, N.B. Ingleby, P.L.F. Andrews, D.M. Barker, J.R. Bray, A.M. Clayton, T. Dalby, D. Li, T.J. Payne and. F.W. Saunders, 2000: *“The Met Office global 3-dimensional variational data assimilation scheme”*. QJRMS. **126** pp 2991–3012.

Rawlins, F., S.P. Ballard, K.J. Bovis, A.M. Clayton, D. Li, G.W., Inverarity, A.C. Lorenc,. and T.J. Payne, 2006: *“The Met Office global four-dimensional variational data assimilation scheme”*, QJRMS, **133**, pp. 347-362.

Seed, A.W., E. Duthie and S. Chumchean, 2007: *“RAINFIELDS: The Australian Bureau of Meteorology System for Quantitative Precipitation Estimation*”. Proceedings of the 33rd AMS Radar Conference, 2007, Cairns.

Vincent, C. L., W. P. Bourke, J. D. Kepert, M. Chattopadhay, Y. Ma, P. J. Steinle, and C. I. W.Tingwell, 2008: *“Verification of a high-resolution mesoscale NWP system”*. Aust. Meteor. Mag., **57**, 213–233.

Vincent, C. L. and J. D. Kepert, 2008: *“Using kinetic energy spectra from NWP to forecast wind variability”*. BMRC Res. Lett., **8**, pp. 27–34. 2007.

Table 1. Aspirational targets for the SREP systems. The resolutions and frequency of updates are subject to computer and software performance.

	Research	***Operational***
2009-10	• 2-5km city based systems **with assimilation**, 00 & 12UTC	
2010-11	• 2-5km systems with assimilation **8xdaily**	• 2-5km systems **with assimilation,** 00 & 12UTC, 24-36hr
2011-12	• 2km city-based **8xdaily**, ~18hr with **Doppler winds**	• 2-5km systems with assimilation operational, **4xdaily**
2012-13	• 10km National with **reflectivity** • 2-5km **relocatable, 8xdaily, Doppler winds**	
2013-14	• 2km city based, 8xdaily with Doppler and **radar reflectivity** • 2km relocatable, 8xdaily with Doppler and **radar reflectivity**	• 10km National with **reflectivity**
2014-15	• 2km city based, **24xdaily** with Doppler and radar reflectivity • 2km relocatable, **24xdaily** with Doppler and radar reflectivity	• 2-5km city based, 8xdaily with Doppler and **radar reflectivity** • 2-5km relocatable, 8xdaily with Doppler and **radar reflectivity**
2015-16		• 2km city based, **24xdaily** with Doppler and radar reflectivity • 2km relocatable, **24xdaily** with Doppler and radar reflectivity

NWP modelling of high impact weather events at JMA

Yuki Honda
Japan Meteorological Agency, Chiyoda, Tokyo, Japan

Introduction

Japan is located at the mid latitude and has been exposed to the various severe weather phenomena / high-impact weather events such as the extra-tropical cyclone, typhoon, BAIU front. To secure the lives and the properties of citizens from the risk of natural disasters, the Japan Meteorological Agency operates a suite of numerical prediction models from global to meso-scale, and also from deterministic and ensemble forecasts. In this paper, a high-resolution limited area model is introduced, which is operated for the main purpose of the disaster prevention.

Meso Scale Model (MSM)

To enhance the disaster prevention weather information, the JMA decided to develop a high-resolution limited area model and started the pre-operational implementation of a Meso Scale Model (MSM) in March, 1998. MSM became operational in March 2001 when the new super computer, HITACHI SR8000, was installed at JMA. Through many major upgrades, current MSM consists of JMA nonhydrostatic model (JMA-NHM, or simply NHM) as a forecast mode and JMA-NHM-based 4D-Var system (JNoVA) as an analysis system and has been executed every 3 hours to produce 15 or 33 hour forecasts with grid spacing of 5km on HITACHI SR11000. The brief history of major upgrades of MSM is shown in Table 1.

Our efforts to improve MSM have been focused especially on the accuracy of quantitative precipitation forecasts (QPFs). Figure 1 shows the history of the score QPFs of MSM since 2001. The steady improvement of QPF is apparently recognized from this figure.

The factors that determine the model performance are mainly initial fields, a forecast model and boundary conditions. In the following sections, past developments implemented to

Table 1: Brief history of MSM

Month / Year	Event
March 1998	Start of the pre-operation of Meso Scale Model (MSM) on HITACHI S3800
March 2001	Replacement of JMA supercomputer: Installation of HITACHI SR8000 Start of the operation of MSM on HITACHI SR8000
March 2002	Replacement of data assimilation system: Introduction of 4D-Var (Meso 4D-Var)
September 2004	Replacement of forecast model: Introduction of JMA nonhydrostatic model (NHM)
March 2006	Replacement of JMA supercomputer: Installation of HITACHI SR11000 Increase of model resolution: From 10km to 5km in horizontal, From 40 to 50 layers in vertical
April 2009	Replacement of data assimilation system: Introduction of a new 4D-Var (JNoVA)

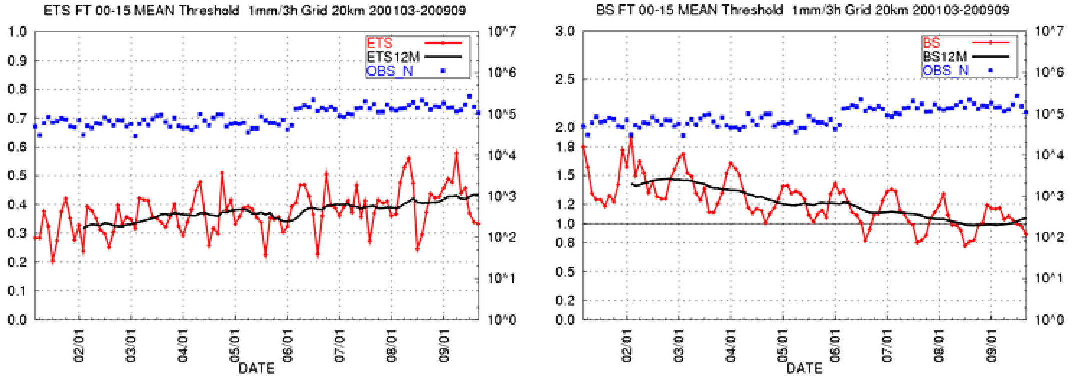

Fig. 1: The history of the score of 3 hourly accumulated precipitation forecast of MSM. Left panel shows the equitable threat score and right one is the bias score. The horizontal axis is a date from March 2001 till September 2009.

MSM are reviewed from each viewpoint.

Initial Fields: 4D-Var and the Dense Observation Data

Whether the severe weather phenomena are analyzed in the initial fields or not is a kind of most important factor that determines the quality of prediction within the forecast range of ~1 day. We would like to introduce the mesoscale analysis system.

Introduction of 4D-Var

The JMA is the first operational NWP center that has introduced the four-dimensional variational data assimilation system (4D-Var) for mesoscale analysis in 2002 (Ishikawa and Koizumi 2002). In the beginning of MSM operation, an hourly analysis system named ‘pre-run’ was used as mesoscale analysis system. The pre-run was a sequential data assimilation system for 3 hours that consisted of the analysis system using the statistical/optical interpolation method (OI) and the physical initialization scheme (PI). PI was used to assimilate the Radar/Raingauge Analyzed Precipitation (RA) that was the quantitative precipitation estimation using Radar data and rain gauge data. This system was used for 1 year and replaced with Meso 4D-Var in March 2002. Meso 4D-Var was an incremental form of 4D-Var using the adjoint model of the hydrostatic spectral model with full physics. Although both OI and 4D-Var consider the statistical error covariance of the background and observation, 4D-Var can also consider the dynamical balance represented by the forecast model. Since the adjoint model included the moist physics, Meso 4D-Var allowed us to assimilate RA directly together with other observation data. By this upgrade of mesoscale analysis, the score of QPF was improved very much. This will be discussed again in the following subsection.

Meso 4D-Var has been operated for 7 years since 2002. During this period, the forecast model of MSM has been upgraded from the hydrostatic spectral model to a nonhydrostatic grid model, NHM, in September 2004. Since then it has been desired to upgrade the mesoscale analysis from Meso 4D-Var to a new 4D-Var based on NHM because the analyzed field should be optimal for a forecast model adopted in 4D-Var in theory. Besides, NHM performs much better than the hydrostatic spectral model. In April 2009, the new 4D-Var named JNoVA (Honda et al. 2005) was successfully introduced to replace Meso 4D-Var. By this upgrade, the analysis resolution is also increased from 10km to 5km in horizontal and from 40 to 50 layers in vertical. It is statistically verified that the QPFs are improved both in summer and in winter (Fig.2) (Honda and Sawada 2009).

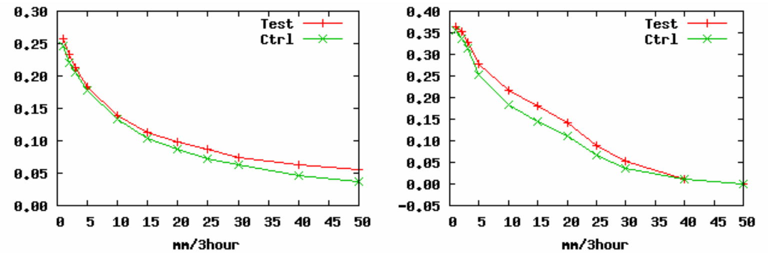

Fig. 2: Equitable threat scores of three-hourly accumulated precipitation forecasts in summer (right) and winter (left). The red and green lines show the results of JNoVA (Test) and Meso 4D-Var (CTRL), respectively. The horizontal axis is the threshold value of the rainfall amount.

Assimilation of Dense Observation Data

In addition to highly sophisticated data assimilation algorithm, it is also important to assimilate the dense observation data that can capture the mesoscale weather phenomena. All observation assimilated in the mesoscale analysis are shown in Table 2. The impact of assimilation of some observation will be shown below.

First of all, direct assimilation of precipitation using 4D-Var is one of the characteristics of the mesoscale analysis. Currently two kinds of surface precipitation data are available. One is RA and the other is the retrieved data from satellite microwave radiometer such as AMSR-E. As described in the previous subsection, RA is the quantitative precipitation estimate that is created by calibrating the low-level composite radar reflectivity data with rain-gauge data. RA is assimilated as hourly accumulated precipitation. Since the probability distribution of observation error of RA is quite different from Gaussian distribution, the exponential distribution is assumed for RA (Koizumi et al 2005). The assimilation of RA improved the QPF of the BAIU front significantly compared to the result of Pre-run (Fig.3). Since October 2009, the total precipitable water retrieved from ground-based GPS data also started to be assimilated over the land so that the moisture fields are analyzed better.

Regarding the satellite microwave radiometer, not only the precipitation but also the

Table 2: the List of observation and elements assimilated into mesoscale analysis

Element	Observation				
Pressure	SYNOP	SHIP	BUOY	TEMP	Typhoon Bogus
Wind	TEMP	PILOT	Wind Profiler	AMDAR	SATOB
	Scattermeter	Doppler Radar	Typhoon Bogus		
Temperature	TEMP	AMDAR	SATEM	ATOVS	
Relative Humidity	TEMP				
Total Precipitable Water	Satellite Microwave Radiometer		Ground-based GPS		
Precipitation	Radar/Raingauge Analyzed Precipitation		Satellite Microwave Radiometer		

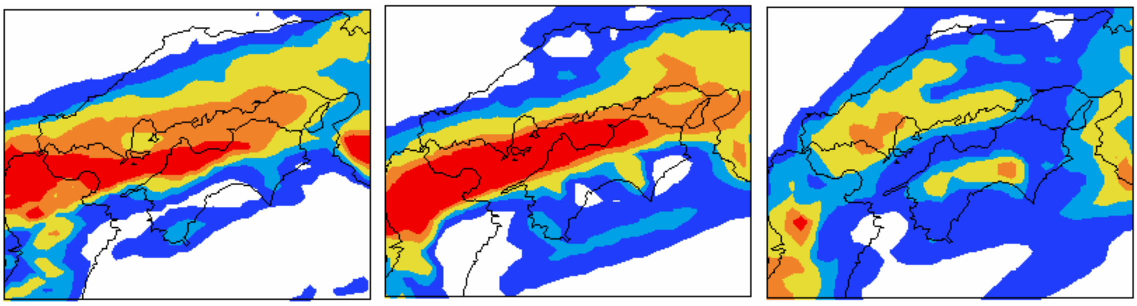

Fig. 3: 3 hour accumulated precipitation of 12-15UTC on 19 June 2001.From the left, the RA and two forecasts from the initial fields of Meso 4D-Var and Pre-run, respectively. Both forecasts are 3 hour forecasts from 12 UTC initial on the same day.

total precipitable water is retrieved over the sea. According to Table 2, it is apparent that there is no other observation relating humidity over the sea except this satellite data. Since the Japan is surrounded by the sea, the moisture from the sea is quite important for the accurate forecast of the precipitation. So the retrieved data are quite useful to improve the initial fields.

Other dense observation data such as the aircraft data, wind profiler data, Doppler radar data and scattermeter data are also essential for the improvement of the initial fields although the detail of their impacts are not shown here. Besides, it should be pointed out that the pseudo observation data, typhoon bogus, is quite useful to analyze the location and the intensity of the typhoon.

Forecast Model: JMA nonhydrostatic model

At the beginning, a forecast model of MSM was a hydrostatic spectral model. Although this model has been used operationally for a long time as another limited area model named RSM (Regional Spectral Model) with coarser grid spacing of 20km, it became obsolescent gradually. Therefore, a new nonhydrostatic model, NHM, was developed and became operational in September 2004 (Saito et al. 2006). The specifications of the NHM used in the current operational MSM are listed in Table 3.

Moist Processes

To avoid the pseudo grid-scale convection, Kain-Fritsch convective scheme (KF scheme) (Kain and Fritsch 1990; Kain 2004) is used with bulk microphysics. The original KF scheme was provided from WRF model in 2002 by the courtesy of Dr. Kain and Dr. Dudhia. To suppress the spread of the weak rain, Kessler type auto-conversion scheme was introduced. (Ohmori and Yamada 2003).

Table 3: Specifications of the NHM used in the current MSM

Iterm	Description
Governing Equation	Fully compressible nonhydrostatic equations with a map factor
Advection	4^{th} order flux form with flux correction in horizontal 2^{nd} order flux form in vertical
Diffusion	4^{th} order linear diffusion and nonlinear diffusion Targeted moisture diffusion
Moist process: grid-scale	2 moment 3-ice bulk microphysics
Moist process: sub-grid scale (convection)	Modified Kain-Fritsch convective scheme
Turbulent process	Mellor-Yamada-Nakanishi-Niino Level3 Similarity theory in bulk formulae for surface layer
Surface flux scheme	Beljaars and Holtslag (1991)
Radiation process	Two-stream with delta-Eddington approximation for shortwave Table look-up and k-distribution methods for longwave
Land surface process	Slab model(Ground temperature predicted by 4-layer diffusive model, Soil moisture: force restored method)

Another main modification was the introduction of a new trigger function that considered the temperature perturbation based on the relative humidity (Narita 2006). The formula of the trigger function follows the one proposed by HIRLAM (Undén et al. 2002) although the latest version of HIRLAM has already removed this trigger. This trigger is effective when the lowest atmosphere is wet and dynamical forcing is weak. This is a kind of typical weather condition of the unstable convective precipitation in summer. The unstable convective activity is difficult to simulate using a forecast model with grid spacing of 5km, but it may cause the natural disaster. Although the precipitation amount is far from the observed one, the model can sometimes simulate the spread of the precipitation by using the new trigger function (Fig. 4). Then it would draw the forecasters' attention.

Several parameters such as life time of deep and shallow convections were tuned to

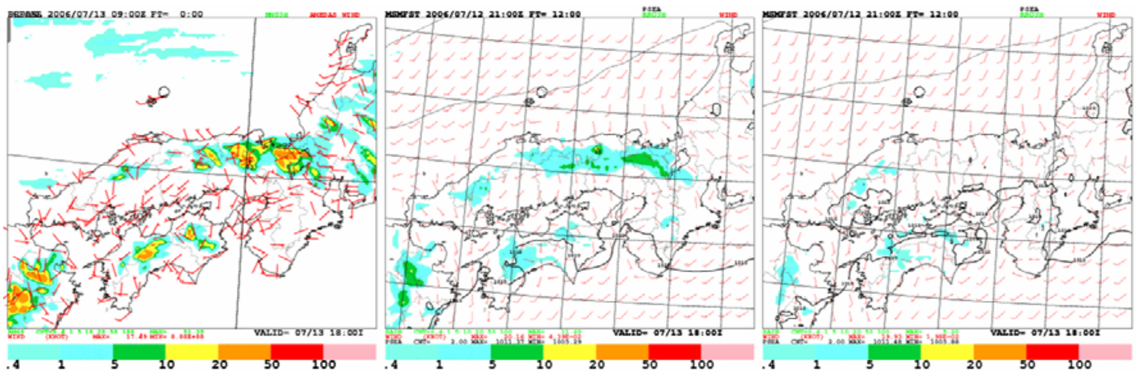

Fig. 4: 3 hour accumulated precipitation of 06-09UTC on 13 Jul. 2006. From the left, RA and two forecasts by NHM with and without the trigger function of the relative humidity in KF scheme, respectively. Both forecasts are 12 hour forecasts from 21UTC initial of 12 Jul. 2006.

match the simulated precipitation frequency with the observation and improve the performance of QPFs by NHM (Ohmori and Yamada 2006)

Turbulent Process

Turbulent Process plays an important role especially in the planetary boundary layer (PBL) from where most convective activity occurs. The improved Mellor-Yamada-Nakanishi -Niino Level 3 scheme (MYNN3) (Nakanishi and Niino 2004, 2006) was introduced into NHM as a new turbulent scheme (Hara 2007). MYNN3 is corrected using the Large Eddy Simulation. Compared to Deardorff turbulent scheme, MYNN3 is the higher order closure scheme and the counter gradient terms are naturally considered to represent the non-local effect in the convective PBL. Simultaneously, partial condensation scheme was also introduced, which estimates cloud fraction and cloud water content for radiation and turbulent processes through the probability density function of the fluctuations (Hara 2007). These new schemes bring the better diurnal changes of surface temperature and wind, vertical profiles of temperature and wind and also give the remarkable impact for a heavy rain case (Fig.5).

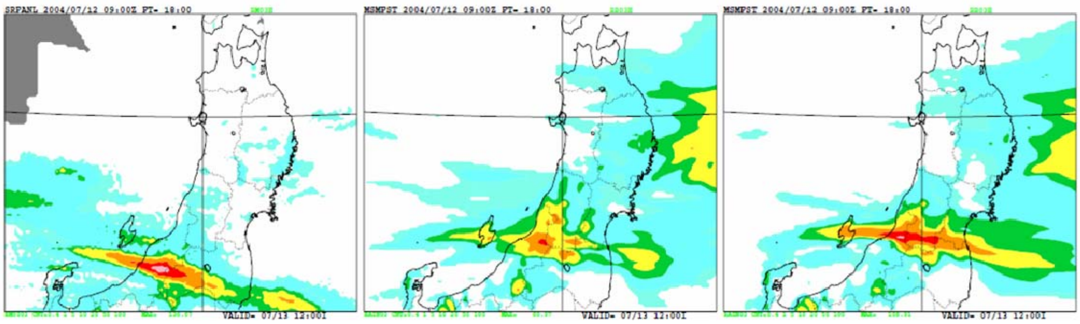

Fig. 5: 3 hour accumulated precipitation at 18 hour forecast from 09UTC initial on 12 Jul. 2004. From the left, RA of 00-03UTC on 13 Jul. 2004 and two forecasts of NHM using Deardorff scheme and MYNN3 with partial condensation scheme, respectively.

Other Processes

Other processes also have some impacts on forecast performance. The developments relating these processes will be also reviewed in the presentation.

Lateral Boundary Condition: From RSM to GSM

MSM used to be nested into Regional Spectral Model (RSM) that was another limited area model with grid spacing of 20km operated since 1996. RSM was retired when the horizontal resolution of Global Spectral Model (GSM) was raised from around 60km (TL319) to around 20km (TL959). MSM has been nested into GSM since then.

The statistical upper-air verification shows that the simulated atmosphere of GSM is better than that of RMS (not shown). This feature affects on MSM and the upper-air verification of MSM is also improved by changing the L.B.C.s from RSM to GSM (not shown). However, it doesn't mean the QPF would be improved. Actually, GSM has a dry bias in middle troposphere and moist bias near surface. This kind of biases also affects on the atmospheric structure and the moist processes of MSM have not been adjusted yet. Therefore the score of QPF is neutral despite the improvement of the atmospheric structure.

Heavy Rain Events in Summer 2008

MSM showed the worst performance of QPFs in summer 2008 since starting the operation of MSM (Fig.1). Mainly in July and August, many events of localized and concentrated heave rainfall occurred unusually and some of them damaged the lives and properties seriously. We investigated the 3 special cases in which MSM failed to forecast the rainfall: (a) Hokuriku/Kinki heavy rainfall around 28 Jul. 2008, (b) Toga River heavy rainfall around 5 Aug. 2008, and (c) "Heavy rainfall in end of August 2008".According to Ikuta (2009), the main reason of the forecast failures in case (a) and (c) is the quality of the initial fields. Especially, moisture fields were not well analyzed in both cases. In case (a), it was verified that the forecast became better using the initial field analyzed by JNoVA instead of the initial field by Meso 4D-Var. Because the low-level moisture flux from the ocean were analyzed better in the analysis of JNoVA. About this case (a), .it was also shown that the modification of the Kain-Fritsch scheme could improve the forecast (Fig. 6) (Narita 2009). Contrary to these 2 cases, MSM forecasted the weak rain over Kanto plain which was created by KF scheme. However, the peak amount was much less than the observed maximum value. Because the rain was produced from the convections whose horizontal scale was around 20km.It is quite hard to simulate accurately by MSM because of the shortage of model resolution. To improve the forecasts of this kind of convective activities, we need a finer resolution NWP system.

Future Plan: Local Forecast Model (LFM)

We plan to operate a new limited-area model named Local Forecast Model (LFM) on next supercomputer. This horizontal resolution of LFM is around 2km. We intend to simulate the deep convection explicitly to improve the forecasts of localized heavy rainfall.

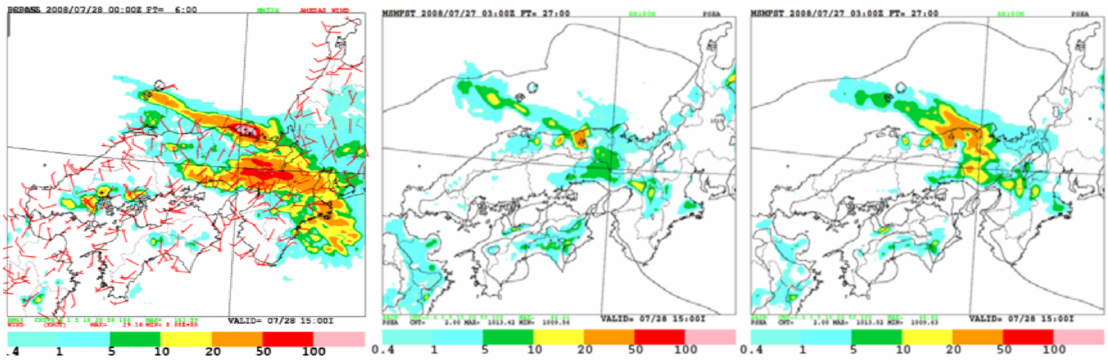

Fig. 6: 3 hour accumulated precipitation of 03-06UTC on 28 Jul. 2008. From the left, RA and two forecasts with original KF scheme and with modified KF scheme, respectively. Two forecasts are 27 hour forecasts of 03UTC initial on 27 Jul..2008.

Acknowledgment

The author would like to thank Dr. Tingwell, Dr. Hollis and Dr. Jemmeson for their support to participate in the 4th CAWCR modeling workshop. The author also thanks our colleagues for kindly providing the figures of their works.

References

Hara, T. 2007. Implementation of improved Mellor-Yamada Level 3 scheme and partial condensation scheme to JMANHM and their performance. *CAS/JSC WGNE Research Activities in Atmospheric and Oceanic Modelling, 36,* 4-07.

Honda, Y., el al. 2005. A pre-operational variational data assimilation system for a non-hydrostatic model at the Japan Meteorological Agency: Formulation and preliminary results. *Quart. J. Roy. Meteorol. Soc., 131*, 3465-3475.

Honda, Y., and Sawada, K. 2009. Upgrade of the Operational Mesoscale 4D-Var System at the Japan Meteorological Agency. *CAS/JSC WGNE Research Activities in Atmospheric and Oceanic Modelling, 39*, 1-11.

Ikuta, Y. 2009: Verification of quantitative precipitation forecasts. *Training Text of Numerical Prediction.* 1-12. (in Japanese)

Ishikawa, Y. and K. Koizumi, 2002: One month cycle experiments of the JMA mesoscale 4-dimensional variational data assimilation (4D-Var) system. *CAS/JSC WGNE Res. Activ. Atmos. Oceanic Modell., 32*, 0126-0127.

Koizumi, K., Y. Ishikawa, and T. Tsuyuki, 2005: Assimilation of precipitation data to JMA mesoscale model with a four-dimensional variational method and its impact on precipitation forecasts. *Sci. Online Letts. Atmos.*, **1**, 45-48.

Kain, J. S. 2004. The Kain-Fritsch convective parameterization: An update. *J. Appl. Meteor., 43*, 170-181.

Kain, J. S. and Fritsch, J. M. 1990. A one-dimensional entraining/detraining plume model and its application in convective parameterization. *J. Atmos. Sci., 47*, 2784-2802.

Nakanishi, M. and Niino, H. 2004. An improved Mellor-Yamada level 3 model with condensation physics : Its design and verification. *Bound.-Layer Meteor., 112*, 1-31.

Nakanishi, M. and Niino, H. 2006. An improved Mellor-Yamada level-3 model: Its numerical stability and application to a regional prediction of advection fog. *Bound.-Layer Meteor., 119*, 397.407.

Ohmori, S. and Yamada, Y. 2003. Introduction of Kain-Fritsch scheme into operational NHM. *5th workshop on nonhydrostatic modeling.* 31-32. (in Japanese)

Ohmori, S. and Yamada, Y. 2006. Development of cumulus parameterization scheme in the nonhydrostatic mesoscale model at the Japan Meteorological Agency. *CAS/JSC WGNE Research Activities in Atmospheric and Oceanic Modelling, 35*, 4-21.

Saito, K., et al. 2006. The operational JMA non- hydrostatic mesoscale model. *Mon. Wea. Rev., 134,* 1266-1298.

Undén, P., et al. 2002. *HIRLAM-5 Scientific Documentation*, pp.144.

Extreme sea levels and coastal vulnerability in a changing climate - a state-wide assessment for Victoria

Kathleen L. McInnes[1], Ian Macadam[2] and Julian O'Grady[1]

[1]Centre for Australian Weather and Climate Research: A partnership between CSIRO and the Bureau of Meteorology, PMB#1 Aspendale, 3195
[2]University of New South Wales, Sydney, NSW, Australia, 2052

Introduction

Victoria's coastline is highly valued for its aesthetic, ecological, recreational and economic assets. Since the late 1990's, a rapid increase in the rate of internal migration from large cities to the coast, has led to an increase in development pressure along the coast, which in turn poses challenges for sustainable management of the coast. Climate change through rising sea levels and possible changes to severe storms has the potential to create significant additional challenges to coastal management. Such issues have prompted the present study which is concerned with the evaluation of storm tides under present and future climate conditions and their possible contribution to coastal inundation.

This study employs hydrodynamic models and statistical techniques to develop information on the extreme sea level hazard along Victoria's coast. These extreme sea levels usually occur as a result of the combination of tides with storm surges associated with weather systems that bring westerly winds to the south coast of Australia. In this study, extreme sea levels are estimated using an approach similar to that of McInnes et al (2009), whereby tide and surge heights are evaluated separately and then combined to estimate 'storm tide' heights. A hydrodynamic model is used to estimate tide and surge heights for the entire Victorian coast and return periods are estimated using extreme value statistical analysis.

The study also explores the impact of a range of plausible climate change scenarios on sea level extremes under future climate conditions. A Digital Elevation Model (DEM) of Victoria's coast, acquired as part of the Future Coasts Program, is used in combination with the extreme sea levels and climate scenarios to evaluate potential inundation at a selection of sites along Victoria's coast.

The remainder of this paper is structured as follows. The following section briefly describes the method and the future climate change scenarios used in this study. Then extreme sea level and inundation results are presented and finally concluding comments are presented.

Method

For the purposes of planning and engineering design, extreme sea level events are commonly expressed in terms of return periods. A return period is defined as the average amount of time between events that exceed a particular level. In this study, maps of 1 in 100 year sea levels are developed. These are then combined with a simple inundation model and the Future Coasts DEM and to identify parts of the Victorian coast that are vulnerable to inundation.

The most important components of extreme sea levels along the Victorian coast are tides and storm surges; sea level elevations caused by the high winds and low mean sea level pressure associated with storms. In this study, these components are evaluated separately and then combined to estimate 'storm tide' heights using the well established Joint Probability Method (JPM) (e.g. Tawn and Vassie (1989). The approach used in this study is illustrated schematically in Figure 1.

The main synoptic weather systems responsible for storm surges along the coastline of Victoria are west-to-east travelling cold fronts, which occur year round but tend to be more frequent and intense in the winter months (McInnes and Hubbert, 2003). The large spatial scale of these systems means that they impact a large stretch of coastline when they occur and so the resultant elevated coastal sea levels are well captured by the available tide gauge network. This is exploited by this study, which uses a selection of tide gauge records to identify a population of significant storm surge events occurring during the 1966-2003 period, for which largely complete tide gauge records were available. Probabilities of extreme storm surge heights, which are required as input to the Joint Probability Method, are developed from an analysis of this population using the approach of McInnes et al. (2009).

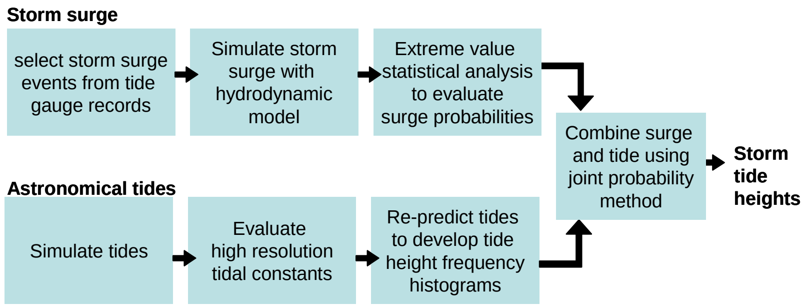

Figure 1: Schematic diagram illustrating modelling approach used in this study.

The hydrodynamic model GCOM2D (Hubbert and McInnes, 1999) was used to simulate each of the storm surge events in the population. In order to capture the evolution of the storm surge along the southern coastline and into the complex embayments along the Victorian coastline, simulations were carried out over a set of grids, the four higher resolution inner grids with resolutions of 50 to 100 m over Port Phillip Bay, Western Port Bay, Corner Inlet and the northern end of Lakes Entrance were nested within an intermediate grid at 1 km resolution covering Bass Strait, which in turn was nested in a 5 km resolution outer grid (Figure 2) extending to the west. NCEP reanalyses provided the atmospheric conditions required to simulate each of the identified storm surges.

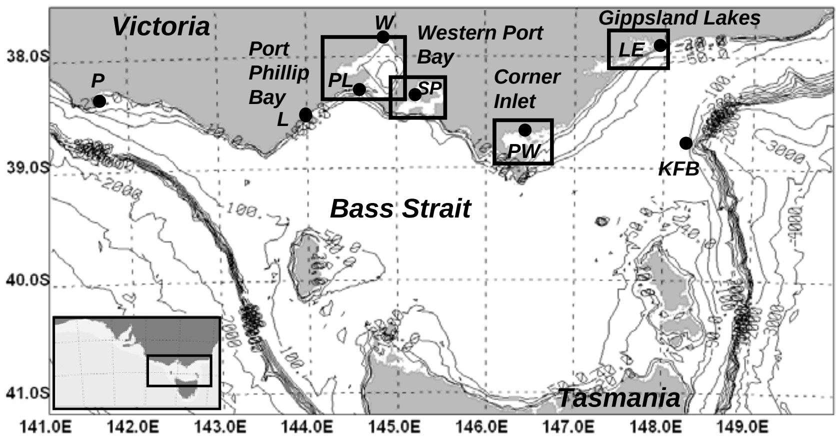

Figure 2: The horizontal domain of the 1 km resolution Bass Strait storm surge model. Land area is shaded in grey and bathymetric contours of 10, 20, 40, 50, 100, every 100 m to 1000m and every 1000m thereafter. P=Portland, PL=Point Lonsdale, SP=Stony Point, PW=Port Welshpool, LE=Lakes Entrance, KFB=Kingfish B oil platform. The insert shows the region covered by the 5 km outer grid while the four rectangles indicate where the higher resolution innermost grids were located.

Future increases in mean sea level and possible changes in wind speed due to climate change will influence the height and frequency of extreme sea level events along the Victorian coast. Two scenarios incorporate estimates of sea level rise by Hunter (2009) that correspond to the IPCC's SRES A1FI scenario for future greenhouse and aerosol emissions (Nakićenović and Swart, 2000) and are considered both with and without consistent high-end estimates of wind speed increases obtained from recent climate change projections developed for Australia (CSIRO and Australian Bureau of Meteorology, 2007) (Scenarios 1 and 2 in Table 1).

The observed rate of global sea-level rise since 1990 corresponds to the upper bound of estimates from the IPCC's Third Assessment Report (IPCC, 2001) projections (Rahmstorf et al., 2007), causing concern that values of sea level rise derived from global climate model simulations may be underestimating one or more of the model contributions to sea level rise. Hence two climate change scenarios incorporating sea level rise estimates higher than those of the IPCC (2007) were also investigated (Scenarios 3 and 4 in Table 1).

The spatial maps of the 1 in 100 year return levels for total sea level (storm surge + tide + mean sea level rise) were used in combination with digital elevation data obtained from an airborne terrestrial LiDAR survey of the Victorian coast to evaluate maps of inundation. Nine regions were selected along the coast (Figure 3) on the basis that they contained extensive areas of terrain below 2 m elevation.

Table 1: Climate change scenarios considered in the present study. Asterisked values were not investigated in the present study.

Future climate scenario			2030	2070	2100
1	IPCC 2007 A1FI scenario Hunter (2009)	Sea level rise (m)	0.15	0.47	0.82
2	IPCC 2007 A1FI scenario in combination with 'high' wind speed scenario from CSIRO and Australian Bureau of Meteorology (2007) averaged over Bass Strait.	Sea level rise (m)	0.15	0.47	0.82
		Wind speed increase (%)	4	13	19
3	Sea level rise based on Netherlands Delta Committee Vellinga (2008)	Sea level rise (m)	0.20*	0.70*	1.10
4	Rahmstorf (2007) upper estimate	Sea level rise (m)	0.23*	0.74*	1.40

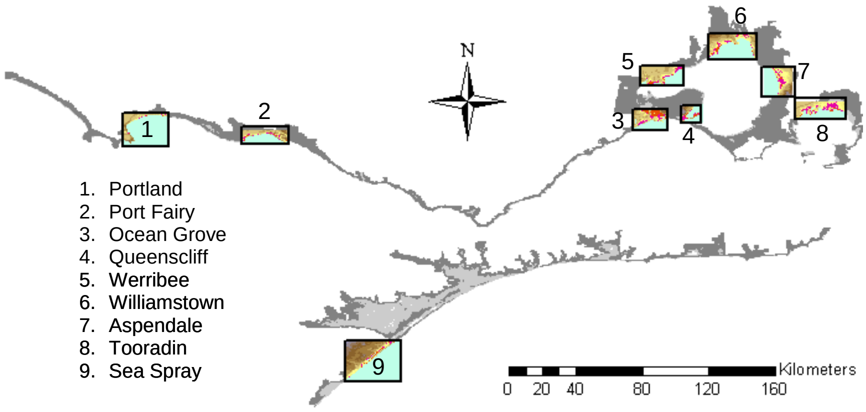

Figure 3: Digital Elevation Data in m (AHD) sourced from the Victorian Department of Sustainability and Environment's 'Future Coasts' LiDAR survey. The 9 rectangular regions were selected for inundation analysis.

Results

The spatial pattern of 1 in 100 year storm tide heights for the Victorian coast under current climate conditions is shown in Figure 4. The highest coastal values, in excess of 2 m, occur in and around Western Port Bay and values of 1.8 to 2.0 m extend from just west of Port Phillip Bay to Wilson's Promontory. These high values are the result of a large contribution from both storm surges and astronomical tides. In Port Phillip Bay, the lower storm tide heights of 1.0 to 1.2 m are due to the strong attenuation of the tides across the entrance to the bay. Values of storm tide heights for the various scenarios are presented in Table 2.

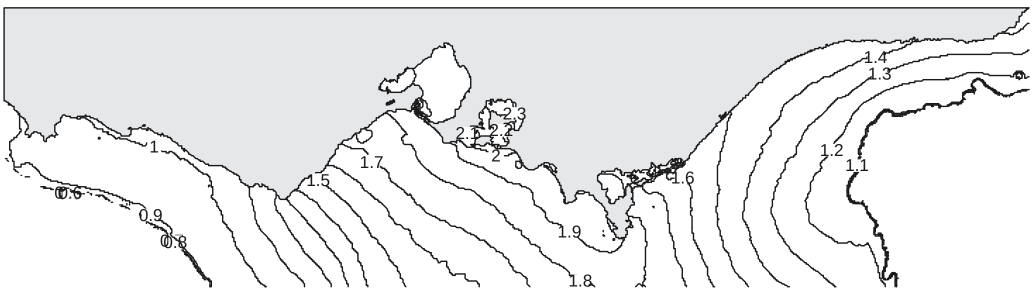

Figure 4: The spatial pattern of 1 in 100 year storm tide heights for the Victorian coast under late 20th Century climate conditions.

The impact of associated increases in coastal inundation depends on the location of coastal assets and the topography of coastal terrain. A simple method is used to identify coastal land that is vulnerable to inundation by extreme sea levels under current climate conditions and the climate change scenarios described in Table 1. The results highlight the non-linear impact that the different climate change scenarios can have on inundation and exposure. This is most dramatically illustrated for Aspendale, between scenarios 1 and 2 for 2070 where a 0.20 m increase in sea level between the scenarios sees the increase in land parcels affected jump from just over 7 times the number affected under current climate conditions to just over 27 times the number affected under current climate conditions.

Conclusions

An efficient method has been developed that enables the development of spatial maps of storm tide return heights under present and future climate conditions. Results indicate that the highest sea levels occur in Western Port Bay and along the central Bass Strait coast. Storm tides are lower in Port Phillip Bay due to the much lower tidal range. The stormtide maps have been used to assess the comparative impact of extreme sea levels on coastal inundation and highlights thresholds of sea level rise that are important in the context of vulnerability and adaptation.

Table 2: The approximate height of the 1 in 100 year storm tide in m (bold), number of land parcels and the area of land in km^2 (in brackets) affected by inundation under the different climate change scenarios. Land parcel data was obtained from the Vicmap property data base (Victorian Department of Sustainability and Environment).

Location	**Current**	**2030**		**2070**		**2100**			
Scenario		**1**	**2**	**1**	**2**	**1**	**2**	**3**	**4**
Portland	**1.01** 168 (0.8)	**1.16** 178 (1.0)	**1.22** 189 (1.0)	**1.48** 180 (1.3)	**1.61** 192 (1.5)	**1.83** 210 (1.7)	**2.05** 220 (2.1)	**2.11** 228 (2.0)	**2.41** 272 (2.5)
Pt Fairy	**1.05** 162 (3.3)	**1.2** 168 (3.7)	**1.25** 189 (4.2)	**1.52** 314 (5.0)	**1.67** 565 (11.3)	**1.87** 680 (12.4)	**2.09** 781 (14.2)	**2.15** 812 (14.0)	**2.45** 968 (15.5)
Ocean Grove	**1.69** 345 (54.2)	**1.84** 460 (56.0)	**1.91** 498 (56.5)	**2.16** 693 (59.6)	**2.33** 751 (60.8)	**2.51** 821 (61.9)	**2.74** 2559 (69.9)	**2.79** 2591 (69.5)	**3.09** 2825 (72.8)
Queenscliff	**1.23** 222 (6.5)	**1.38** 623 (8.9)	**1.46** 819 (9.4)	**1.70** 1379 (10.9)	**1.90** 1667 (11.8)	**2.05** 1937 (67.8)	**2.34** 2094 (73.3)	**2.33** 2094 (73.3)	**2.63** 2254 (75.3)
Pt Wilson	**1.06** 62 (9.1)	**1.21** 64 (10.4)	**1.28** 65 (10.9)	**1.53** 71 (14.3)	**1.72** 75 (17.1)	**1.88** 79 (21.0)	**2.16** 96 (24.0)	**2.16** 97 (23.9)	**2.46** 100 (26.9)
Williams town	**1.12** 303 (6.9)	**1.27** 415 (7.8)	**1.36** 491 (8.3)	**1.59** 1187 (10.0)	**1.81** 2240 (13.1)	**1.94** 3373 (15.5)	**2.26** 10409 (23.5)	**2.22** 9531 (23.2)	**2.52** 15568 (32.0)
Aspendale	**1.14** 257 (2.1)	**1.29** 425 (2.3)	**1.39** 484 (2.4)	**1.61** 1905 (4.0)	**1.83** 6995 (7.8)	**1.96** 9891 (13.3)	**2.29** 16793 (22.6)	**2.24** 15520 (20.9)	**2.54** 19648 (28.8)
Tooradin	**2.08** 554 (42.6)	**2.23** 711 (49.1)	**2.30** 822 (52.5)	**2.55** 1161 (65.4)	**2.73** 1343 (76.2)	**2.90** 1425 (81.7)	**3.14** 1587 (96.4)	**3.18** 1574 (97.5)	**3.48** 1704 (109.8)
Sea Spray	**1.50** 289 (27.4)	**1.65** 548 (30.5)	**1.73** 579 (31.3)	**1.97** 1867 (36.8)	**2.18** 2720 (39.6)	**2.32** 2984 (40.7)	**2.64** 3341 (42.6)	**2.60** 3346 (42.6)	**2.90** 3763 (44.1)

References

CSIRO and Australian Bureau of Meteorology, 2007: Climate Change in Australia, CSIRO and Bureau of Meteorology Technical Report, 140 pp. www.climatechangeinaustralia.gov.au.

Hubbert, G.D., and McInnes, K.L., 1999: A storm surge inundation model for coastal planning and impact studies., J. Coastal Research, 15, 168-185.

Hunter, J., 2009: Estimating Sea-Level Extremes Under Conditions of Uncertain Sea-Level Rise. Climatic Change. DOI 10.1007/s10584-009-9671-6.

IPCC, 2001: Climate Change 2001: The Science of Climate Change. Summary for Policymakers and Technical Summary of the Working Group I Report. Intergovernmental Panel on Climate Change. Cambridge University Press, v+ 98 pp.

IPCC, 2007: Contribution of Working Group I to the Fourth Assessment Report of the Intergovernmental Panel on Climate Change. Summary for Policymakers. 18pp http://www.ipcc.ch/SPM2feb07.pdf

McInnes, K.L., and Hubbert, G.D., 2003: A numerical modeling study of storm surges in Bass Strait. Aust. Met. Mag. 52, 143-156.

McInnes, K.L., Macadam, I., Hubbert, G.D., and O'Grady, J.G., 2009: A Modelling Approach for Estimating the Frequency of Sea Level Extremes and the Impact of Climate Change in Southeast Australia. Natural Hazards DOI 10.1007/s11069-009-9383-2.

Nakićenović, N., and Swart, R., (eds.), 2000: Special Report on Emissions Scenarios. A Special Report of Working Group III of the Intergovernmental Panel on Climate Change, Cambridge University Press, Cambridge, United Kingdom and New York, NY, USA, 599pp.

Rahmstorf, S., 2007: A semi-empirical approach to projecting future sea-level rise. Science, 315(5810), 368–370.

Tawn, J.A, and Vassie, J.M., 1990: Spatial transfer of extreme sea level data for use in the revised joint probability method. Proc Inst Civil Eng Part 2 89:433–438.

Vellinga, P., 2008: Exploring high end climate change scenarios for flood protection of the Netherlands. International Scientific Assessment, 136pp.

Trends and variability in storminess over south-east Australia since the end of the 19th century

Lisa Alexander
Climate Change Research Centre, University of New South Wales, Sydney, Australia

Xiaolan L. Wang, Hui Wan
Climate Research Division, Science and Technology Branch, Environment Canada, Toronto, Canada

Blair Trewin
National Climate Centre, Bureau of Meteorology, Melbourne, Australia

Introduction

Recent studies suggest that there is some evidence that changes in synoptic weather patterns have led to a decline in the frequency of rain bearing and/or storm systems reaching southern Australia [e.g. Hope et al. 2006; Verdon-Kidd and Kiem 2008; Alexander et al. 2009]. However, previous studies of “storminess” have mostly had to rely on reanalysis data because of the lack of access to early observational data across Australia prior to the mid-20th century. The aim of this study is to extend analysis of storminess across south-east Australia back to the end of the 19th century using geostrophic winds deduced from station triangles of pressure observations. Understanding the long term variability of storm activity would give a much better perspective on how unusual recent climate variations have been.

Geostrophic wind speeds or ‘geo-winds’ have been used in a number of studies of North Atlantic and European storminess using centennial and longer time scale *in situ* observations [e.g. Schmidt and von Storch 1993; Matulla et al. 2008; Wang et al. 2009]. The assumption is that outside of the tropics geo-winds form a reasonably good first approximation for actual wind speeds and provide a much more reliable and homogeneous measure for long term storminess than wind speed measurements which are very sensitive to site moves and instrumentation changes [WASA 1998; Wan et al. 2009]. We apply this method to quality controlled sub-daily mean sea level pressure (MSLP) observations at eight sites across south-eastern Australia (see Table 1) to form eight station triangles. These data, the earliest observations dating back to 1859, have only recently become available following a digitization project by the Australian Bureau of Meteorology (BoM) and they are used here to reconstruct long-term measures of storminess for south-east Australia.

Table 1: The eight sites and the related stations of MSLP data analyzed in this study. A site usually refers to a combination of the stations listed in the second column.

Site	Name of station(s)	Station IDs	Start date (YYYY.MM.DD.HH)
Rob	Robe	026026	1884.09.01.00
Cap	Cape Otway	090015	1861.01.11.00
Hob	Hobart	094029	1893.05.11.06
Por	Port Lincoln; Port Lincoln AWS	018070; 018192	1892.01.01.00
Den	Deniliquin; Deniliquin Airport AWS	074128; 074258	1859.09.01.00
Mil	Mildura Post Office; Mildura Airport	076077; 076031	1891.02.05.00
Bou	Bourke; Bourke Airport; Bourke Airport AWS	048013; 048239; 048245	1892.03.16.00
Goo	Goondiwindi; Goondiwindi Airport	041038; 041521	1891.03.18.00

Each station recorded at least twice a day but all recorded at 0900 and 1500 local time. The quality of the data was tested by analyzing pressure tendencies (i.e. the difference in hPa between two subsequent MSLP observations) both within and between stations to highlight unusually large values. In addition, the consistency of the MSLP time series was tested using the method of Wang (2008) and any mean shifts detected were adjusted accordingly.

Using these high quality, consistent sub-daily MSLP time series we were able to closely follow the method of Wang et al. (2009) who assessed trends and variability in storminess in the north-east Atlantic since 1874 using geostrophic wind speed triangles, and apply it to south-east Australia. A detailed description of the method is given by Wang et al. (2009) but essentially geo-winds, w_g, are calculated from meridional (u) and zonal (v) wind inferred components such that:

$$w_g = (u_g^2 + v_g^2)^{1/2}$$

where u and v are functions of air density, the Coriolis parameter and the zonal and meridional pressure gradients respectively of the instantaneous MSLP values at the three locations making up the station triangle.

From the sub-daily geo-wind values it was then possible to calculate standardized annual and seasonal 95th and 99th percentiles to represent what we hereafter refer to as the “storm” or “severe storm” percentiles respectively. Percentiles were calculated from the earliest possible date when all stations in the triangle were reporting for the full year e.g. the RDC geo-winds can be calculated from 1885 (see Table 1). The decadal variability of the resulting storm and severe storm percentile timeseries was assessed using an 11-point Gaussian smoother [Wang et al. 2009; Alexandersson et al. 2000] and long term trends were also calculated using a modified non-parametric Mann Kendall slope estimator [Mann 1945; Kendall 1955; Wang and Swail 2001; Wang et al. 2009].

Results

Results indicate a consistent decrease in both storm and severe storm activity in nearly all regions and seasons. In the majority of cases these trends are significant at the 5% level. In autumn (MAM) and winter (JJA) significant declines are apparent in all regions in the 95th percentile results, except for CDH (the most southerly triangle). When the results are combined to form regional series, all seasons show statistically significant declines, with the largest reductions in storminess in autumn and winter for both storm and severe storm percentiles.

However, trends on their own mask some of the low frequency variability that is present in these storm indices. Fig. 1 shows the 11-point Gaussian filtered winter (JJA) storm percentile results. In the late 19th century and early 20th century, decadal variability is large in all regions but this has reduced in later decades. The results are similar for all seasons and also the severe storm percentile (not shown). Of course the results are not independent between triangles because in a lot of cases they share a common vertex or vertices. However, there is a remarkable consistency between the timeseries and trends from each of the regions even between those triangles that do not share station locations. This gives us confidence in the robustness of the results.

Fig. 2 shows the south-east Australian regional results for all seasons. The storm and severe storm percentiles are highly positively correlated (0.84, 0.77, 0.81 and 0.83 for DJF, MAM, JJA and SON respectively). For both storm indicators there is larger decadal variability in the earlier part of the record. In all seasons there appears to be a peak in storminess around the 1920s with least activity around the 1960s. To some extent in the last couple of decades, storminess has “rebounded” somewhat, except perhaps in spring (SON), but not nearly to the levels of the storminess peaks of the earlier part of the 20th century.

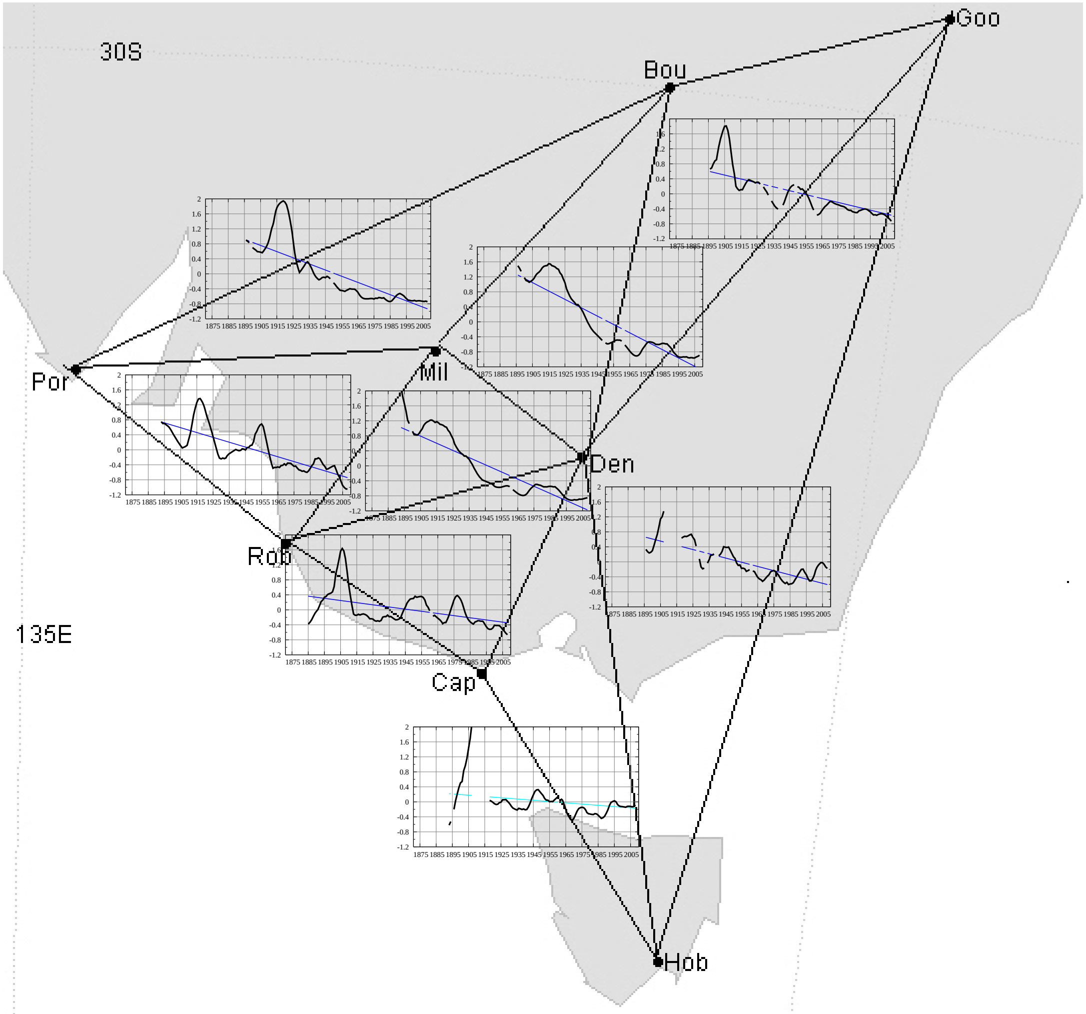

Fig. 1: Low-frequency variability and linear trends of JJA 95th percentiles for each triangle. In the text, the Cape Otway-Deniliquin- Hobart triangle will be referred to as CDH. All trends shown are statistically significant at the 5% level, except for CDH.

Conclusions

Using geostrophic wind speeds derived from eight triangles of sub-daily mean sea level pressure observations, we calculated measures of storminess for the south-east Australian region from the end of the 19th century through to 2008 for all seasons. Storminess has reduced in almost all triangles and seasons across the region since the end of the 19th century but particularly in autumn and winter. Reductions are statistically significant at the 5% level in nearly all regions and seasons. Using data from all the station triangles to create a combined index for south-east Australia, our results indicate statistically significant declines in all seasons in both storm and severe storm activity. There is strong decadal variability in storm activity particularly in the early part of the record, with storminess peaking in the 1920s. Decadal variability in storm activity has reduced in more recent decades in all seasons.

The results show strong evidence for a significant reduction in westerly flow across south-east Australia over the past century, consistent with a southward movement of Southern Hemisphere storm tracks. While these changes can not fully explain the significant reductions that have been observed in rainfall in the region it is likely that reductions in storminess are exacerbating observed drought conditions.

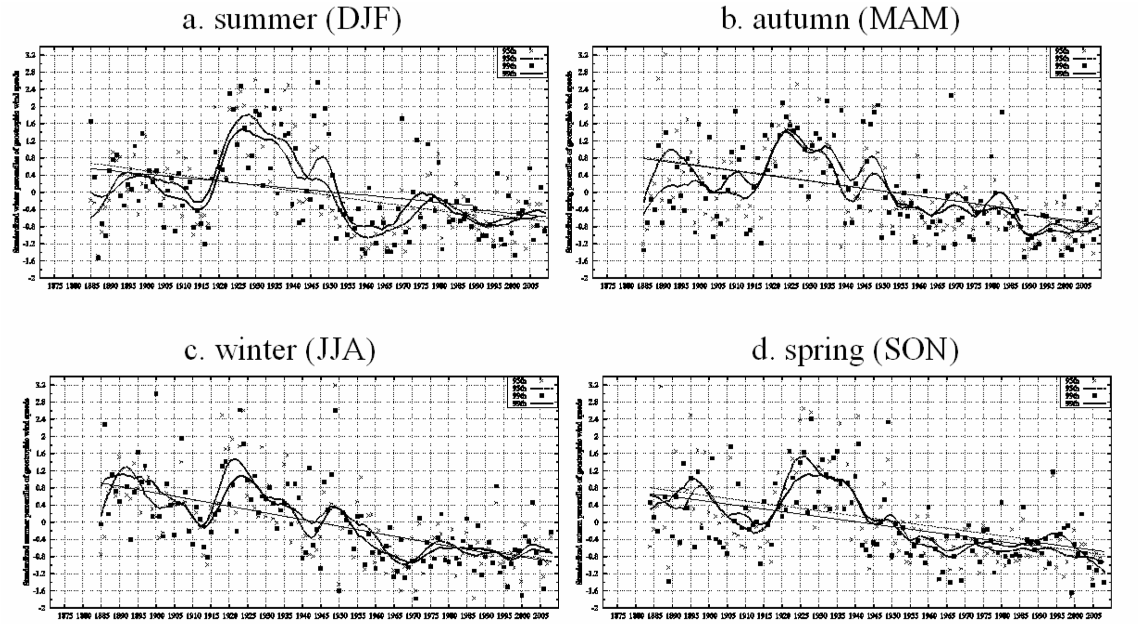

Fig. 2: South-east Australian region area averages between 1885 and 2008 of standardized 95th and 99th percentiles of geo-winds along with Gaussian low-pass filters and linear trends for the indicated seasons.

References

Alexander, L.V., P. Uotila, N. Nicholls and A. Lynch. 2009. A new daily pressure dataset for Australia and its application to the assessment of changes in synoptic patterns during the last century, *J. Clim.*, in press.

Alexandersson, H., H. Tuomenvirta, T. Schmith, and K. Iden. 2000. Trends of storms in NW Europe derived from an updated pressure data set, *Clim. Res.*, 14, 71-73.

Hope, P. K., W. Drosdowsky, and N. Nicholls. 2006. Shifts in the synoptic systems influencing southwest Western Australia. *Clim. Dyn.*, **26**, 751-764.

Kendall, M. G. 1955. Rank Correlation Methods, Charles Griffin, 196pp.

Mann, H. B. 1945. Non-parametric tests against trend, *Econometrica*, 13, 245-259.

Matulla, C., W. Schöner, H. Alexandersson, H. von Storch and X. L. Wang. 2008. European Storminess: Late 19th Century to Present. *Clim. Dyn.*, 31, 125-130. DOI: 10.1007/s00382-007-0333-y.

Schmidt, H. and H. von Storch. 1993. German Bight storms analyzed, *Nature*, 365, 791

Verdon-Kidd, D. and A. S. Kiem, 2008, On the relationship between large-scale climate modes and regional synoptic patterns that drive Victorian rainfall, *Hydrol. E. Sys. Sci. Discuss.*, **5**, 2791-2815.

Wang, X. L. and V. R. Swail. 2001. Changes of extreme wave heights in Northern Hemisphere oceans and related atmospheric circulation regimes. J. Clim 14:2204-2221.

Wang, X. L. 2008. Accounting for autocorrelation in detecting mean shifts in climate data series using the penalized maximal t or F test, *J. Appl. Meteor. Climatol.*, 47, 2423-2444. Doi:10.1175/2008JAMC1741.1

Wang, X. L. et al. 2009. Trends and variability of storminess in the Northeast Atlantic region, 1874-2007, *Clim. Dyn.*, in press. DOI 10.1007/s00382-008-0504-5

Wan, H., X.L. Wang, and V. R. Swail, 2009: Homogenization and Trend Analysis of Canadian Near-Surface Wind Speeds. *J. Climate*, in press.

WASA Group. 1998. Changing waves and storms in the northeast Atlantic? *Bull. Amer. Met. Soc.*, 79, 741–760.

Modelling challenges from the Black Saturday 2009 event

Tony Bannister
Victorian Regional Office
Bureau of Meteorology
GPO Box 1636 Melbourne
Vic 3001, Australia
Email: t.bannister@bom.gov.au

Introduction

A defining Australian natural disaster occurred in Victoria on Saturday 7 February 2009 (Black Saturday). On a day of unprecedented heat in Victoria, fires in central and southeast parts of the State caused a level of death and destruction that surpassed previous fire events in the recorded history of Australia. 173 people lost their lives. 'Around 78 communities were directly impacted and entire towns were left unrecognisable. The fires burnt more than 2,000 properties and 61 businesses. Police stations, schools and kindergartens, fire and emergency services facilities, churches, community halls and sporting clubs were also destroyed or badly damaged' (Department of Sustainability and Environment website).

Fig. 1: Map of the major fires that occurred on Black Saturday in Victoria (sourced from the Victorian Country Fire Authority website)

Weather background

The context for the weather on Black Saturday was the whole of southeast Australia suffering a severe and protracted drought that is without historical precedent. After a relatively mild start to 2009, exceptional heatwave conditions developed across southeast Australia in late January. In addition to its peak intensity, the 2009 heatwave was also notable for its duration. While there was some respite in temperatures across coastal southern Victoria in the few days preceding Saturday 7 February, the prolonged period of extreme heat persisted for inland Victoria.

As a cold front moved towards southeastern Australia, a pre-frontal trough moved eastward from South Australia across Victoria during Saturday 7 February, see Fig. 2 for the weather chart valid at 11am Eastern Daylight Time (EDT) 7 February. Dry, strong to gale-force, north to northwesterly winds blew the pool of extreme heat through Victoria ahead of the pre-frontal trough wind change. Record high temperatures for February were set in over 87% of Victoria on this day. The combination of exceptional heat, low humidity, wind speed and dry fuels produced extreme fire weather conditions over Victoria from early on the Saturday. Winds averaged 40 – 60 km/h with gusts to 115 km/h reported. Fire dangers did not drop below Extreme until up to an hour after the strong and gusty wind change in central parts of the State. A general cooler southwesterly wind flow extended throughout Victoria, apart from the alpine region, by early Sunday 8 February, with the weather event essentially over.

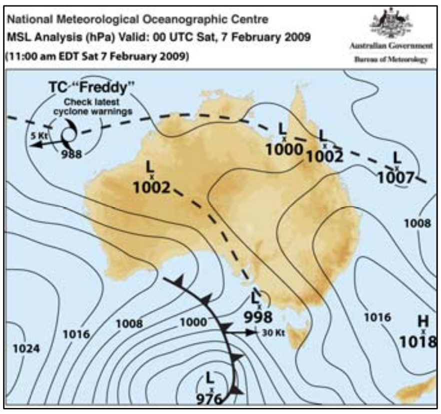

Fig. 2: Mean sea level pressure chart valid for 11am Black Saturday.

Model challenges

Long term

The computer weather model guidance for this event was incredibly good. Most of the long term guidance depicted the same scenario for the Saturday, starting from about a week before the event.

The consistency of the global model output during the week prior to 7 February gave the meteorologists the confidence to emphasise to the fire agencies, government officials and the public the extreme conditions expected, for example refer to Fig. 3 for the Black Saturday fire agency forecast issued Sunday 1 February 2009. This led to the Premier of Victoria conducting a press conference on Thursday 5 February to highlight the seriousness of the situation.

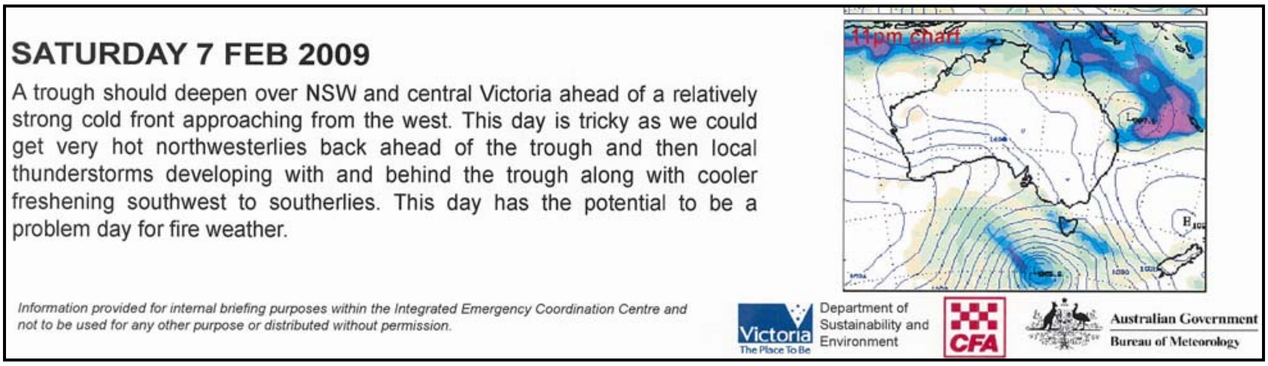

Fig. 3: Interagency Emergency Coordination Centre (iECC) forecast issued Sunday 1 February 2009 for Black Saturday.

Short term

In general the short term model guidance was very good in providing guidance as to the extreme conditions experienced on the Saturday. The models captured well the development of the pre-frontal northwesterlies, the development and movement of the wind change and the easing of conditions overnight, however there were some specific areas where more accurate guidance would have made a good forecasting effort even better.

Wind change timing

A critical element of the day was the timing of the prefrontal wind change as it swept across Victoria, especially expected timing at the main fire locations in Central Victoria. Fig. 4 illustrates the development and movement of the wind change, both in reality and as indicated by the 10m winds from the 6 February 2009 12 UTC run of the MesoLAPS (Puri et al., 1998) 5km resolution model. Initially the model guidance moved the change across the coast earlier than in reality, then during the afternoon the actual change movement generally became faster than the guidance. Also as indicated by Fig. 4, discerning the model wind change position became very difficult later in the afternoon as model instabilities produced spurious wind outflow boundaries. Although not show, the wind change position in the 7 February 2009 00 UTC run of the MesoLAPS 0.05 degree resolution model was even more difficult to discern due to these spurious wind boundaries. Operationally the timing of the wind change was the highest priority forecast on Black Saturday; it was literally a life or death forecast.

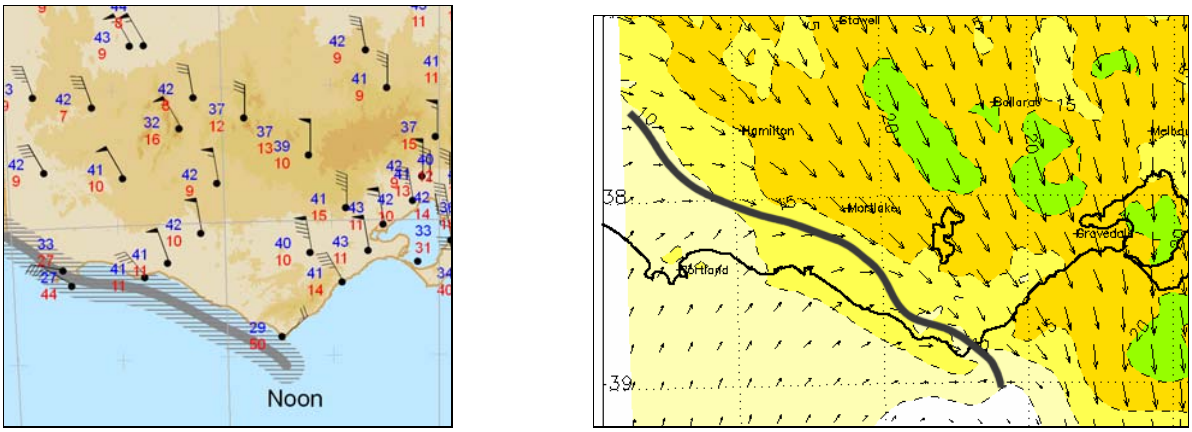

(a) (b)

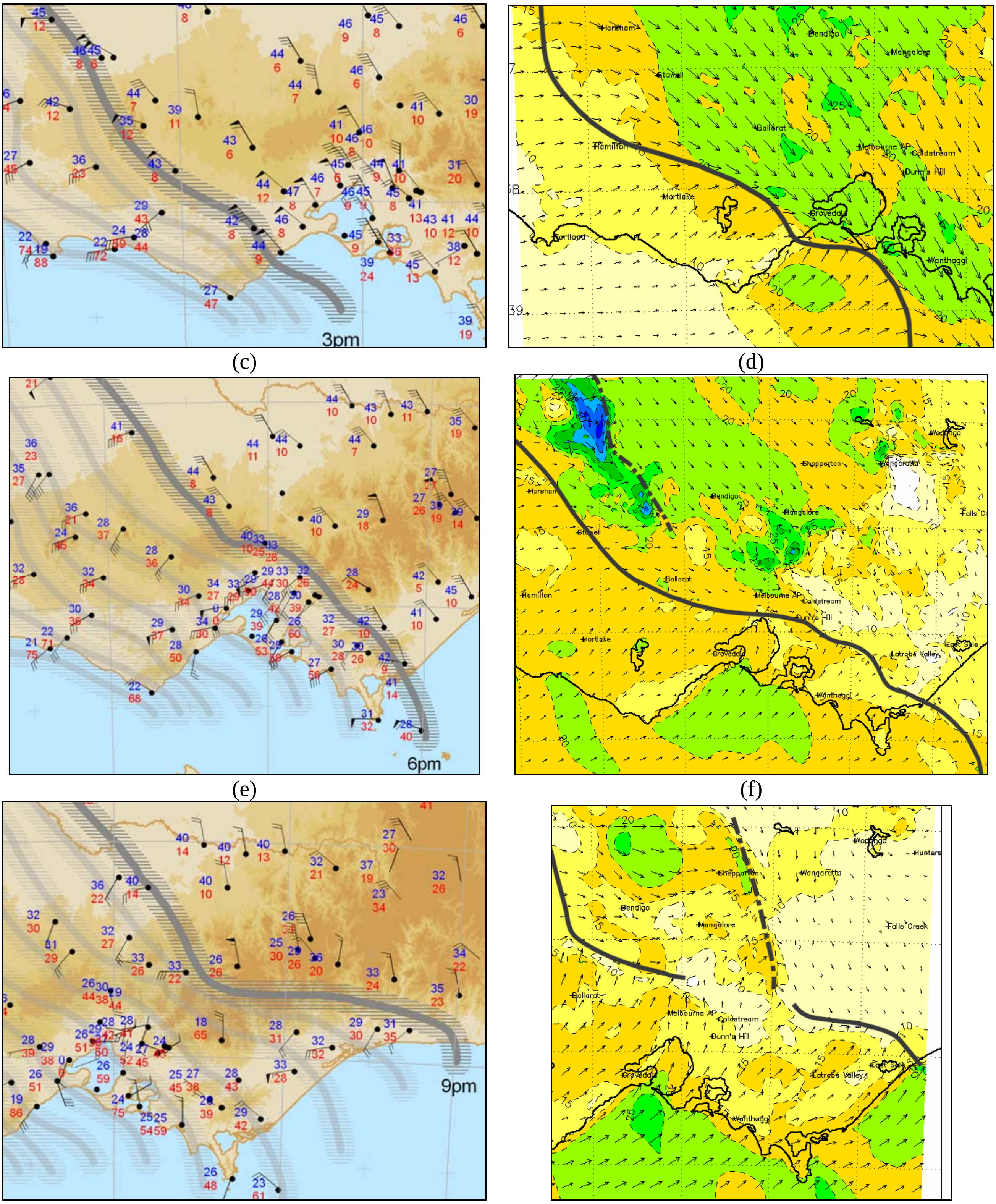

Fig. 4: Actual and MesoLAPS (0.05 degree resolution) wind change location on 7 February 2009 at (a)&(b) noon, (c)&(d) 3pm, (e)&(f) 6pm and (g)&(h) 9pm EDT. Note that the wind barb convention is non-WMO standard and is in km/h. Temperature (upper) and relative humidity (lower) values at Automatic Weather Station sites are indicated. Current and past actual hourly wind change positions are shown with indicative uncertainty. Model isotachs are in knots.

Mesoscale high behind the wind change

Winds immediately behind the wind change were strong and gusty with fire dangers not dropping below Extreme until up to an hour after the change in central parts of the State. However winds in the Melbourne area and nearby fire areas to the north east then became light and variable and it took three to four hours after the initial cool change for the general southerly push to overwhelm this variable wind flow and allow a secondary southerly surge through the Metropolitan area and West Gippsland. No operational computer weather model guidance gave any indication of this scenario occurring and it took the fire weather forecasters completely by surprise. The forecasters could see the secondary surge to the southwest of Melbourne and the then current spot fire forecasts were amended to allow a period of light winds before this surge reached the fire grounds. However the forecasters at the time did not know how long the light winds would persist. Fig. 5 indicates the actual conditions at 9pm and the 6 February 2009 12 UTC MesoLAPS 0.05 degree resolution guidance for the same time. Better model guidance for this mesoscale process would have enabled the forecasters to provide more accurate spot fire forecasts to the fire agencies.

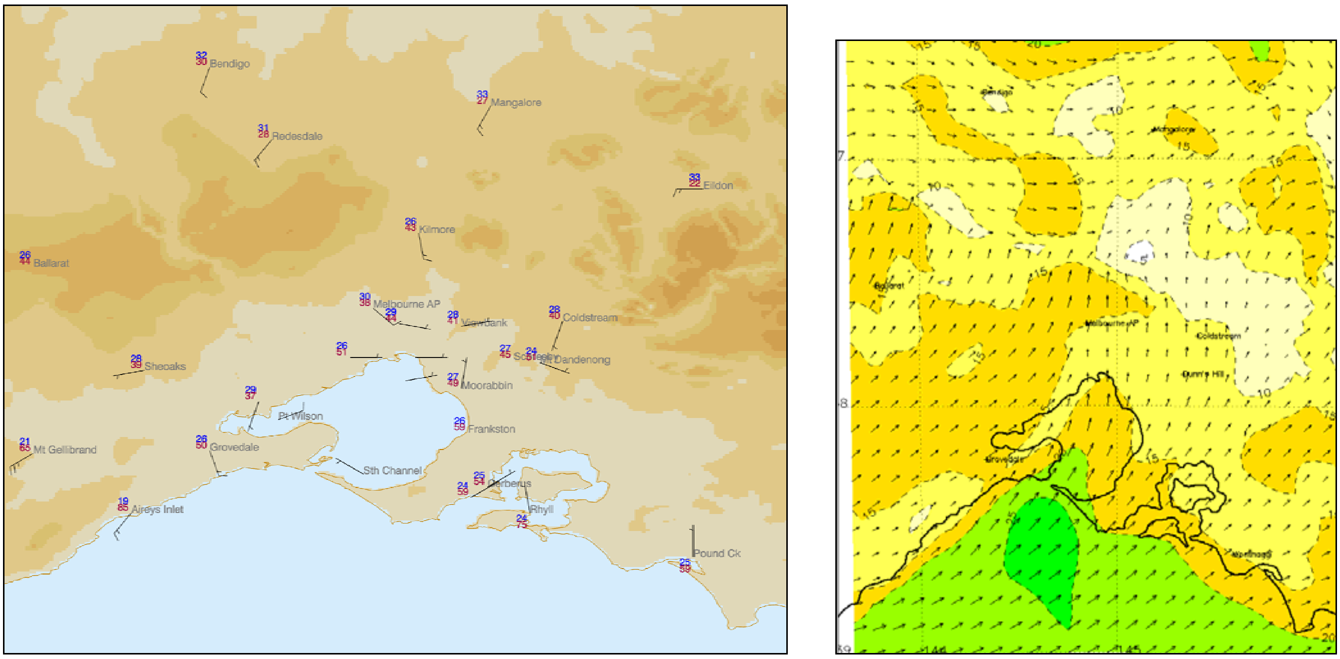

(a) (b)

Fig. 5: 9pm EDT, 7 February 2009 (a) actual observations and (b) MesoLAPS 5km resolution 10m wind output for the Melbourne area. Wind barbs and isotachs are in knots.

Forecaster guidance for possible pyrocumulonimbus development

In the days leading up to Black Saturday, as well as on the day, the fire agencies were very concerned about the potential for formation of pyrocumulonimbus (pyro-cb) above any fire that formed. These fire-induced thunderstorms provide a feedback mechanism to increase the intensity of the fire, as well as producing lightning which can start new fires and create a situation where winds around and in the fire ground can become violent and even more unpredictable.

Normal model thunderstorm guidance is not usually helpful for pyro-cb development because there is no representation of fire in the atmospheric model to provide extra heat and moisture. For Black Saturday the lack of lower level moisture was the reason for no model signature of normal thunderstorm development. Specific model guidance for this possibility would greatly add to the forecaster service to the fire agencies. Mills and McCaw (2009) have developed both a modified Haines Index, C-HAINES, based on the Haines Index (Haines 1988), as well as a modified Convective Available Potential Energy, FIRECAPE, which both show some promise in distinguishing these extreme conditions where pyro-cb are possible.

The operational forecasters who worked up to and on Black Saturday have nothing but praise for the performance of the global and mesoscale models for this signature event. However there are still some areas where better guidance would have meant better forecasts, which may have had impact in terms of the human cost of Black Saturday.

References

Haines, D.A. 1988. A lower atmospheric severity index for wildland fires. *National Weather Digest*, **13**(2), 23-27.

Mills, G. A. and McCaw, L. 2009. Atmospheric Stability Environments and Fire Weather in Australia – extending the Haines Index. *In press*, CAWCR Research Report. (http://www.cawcr.gov.au/publications/technicalreports.php).

Puri, K., G. S. Dietachmayer, G. A. Mills, N. E. Davidson, R. A. Bowen, and L. W. Logan, 1998: The new BMRC Limited Area Prediction System, LAPS. *Aust. Meteor. Mag.*, **47,** 203–223.

Modelling of convective events for climate change applications

Debbie Abbs
Centre for Australian Weather and Climate Research
CSIRO Marine and Atmospheric Research,
Private Bag 1, Aspendale, Victoria 3195
Email: Deborah.Abbs@csiro.au

In human systems, the key features of climate change for vulnerability and adaptation are related to coping with variability and extremes, not simply average conditions. In many cases these extreme events are convective in nature and can cause extreme rainfall, severe winds, coastal erosion and in some cases be accompanied by hail and/or tornadoes. Impacts to the community from these events include loss of life, damage to infrastructure, housing and agriculture, disruption to businesses and loss of income.

An important consideration for climate change science however is that these extreme weather events are often of a spatial scale that is too small to be adequately represented in global climate models. Thus other methods need to be developed that enable the climate science community to develop projections for changes in the intensity and frequency of these events. The development of these techniques relies on the “marriage” of traditional weather-related research with climate change research.

This talk will review some of these techniques and present results from a selection of high resolution simulations. These simulations aim to demonstrate that it may be feasible to use event-based modelling of extreme convective events to quantify changes in the intensity of such events arising from human-induced climate change. Examples to be covered include east coast lows and severe thunderstorms.

The Centre for Australian Weather and Climate Research is a partnership between CSIRO and the Bureau of Meteorology.